DOCTORAL THESIS

Analysis and control of nonlinear dynamic systems using novel computational methods

Author:
Balázs Csutak

Thesis advisor:
Dr. Gábor Szederkényi, DSc

Pázmány Péter Catholic University
Faculty of Information Technology and Bionics
Roska Tamás Doctoral School of Sciences and Technology
2025

Acknowledgements

First and foremost, I would like to thank my supervisor, Dr. Gábor Szederkényi, for introducing me to the world of science and for all the guidance and support he has provided over the past eight years. Without his precise professional direction, endless patience, and consistently positive and supportive attitude, this thesis would not have been completed. I am grateful to be part of his team.

I thank Dr. Tamás Péni, senior research fellow at SZTAKI, for the opportunity to explore so many fascinating scientific topics over the years, and to co-author the resulting papers. I am grateful for the support, collaboration, and many joyful moments.

I also wish to thank Dr. Péter Polcz for his invaluable professional assistance, our joint work, his thorough explanations, and thought-provoking discussions. I am grateful to Dr. Gergely Röst and Dr. Ferenc Bartha, researchers at the Bolyai Institute of the University of Szeged, for our collaboration in the field of epidemic control. Thanks also to Koppány Jenei for his contribution to our joint conference paper.

Many thanks to Judit Juhász for her help with editing the thesis and organizing the references.

Last but most importantly, I thank my family, and especially my parents, for setting me on this path many-many years ago. I am deeply grateful for the years of learning together, their unwavering patience, encouragement, and — well needed —constructive criticism and nudging.

Finally, my heartfelt thanks to teacher Judit Bíró for the many math lessons that taught me the importance of true understanding, critical thinking, and problem-solving—skills that have proven invaluable in everything I've undertaken since.

Abstract

This thesis contributes to the control, trajectory reconstruction and parameter synthesis of nonlinear nonnegative compartmental models. It presents novel applications of computation-based methodologies, addressing practical challenges in epidemic intervention planning, state estimation under uncertainty, and qualitative design of system behavior.

In the first part, a model predictive control-based framework is introduced for the optimal control of compartmental epidemic models under realistic intervention possibilities and constraints. The method supports the formal specification of complex public health requirements and policy expectations using temporal logic, and can handle discrete intervention levels, balancing between the often contradicting objectives. Later, the control framework is extended to integrate non-pharmaceutical interventions, testing, and vaccination strategies by introducing additional inputs and compartments. The method accounts for limited resources and logical interdependencies between these interventions, allowing the derivation of coordinated strategies.

The second part addresses the retrospective trajectory reconstruction of nonlinear nonnegative models in the presence of model mismatch, parameter uncertainties, and observation inaccuracies. Two complementary methodologies are developed. Both of them leverage the fact, that such reconstruction tasks can be transformed into a control problem by considering the measurable quantities as a reference signal to be tracked, effectively performing a model inversion. First, a stochastic and deterministic optimization-based method is presented for inferring directly unmeasurable epidemic states and parameters, such as the time-varying transmission rate, latent infections, and asymptomatic cases, along with uncertainty estimates. The second approach uses a robustified feedback-linearization based asymptotic output tracking technique with nonlinear state estimation.

The proposed methods are evaluated through various realistic case studies and simulations using genuine epidemiological data. Both hypothetic and real-world scenarios are discussed, including actual intervention strategies applied in different European countries during the COVID-19 pandemic. The computed outcomes are compared to independent results from the related scientific literature.

Finally, the third contribution is a general parameter synthesis method, capable to ensure predefined qualitative behavior in nonnegative dynamical systems. The technique is illustrated by inducing autonomous oscillations with desired frequency characteristics in different kinetic models, underlining its application potential in biochemical and epidemiological domains.

Contents

Chapter 1

Introduction

Nonlinear dynamical systems play a fundamental role in almost every field of natural sciences. Starting from physical and mechanical systems, through all kinds of biological, chemical, and even sociological processes, these abstractions can accurately describe a wide range of the inherently continuous and nonlinear phenomena of nature [1].

Not surprisingly, the theory of dynamical systems has been an intensively studied topic for centuries, creating an abstract, generic field of science with strong mathematical foundations and extensive literature, all aimed at the analysis, synthesis, monitoring, and control of these systems. Numerous subclasses of dynamical systems have been defined, followed by the proposal and development of countless ideas and methods revolving around the related problems [2].

While some of these subclasses are well explored with comprehensive tools available for all kinds of practical problems, most of them - especially the nonlinear ones - still offer open questions. Most of the theoretical contributions in the field of nonlinear systems are generally applicable only to a well-defined subclass of the area. Thus, the analysis and control of such systems remain a challenge due to the complex dynamical behavior, possible singularities, and state-dependent nature of fundamental properties like reachability and observability. The complexity of the underlying mathematical structure required to provide theoretical guarantees for the expected dynamical behavior often exceeds the capabilities of the present state of scientific knowledge [3].

The emergence of modern computational hardware, tools, and methodologies, however, has opened the gate for a range of novel approaches, based on extensive simulations or high-complexity optimization problems. With rapidly evolving numerical solvers becoming available, some of these problems - previously non-tractable due to the high computational cost - are becoming solvable in an acceptable timeframe [4, 5].

In this thesis, I explore multiple novel computational methods aimed at the observation, control, and parameter synthesis of nonlinear, nonnegative systems, with a special focus on the compartmental epidemic models, which have gained never-before-seen popularity in the shadow of the recent COVID-19 pandemic.

1.1 Nonnegative dynamic systems

A special subset of nonlinear dynamical systems is the class of nonnegative (also called positive) dynamical systems, which are widely applied in different fields of science where the modeled quantities (e.g. mass, concentration, pressure, population number or density, object count) are

nonnegative by nature [6]. In the essential book [7], the authors write: *"One is tempted to assert that positive systems are the most often encountered systems in almost all areas of science and technology, except electro mechanics ... "*.

An important subset of nonnegative systems is the class of kinetic models (also called chemical reaction networks), the dynamics of which can be formally represented by chemical reactions assuming certain reaction rates. The state variables of such models are the (generalized) concentrations. Chemical reaction network theory (CRNT) is mathematically well-founded and has been continuously developing since the 1970s [8]. It is often possible to transform originally non-kinetic models into kinetic form; therefore, reaction networks form a really wide system class which is sometimes called a "prototype of nonlinear science" [9]. This implies that it might be beneficial to write non-chemical models into reaction network form [10], and apply CRNT for analysis or control design [11]. One recent example of that is the kinetic modeling of vehicle traffic flows, where the reacting 'molecules' are vehicles and units of free space on highways [12].

The topic of oscillating (bio)chemical reactions has been an intensively studied field since the discovery of the Belousov-Zhabotinsky reaction [13]. It is now known that chemical oscillators together with other switching subsystems are widely present in living organisms, regulating physiological processes and influencing important cell decisions [14]. The possibility of complex dynamical behaviour is also a central problem in CRNT, where there exist several strong mathematical conditions for this (see, e.g. [15, 16]). However, finding the parameter values that guarantee the desired dynamic properties of the solutions of such a system still remains a complex problem.

1.1.1 Parameter synthesis for qualitative behavior

Numerous classical and novel computational approaches exist for solving these kinds of problems. In [17], a mathematical and chemical approach is presented on the Belousov-Zhabotinskii reaction, aiming to formalize the connection between oscillating reactions and the properties of nonlinear differential equations, and promising a systematic approach for synthesizing new chemical reactions showing oscillatory behavior. Similarly, the authors of [18] study analytically and numerically the transition of two-variable chemical models from stable steady states to oscillatory states.

The already mentioned increase in computational power has shifted the focus towards numerical approaches for setting the behavior of biochemical systems as well. One of the most functionally rich solutions is [19], where a multi-level optimization solution is proposed for the automated design of synthetic biological circuits from predefined components. Here, the model parameters belong to the decision variables, and several simulation-based optimization runs are needed to compute a feasible solution.

Another possibility is to introduce compact formalisms, such as different versions of Temporal Logic (Linear Temporal Logic, Signal Temporal Logic, Computational Tree Logic, etc.) for describing the required dynamical behavior. Such solutions are mostly used for model checking, and not as part of the synthesis process itself (see, e.g. [20–24]). Thus, looking for the right parameter settings becomes more like an exhaustive search, at the end of which a validation step is carried out using the respective temporal logic methodology. There are even machine learning-based approaches, for completing or correcting biological models semi-automatically, starting from temporal logic formulae [25]. Optimization, however, can be directly used for controller and parameter synthesis as well. Derived manually or translated algorithmically from temporal logic

formulae [26], optimization constraints describing the desired model behavior can be directly applied to find the correct parameter values. A temporal logic-based model synthesis was shown for reaction-diffusion networks in [27, 28].

Another particularly successful application of this computation framework is model predictive control, where the requirements can be automatically translated to a mixed integer programming problem taking into consideration the system dynamics as constraints [29]. Using signal temporal logic, complex specifications and constraints can be given for the required dynamical behaviour of a model in a compressed form. Most often, linear dynamical models are preferred for control design with temporal logic, since those can be put into the framework of mixed integer linear programming. However, there exist really powerful solvers capable of efficiently handling nonlinear models as well [30].

1.2 Model-based epidemic management

1.2.1 Early course of COVID-19 and intervention strategies

On December 31, 2019, China alerted the World Health Organization (WHO) on a cluster of pneumonia cases of unknown origin in Wuhan, China. On January 7, 2020, the causative pathogen of the outbreak was identified as a novel coronavirus, later named SARS-CoV-2, and the disease it causes as COVID-19. SARS-CoV-2 infections quickly spread: the first case outside China was identified in Thailand, on 14 January, followed by reported cases from a number of countries [31, 32].

In Europe, the first cases were confirmed on January 24, 2020, in France (where, later in April, COVID-19 was retrospectively confirmed for a patient hospitalized in late December 2019) [33,34], and on January 27, in Germany, Bavaria, leading to a local outbreak [35]. The first epidemic in Europe started in the Lombardy region of Italy with the first detection on February 20, 2020 [36]. Control measures started in mid-March in most of the European countries, including social distancing measures that reflect a strong effort to suppress, or at least to slow down, the spread of COVID-19. Because of the differences in timing and stringency of the applied measures, the peak daily incidence varied substantially among countries, with occasional resurgence of cases observed [37]. By the end of July 2020, around seventeen million cases and seven hundred thousand deaths had been reported worldwide, with significant spreading in the Americas, Eastern Mediterranean, and Southeast Asia [38].

In the initial absence of vaccine and effective treatment, the available non-pharmaceutical intervention strategies could roughly be divided into two main categories, targeting the mitigation or the complete suppression of the epidemics [39]. Mitigation does not aim to completely stop the transmission of the virus, only to slow it down to keep the number of infected people below the capacity of the healthcare system. Sweden is an example of such a strategy. On the other hand, suppression aims to reduce the incidence to a very low level by strict social distancing, and then keep that number low by localized and targeted measures, such as efficient surveillance, testing, tracing, and quick isolation of cases. The first outbreak was suppressed in most European and East Asian countries, Australia, and New Zealand. Afterwards, following a relaxation of such measures, a resurgence has been observed in the Western Balkans [37].

Mathematical models have been commonly used in epidemiology to evaluate such disease control strategies. However, disease control in this context usually refers to a single intervention measure that is sufficient to reduce the reproduction number below one, leading to the eradication of the

disease. The most commonly used measures are widespread vaccination and drug treatment [40], or, in the case of vector-borne diseases, culling of mosquitoes and other arthropods that transmit the pathogen into other living organisms.

The COVID-19 situation was unprecedented in the sense that governments were constantly tuning their control measures, trying to find balance between public health concerns and the costs of social distancing measures to the society and the economy [41, 42]. Thus, using more refined approaches, such as feedback and optimization, which are standard tools of control theory, is necessary to dynamically manage our response to the pandemic and tailor policies to stabilize the situation.

To place the problem of epidemic management in a control theoretic framework, some key concepts must be reiterated. In this approach, dynamical systems are considered as operators mapping from an input signal (function) space to an output space [43]. A distinction must be made between manipulable inputs, which can be set (often between certain limits) by the user, and disturbance inputs from the environment that cannot be directly influenced. The outputs are either directly measured quantities or they are computed from measurements. The control goals are usually prescribed using the outputs, e.g. they have to track a reference trajectory or just stay between predefined limits. Such goals are often equipped with additional constraints (e.g. physical or strategic bounds on the inputs and/or on the state variables) and optimality criteria (e.g. cost or operation time). This kind of complex control problem can most often be expressed in the form of constrained optimization.

There is a wide literature on the model-based targeted manipulation of diseases either within the host or across an entire population [44–48]. In the case of mitigation and suppression strategies, typically the key manipulated input variables are the infection rate and the recovery speed if there is any efficient therapy for the disease [49]. Moreover, vaccination intensity can also be considered as a possible input [50, 51].

In addition to the control goals of intervention strategies, several important constraints must be taken into consideration, related to e.g. the capacity of the healthcare system, the costs of the introduced measures, or the tolerance level of the population. A reasonable choice to balance between these often contradicting considerations while still handling the nonlinear dynamics in an appropriate way is the application of model predictive control (MPC) [52,53]. Social distancing is used as input in [54,55] and [56] to suppress the peak of infections together with the minimization of economic loss using the MPC framework.

It is worth mentioning that the vast majority of the available control approaches assume a manipulable control input with continuous range, which is clearly useful for strategic planning, but not straightforward to put into practice if there are distinct levels of intervention. A notable exception is [55], where starting and stopping strict social distancing is a binary control input applied in a nonlinear model predictive framework, and tested through simulations on nominal and uncertain models of the COVID-19 pandemic in Brazil.

For this reason, in Chapter 3 we focus on developing an MPC-based solution capable of choosing the input value from a predefined discrete set of intervention levels, even though this makes the already expensive optimization problem even more challenging. Related to this, [57] proposes a suboptimal solution for the computation of the output feedback law, requiring only convex optimization, and thus resulting in a faster solution.

By the beginning of 2021, in most developed countries, the resources for large-scale testing and vaccination started to gradually become available. While both of these measures also have cost and limited availability, the economic impact can be reduced by combining them with quaran-

tining and the already implemented restrictive measures.

In [58], model predictive control is used for the optimal allocation of vaccination resources between different risk groups and regions. A robust model predictive approach for stochastic epidemic models is proposed in [59], where quarantine policy design is shown as a possible control input.

In [60, 61] it was shown that testing together with an appropriate quarantine policy may have a significant effect in suppressing epidemic waves. China and Taiwan are well-known examples of mass testing, efficient contact tracing, and extremely strict quarantining during the COVID-19 pandemic [32]. In Europe, Denmark has successfully applied the combination of intensive testing and other non-pharmaceutical measures to minimize the burden on its healthcare system [62].

The effect of testing seems to weaken with the increasing infectiousness of newer virus variants such as the Omicron (B.1.1.529). These observations have been mathematically supported and explained by the symptom-based testing model introduced and analyzed in [63].

With the introduction of testing and vaccination, finding the optimal management policy becomes an even more complex problem. In section 3.2, we show an MPC-based solution, balancing between the different objectives while several (new) constraints and limitations have to be satisfied.

1.2.2 Modeling approaches for epidemic processes

Reliable quantitative models are of key importance in the development of any system control methodology, different goals and needs requiring various modeling approaches with models of different levels of detail and descriptive power [64]. Epidemic management is no exception, resulting in epidemic modeling gaining unforeseen significance during the COVID-19 pandemic [49, 65–68]. Efficient description of the underlying process is inevitable for the analysis, reconstruction, prediction, and control of the infections' transmission dynamics [69–72].

Population-level deterministic epidemic models are most often written in a nonnegative compartmental form with polynomial nonlinearities representing the infection mechanism and linear subsystems describing the transitions between certain compartments. Mathematically, these are represented in the form of a nonlinear ordinary differential equation (ODE) system, usually derived from a susceptible–(exposed)–infected–recovered (SEIR)-type description [45, 73–77].

A quantitative model is presented in [78] for the COVID-19 outbreak in Wuhan, China, taking into consideration the effect of different interventions. In [66] an 8-compartment ODE model is presented for describing and analyzing the COVID-19 epidemic in Italy, where the authors show different scenarios for the implementation of countermeasures. The same model structure is used in [53], adapted to the data from Germany. Detailed control-related model analysis and vaccination input design are proposed in [79], which tracks a prescribed output given in terms of susceptible and infected people.

It has to be noted that the general assumption of a homogeneous population and constant model parameters in compartmental models often oversimplifies the problem and prevents the sufficiently accurate description of the epidemic process in complex environments. Therefore, it was already proposed in [80] that the probabilities of infection and death should depend on the different stages of the disease. To address the homogeneity problem, [81] gives a comprehensive overview of the modeling of infection mechanisms in heterogeneous networks using the notions of network science. In [82], the authors separate the infection dynamics for symptomatic and asymptomatic COVID-19-carriers, and also assume heterogeneous connectivity between people. With this modeling setup, it is shown that a more realistic picture of the pandemic in Italy can be reconstructed than by using classical models.

Another important property worth mentioning is that even the simplest epidemic models are nonlinear, which makes the corresponding control problems challenging due to complex dynamical behaviour, possible singularities, and the state-dependent nature of fundamental properties like reachability or observability [83]. Parameter and input uncertainties or the lack of measurements of sufficient quality often add further difficulties to the problem [49, 84].

As another solution addressing the homogeneity concerns, agent-based models have also become popular for modeling epidemics and forecasting the effect of control possibilities. Tracking the stochastic process of consecutive infections on an individual level, possibly with detailed spatial information and time-varying probabilities, these models offer accurate validation of possible real-world constraint combinations in terms of their influence on the transmission dynamics [85–89]. In [90] a hybrid approach is presented, combining robust control based on a population-level model with the agent-based simulation introduced in [88].

Yet another popular direction is the application of artificial intelligence and machine learning for epidemic modeling and prediction [91–93]. In [94], a hybrid machine learning approach is proposed to predict the number of infected individuals and the mortality rates of the first wave of the COVID-19 outbreak in Hungary. In [95] the authors show that epidemic outbreak prediction can be efficiently supported by integrating machine learning and SEIR models. Logistic wavelets were used in [96] to compute the possible cumulative number of people infected with COVID-19.

1.2.3 Reconstruction of uncertain parameters and historical data

The accuracy and efficiency of any kind of epidemic modeling and management efforts largely depend on the quality of measurable and computable parameter and past trajectory data. E.g. it is of fundamental importance to track the evolution of the epidemic process in real-time, in order to prepare healthcare capacities, or to design efficient measures and vaccination policies against the disease spread.

Majority of the data analysis approaches use primarily the daily infected data, possibly together with the recovery statistics. However, it is well-known that only a fraction of the actually infected persons get registered into the official databases. This ratio varies widely between countries depending on the testing activity and related policies. e.g. as of Apr. 28., 2021, the official data for the cumulative numbers of infected in Czechia and Hungary were 1.626.033 [97] and 774.399 [98], respectively. Considering the similarities between these two countries in terms of geographic location, area, population size, the stringency of interventions, the organization of healthcare, and the number of reported COVID-19 deaths, it is highly unlikely that there could be such a huge difference in the true numbers.

There exist several attempts in the literature for the reconstruction of real epidemic data. In [99] a robust statistical estimate with uncertainty analysis was given for the detection rate in several countries. It turns out from the published results that during the 2020 spring wave of the pandemic, the detection rate could be as small or even lower than 10% for e.g. Sweden, Italy, Spain, or may have reached 40-50% in the case of Australia and South Korea, where huge effort was put into immediate contact tracing and testing. Somewhat tighter upper bounds were computed for the possible total number of cases in several European countries in [100] using a data-driven estimator from the distributions of daily cases and deaths. It is clear from the above that the recorded number of infected people alone is generally not a reliable source for tracking the epidemics.

Moreover, it is also visible from the Hungarian data that recoveries were not followed and recorded

precisely in the second wave of the pandemic until the middle of December 2020 (see, e.g. at [101]). Therefore, the epidemic curve showing the active cases cannot reflect the real situation, not even in a qualitative way. After the spring wave of COVID-19, a representative serological test was designed and carried out in Hungary, which estimated that exposure was approximately 0.68% among the total population by the middle of May, 2020 [102].

In systems and control theory, it is a common practice to estimate unknown quantities (e.g. states or parameters) from measurement data using dynamical models of the observed phenomena [103, 104]. There exist several studies aimed at the reconstruction of past epidemiological data using a model-based approach.

A key parameter in such analyses is the time-varying reproduction number (R_t), which is the population-level transmission potential of the disease at time t, and which is known to be non-trivial to estimate [105]. Therefore, several different computational approaches have been proposed to track this quantity for epidemic outbreaks [106, 107]. In [108], the authors fitted a stochastic compartmental model defined by a random walk to estimate the time-dependent reproduction number of the COVID-19 epidemic in Wuhan from publicly available datasets. A discrete-time Hawkes process was used for the estimation of R_t in [109], which allowed the detection of events such as restrictions and their relaxation. The estimation of other non-measured variables, such as the number of people in latent or asymptomatic stages, is also a relevant problem in data reconstruction [110].

Later, in Chapter 4, multiple computationally different approaches are presented for the reconstruction of such epidemiological quantities. As a preliminary, in Chapter 3, a state estimator is proposed for the 8-compartment epidemic model to provide real-time full state information required for control. However, due to some inherent assumptions, this is unfeasible for historical reconstruction in itself. We also carried out our preliminary experiments in [C1], first by directly inverting the transfer function of a linear subsystem, followed by the application of an unknown-input observer.

The basic system theoretic idea behind our proposed solutions is that the transmission parameter β, which is closely related to R_t, can be considered as an input of a nonlinear system model describing epidemic spread, and its estimation can be traced back to a trajectory tracking control problem, where the output to be tracked is the true reported number of hospitalized people. This is a well-known approach in control theory, with some fundamental textbooks like [83] even referring to this kind of control as *inversion*. The idea of using the number of hospitalizations as reference also appears in [111], and is based on the assumption that the testing rules and protocols in hospitals give sufficiently reliable and timely information in most developed countries. Even with these in place, however, sometimes intensive preprocessing is required to obtain sufficiently clean time-series on the number of true hospitalizations.

One straightforward choice for the solution is stochastic MPC, where we can computationally handle model nonlinearities and parametric uncertainties [112]. The theory of optimization- and prediction-based simultaneous state and parameter estimation is well founded in the literature [113–116], and it is applied in a wide spectrum of sciences, e.g. in geosciences [114], in medicine [117], in agriculture [118,119], in aerospace [120], or in meteorology [121]. The classical approaches [114, 121] use variational principles and consider continuous-time models. Due to its simplicity and transparency, the MPC approaches with discrete-time model descriptions are widely used to solve optimal filtering problems, e.g. [116–119] addressed model predictive *data assimilation*, i.e., optimal state/parameter reconstruction to minimize the deviation between the measurement and model output. In [120], an optimal design parameter was computed through a constrained

MPC for a small satellite system, which provides constraint satisfaction during operation time. Furthermore, optimal dosing of cancer chemotherapy is addressed in [117] by solving a predictive control problem with joint state and parameter estimation.

In general, the nonlinear MPC (NMPC) approaches result in a cumbersome optimization problem, especially when the model equations are stochastic. However, the available sequential convex programing approaches [122, 123], the algorithmic differentiation techniques [124, 125], and the numerical software tools [126,127] exploit the special structure of a typical MPC problem and provide an efficient toolkit to solve the nonlinear problems precisely in a reasonable time. Among the several approaches to cope with stochastic dynamics [128], we mention two groups of techniques, which are popular in control theory. First, the particle-based approaches [129–133] with scenario trees allow to cope with general (not necessarily Gaussian) models. Secondly, the tube-based approaches [134–137] approximate each predicted state and input by a Gaussian distribution. Therefore, the dynamic equations in these references are recast as a deterministic mean-variance recursion.

However, general nonlinear model predictive control is a primarily numerical approach, which sometimes does not give enough insight into certain fundamental properties and limitations of the solution. For this reason, as an alternative approach, feedback-based robust controller methodologies can be used. E.g. a robust sliding mode approach has been successfully applied in the field of epidemic control in [138, 139].

Feedback linearization is typically applied for nonlinear systems where the models are known with sufficient precision, such as (electro) mechanical systems [140–142]. The robustness analysis of feedback linearized loops is known to be a difficult problem, and it has been the target of intensive research for several decades [143,144]. A critical point in such an analysis is checking the stability of the zero dynamics [83]. Therefore, feedback linearization is usually not the first choice for epidemiological or biological systems, where researchers are often faced with non-negligible model uncertainties and measurement data of questionable quantity or quality. However, there exist some successful applications in this area, such as [145] and [146], where vaccination inputs were computed through the feedback linearization of nonlinear models. Moreover, the stability of the zero dynamics for any meaningful parameter values of an SEIR-type model was also proved in [145].

1.2.4 State observer design for real-time epidemic control

Most advanced feedback control methods, like MPC, need the whole state information for computing the input. Epidemic models, however, (depending on the level of detail) typically contain several directly non-measurable states such as the number of susceptible, exposed, or asymptomatic people. While different statistical approaches exist for estimation (e. g. from large-scale serological surveys), it is not realistic to assume that these quantities can be continuously measured with the required accuracy. Therefore, a state estimator is needed in practice, which is known to be non-trivial to design for nonlinear systems, and most often its stability has to be proved on a case-by-case basis [83]. A general observer class with convergence proof is proposed for low-dimensional continuous time epidemic models in [147]. An implicit observer design approach for specially discretized SEIR models with global convergence proof is described in [138, 139].

Estimation of non-measured states is a fundamentally important task for model-based feedback control as well [148]. The literature on the state estimation of epidemics is wide, where popular techniques include Kalman filtering, particle filtering, and maximum likelihood estima-

tion [149–151]. We also highlight [152] and [153], where Kalman filter-based state estimation is successfully combined with feedback control. In [147], continuous time observers with guaranteed convergence were proposed for low-dimensional epidemic models. A discrete-time observer for SEIR models with efficiently computable stability conditions was presented in [154]. Feedback linearization combined with a state observer was proposed in [51] to compute a vaccination input that guarantees the asymptotic eradication of an epidemic described by an SEIR model. The convergence of the observation error to zero, the feasibility of the input, as well as the asymptotic stability of the desired state were proved.

1.3 Structure of the dissertation

The thesis revolves around three main topics: the control, reconstruction, and parameter synthesis of different nonlinear, nonnegative, (compartmental) systems. Thus, it is structured as follows.

Chapter 1

In Chapter 1, I present a comprehensive overview of the related scientific literature. First, I review the importance of nonnegative dynamic systems (Section 1.1), followed by the question of synthesizing parameters that guarantee predefined - in this case, oscillatory - behavior in such models. The topic is discussed in detail in Chapter 5, where I propose an optimization-based solution for the problem.

Second, I outline the vast amount of literature related to the COVID-19 pandemic in Section 1.2. I present the course of the epidemic after the initial outbreak, the first governmental interventions aimed to mitigate its effects, and the modeling and planning efforts shown by the scientific community to aid conscious intervention planning (Section 1.2.1). Then, I give a more general overview for the epidemic modeling (Section 1.2.2), data estimation and reconstruction approaches taking into account the uncertain, inaccurate and stochastic nature of information recorded in a real-life epidemic situation (Section 1.2.3), and also present candidates for state observers required for model-based control methodologies (Section 1.2.4).

Chapter 2

Chapter 2 presents the theoretical and methodological foundations of the area of dynamic systems and control. It states fundamental definitions for system classes, their structural and behavioral properties, and theorems, followed by a more general, theoretical presentation of widely applied modeling, control, and reconstruction methodologies (like temporal logic, model predictive control, feedback linearization, etc.).

Chapter 3

Chapter 3 has optimization-based epidemic control in its focus. Supported by papers [J1, J2], it presents a comprehensive solution for planning discrete-level control levels satisfying complex constraints specified using signal temporal logic on a finite horizon. The chapter investigates multiple realistic scenarios in different circumstances and with different goals, and explores the effect, potential benefits, limits, applicability, ideal timing, and inevitable cost of multiple (alternative) inputs like social distancing, testing intensity, and vaccination.

Chapter 4

In chapter 4, I present two different approaches for the reconstruction of epidemiological data.

Based on [C1], [J3], Section 4.1 tries to to reconstruct epidemiological data through the approximation of unknown time-dependent quantities (such as state, unknown input, or parameter) of a class of discrete-time nonlinear stochastic dynamical models by a sequence of Gaussian distributions, using the second wave of the COVID-19 pandemic in Hungary as a case study. The problem is formulated as a single stochastic nonlinear MPC computation.

In Section 4.2 a robustified feedback-linearization-based asymptotic output tracking control is shown for the same purpose, based on the studies [C2–C4] [J4]. Transforming the problem of reconstruction into a control problem with uncertain parameters and serious model mismatch, we try to push the (theoretical) limits of controllability and observability, depending on the accuracy of our initial assumptions. The solutions - with increasing complexity - are illustrated on real COVID-19 data from Sweden and Hungary.

Chapter 5

Finally, in chapter 5 I present an optimization-based methodology, somewhat similar to the theory of MPC, for synthesizing parameters guaranteeing predefined qualitative behavior [J5]. I illustrate the technique on three nonnegative models with increasing complexity: a two-dimensional Brussellator (mostly for validation, as the behavior of this has strong theoretical limits), a three-species Lotka-Volterra food chain model, and finally a SEIR(S)-type epidemic model with re-infection (capable of showing oscillatory behavior even without seasonability or time-variant parameters).

Chapter 6

In chapter 6 I reiterate the theoretical contributions of this thesis and outline the possible future research directions and the practical applicability of the results.

Appendix

Some of the more detailed mathematical derivations, required to theoretically support some of our statements, can be found in the Appendix Chapter at the end of the document.

Chapter 2

Background

In this Chapter, I present the theoretical and methodological foundations necessary for understanding the techniques and results developed throughout this thesis. The focus is on concepts and tools relevant to the analysis and control of nonlinear dynamic systems, with emphasis on nonnegative compartmental systems used in describing biological and chemical processes, like epidemiological modeling or population dynamics.

In the beginning, the general theory of dynamic systems is introduced. I discuss the essential system-theoretic properties, such as controllability and observability, needed for determining the extent to which system behavior can be influenced or inferred. Special attention is given to linear time-invariant (LTI) systems, which have a mathematically well-founded theoretical framework for analysis and control, and thus often serve as a stepping stone toward understanding more complex nonlinear models. Furthermore, I address the role of constraints in dynamic systems, particularly the importance of restricting system evolution within physically meaningful bounds—such as polytopic regions in the state-space. Finally, I cover the standard numerical methods for discretization of continuous-time system dynamics (the Euler and 4th-order Runge-Kutta methods), required both for computational implementations and for model-predictive control computation.

Further, the chapter contains a discussion focused on nonlinear systems, more specifically nonnegative compartmental models, that arise in epidemiological applications and more generally, when dealing with biological and chemical processes. The special structure and properties of these system classes are essential for the techniques developed and applied throughout the thesis.

For formal specification of desired system behaviors over time, I introduce two versions of temporal logic. Both linear temporal logic (LTL) and signal temporal logic (STL) are reviewed, as they offer expressive tools for encoding complex temporal specifications, which are later leveraged in (automated) control synthesis and system analysis.

Subsequently, I explore optimization-based control strategies, with a particular focus on model predictive control (MPC). This serves as a base for several control approaches and experiments developed and discussed in later chapters, ideal for dealing with complex logical constraints and partially contradicting control goals. Since real-world control scenarios generally involve a degree of parameter uncertainty, and only a part of the states are measurable directly, I also introduce the extended Kalman filter as a tool for state estimation in nonlinear settings.

I conclude the chapter with an overview of the computational tools employed throughout this research. I shortly mention or introduce the programming languages, software environments, different libraries, and optimization solvers used for this research, such as MATLAB/Simulink, YALMIP, BARON, Casadi, and BluSTL.

2.1 Dynamic systems

In the context of system theory, a dynamic system can be viewed as an abstraction of a specific, isolated part of the real world, the behavior of which is to be examined or controlled. Its behavior can be influenced by the surrounding world, modelled as inputs changing in time, and it can influence this external environment through so-called outputs.

These inputs and outputs, representing the interactions between the system and the outer world, can be described using scalar- or vector-valued functions, called signals.

Definition 1 (Signal)**.** A signal is a vector-valued time-dependent function $x : \mathbb{R} \to \mathbb{R}^n$.

The value of a signal can, in some cases, also depend on other independent variables (e.g. on space). The set of all possible realizations of a given signal x forms a signal space $\mathcal{X}$.

Using these definitions and looking at the system as a closed black box with well-defined boundaries, it can be treated as an abstract operator, transforming the time-dependent input signals into the corresponding outputs. Formally:

Definition 2 (Dynamic input-output system)**.** A dynamic input-output system is an operator $S : \mathcal{U} \to \mathcal{Y}$, where $\mathcal{U}$ is a space of all possible input signals $u(t)$, and $\mathcal{Y}$ is a space of all possible output signals $y(t)$.

In this interpretation, inputs can be functions consciously manipulable by some external entity (like someone trying to influence the behavior of the system and achieve desired outputs), or can be functions resulting from the environment itself, like disturbances and noise. From now on, the term *disturbance input* is used collectively for the latter. Naturally, the space of the input signals can also be empty, resulting in an *autonomous system* without (manipulable) inputs.

Dynamic systems can be classified based on a number of properties, regarding their model and behavior, forming easy, interesting and challenging categories in terms of analysis and control.

An important property is how the system's behavior is described in time. In case of *continuous-time systems*, time is a continuous interval of the real numbers ($t \in \mathcal{T} \subset \mathbb{R}$). *Discrete-time systems*, on the other hand, treat time as an ordered set of discrete points in time ($t \in \mathcal{T} = \{\dots, t_0, t_1, t_2, \dots\}$), and the values of input and output signals are only given at those moments.

The first principle physical models of real-world systems (like physical, chemical or biological processes) tend to be inherently continuous, even if their representation for a given objective (eg. calculating or simulating their behavior) may vary. Computer-based solutions are a typical example of discrete-time systems, where the inputs and outputs are sampled in time, based on internal factors like processor clock frequency and other high-level constraints.

Another interesting property is time (in)variance. *Time-invariant systems* are invariant to shifting the time of their signals, producing the same outputs if the same inputs are applied to them at a later time. These systems do not change their properties in time; repeating an experiment (under the same circumstances) produces the same response.

Introducing the time shift operator:

Definition 3 (Time shift operator)**.** The time shift operator $\mathbf{T}(\tau)[u(t)] = u(t + \tau)\ \forall t \in \mathbb{R}$

we can formally define time invariance:

Definition 4 (Time-invariant system)**.** A system $\mathbf{S}$ is time-invariant if $\mathbf{T}(\tau) \circ \mathbf{S} = \mathbf{S} \circ \mathbf{T}(\tau)$, where $\circ$ is the composition operator (i.e $(f \circ g)(x) = f(g(x))$).

The third property worth mentioning is linearity.

Definition 5 (Linear system)**.** We call the system $\mathbf{S}$ linear, if:

$$\mathbf{S}[c_1 \cdot u_1 + c_2 \cdot u_2] = c_1 \cdot \mathbf{S}[u_1] + c_2 \cdot \mathbf{S}[u_2],$$

where $c_1, c_2 \in \mathbb{R}; u_1, u_2 \in \mathcal{U}$. This means that any linear combination of the system's possible inputs produces the same linear combination of the respective outputs.

The theory of analysis and control of linear systems is mathematically well-founded, which means that mathematically proven, correct-by-design solutions exist for numerous problems using the tools of mathematical and computational theory. For this reason, even though many real-world systems are inherently nonlinear, they can be handled by reaching back to the well-explored class of linear systems through locally valid approximations and other linearization techniques.

2.1.1 State-space representation

Describing the behavior of a system using the abstract operator notation is usually inefficient for addressing the problems of analysis or control. Instead, typically different system models are used to represent the inner operation of the "box", possibly incorporating prior engineering knowledge about how the elements of the system interact with each other.

One of these representations is the *state-space model*, where information about the history of the system is introduced. In this approach, we assume that the current state of the system (at $t = t_0$) contains all knowledge about the initial conditions and the past input and output values up to this point in time. This way, the future outputs $y(t), t > t_0$ depend on the current state and the future inputs $u(t), t \geq t_0$ only.

Definition 6 (Continuous-time state-space model)**.** The state-space representation of a continuous-time system is a pair (f, g) of a state-transition (f) and an output (g) function:

$$\dot{x}(t) = f\left(t, x(t), u(t)\right), \quad \text{(state equation)} \tag{2.1a}$$

$$y(t) = g\left(t, x(t), u(t)\right), \quad \text{(output equation)} \tag{2.1b}$$

where $t \in \mathbb{R}, x \in \mathcal{X} \subset \mathbb{R}^n,\ u \in \mathcal{U} \subset \mathbb{R}^p,\ y \in \mathcal{Y} \subset \mathbb{R}^r$. The state of the system is described using a multi-valued time-dependent function similar to the input and output, noted by x, and belonging to the space of all possible states $\mathcal{X}$.

There are some important remarks which are worth noting.

1. As the system described is continuous, the state-transition function f describes the evolution of the state (in function of the current state, current input, and time) by giving the time derivative of x at the given time. Thus, calculating the future states of the system (the system's *trajectory*) can be realized by integrating the differential equation. Based on the complexity of f and u, this task can be analytically challenging or impossible, in which case numerical methods are typically used.

2. The evolution of the system's state depends only on the current state and the current value of the input (and possibly directly on the time). As the state incorporates all past events which happened to the system, to calculate the system's state at a future time t_1, only knowledge of the system's *initial state* $x(t_0) = x_0$ and input $u(t), t \in [t_0, t_1]$ is required.

3. The output of the system depends only on the system's current state and input (and possibly directly on the time). Obtaining the system's output can be achieved by determining the system's trajectory and calculating the value of the output function.

4. The system classes mentioned above introduce special properties f and g:

   - In case of a time-invariant system, $f\left(t, x(t), u(t)\right) = f\left(x(t), u(t)\right)$, without direct dependence on the time. Analoguously, $g\left(t, x(t), u(t)\right) = g\left(x(t), u(t)\right)$.
   - In case of a linear time-varying (LTV) system, f and g can be written using matrix-vector multiplications:

$$f\left(t, x(t), u(t)\right) = A(t) \cdot x(t) + B(t) \cdot u(t) \tag{2.2a}$$
$$f\left(t, x(t), u(t)\right) = C(t) \cdot x(t) + D(t) \cdot u(t) \tag{2.2b}$$

   - In case of linear, time-invariant (LTI) systems, the state-space model is essentially a quadruple (A, B, C, D) of matrices:

$$\dot{x}(t) = f(x(t), u(t)) = A \cdot x(t) + B \cdot u(t) \tag{2.3a}$$
$$y(t) = g(x(t), u(t)) = C \cdot x(t) + D \cdot u(t), \tag{2.3b}$$
$$A \in \mathbb{R}^{n \times n}, B \in \mathbb{R}^{n \times r}, C \in \mathbb{R}^{p \times n}, D \in \mathbb{R}^{p \times r} \tag{2.3c}$$

Definition 7 (Discrete-time state-space model)**.** The state-space representation of a continuous-time system is a pair (f, g) of a state-transition (f) and an output (g) function:

$$x(t_{k+1}) = f\left(t_k, x(t_k), u(t_k)\right), \quad \text{(state equation)} \tag{2.4a}$$
$$y(t_k) = g\left(t_k, x(t_k), u(t_k)\right), \quad \text{(output equation)} \tag{2.4b}$$

Opposed to the continuous-time model, here obtaining future state values does not require the solution of a differential equation, only iterative calculation of the future states, starting from the initial values. However, as the continuous differential equations are seldom solved analytically, and rather the solution is approximated using some kind of numerical method, the two cases effectively boil down to quite similar steps.

2.1.2 Controllability of dynamic systems

One fundamental problem of system theory is controlling the behavior and outputs of a given system by manipulating (some of) the inputs. Loosely speaking, the ability to drive a system from one state to another using the manipulable inputs is called controllability.

Definition 8 (Controllability)**.** A state-space representation (2.1) of a system is (full state) *controllable*, if $\forall x_1 = x(t_1), x_2 \neq x_1$ states $\exists\, u \in \mathcal{U}$ which drives the system from x_1 to $x_2 = x(t_2)$ in finite $(t_2 - t_1)$ time.

There are many approaches to computing the input, which makes a system achieve the defined control goal. For LTI systems, such input can be computed even analytically; however, such computations rarely work in practice, due to external factors (stochastic behavior, noise, modelling error, etc.) which influence the states of the system. For this reason, the input is typically computed as a function of the current output or states, and their current relation to the desired outcome. This methodology is called *feedback*, and results in a new, closed-loop system with (ideally) better properties than the original one.

Definition 9 (Static output feedback)**.** In case of static output feedback, the input depends only on the system's current output: $u(t) = F(y(t))$.

Definition 10 (Static state feedback)**.** In case of static state feedback, the input depends on the system's current state: $u(t) = F(x(t))$. If every state variable is required, it is called *full* state feedback.

It must be noted, that the input above can depend solely on the state/output signals themselves, or might include their derivatives as well.

A common problem in control theory is (asymptotic) output tracking, when instead of driving the system into a desired state, the control goal is tracking a so-called *reference signal* $r(t)$ with the output(s) of the system.

Definition 11 (Output tracking)**.** Given a dynamic system S with input $u(t)$ and output $y(t)$, and given a reference signal $r(t)$, the aim of (asymptotic) output tracking is the computation of an $u(t)$ input, for which the tracking error converges to 0, i.e. $\lim_{t\to\infty} e(t) = \lim_{t\to\infty} (r(t) - y(t)) = 0$.

This output tracking is typically realized using a feedback loop, in which the tracking error is fed back into the controller.

2.1.3 Observability of dynamic systems

Another fundamental problem of system theory is the ability to measure or otherwise compute the state variables of a state-space model. Apart from possibly needing this information for control (as in the case of full state feedback), obtaining information on non-measurable state variables might be necessary for properly understanding and analysing the underlying process or phenomenon.

Definition 12 (Observability)**.** A state-space model (2.1) is *observable*, if the initial state $x_0 = x(t_0)$ can be determined from a finite measurement of $u(t)$ and $y(t) : t \in [t_0, t_1]$.

It must be noted, that by being able to determine the initial state of the system, the whole trajectory can be computed.

There are also cases in which the inputs of the system can not be directly measured. Even in the case of a controlled system, the actual input applied to the system might differ from that computed by the controller, e.g. due to external noise or other constraints introduced by the surrounding world. Thus, we also define the ability to compute the state variables without knowing the input:

Definition 13 (Unknown-input observability)**.** A state-space model in *unknown-input observable*, if the trajectory $x(t), t \in [t_0, t_1]$ of the system can be reconstructed from a finite measurement of its outputs $y(t)$, even if the inputs $u(t)$ are not known.

There are special conditions for both controllability and observability of LTI systems, as there exist well-defined techniques for designing a full-state feedback controller and observer for controllable and observable systems, respectively. However, these tasks can quickly become challenging in the nonlinear case, where only special system classes under specific assumptions can be accurately handled.

2.1.4 Special notions on LTI systems

There are some special properties for linear time-invariant systems, which are worth mentioning.

The first is joint controllability and observability, which, contrary to controllability and observability, is not a property of the realization, but the system itself.

Definition 14 (Joint controllability and observability)**.** A system is jointly controllable and observable if it is both controllable and observable.

There are several useful theorems and lemmas [155] for determining whether an LTI system is jointly controllable and observable.
Another useful property of LTI systems is the separation principle.

Definition 15 (Separation principle)**.** The principle of *separation of estimation and control* states that if a stable observer and a stabilizing state feedback are designed for a linear time-invariant system, then the combined observer and feedback is stable.

This property is rarely true in nonlinear systems, meaning that even by computing the exact stability region for both the controller and observer (which, again, can be cumbersome or impossible for some cases), the correctness of the combined setup can not be guaranteed. In these cases, finding the domain in which the controlled system remains stable can become tedious, and might require a more empirical approach like running large amounts of simulations - all without a formal guarantee for the desired behavior.

2.1.5 Constraints on dynamic systems

In many real-world applications, dynamic systems are subject to inherent constraints — arising from physical, safety, or design limitations — which must be accounted for in both analysis and control. Moreover, in the case of nonlinear systems, important properties like stability or controllability typically hold only within specific regions of the state-space.
In this section, I introduce common mathematical representations of such constraints (like convex sets and polytopes), essential for accurately characterizing these regions for further analysis. Especially, in model predictive control (MPC), constraints are an integral part of the optimization problem, governing feasible trajectories and admissible control inputs.

Convex sets

Definition 16 (Convex set)**.** A set S is called *convex*, if:

$$\forall x_1, x_2 \in S \ : \ \theta x_1 + (1-\theta)x_2 \in S, \ 0 \leq \theta \leq 1 \tag{2.5}$$

Equivalent definition: a set S is called convex, if

$$\forall \{x_i | 0 \leq i \leq n\} \subset S : \sum_{i=0}^{n} x_i \theta_i \in S, \ 0 \leq \theta_i \leq 1 \ \forall i = 1...N, \ \sum_{i=0}^{n} \theta_i = 1 \tag{2.6}$$

Definition 17 (Convex hull)**.** The *convex hull* of a finite set of points $\{x_i | 0 \leq i \leq n\}$:

$$S = \text{Conv}(\{x_i | 0 \leq i \leq n\}) = \left\{ x \ \middle| \ \sum_{i=0}^{n} x_i \theta_i \in S, \ 0 \leq \theta_i \leq 1 \ \forall i = 1...N, \ \sum_{i=0}^{n} \theta_i = 1 \right\} \tag{2.7}$$

There are several mathematical operations used for convex sets, which may or may not preserve the convex property. These are:

- intersection (convex), union (not necessarily convex)

- affine function: $A \cdot S + B = \{y \mid y = A \cdot x + B \;\; x \in S\}$ (convex)
- Minkowski sum: $S_1 \oplus S_2 = \{y \mid y = x_1 + x_2,\; x_1 \in S_1 \; and \; x_2 \in S_2\}$
- Minkowski difference (also called erosion): $S_1 \ominus S_2 = \{y \mid y \in S_1 \; and \; \{y\} \oplus S_2 \in S_1\}$
- projection along a set of coordinates (convex)

Special convex sets

Definition 18 (Ellipse)**.** An ellipse is a convex set, given by the equation:

$$\epsilon = \left\{x \middle| (x - x_0)^T P (x - x_0) \leq 1,\; P \succ 0 \text{ (positive definite)}\right\}, x_0 \in \mathbb{R}^n, x \in \mathbb{R}^n \tag{2.8}$$

This set has the following important properties:

- intersection of an ellipsoid with a plane or projection to a plane is an ellipsoid
- can be given using a quadratic formula (good for optimization tasks)
- volume is easy to compute: $V(eps) \sim \det(P^{-1})$
- it depends only on a "few" parameters: in $\mathbb{R}^n$ a matrix of $n \times n$

Due to its simple structure, an ellipse is easy to work with; however, as I present below, it might not have the complexity required to describe a more complicated system behavior.

Definition 19 (Polytope)**.** A polytope is a finite convex set, given with vertices and bounding faces, using one of the following equations:

$$\mathcal{P} = \{x | Hx \leq h\} = \{x | V\lambda,\; \sum \lambda_i = 1, \lambda_i \geq 0\} \tag{2.9}$$

Note. The representation might be redundant, with a non-minimum number of planes in H or vertices in V, but there are algorithms to get rid of unnecessary constraints [156].

There are also algorithms to calculate one representation from another (noted by HR and VR). This operation is generally computationally expensive, and the numerical computation in some cases might not give a mathematically equivalent result; nevertheless, it might be necessary for some operations. For example, the computation of an intersection in HR is a simple concatenation of the matrices:

$$P_1 = \{x \mid H_1 x \leq h_1\} \quad P_2 = \{x \mid H_2 x \leq h_2\} \tag{2.10a}$$

$$P_1 \cap P_2 = \left\{ x \;\middle|\; \begin{pmatrix} H_1 \\ H_2 \end{pmatrix} x \leq \begin{pmatrix} h_1 \\ h_2 \end{pmatrix} \right\} + \text{eliminate redundant planes} \tag{2.10b}$$

However, for a projection, only the VR representation enables a straightforward transformation.

2.1.6 Discretization of dynamic systems

As mentioned earlier, models depicting real-world systems and processes are generally continuous by nature, so analyzing and predicting their behavior usually involves solving differential equation systems. Due to the complexity of these, giving an analytical solution is generally not possible. Moreover, the practically available controllers for such dynamic systems are often realized by some kind of software running on a digital computer, operating at a given clock frequency, and thus resulting in a discrete behavior.

Furthermore, control techniques using an explicit process model for forecasting system behavior (like MPC) require numerically simple operations for expressing the future states as a function of the possible planned inputs.

For the above reasons, there are numerous discretization techniques for representing a continuous system with a discrete-time model, much better usable for simulations and computer-based control. These techniques offer different complexity and precision, with special caveats (like quickly accumulating error in some cases) and tunable parameters. Below, the two most common techniques (used throughout this thesis) are presented.

Euler method

Given a continuous-time (time-invariant) system model:

$$\dot{x}(t) = f\left(x(t), u(t)\right), \tag{2.11a}$$

$$y(t) = g\left(x(t), u(t)\right) \tag{2.11b}$$

the aim of the discretization is creating a discrete-time representation with sampling time dt, containing only a difference equation for computing the next state:

$$x_{k+1} = F(x_k, p) \tag{2.12a}$$

$$x_k = x(k \cdot dt) \tag{2.12b}$$

In case of an accurate discretization, it should be true that $x_k \approx x(k \cdot dt)$ for any piece-wise constant input $u(t) = u_k$, $t \in [k \cdot dt, (k+1) \cdot dt)$.

The Euler method is known for its simplicity, as it uses only the first derivative at time instant k to estimate the next state:

$$F(x_k, p) = x_k + dt \cdot f(x_k, p) \tag{2.13}$$

While having the well-known drawback of quickly cumulating the error in case of larger derivatives, an appropriately small dt can be sufficiently reliable for integrating the differential equation and ensuring that the behavioral constraints are satisfied.

In the thesis, discrete models obtained through the Euler method are generally used for MPC and parameter synthesis, as the equations for future states expressed using these lack the higher-order terms introduced by more complex approaches, and thus are more easily handled by optimization frameworks.

It must be emphasized that system behavior computed using Euler-discretized systems can not be taken for granted. In the thesis, every parameter synthesized and every system input computed involving the Euler method is applied to systems simulated using more accurate ODE-solving techniques involving high-order terms, and thus validated in a more realistic setup.

Runge-Kutta method

Using the notations introduced for the Euler method, the 4th-order Runge-Kutta method divides the computation of the next state x_{k+1} into four consecutive steps, averaging the estimated

current and future derivatives of state variables:

$$a_k = f(x_k, p) \tag{2.14a}$$
$$b_k = f(x_k + 0.5 \cdot dt \cdot a_k, p); \tag{2.14b}$$
$$c_k = f(x_k + 0.5 \cdot dt \cdot b_k, p); \tag{2.14c}$$
$$d_k = f(x_k + dt \cdot c_k, p); \tag{2.14d}$$
$$F(x_k, p) = x_k + dt \cdot (a_k + 2 \cdot b_k + 2 \cdot c_k + d_k)/6; \tag{2.14e}$$

While being a more precise approximation of the derivatives, and therefore generally working with longer dt timesteps, this discretization might be substantially harder to tackle by optimization solvers due to the increased number of dynamical constraints.

The Runge-Kutta method serves as a base for standard ODE solvers, like the ODE45 and ODE89 used by MATLAB and Simulink.

2.2 Nonlinear systems

2.2.1 Nonnegative and compartmental systems

A wide range of physical, chemical and biological systems are derived from mass balance considerations. Many of these models show a specific, constrained structure for their system of differential equations, and are called compartmental systems.

Due to this structure, the solution of these systems also follows a specific pattern, which has led to the development of a complete mathematical framework for dealing with compartmental systems, as a simplified alternative to handling them as generic nonlinear ones. Such a unified theory is presented in e.g. [157], and used in this thesis for addressing the challenges posed by the analysis and control of complex epidemic processes.

In this subsection, the key notations and definitions are introduced, with more details present in the description of the estimation or control technique itself.

Definition 20 (Nonnegative system)**.** We call a dynamic system (2.1) nonnegative, if all of its state variables are positive or zero at any given time $x_i(t) \geq 0 \;\; \forall i \;\; \forall t \in \mathbb{R}$.

Definition 21 (Compartment)**.** A *compartment* represents a virtual / logical storage, containing an amount of kinetically homogeneous material.

Definition 22 (Flow)**.** A flow is a function $F : \mathbb{R} \to \mathbb{R}_0^+$ representing the rate at which the material is entering or exiting a compartment at a given moment.

It must be noted, that all flows are *positive by definition*, and thus any amount of material moving in the opposite direction is represented by another flow.

Now, considering a dynamic system of n compartments, in which the amount of material in the i-th compartment is noted by x_i, different types of flows can be defined:

Definition 23 (Inflow)**.** The flow I_i representing the material entering a compartment i from outside the system is called *inflow*.

Definition 24 (Outflow)**.** The flow F_{0i} representing the material leaving a compartment i and the whole system is called *outflow*.

Definition 25 (Transfer)**.** The flow F_{ji} representing the material leaving a compartment i and entering compartment j is called a *transfer*.

In such a system, the state-space model can be obtained by writing the instantaneous mass-balance equation for each compartment:

$$\dot{x}_i = \sum_{j \neq i} (F_{ij} - F_{ji}) + I_i - F_{0i} \;\; \forall i = 1, 2, \ldots, N \tag{2.15a}$$

It must be noted, that since *negative masses* are impossible, $x_i(t) \geq 0 \; \forall t$. Moreover, by definition, $F_{ii} = 0 \; \forall t$.

Another important property is, that the functions F_{ij} are required to be functions of $\mathbf{x} = (x_1, x_2, \ldots, x_n)$ and possibly t. Due to additional constraints (as presented in [158]) it can be shown, that $\mathbf{F}$ must be enough times continuously differentiable, and that $F_{ij}(\mathbf{x}) = f_{ij}(\mathbf{x}) \cdot x_i$.

Using this, the state-space model of a compartmental system can be rewritten as:

$$\dot{x}_i = -\left(f_{0i} + \sum_{j \neq i} f_{ji} \right) + \sum_{j \neq i} f_{ij} x_j + I_i \;\; \forall i = 1, 2, \ldots, N \tag{2.16a}$$

Here, the terms f_{ij} are called *fractional transfer coefficients*. By definition, $f_{ii} = f_{0i} + \sum_{j \neq i} f_{ji}$, leading to a more compact equation:

$$\dot{x}_i = \sum_j f_{ij} x_j + I_i \tag{2.17}$$

Definition 26. An n-dimensional dynamic system with state variables $\mathbf{x} = (x_1, \ldots, x_n)$ is called compartmental, if the below properties hold:

1. $\dot{x}_i = \sum_j f_{ij} x_j + I_i \quad (\forall\ i = 1 \ldots n)$
2. $f_{ii} \leq 0 \quad (\forall\ i, t \geq 0)$
3. $f_{ij} \geq 0 \quad (\forall\ i \neq j,\ t \geq 0)$
4. $\sum_{i=1}^{n} f_{ij} = \sum_{j \neq i} f_{ji} + f_{jj} = -f_{0j} \leq 0 \quad (\forall\ j, t \geq 0)$

It must be emphasized, that compartmental systems are a generic class for describing nonnegative systems. As shown in [158], any stable nonnegative linear dynamics can be linearly transformed into compartmental form, and any bounded dynamics in $\mathbb{R}^n$ can be embedded into a compartmental system having $n+1$ compartments. The article contains a key theorem with constructive proof:

Theorem (Jacquez, Simon 1993 [158])**.** Let $\dot{x} = f(x)$ be a C^k system of n differential equations on an n-dimensional simplex

$$\Sigma_1^n = \left\{ (x_1, \ldots, x_n)\ :\ x_i \geq 0,\ \sum_{i=1}^{n} x_i \leq 1 \right\} \tag{2.18}$$

which points into Σ_1^n on its boundary. Then, there exists an autonomous C^k closed compartmental system $\dot{x} = \tilde{f}(x)$ defined on an $(n+1)$-dimensional simplex $\Sigma_{1+\epsilon}^{n+1}$ and an invariant n-dimensional subsimplex Σ of $\Sigma_{1+\epsilon}^{n+1}$ isomorphic to Σ_1^n such that $\tilde{f}$ restricted to Σ is the original f.

2.3 Temporal Logic

2.3.1 Linear Temporal Logic

Linear Temporal Logic (LTL) is a formalism developed for formal verification and planning of computer programs in 1977. In essence, LTL extends the set of operators familiar from Boolean logic with tools to describe time dependencies between the statements (eg. always, never, eventually, next step, etc.). This makes temporal logic a powerful tool for describing complex system behavior, and provides a method for planning and verification of safe and lively system operation. Linear Temporal Logic is presented below based on [159].

The Linear Temporal Logic works with the following operators:

- Boolean operators: T (true), $\neg$ (negation, not), $\wedge$ (and)
- Until operator: **U**
- Next operator: $\bigcirc$

Consequently, an LTL formula can be recursively defined as:

$$\phi = T|o|\phi_1 \wedge \phi_2|\neg\phi|\bigcirc\phi|\phi_1\mathbf{U}\phi_2 \tag{2.19}$$

In the expression, ϕ, ϕ_1, ϕ_2 are LTL formulae, $o \in O$ is an observation (ie. some condition - eg. inequality for some state variables - becoming true in a dynamic system).

The $\bigcirc\phi$ (next) is a unary operator, without further need for explanation. It will be true at timestep t, if ϕ becomes true in step $(t+1)$. The $\phi_1\mathbf{U}\phi_2$ is a binary operator, which is true if ϕ_1 is true in every timestep before ϕ_2 becomes true.

Moreover, operators from Boolean logic can be used: $\vee$ (or), $\rightarrow$ (implication) and $\leftrightarrow$ (equivalency)

To simplify LTL expressions, two derived operators are introduced:

- Eventually: $\Diamond\phi = T\mathbf{U}\phi$
- Always: $\Box\phi = \neg\Diamond\neg\phi$

These operators are often used in combination to describe behavior like following a reference signal or assuring periodic behavior.

The expression $\Diamond\Box\phi$ means that ϕ will become true sometimes in the future, and it will remain true afterwards. This can be, for example, arriving in the ϵ range of the reference signal or the target state, and remaining there forever.

The $\Box\Diamond$ is good for periodic behavior. Meaning of $\phi = \Box\Diamond o$ is that the observation o must repeat from time to time, which can be used to ensure the liveliness of a system.

2.3.2 Signal Temporal Logic

Signal Temporal Logic (STL) further extends the possibilities offered by LTL, by introducing quantitative operators regarding time in LTL formulae. For instance, in LTL, there is no way to know for sure when an expression preceded by $\Diamond$ (eventually) will actually happen. As we have a finite time horizon in practice, this must be somehow specified. Signal Temporal Logic is presented based on [160].

In STL, the following notation is introduced for the operators:

$$\varphi\mathbf{U}_{[a,b]}\psi \text{ is true at } t \iff \exists t' \in [t+a, t+b] \text{ st. } \psi \text{ is true} \wedge \forall t'' \in [t, t'] \ \varphi \text{ is true} \tag{2.20a}$$

$$\Box_{[a,b]}\phi \text{ is true at time } t \iff \forall t' \in [t+a, t+b] \text{ the formula } \phi \text{ is true} \tag{2.20b}$$

$$\Diamond_{[a,b]}\phi = \top\mathbf{U}_{[a,b]}\phi \tag{2.20c}$$

We must define the *bound* of a formula as well: this value is the sum of the upper bound b of the nested formulae (eg. $\Diamond_{[0,1]}\Box_{[2,3]}\phi$ has a bound of $1+3=4$).

2.4 Model predictive control

Model predictive control (MPC) is commonly used to refer to a class of control algorithms that use an explicit process model to predict the future output of a dynamic system.

Commonly used for complex systems, with high-order dynamics, nonlinear dependencies or large time delays, MPC algorithms compute a series of control inputs, based on the current and the predicted future values of the state variables for a given finite time interval. For discrete (or discretized) systems, this time interval means a predefined number of steps (noted by N), called horizon.

Typically, MPC algorithms are used in a closed-loop scenario, so that only the first computed input is applied to the system, followed by repetition of the whole prediction and planning procedure. It must be noted, that this behavior requires serious online optimization, but due to its ability to handle a wide variety of complex systems, it is extensively used in industrial environments.

To understand the workings of the algorithm, let us consider the following discrete dynamic system:

$$x_{k+1} = F(x_k, u_k) \tag{2.21}$$

With constraints given in the form:

$$G_x(x_k) \leq h_x,\ G_u(u_k) \leq h_u \tag{2.22}$$

The aim of the controller is to drive the system to a desired state, while minimizing a (typically linear or quadratic) cost function $J(x, u)$.

Normally, in case of discrete-time models and full state measurement, the main steps of the MPC algorithm can be summarized as follows:

1. A suitable control horizon $M \in \mathbb{N}_+$ is chosen, the time counter k is set to 0.

2. At time $k \cdot T_s$, state x_k is measured. MPC is based on the prediction of the future states, therefore the following notation is introduced: the $(k+i)$th state predicted from the measurement made at time k will be denoted by $x_{k+i|k}$. By definition, $x_{k|k} = x_k$.

3. By applying the state update equation $x_{k+1} = F(x_k, u_k)$, the M predicted future states $\mathbf{x}_k = \{x_{k+1|k},\ldots,x_{k+M|k}\}$ can be expressed as a function of the (yet unknown) future control actions $\mathbf{u}_k = \{u_{k|k}, \ldots, u_{k+M-1|k}\}$. Using this formulation, an optimization problem can be defined:

$$\min_{\mathbf{u}_k} J(\mathbf{u}_k, \mathbf{x}_k) \tag{2.23a}$$

$$\text{w.r.t. } x_{k+i+1|k} = F(x_{k+i|k}, u_{k+i|k}) \tag{2.23b}$$

$$G_x(\mathbf{x}_k) \leq h_x,\ G_u(\mathbf{u}_k) \leq h_u \tag{2.23c}$$

   The objective function J and constraints (2.23c) are constructed to encode all design specifications to be satisfied by the controller and the closed-loop system. To solve (2.23), an appropriate numerical solver has to be used. The result is the optimal input sequence $\mathbf{u}_k^* = \{u_{k|k}^*, \ldots, u_{k+N-1|k}^*\}$.

4. The first element of $\mathbf{u}_k^*$ is applied to the process, i.e. $u_k := u_{k|k}^*$. This control input is kept constant for a T_s time period. Then k is incremented, i.e. $k := k + 1$, and the iteration continues at step 2.

The cost / objective function is typically defined as one of the following:

- quadratic: $J(x, u) = \sum_{i=1}^{N} \{x_{k+i|k}^T Q x_{k+i|k} + u_{k+i|k}^T R u_{k+i|k}\}$, where $Q, R \succ 0$
- linear: $J(x, u) = \sum_{i=1}^{N} \{|q^T x_{k+i|k}| + |\gamma^T u_{k+i|k}|\} \leq \sum_{i=1}^{N} \alpha_i + \beta_i$

The following important remarks must be added to the MPC algorithm described above:

(a) In the description of the MPC above, we implicitly assumed that the system model is perfect: the model used for prediction is the same as that which describes the true system behavior. In practical situations, this rarely holds: there are modelling uncertainties that may corrupt the prediction and thus the control input obtained. It is known that an appropriate feedback can significantly reduce the effect of uncertainties in itself [43, 83]. Moreover, there exist advanced methods for robust control synthesis and the robustness analysis of the closed loop [161]. In this work, different levels of uncertainty are assumed in the individual chapters, some of which contain considerations for robustifying the control setup.

(b) The numerical complexity of the optimization problem depends on the structure of the cost functions and the constraints. Since the model is nonlinear, (2.23) becomes a nonlinear optimization problem. In the first control scenarios we are going to investigate, a quadratic cost function and linear constraints are used. Later, to formulate more complicated requirements, temporal logic constraints are also introduced, which turn the optimization task into a mixed integer nonlinear programming (MINLP) problem.

(c) A time horizon over which we intend to control the system has to be chosen at the beginning. It is assumed that the external conditions do not significantly change during this time period. Therefore, the behavior of the model beyond the horizon is not taken into consideration (if further control is needed, new computations must be performed after the horizon's end). Since the endpoint is fixed, the MPC is solved over shrinking horizon, i.e. M is time-dependent and defined by $M_k = M_0 - k$. As a convenience, in some works the k index is omitted, and only M is used to generally refer to the end of the horizon in the given step (even though this is obviously not equal to the M value at the beginning of the calculation, which represents the initial length of the horizon). To ensure that recalculation after the horizon's end remains feasible, a safety interval and safety constraints might be added. This prohibits the controller from optimizing e.g. by setting the system on a trajectory exiting the stability region right after the end of the horizon, and sustains the possibility of shifting/rolling the horizon forward in time.

(d) If the entire state vector cannot be measured, the standard procedure is to augment the controller with a dynamical observer providing estimation for the true state. If the system is nonlinear, there is no general procedure for estimator design. This task can therefore be challenging: different existing methods have to be combined and adapted to the specific system model. In Section 3.1.4 a possible state estimator is presented for the epidemic model discussed later, and we show how it can be applied together with the MPC control.

(e) Although in the algorithm above the control input changes in every T_s time period, this is not necessary: the frequency of control update can be easily decreased by simple constraints on u.

2.5 Extended Kalman filter

Designing observers for nonlinear systems is a complex problem with numerous open theoretical questions. Existing methods typically work with known limitations and boundaries: stability is often guaranteed only in certain regions of the state-space, and their accuracy highly depends on

model uncertainties and external disturbances such as measurement noise [83]. One widely used practical solution is the extended Kalman filter (EKF), which builds an adaptive (statistical) model by comparing measured outputs with model-based predictions with tunable confidence in each. This methodology enables a somewhat robust state estimation in the presence of noise and system nonlinearities. In this work, we used EKF to estimate directly unmeasurable internal states of various epidemic models (like the number of asymptomatic individuals), providing the necessary information for full-state-based controllers.

For the state estimation, the EKF assumes a discrete-time nonlinear system model formally described as:

$$x_{k+1} = f(x_k, u_k) + w_k \tag{2.24a}$$

$$y_{k+1} = h(x_k) + v_k, \tag{2.24b}$$

where w and v are additive process and output noise terms, i.e., independent random variables with Gaussian distribution, having zero mean and covariance matrices Q and R, respectively.

Around this model, an EKF state estimator can be constructed with the following two key attributes:

- $\hat{x}_{k|j}$ represents the state estimated for time k at time j ($j \leq k$), initialized as $\hat{x}_{0|-1} = \mathbb{E}_{x_0}$, which is the expected value based on prior knowledge of the system, without any measurements taken.
- $P_{k|j}$ denotes the state estimation error covariance matrix (i.e., the uncertainty of the estimation) for time k calculated at time j, initialized as $P_{0|-1} = \mathbb{E}(x_0 - \hat{x}_{0|-1})(x_0 - \hat{x}_{0|-1})^T$ and also based on prior knowledge.

At each time step $k = 0, 1, 2, ...$ the EKF algorithm executes two main steps:

1. Update (correction) of the current state estimate $\hat{x}_{k|k}$ and current uncertainty $Pk|k$, based on the previously predicted state $\hat{x}_{k|k-1}$, previously assumed uncertainty $P_{k|k-1}$, and the current measurement y_k.
2. Prediction of the state at the next time instance $\hat{x}_{k+1|k}$ using the currently available state estimate $\hat{x}_{k|k}$ and the state transition function of the estimated model, ie. $f(x_k, u_k)$ from Eq. (2.24).

Due to the fact, that functions (f, h) can be nonlinear, the EKF extends the operating principle of the linear Kalman filter algorithm by approximating the state transition and output matrices (A and C) of a linear time-invariant (LTI) system using the Jacobians $A_k = \frac{\partial f}{\partial x}\Big|_{\hat{x}_{k|k}}$ and $C_k = \frac{\partial h}{\partial x}\Big|_{\hat{x}_{k|k-1}}$. Using this notation, the above steps can be computed as:

1. Correction:

$$K_k = P_{k|k-1}C_k^T(C_k P_{k|k-1} C_k^T + R_k)^{-1} \tag{2.25a}$$

$$\hat{x}_{k|k} = \hat{x}_{k|k-1} + K_k(y_k - h(\hat{x}_{k|k-1}, u_k)) \tag{2.25b}$$

$$P_{k|k} = P_{k|k-1} - K_k C_k P_{k|k-1}. \tag{2.25c}$$

2. Prediction:

$$P_{k+1|k} = A_k P_{k|k} A_k^T + Q_k \tag{2.26a}$$

$$\hat{x}_{k+1|k} = f(\hat{x}_{k|k}, u_k). \tag{2.26b}$$

By running the above steps iteratively for the measured (and sampled) output of a continuous-time nonlinear model, the EKF's internal states give an estimation for the unavailable continuous state variables.

2.6 Computational tools

Following the theoretical development and calculations, all methods and algorithms presented in this thesis were implemented and tested on real-world (or real-world-inspired) data. For these implementations, a collection of widely used computational tools and frameworks from the field of systems theory has been employed. Providing a robust environment for modeling, simulation, optimization, estimation, prediction, and analysis, these tools supported the quick implementation and evaluation of the chosen control setups and methods. Below, I present the main software components and their usage in the different parts of this thesis.

2.6.1 MATLAB / Simulink

MATLAB and Simulink served as the primary platform for algorithm development, simulation, and analysis. As the de facto standard for prototyping controlled dynamical systems, this environment offers a vast collection of built-in functions and modular components, while Simulink enables the graphical construction of control setups (made of blocks for input computation, simulation, and state estimation of dynamic models). Preprocessing of real-world input data (cleansing, merging, smoothing via moving averages and spline fitting, and interpolation for the missing values) was also performed using MATLAB's statistical toolbox. For the simulation of compartmental models and controllers, I used Simulink's built-in ODE solvers (e.g., ode45, ode89), based on high-order Runge-Kutta discretization. Additionally, I used Simulink's built-in Extended Kalman Filter block and signal processing tools (e.g., zero-order hold) for the construction and assembly of complex control loops for the feedback-linearization-based reconstruction and control.

2.6.2 YALMIP

YALMIP [162] is a modeling toolbox that simplifies the representation and solution of optimization and control problems. It supports semidefinite, nonconvex, and integer programming, as well as polynomial and rational functions, producing output compatible with various solvers. It fully integrates with MATLAB and Simulink, which makes it ideal for constructing the constrained optimization problems needed for MPC and for the parameter synthesis tasks. Moreover, its output is compatible with the BARON solver, which I used for the epidemic control and reconstruction scenarios.

2.6.3 BARON

BARON (Branch-and-Reduce Optimization Navigator) [163] was used to solve the nonconvex optimization problems resulting from MPC formulations and parameter synthesis tasks. It is a commercially available software for solving nonconvex optimization problems to global optimality. It handles purely continuous, purely integer, and mixed-integer nonlinear problems, and combines

constraint propagation, interval analysis, and duality in its reduce arsenal with advanced branch-and-bound optimization concepts.

In this thesis, BARON proved highly effective due to its informative diagnostics (eg. feasibility analysis, branching progress), and speed in solving complex problem classes.

2.6.4 CasADI

CasADi [124] is an alternative optimization tool that was used to solve (stochastic) MPC problems without integer constraints for reconstruction of past epidemiological data.

CasADi is an open-source tool for nonlinear optimization and algorithmic differentiation. It can handle various convex and nonconvex optimization problems (NLP, MINLP, SQP) and also offer interfaces for integrating with other solvers (eg. IPOPT).

In our experiments, it turned out to be more effective for a subset of the optimization problems encountered during our experiments.

2.6.5 BluSTL

BluSTL [160] is a MATLAB toolkit for automatically generating hybrid controllers from specifications written in Signal Temporal Logic. It first transforms STL formulas (written using its own, text-based language and interpreted by its integrated parser) into equivalent mixed-integer optimization problems, then tries to solve the resulting constrained problem using any solver that YALMIP is compatible with. Although its developers recommend Gurobi as a backend, (after some modifications) it turned out to work with BARON as well.

In our experiments, primarily the parser part was used: with STL, we formulated the complex time-varying logical constraints for epidemic control (like temporarily releasable capacity in hospitals or distribution possibilities of vaccinations), which were transformed into a constraint set for the MPC framework. For identifying the correct parts, we also took inspiration from the works of János Rudán (e.g. [164]).

2.6.6 Hardware

All computational experiments presented in this thesis were run on simple, consumer-grade laptops with Intel Core i7-8565u or Core i7-8550u (4 core, 8 threads, 1.8 - 4.6 GHz) and 8-16GB RAM, without any specific components (e.g. GPU) for acceleration. Depending on the experiment, it took from 30 seconds to a maximum of 12 hours to complete a full simulation / calculation scenario, detailed in the results subsection of the respective application.

Chapter 3

Optimization-based nonlinear epidemic control

This chapter presents the development and application of two optimization-based predictive control strategies on nonlinear epidemiological models, aimed at supporting decision-makers in managing infectious outbreaks, with a specific focus on the dynamics and control challenges of COVID-19.

The contributions presented here were published in [J1] (2020) and [J2] (2022), simulating and optimizing different pandemic mitigation strategies under practical and possibly contradicting constraints. They explore a combination of pharmaceutical and non-pharmaceutical measures (such as testing, lockdown and quarantines), take into account limited resources (like the number of available tests and healthcare system capacity), and optimize for different goals (as minimal economical impact, long-term solution by herd immunity or mass vaccination, minimal number of fatal outcomes, etc).

In the first study [J1], we showed a constrained control framework for a complex nonlinear compartmental model of COVID-19, and explored the short- and long-term effects of possible intervention strategies. The control loop also contained a state observer to estimate directly unmeasurable states — especially the susceptible and asymptomatically infected population — based on observed hospitalization data. Using a combination of different cost functions and constraints, the paper investigated multiple realistic scenarios.

Building on this framework, in the second study [J2] (written around the end of 2021, when vaccines and large-scale testing were just becoming available), we expanded the model by incorporating vaccination dynamics and introducing testing intensity as a second control input alongside the already explored non-pharmaceutical interventions. The resulting 14-compartment model captures a broader range of the real-world phenomena, including resource availability (hospitalization limits and testing capacity) and vaccine-induced immunity.

Combining the two papers, this chapter proposes a comprehensive, optimization-based framework for optimal epidemic control, and explores various real-time epidemic management strategies seen in different countries during the COVID-19 pandemic.

3.1 Nonlinear MPC with logic constraints for COVID-19 management

This section presents a model-predictive control-based framework developed in the early stages of the COVID-19 pandemic, with the objective of exploring and optimizing possible governmental intervention strategies, as well as providing guidance and prediction regarding the effects of the applied non-pharmaceutical measures.

The framework includes an 8-compartment nonlinear compartmental model tailored to COVID-19's dynamics, based on Hungarian epidemiological data measured during the first wave in the spring of 2020. The model captures the key phases of the infection process (including the specifically long latent period and taking into consideration the high ratio of asymptomatic, undetected infections) and hospitalization. The primary manipulable input is the time-varying transmission rate, which reflects the intensity and timing of non-pharmaceutical interventions such as lockdowns and social distancing measures.

The approach allows for both mitigation- and suppression-oriented strategies by adjusting the cost function to prioritize either minimal intervention effort or minimized health burden (in terms of infections, hospitalizations, and/or fatalities).

Five control scenarios are explored, each featuring a different policy goal and set of constraints. These include classical mitigation strategies aimed at keeping hospital occupancy within bounds, and more aggressive suppression strategies that reduce the overall transmission at the cost of a probable new wave emerging after lifting the lockdowns.

3.1.1 Transmission dynamics model

Model description

We construct a compartmental model to describe the transmission dynamics of the infection, incorporating specific characteristics of COVID-19. As illustrated in figure 3.1, our population of N individuals is divided into the following classes, tracking the disease status of them: by S we denote the susceptibles, i.e. those who can be infected by the disease. Latent (L) are those who have already contracted the disease but do not show symptoms and are not infectious yet. Since transmission may occur in the two days before the onset of symptoms [165], we consider a pre-symptomatic infectious compartment P. Since a large fraction of infected individuals show only mild or no symptoms, after the incubation period, we differentiate infected individuals into asymptomatic (A) and symptomatic infected (I) compartments. Those in A will always recover, while the more severe cases in I may require hospitalization, in which case they move to compartment H, from where they may eventually recover (R) or die (D). We note that most transmission occurs within a few days after symptom onset, and the compartment I reflects this

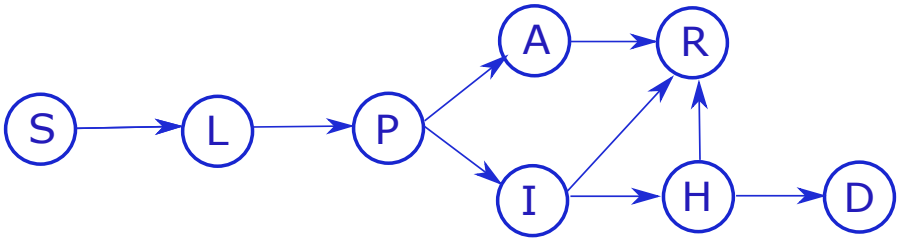

Figure 3.1: Transition diagram of the applied 8-compartment nonlinear epidemic model. Circles represent compartments and arrows represent transitions between these compartments.

period of effective infectivity, rather than clinical status or PCR positivity, which may continue for weeks, yet we remove them from I and place them in R as they do not participate in chains of transmission anymore. Several studies [31, 166–170] have proposed somewhat similar models for COVID-19.

The compartmental model without any control terms reads as:

$$\begin{aligned}
S'(t) &= -\beta\left[P(t)+I(t)+\delta A(t)\right]S(t)/N, && (3.1)\\
L'(t) &= \beta\left[P(t)+I(t)+\delta A(t)\right]S(t)/N-\alpha L(t), && (3.2)\\
P'(t) &= \alpha L(t)-pP(t), && (3.3)\\
I'(t) &= qpP(t)-\rho_I I(t), && (3.4)\\
A'(t) &= (1-q)pP(t)-\rho_A A(t), && (3.5)\\
H'(t) &= \rho_I \eta I(t)-hH(t), && (3.6)\\
R'(t) &= \rho_I(1-\eta)I(t)+\rho_A A(t)+(1-\mu)hH(t), && (3.7)\\
D'(t) &= \mu hH(t). && (3.8)
\end{aligned}$$

Model parameters

From the infectivity profile of COVID-19 [165], we can see that most transmissions occur between 3 days prior to and 4 days after symptom onset, with the pre-symptomatic infection fraction 43.7%. It is a good approximation to set the pre-symptomatic period p^{-1} as three days, and the symptomatic infectious period ρ_I^{-1} as four days, with the same infectiousness β during this period. The estimated mean incubation period (which is the latent and pre-symptomatic period together) of the coronavirus disease is 5.5 days [171], thus the latent period α^{-1} is 2.5 days. Studies have shown similar durations of viral shedding between symptomatic and asymptomatic cases [172], so we set ρ_A^{-1} as four days as well. For the probability of developing symptoms, and the relative infectiousness of asymptomatic individuals, we use the CDC best estimate $q = 0.6$ and $\delta = 0.75$ [173]. The average stay in hospital is assumed to be 10 days, in accordance with the seven-day median reported in [174]. The in-hospital death ratio (μ) in the USA is 0.145 [175]. The best estimate for the infection fatality rate (IFR) is 0.0065 [173], thus the hospitalization probability η of symptomatic cases can be inferred from the relation IFR $= q\eta\mu$ as $\eta \approx 0.076$.

The basic reproduction number, expressing the average number of new infections generated by a single infected individual in a fully susceptible population, is given as

$$R_0 = \beta\left(\frac{1}{p}+\frac{q}{\rho_I}+\frac{\delta(1-q)}{\rho_A}\right). \qquad (3.9)$$

This formula can be derived as follows. Introduce a single infected individual into a susceptible population, then $S(t)/N \approx 1$. A newly infected individual, after passing through the latent phase, spends p^{-1} time in the pre-symptomatic compartment, while infecting others at rate β. Then transits to the symptomatic infected compartment with probability q, where it spends ρ_I^{-1} time infecting others again with rate β. Asymptomatic infection occurs with probability $1-q$, in which case the individual infects with reduced rate $\delta\beta$, for time ρ_A^{-1} on average. Summing up these terms, we obtain (3.9). We assume that hospitalized individuals are properly isolated and do not cause significant numbers of infections.

Many studies have investigated R_0 for different countries; here we use $R_0 = 2.2$ estimated from the Hungarian data [31]. From relation (3.9), given that all other parameters are determined, we can calculate $\beta = 1/3$. We use Hungary's population size for N. The parameter values are summarized in Table 1.

Parameter	Interpretation	Value	Reference
R_0	Basic reproduction number	2.2	[31]
α^{-1}	Latent period	2.5 (days)	[171]
p^{-1}	Pre-symptomatic infectious period	3 (days)	[165]
β	Transmission rate	1/3	calculated
δ	Relative transmissibility of asymptomatic	0.75	[173]
q	Prob. of developing symptoms	0.6	[173]
ρ_I^{-1}, ρ_A^{-1}	Infectious period	4 (days)	[165]
η	Hospitalization probability of symptomatic cases	0.076	[173]
h^{-1}	Average length of hospitalization	10 (days)	[174]
μ	Probability of fatal outcome, given hospitalization	0.145	[175]
N	Population size (Hungary)	9800000	[176]

Table 3.1: List of parameters and their values used in the simulations

3.1.2 The transmission dynamics model as a control system

To design a controller for the epidemic process, the first step is to define the manipulable parameters (control inputs) and identify the measured outputs. The latter comprises all relevant state-dependent variables that are available for measurement. In the absence of vaccination, one needs to rely on a variety of non-pharmaceutical measures, which aim to prevent the transmission of the virus. In our model, the control input, denoted by u, reflects the effect of the measures implemented to reduce the transmission rate. This variable is introduced in the model as a scaling factor of β, i.e. β is replaced by $\beta(1-u)$ in Eqs. (3.1) and (3.2) which are therefore modified to

$$S'(t) = -\beta(1-u(t))\left[P(t)+I(t)+\delta A(t)\right]S(t)/N, \tag{3.10}$$

$$L'(t) = \beta(1-u(t))\left[P(t)+I(t)+\delta A(t)\right]S(t)/N - \alpha L(t), \tag{3.11}$$

where $0 \le u(t) \le u_{max} < 1, \forall t \ge 0$. It is clear from the above equations that $u(t) = 0$ corresponds to unmitigated disease spread without any restriction, and $u(t) = u_{max}$ represents the strictest possible intervention level.

Analogously to R_0, the time dependent effective control reproduction number, denoted by $R_c(t)$, can be given by

$$R_c(t) = \beta\left(1-u(t)\right)\frac{S(t)}{N}\left(\frac{1}{p}+\frac{q}{\rho_I}+\frac{\delta(1-q)}{\rho_A}\right). \tag{3.12}$$

An analysis of eleven European countries [177] revealed that the reproduction number (3.6 on average) dropped to 0.66 after the strictest lockdowns, hence we can assume $u_{max} = 0.82$.

Realization of the control input by specific control measures

Public health authorities are implementing a wide range of measures in response to the COVID-19 outbreak, see Table 3.2. Multiple works appeared at the beginning of the pandemic about the quantitative effect of different measures, usually in terms of the reduction of infection probabilities in different locations, e.g. in [178,179]. These can be used to match input value ranges and various possible restrictions. The Oxford COVID-19 Government Response Tracker [180] is a tool that systematically collects information on several different common policy responses on 17 indicators such as school closures and travel restrictions. Such indicators can be composed into indices, such as the government response stringency index. Having data from more than 160 countries, one can rigorously track the evolving policy responses around the world and compare various

Banned visits to health care institutions and long-term care facilities
Suspension of flights, international travel restrictions
University and school closures
Shortened opening time of shops
Stay at home measures
Restriction of gatherings, cancel public events
Suspend public transportation
Test, trace, isolate
Closing non-essential businesses
Emergency notification
Public information and awareness campaign
Mask wearing requirements

Table 3.2: Typical measures applied in various countries

countries. We have plotted the stringency index of selected European countries (that are similar to Hungary in population size) in Figure 3.2. Later, we will see that the government responses of countries are very similar to constructed control inputs optimizing interventions with different cost functions and constraints.

Non-pharmaceutical measures aim to reduce the number of contacts between individuals or reduce the probability of transmission when contact is made. The transmission rate can be considered as β = daily number of contacts $\times$ transmission probability. Social distancing measures, such as school closures, banning of gatherings, and so on, reduce the average number of daily contacts made by an individual, while improved hygiene, mask wearing reduce the transmission probability. In our control system, we realize any combination of measures by changing β to $\beta(1-u)$, where the control input u represents the overall effect of measures in reducing transmission. For example, if the number of contacts is reduced to half by social distancing measures, then $\beta(1-u) = 0.5\beta$, thus $u = 0.5$. If both the contact number and the transmission probability are reduced to half by a combination of measures, then the transmission rate is reduced to its quarter, corresponding to $\beta(1-u) = 0.25\beta$, meaning that our control input is $u = 0.75$. More recently, works providing a more exact mapping between the applied measures and their effective stringency were published [90], which combine agent-based, high-precision models and simulations with the compartmental model-based controller presented in this thesis. By computing the required β using an optimization-based controller, mapping the obtained value (which is part of a predefined discrete set of intervention levels) to actual interventions (eg. school closure combined with mask-wearing obligation), and finally running the agent-based simulation with these interventions in place, they ensure and prove, that the output of our controller is in fact usable in real-world epidemic situations.

Discretization

The predictive control algorithm proposed in the next section requires a discrete-time dynamical model given in the general form $x_{k+1} = F(x_k, u_k)$. Therefore, the epidemic model (3.1) has to be discretized: function F has to be constructed s.t. $x_k \approx x(k \cdot T_s)$ for any piece-wise constant input $u(t) = u_k$, $t \in [k \cdot T_s, (k+1) \cdot T_s)$, where T_s is the sampling time and x_k is a state vector. From the different possible discretization methods, we found that the simple forward Euler method is suitable for our purposes. It provides sufficient accuracy and preserves the structure of the continuous time model. We used a sampling time $T_s = 0.5$ days to get the discrete time model for

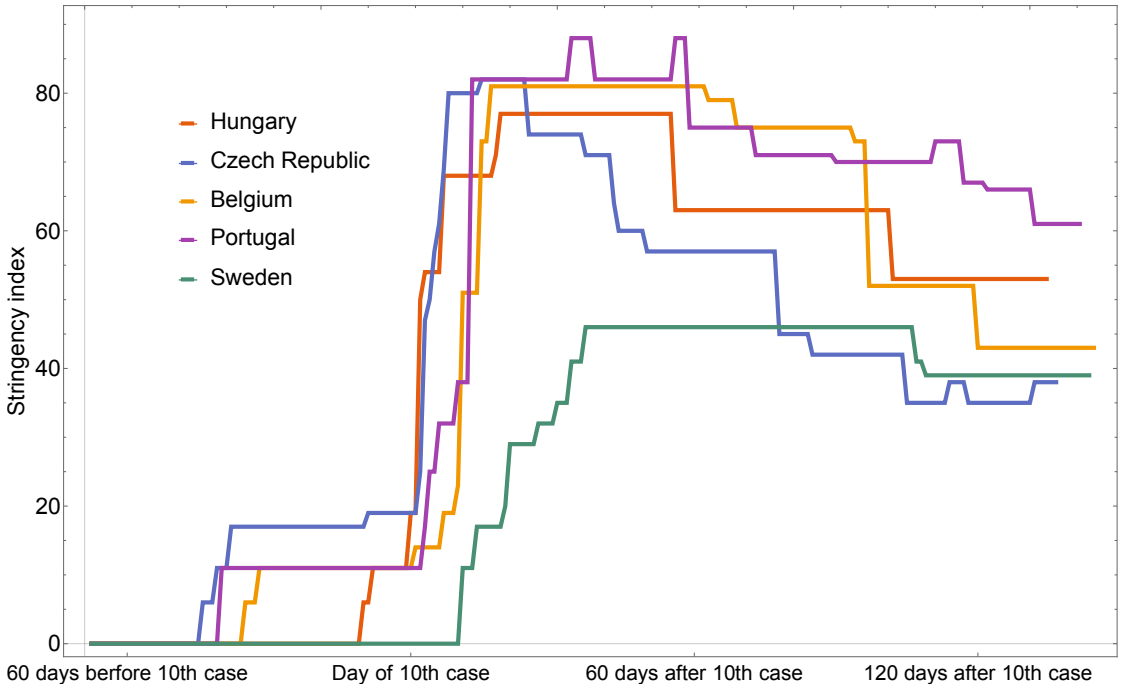

Figure 3.2: Stringency index of control measures in some countries of similar population sizes (Hungary, Czech Republic, Sweden, Belgium, Portugal). The data is taken from [180], and shifted in time to match the day of the 10th confirmed case in each country.

control synthesis. It is important to note that the discrete time model is used for control input design, but the actual trajectories of the system between the sampling instants are computed by an appropriate ODE solver using a standard explicit Runge-Kutta (4,5) method. In Section 3.1.4 a dynamic observer is designed for the epidemic model, which also requires a discrete-time model. To increase the accuracy, that model is generated by a smaller ($T_s = 0.1$ days) sampling time.

3.1.3 Constrained state feedback control for mitigation: control scenarios

In the first control scenarios the entire state vector is assumed to be known. This assumption is not realistic, but the corresponding simulation results will show the physical limitations for controlling the epidemic process in the ideal situation when full information is available. In Scenario 6, this assumption will be relaxed, and only the number of hospitalized COVID-19 patients (state H in the model) and the number of deceased (state D in the model) will be considered available.

In all scenarios we design a feedback controller, i.e. the control input is periodically updated based on the actual measurements.

To formulate the control problem, the next step is to define the performance specifications that have to be satisfied by the controller and the controlled (closed-loop) system. Most of the criteria we expect from a conscious epidemic management can naturally be formulated by cost functions to be minimized (e.g., healthcare costs, or the harmful effects of restrictions on economy and society) and constraints to be satisfied (e.g., upper bounds for the number of hospitalized people and/or on the number of deaths). Model Predictive Control (MPC) methodology is therefore a promising approach for solving this problem. In the MPC framework the control synthesis is transformed into a constrained optimization task solved in every discrete time step, when the control input

has to be updated. Since the synthesis procedure boils down to a standard optimization problem, theoretically a wide set of possible cost functions and complicated constraints can be handled.

Formally, we formulate the MPC problem using the assumptions described in section 2.4. We intend to control the epidemic process in a shrinking-horizon approach, with an initial length of $M = 180$ days. In subsection 3.1.4 a state observer is included in the control loop to estimate the unmeasurable states of the epidemic model. The control input is allowed to change once every week, as changing the stringency of governmental interventions is unrealistic with a higher frequency. This section presents five control scenarios defined for the epidemic model. Each scenario addresses a different public health goal and presents a different control strategy. In all cases, full state measurement is assumed, and all simulations start from the same initial condition: $S_0 = N - L_0$, $L_0 = 40$, $P_0 = I_0 = A_0 = H_0 = D_0 = R_0 = 0$, where N is the population of Hungary according to Table 1. We assume that the epidemic remains undetected until the number of hospitalized patients exceeds a small threshold H_{thr}. Technically, this means that the simulation runs open-loop until this threshold is reached, and the controller is switched on only thereafter. In the case studies we examined, $H_{thr} = 10$ was used. As mentioned before, the sampling time is $T_s = 0.5$ days, but in each scenario the control input is updated only weekly, i.e. in every 14th time instant. The simulations were run on a Dell Vostro 5471 computer with i7-8550U (4 cores, 1.8-4.0 GHz) processor and 8GB RAM under MATLAB R2019b using the BARON 19.3.24 solver [163] and YALMIP version R20200116 [181]. The code for the translation of specifications containing temporal logic expressions to optimization problems was based on the BluSTL toolbox [160].

Scenario 1: Mitigation and suppression with continuous control input

In this scenario the control input is allowed to take arbitrary (continuous) values between 0 and an a priori defined u_{max}. The cost function and constraints used in the MPC design are defined as follows:

$$J(x,u) = \sum_{i=0}^{M_k} u_{k+i|k}^2 + w_H H_{M_k} + w_D D_{M_k} + w_\varepsilon \varepsilon, \tag{3.13a}$$

$$H_{k+i+1|k} \leq \overline{H} + \varepsilon, \quad 0 \leq \varepsilon, \quad 0 \leq u_{k+i|k} \leq u_{max}, \quad \forall i = 0 \dots M-1. \tag{3.13b}$$

So, we would like to minimize the direct harmful effects of the restrictions (measured in a 2-norm), and keep the number of hospitalized patients under a predefined upper bound, not to overload the healthcare system. The weighting factor w_D penalizing the number of deceased at the end of the horizon can be used to balance between *mitigation* and *suppression*, the two typical goals of COVID-19 management [182].

Note: as explained in Section 2.4, Remark c), the term $M_k = M - k$ here is used to indicate the end of the horizon when iteratively re-computing the MPC problem in the k-th timestep in a shrinking horizon setup. Consequently, D_{M_k} and H_{M_k} denote the number of people in the D and H compartments at the current end of the horizon.

In the first case $w_D = w_H = 0$, so the focus is only on the direct cost of the control measures. The controller is expected to avoid strict measures and thus only mitigates the effects of the epidemic to the extent that the hospitalization remains below the given bound. In the second case, $w_D \gg 0$, $w_H \gg 0$ are set such that the corresponding terms in the cost function are comparable with $\sum_{i=0}^{M} u_{k+i|k}^2$, so the controller tries to suppress the epidemic even if the control actions are expensive (i.e., they have harmful effects). The upper bound $\overline{H}$ represents the limit of the healthcare capacity. Parameters w_ε and ε are the ingredients of the soft constraint formulation.

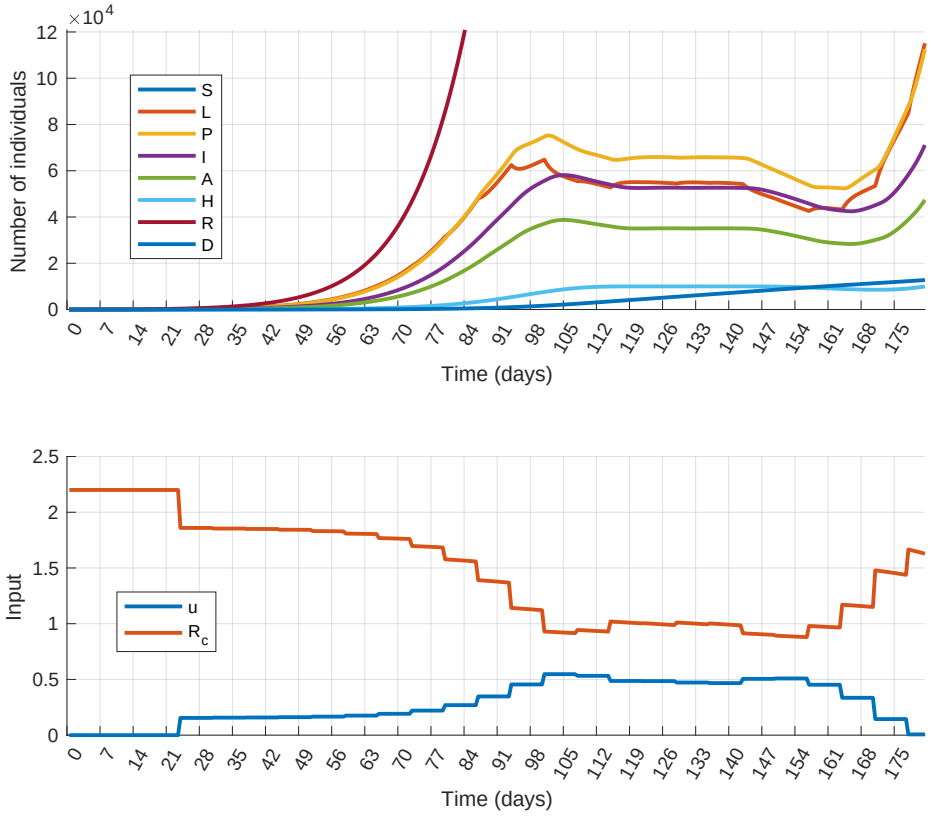

Figure 3.3: Simulation results of Scenario 1.a (Mitigation): state trajectories (top) and control inputs with the corresponding effective reproduction number R_c (bottom).

A soft constraint is applied to avoid the possible numerical infeasibility that can occur in the vicinity of $\overline{H}$ by the slight difference between the simulated continuous and the predicted discrete trajectories.

First, the *mitigation* scenario is investigated. For this, simulations have been performed with the following parameter values: $\overline{H} = 10000$, $u_{max} = 0.82$. The results obtained are shown in Fig. 3.3. At the beginning of the control period the control input is small. This shows that less strict measures are sufficient during this time. As the epidemic progresses, the control input slowly increases, but only until the 98th day, when it reaches a higher but still moderate value that is significantly smaller than the allowed maximum u_{max}. After the 98th day, the epidemic can be successfully mitigated. At the end of the control period (from day 154) the controller eases the restrictions (the control input decreases) since the control specifications have to be fulfilled only up to the 180th day, and this can be achieved even if the measures are relaxed (the control cost is decreased) in the last few weeks. If the constraints have to be satisfied over a longer time period, the control horizon has to be increased. From this result the following conclusion can be drawn: first, if we can intervene in time, there is no need to immediately implement strict measures, and second, the epidemic can be mitigated by applying only moderate restrictions. The total cost of the control strategy is $J^*_{1m} = 42.86$.

It is important to notice the increase of the state variables at the end of the horizon. Since a finite time control policy is computed, it is not surprising that close to the end of the control period, the controller decreases the control input to minimize the cost. As a response, the state variables start to increase, but this does not cause a feasibility problem as long as the constraints are not violated till the end of the horizon. This so-called "turnpike" behavior shows that easing the measures would result in an epidemic peak. With a strict constraint on the healthcare capacity,

this could be satisfactorily avoided only if a suitable herd immunity is reached by the end of the control horizon. It has been documented in several papers, e.g. [183] and [184], that in the case of the COVID-19 pandemic, to reach herd immunity without overwhelming the healthcare system would take years. Consequently, defining a good terminal constraint for this relatively small time period is not possible. What can be done is to directly constrain the increase of the states at the final (M and $M-1$-th) time instants [183], to preserve the possibility of extending the control horizon at a later time. We are going to show an example for this in Scenario 3.

Using the mitigation setup, we have analyzed the maximum delay that the system can tolerate before implementing any measure. From a control perspective, this means that the system runs open loop (i.e., uncontrolled) in the time interval $[0, d \cdot T_s]$, where $d \in \mathbb{N}_+$ and then the controller is turned on. We seek the maximal d, for which the MPC optimization problem has a feasible solution. For the maximal tolerable delay we have obtained 74 days (i.e. $d = 144$). For larger values of d the MPC optimization has no feasible solution. (To detect infeasibility, a hard upper bound has been introduced for the soft constraint violation. Specifically, in this scenario, $\varepsilon \leq 0.01$ has been used.) The simulation results are plotted in Figure 3.6. Considering the control input, it can be seen that, as expected, the larger the delay, the stricter the measures that have to be applied. The maximal control input is 0.82, which corresponds to a total lockdown.

The controller for epidemic *suppression* has been designed by the following weights in the cost function: $w_D = 0.0267$ and $w_H = 0.0033$. The simulation results are plotted in Fig. 3.4. It is visible that the outbreak can be successfully suppressed for the price of a strict and early lockdown, followed by a slow, gradual easing of the measures. However, a second wave of the epidemic appears at the end of the horizon, as it has been observed in several countries; for example, the curves in Figure 4 show a striking resemblance to the true epidemic curve of Hungary. The total cost of the control strategy is $J_{1s}^* = 101.8$ from which the cost of the control input is $\sum_k u_k^2 = 89.27$.

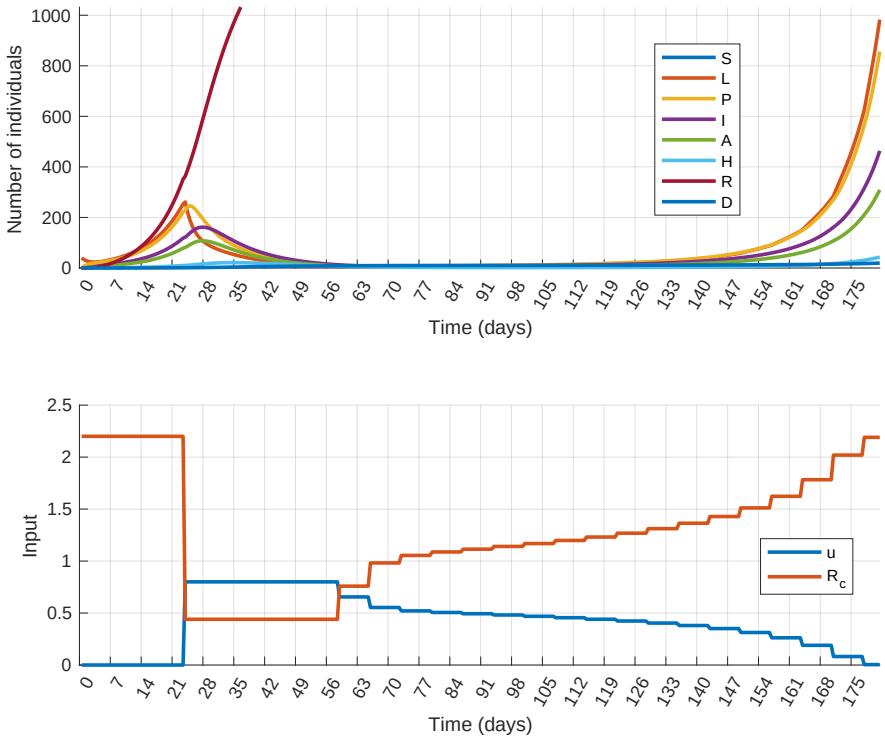

Figure 3.4: Simulation results of Scenario 1.b (Suppression): state trajectories (top) and control inputs with the corresponding effective reproduction number R_c (bottom).

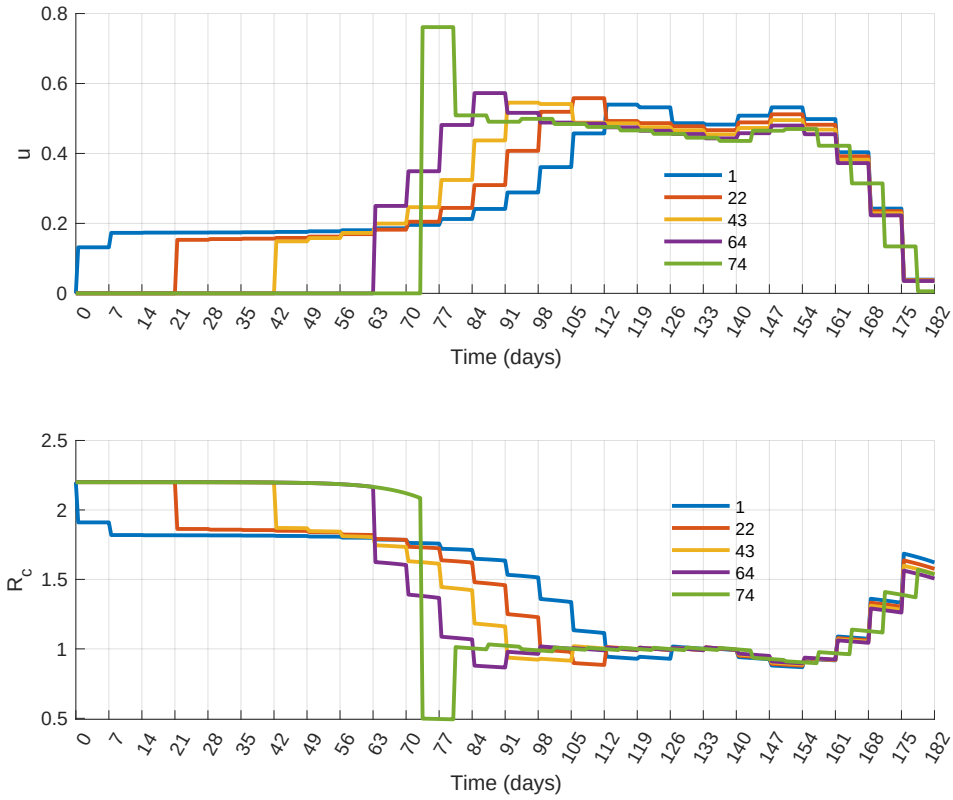

Figure 3.5: Simulation results of Scenario 1.a with delayed intervention. Control inputs (u) and the corresponding effective reproduction number (R_c) obtained at different values of delay.

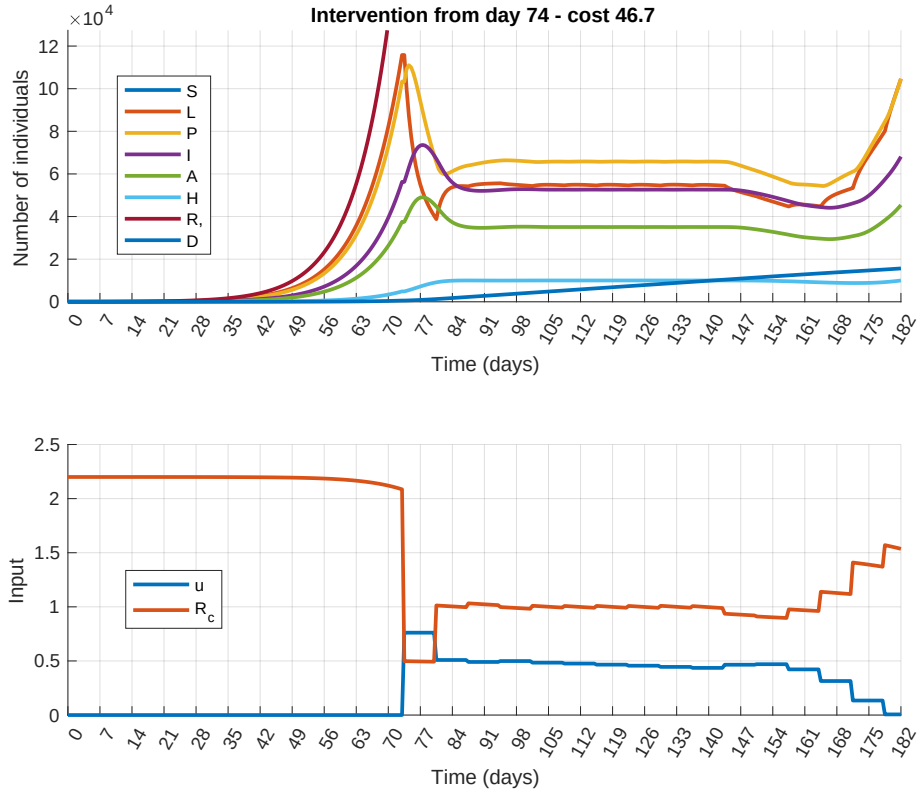

Figure 3.6: Simulation results of Scenario 1.a with delayed intervention. Simulation results obtained at the maximal tolerable input delay ($d = 74$ days)

Scenario 2: The effect of control input quantization

By definition, the control input u reflects the effect of different measures implemented by the government in the society. Since there is a finite number of measures that can be applied (see Table 1), a control input with truly continuous range cannot be realized in practice. Motivated by this, we assume now that the control input is quantized and can take only 4 different values. Each value corresponds to a specific measure as follows: $u^{(1)} = 0, u^{(2)} = 0.19, u^{(3)} = 0.41, u^{(4)} = 0.6$. Here, as an example, $u^{(2)}$ may correspond to school closures, $u^{(3)}$ to stay-at-home orders, and $u^{(4)}$ can be interpreted as a combination of the two. To force $u_k \in \{u^{(1)}, u^{(2)}, u^{(3)}, u^{(4)}\}$ for all k, an additional constraint is added to the MPC synthesis:

$$\square(u = u^{(1)} \vee u = u^{(2)} \vee u = u^{(1)} \vee u = u^{(4)}), \tag{3.14}$$

where $\square$ is a temporal logic operator called 'always' and is defined as follows: if ϕ is an arbitrary logical expression, then

$$\square_{[a,b]}\phi \text{ is true at time } t \Leftrightarrow \ \forall t' \in [t+a, t+b] \text{ the formula } \phi \text{ is true.} \tag{3.15}$$

Using this definition, constraint (3.14) prescribes that one of the four equations $u = u^{(i)}$, $i \in \{1, 2, 3, 4\}$ has always to be true. (More details on temporal logic operators can be found, e.g., in [29]). We remark that the discrete inputs alone do not necessitate the application of temporal logic (see, e.g. [55]). However, this notation is intuitive, and using the temporal logic framework it is straightforward to add more complex (possibly time-varying) constraints, as will be shown by the next scenario.

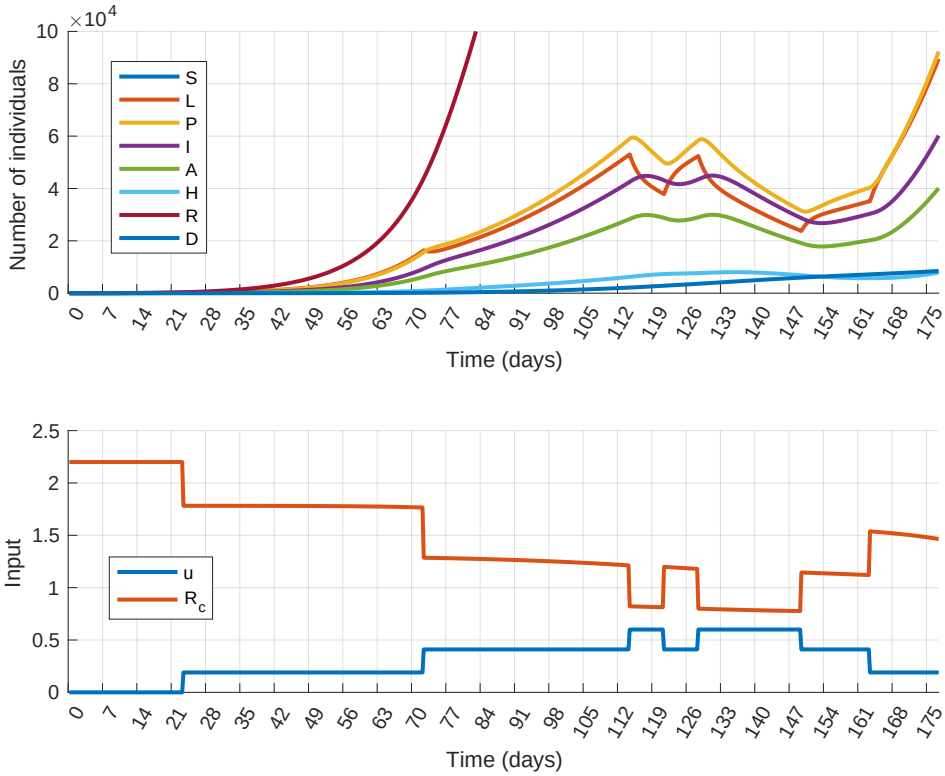

Figure 3.7: Simulation results of Scenario 2 (Control input quantization): state trajectories (top) and control inputs with the corresponding effective reproduction number R_c (bottom).

To analyze the effect of input quantization, we have performed the mitigation scenario defined in the previous section with the additional constraint (3.14). The results are plotted in Fig. 3.7.

It can be seen that the primary control goal, i.e. the mitigation of the epidemic, is achieved and the input and state constraints are satisfied. It is also important to mention that the quantized control input is similar to the continuous one obtained in Scenario 1, which means that the optimal control strategy is very similar in the two cases. On the other hand, the quantization allows less freedom to the controller, so the total cost is now higher: $J_2^* = 45.88$.

Scenario 3: Refined constraint for healthcare capacity

In this scenario we allow, but only once and only for a limited time period, that the number of hospitalized patients (H) exceeds the limit $\overline{H}$. This scenario represents the case when there is an extra, but possibly costly reserve in the healthcare system that can be activated if necessary, or resources are reallocated to COVID-19 from other areas of healthcare. Formally, we introduce two new parameters: T_r and $\overline{\overline{H}}$, such that $\overline{H} < \overline{\overline{H}}$ and the MPC design is completed with the following constraint:

$$\square(H \leq \overline{H}) \ \mathbf{U} \left(\square_{[0,\ T_r]}(H \leq \overline{\overline{H}}) \wedge \square_{[T_r,\ N]}(H \leq \overline{H}) \right) \tag{3.16}$$

where the temporal logic operator $\mathbf{U}$ (called 'until') is defined as follows:

$$\varphi \mathbf{U}_{[a,b]} \psi \text{ is true at time } t \Leftrightarrow \ \exists t' \in [t+a, t+b] \text{ st. } \psi \text{ is true } \ \wedge \tag{3.17a}$$

$$\forall t'' \in [t, t'] \ \varphi \text{ is true} \tag{3.17b}$$

In expression (3.16), $\overline{\overline{H}}$ denotes a new upper bound that is never to be violated, and T_r is the maximal time period for which $H > \overline{H}$ is allowed. The numerical simulation for this scenario was performed with the following parameter values: $\overline{\overline{H}} = 15000$ and $T_r = 21$ days. The results obtained by performing a mitigation scenario are depicted in Fig. 3.8 and 3.9, respectively. Compared to the results of Scenario 1, it can be seen that the shapes of the control inputs are similar. The main difference is that the controller in Scenario 3 applies smaller control actions over almost the entire horizon. The control input is larger only for a short period after T_r has elapsed. This is necessary to stop the increase of the constrained state variables, which would result in the violation of the constraints and the loss of feasibility. Since the control input is smaller at most times than in Scenario 1, the total cost of the control is smaller: $J_{1m}^* = 42.86$ in Scenario 1 and $J_3^* = 41.43$ in Scenario 3.

Similar to the other scenarios investigated so far, the state variables start to increase at the end of the control horizon. To avoid this behavior we introduce the following simple terminal constraint:

$$H_{k+M|k} + 1 \leq H_{k+M-1|k} \tag{3.18}$$

i.e. the number of hospitalized individuals must decrease in the last step. This constraint prevents H and the other states from increasing: strict control measures are applied till the very end of the horizon. Though the characteristic of the state variation has been significantly improved, nothing can be guaranteed for the process behavior beyond the control horizon. A later outbreak can be avoided only if the implementation of the carefully planned, strict control policy is continued.

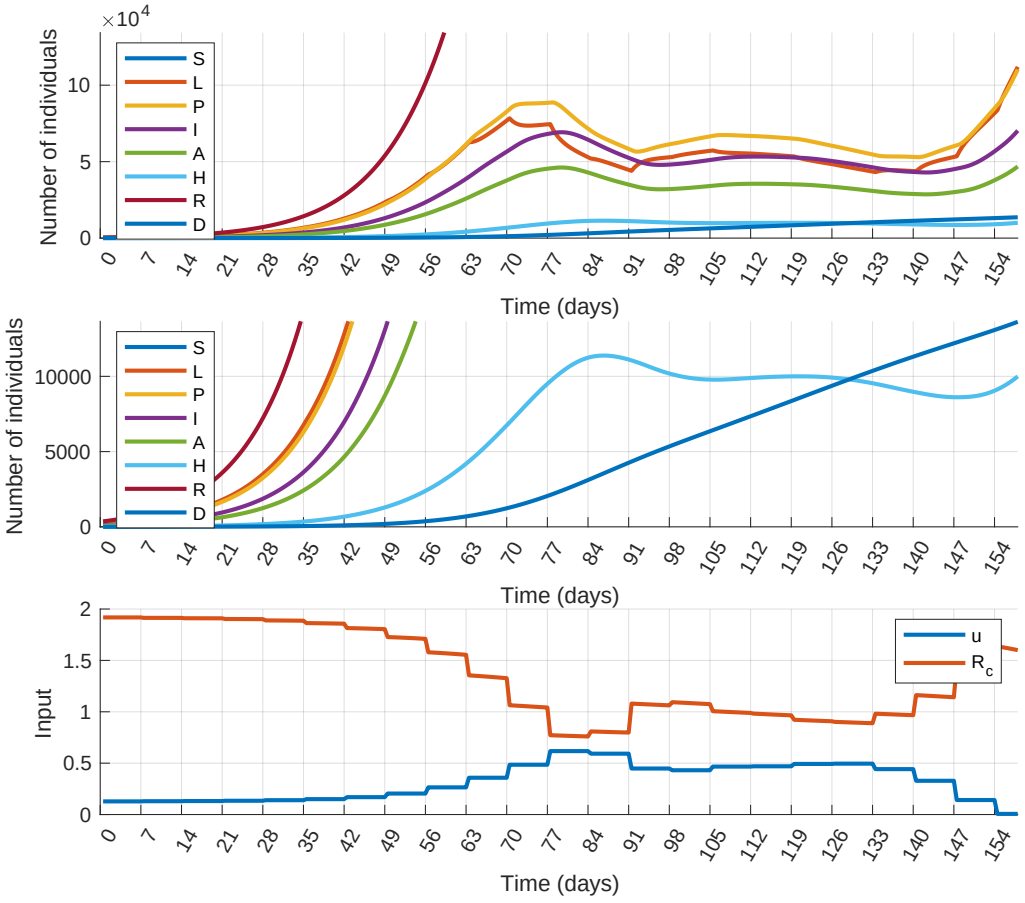

Figure 3.8: Simulation results of Scenario 3 (Temporal increase of healthcare capacity): state trajectories (top) and control inputs (bottom) obtained with $T_r = 21$ and $\overline{\overline{H}} = 15000$. H is above 10000 between days 79 and 100.

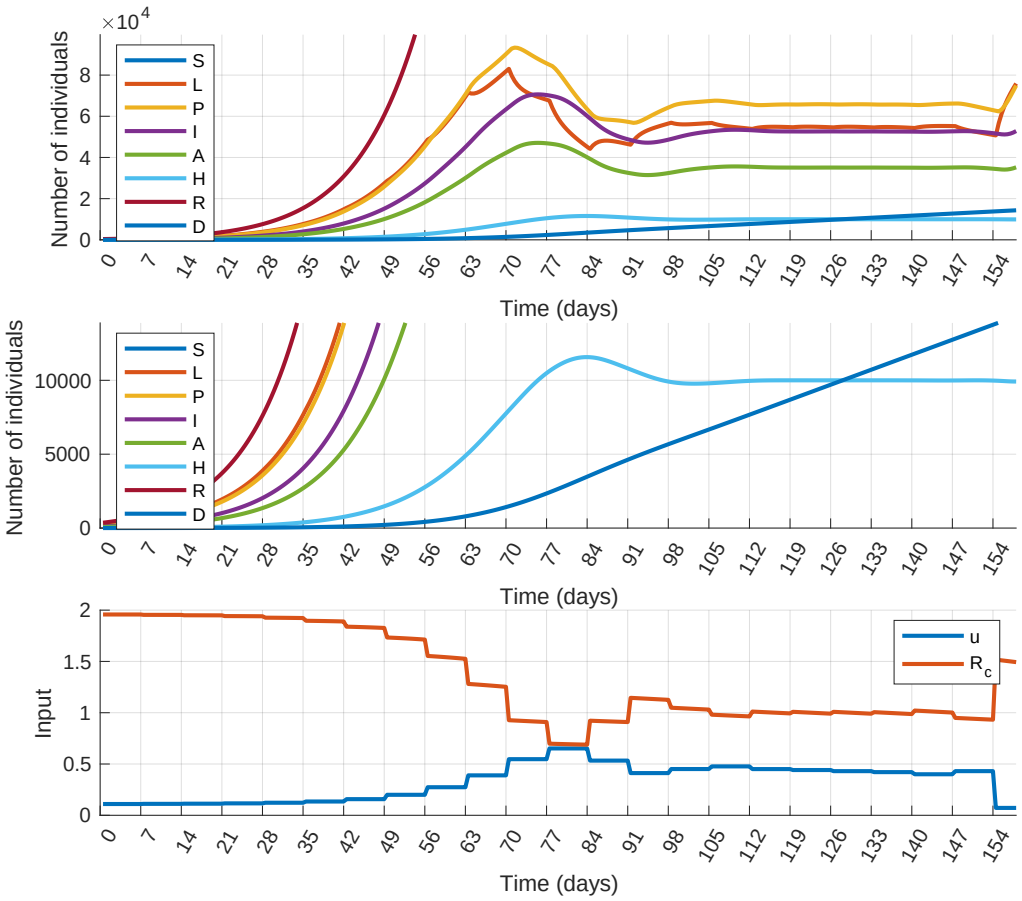

Figure 3.9: Simulation results of Scenario 3 (Temporal increase of healthcare capacity): state trajectories (top) and control inputs (bottom) obtained with $T_r = 21$ and $\overline{\overline{H}} = 15000$. In this simulation a terminal constraint for the number of hospitalized individuals has also been introduced. H is above 10000 between days 76 and 97.

3.1.4 State estimator design and output feedback control

In this section the assumption of full state measurement is dropped, and aligned with the common practice, only the number of the deceased (D) and the number of the hospitalized individuals (H) are monitored. There are examples in the COVID-19 literature, where the global dynamics and the epidemic curve were reconstructed from the data of hospitalized or deceased individuals [185, 186]. In order to use the state feedback MPC controller, a dynamical observer is designed to estimate the remaining non-measured states.

As the design and implementation of the presented observer is entirely the work of Dr. Tamás Péni, only some key ideas and numerical results are highlighted in this thesis. A more detailed discussion of the LPV observer design and analysis can be found in the original paper [J1].

LPV observer design for the epidemic model

To design the estimator, the states are normalized first and the dynamical model is divided into three parts. According to the three subsystems, the state vector is partitioned as follows: $s := S/N$, $\bar{x} = [L, P, I, A, H]/N$ and $r = R/N$. Focusing on x, we notice that the corresponding dynamical equations can be rewritten in linear parameter varying (LPV) form:

$$\bar{x}_{k+1} = (I + T_s A_0 + \rho_k T_s A_1)\bar{x}_k \doteq A(\rho_k)\bar{x}_k \tag{3.19}$$

where $\rho_k = s_k v_k$ with $v_k = 1 - u_k$ is the scheduling variable and

$$A_0 = \begin{bmatrix} -\alpha & 0 & 0 & 0 & 0 \\ \alpha & -p & 0 & 0 & 0 \\ 0 & qp & -\rho_I & 0 & 0 \\ 0 & (1-q)p & 0 & -\rho_A & 0 \\ 0 & 0 & \rho_I \eta & 0 & -h \end{bmatrix}, \quad A_1 = \begin{bmatrix} 0 & \beta & \beta & \delta\beta & 0 \\ 0 & 0 & 0 & 0 & 0 \\ 0 & 0 & 0 & 0 & 0 \\ 0 & 0 & 0 & 0 & 0 \end{bmatrix} \tag{3.20}$$

follow from (3.1). By introducing $C = [0\ 0\ 0\ 0\ 1]$, a measurement equation is added to the model: $y_H = C\bar{x}$, where $y_H = \bar{x}_5 = H/N$. We can safely assume that some variables are bounded:$s \in [0.5, 1]$, $u \in [0,\ 0.7]$, $\rho \in [0.15, 1]$. Using these bounds, a parameter-varying observer can be designed, but the scheduling variable is unknown and must be estimated. Since in our case s_k is not available for measurement, we can only approximate it by using its difference equation, as follows:

$$\hat{s}_{k+1} = \hat{s}_k - T_s \hat{s}_k v_k \,[0\ -\beta\ -\beta\ -\beta\delta\ 0]\,\hat{\bar{x}} \tag{3.21}$$

Scheduling the model with $\hat{\rho} = \hat{s}v$ leads to the problem of observer design for LPV systems with inaccurately measured scheduling variables, which is well identified in control literature, and one possible solution is proposed in [187–189]. The method constructs a parameter varying observer, scheduled by $\hat{\rho}$ such that the boundedness of the estimation error is guaranteed as long as $\rho - \hat{\rho}$ is bounded.

Before applying this method, it is important to check the observability properties of the LPV model, which was realized by computing the observability matrix at 10 different frozen (fixed) parameter values. In all cases, the observability matrix was full rank but badly conditioned.

Starting from the LPV model, the state estimator is defined in the following form:

$$\hat{\bar{x}}_{k+1} = A(\hat{\rho})\hat{\bar{x}}_k + L(\hat{\rho})(y_H - \hat{y}_H) \tag{3.22}$$

where $\hat{y}_H = C\hat{x}$.

The above methodology assumes perfect knowledge of the model parameters, which is admittedly unrealistic. Therefore, tracking the number of hospitalized people only may not be enough in practice to compute the population in other compartments with the required precision using this method. However, as examined in Subsection 3.1.4, the obtained results are suitably accurate for the controller.

Numerical results obtained by the LPV observer

During the simulations, we use the observer gain $L(\hat{p}) = L_0 + \hat{p}L_1$ with:

$$L_0 = \begin{bmatrix} 13.4913 \\ 14.1086. \\ 8.3603 \\ 5.5759 \\ 1.0058 \end{bmatrix}, \quad L_1 = \begin{bmatrix} 1.3190 \\ 0.0767 \\ -0.0009 \\ -0.0019 \\ 0.0001 \end{bmatrix}. \tag{3.23}$$

Due to the weak observability, the error dynamics is close to the boundary of stability, and further analysis would be necessary to reveal the exact performance of the observer. However, as this was out of the scope of the original paper, as well as of this chapter, the observer is only examined in numerical simulations, focusing on its applicability in the control loop.

Figure 3.10 presents the simulation results obtained by running the system open-loop with the control input depicted in the same figure. The initial state was the same as we chose above, i.e. $L(0) = 40$, $S = N - L$, and the other states are 0. In the simulation the normalized states were estimated, but they were re-scaled to plot the results. It can be seen that a noticeable, but still not significant estimation error can be detected only in variables S and R and only in the neighborhood of the peak of the epidemic. This is not relevant, however, since the estimator is intended to be used together with a controller, which mitigates or suppresses the epidemic peak.

Scenario 4: Output feedback control

In this section we examine how the state observer works together with the MPC controller. For this, we repeat the simulation of Scenario 1 (subsection 3.1.3) with the following modification: the precise state measurement x_k is replaced by the estimated value $\hat{x}_k$. The simulation results are plotted in Figure 3.11. The control input and state trajectories obtained in the two scenarios can hardly be distinguished. Since the epidemic peak, where the estimation error would be noticeable, is mitigated, the state estimation is almost perfect over the entire horizon. Consequently, using $\hat{x}_k$ in the control input computation has only negligible effect on the closed-loop behavior. Compared to Scenario 1, the control costs are almost equal in the two scenarios: $J_1^* = 42.86$, $J_4^* = 42.98$. We can conclude that the lack of direct measurement of S is not crucial from the point of view of state measurement if the observer is used in closed-loop control.

Scenario 5: Effect of parameter uncertainty

We have assumed so far that the dynamical model of the epidemic is precisely known, that is the model (3.1)-(3.8) with parameters in table 3.1 accurately describes the dynamical behavior of the epidemic process. This is hardly the case in a real situation. Therefore, the possible parameter uncertainties have to be taken into account during the control design process. This leads to a robust synthesis, which is addressed later, in Chapter 4. On the other hand, to study the applicability of the proposed control method, it is important to examine how it works

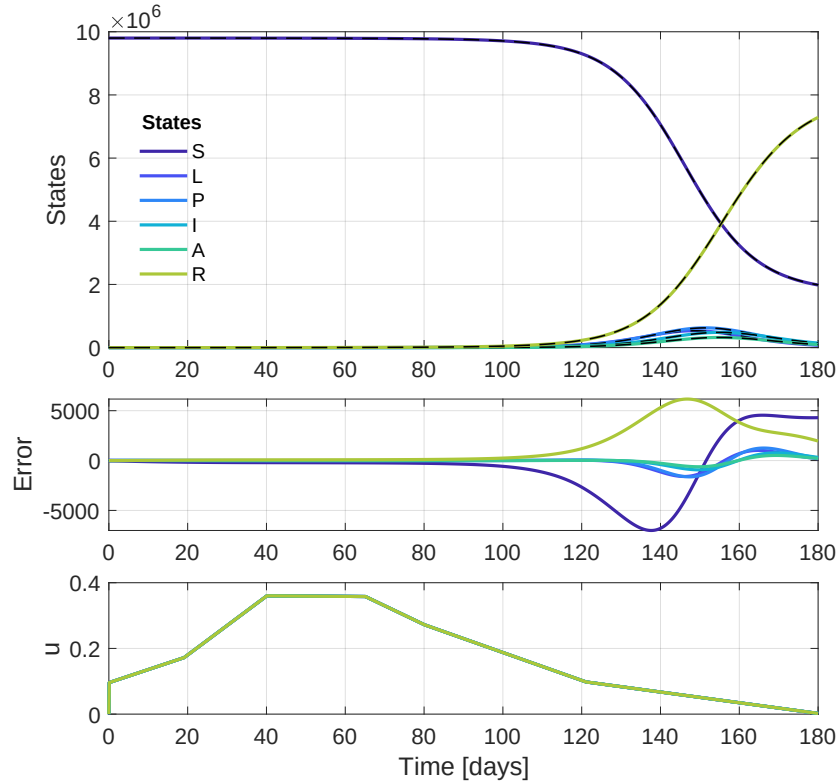

Figure 3.10: True (coloured solid line) and estimated states (dashed black line) (top figure) and estimation error (middle figure) obtained by the state observer. The control input applied during the simulation is plotted in the bottom figure.

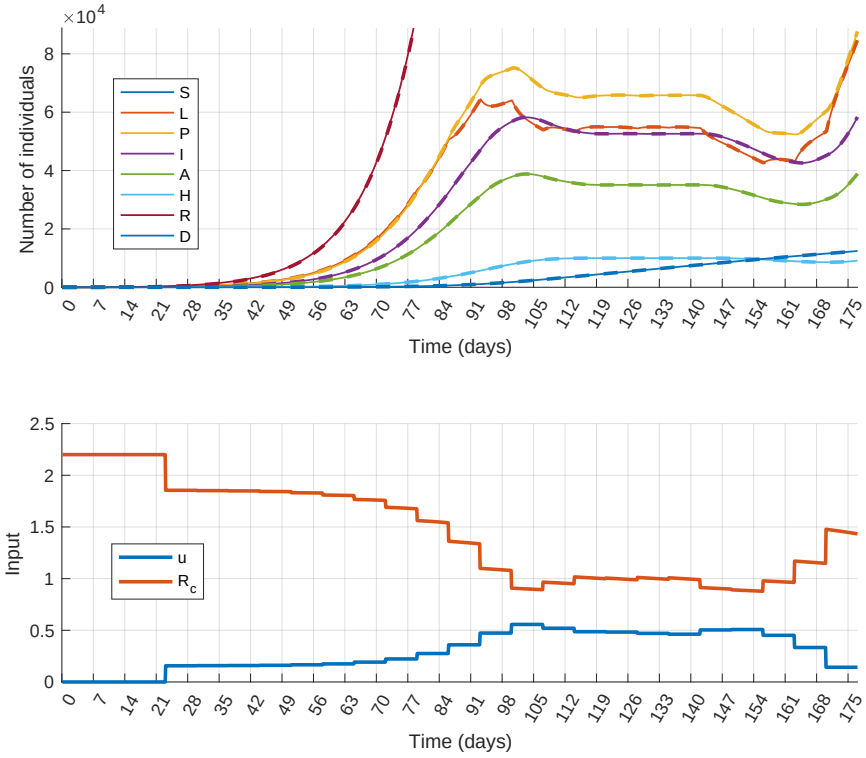

Figure 3.11: Simulation results of Scenario 4 (Output feedback control): state trajectories (top) and control inputs with the corresponding effective reproduction number R_c (bottom). The true and estimated state trajectories are plotted by the solid and dashed lines, respectively.

Case number	α^{-1}	δ	**q**	η	**cost**	**maxH**
0	3.00	0.70	0.50	0.69	33.54	9305
1	3.00	0.70	0.50	0.83	35.33	9608
2	3.00	0.70	0.70	0.69	41.22	10290
3	3.00	0.70	0.70	0.83	43.79	10504
4	3.00	0.80	0.50	0.69	36.86	9738
5	3.00	0.80	0.50	0.83	38.96	9939
6	3.00	0.80	0.70	0.69	43.38	10781
7	3.00	0.80	0.70	0.83	46.30	10893
8	2.00	0.70	0.50	0.69	37.37	9336
9	2.00	0.70	0.50	0.83	39.65	9545
10	2.00	0.70	0.70	0.69	46.03	10242
11	2.00	0.70	0.70	0.83	49.20	10765
12	2.00	0.80	0.50	0.69	40.24	9691
13	2.00	0.80	0.50	0.83	44.64	9834
14	2.00	0.80	0.70	0.69	48.28	10651
15	2.00	0.80	0.70	0.83	51.70	11105

Table 3.3: Model parameters of the experiments performed for uncertainty analysis.

in the presence of model mismatch. In this subsection we show several simulations with the output feedback scenario presented above with the following settings: the model structure used for prediction and state observation is the same, but certain parameters of the controlled system are different in each experiment. We assume that 4 parameters, namely α, q, δ, η are uncertain, they take values from the following intervals:

$$\alpha \in [1/3,\ 1/2],\ \delta \in [0.7,\ 0.8],\ q \in [0.5,\ 0.7],\ \eta \in [0.069,\ 0.083], \tag{3.24}$$

The upper and lower bounds of the parameter domains have been determined using the references in Table 1. Further, we assume that the other model parameters are more precisely known, and therefore their nominal values were used in the simulations. We remark that possible uncertainty in β can be handled, since due to the model structure, designing for larger β gives a feasible controller for smaller values as well. To analyze the robustness, 16 simulations defined by the possible combinations of the min-max values of the uncertain parameters have been performed. Table 3.3 collects the parameters of the experiments with the results obtained. The detailed simulation results obtained for cases 7 and 15 are plotted in Figs. 3.12 and 3.13, respectively.

It can be seen that the controller worked acceptably well with uncertain models, although the cost varied visibly for the different cases. Regarding the constraint on the health care capacity, it is only violated in half of the simulations and the transgression of the limit is not critical. On the other hand, there is room for performance improvement, and thus improving the robustness of the controller is an important task in the future.

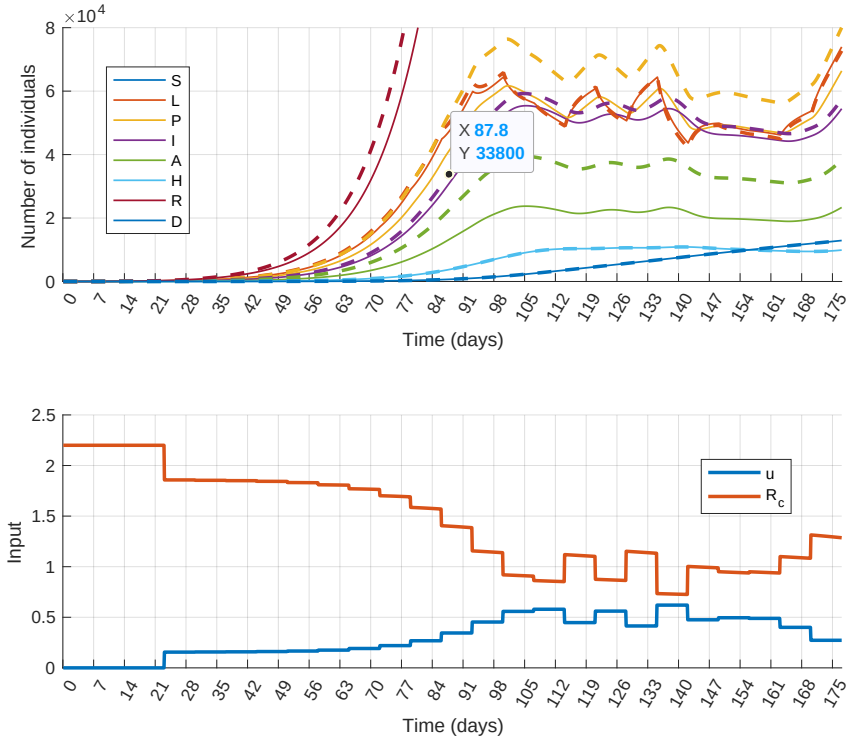

Figure 3.12: Simulation results of Scenario 5 (Output feedback control) with model uncertainties. State trajectories (top) and control inputs with the corresponding effective reproduction number R_c (bottom) in case 7 of table 3.3. The true and estimated state trajectories are plotted by the solid and dashed lines, respectively.

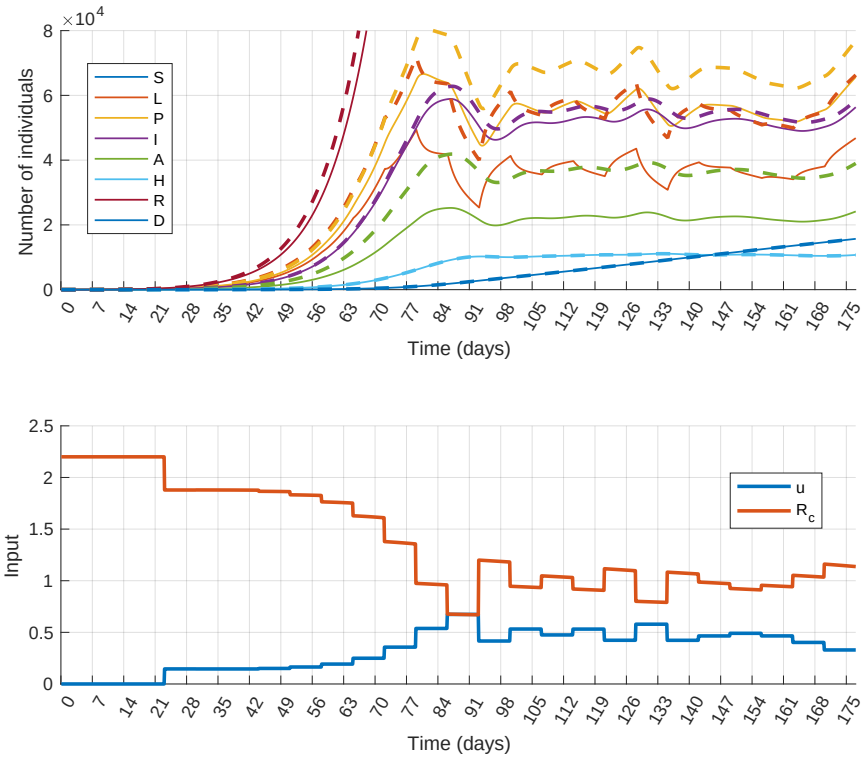

Figure 3.13: Simulation results of Scenario 5 (Output feedback control) with model uncertainties. State trajectories (top) and control inputs with the corresponding effective reproduction number R_c (bottom) in case 15 of table 3.3. The true and estimated state trajectories are plotted by the solid and dashed lines, respectively.

3.2 Optimizing symptom-based testing strategies

Based on [J2], in this section a predictive-control-based approach is proposed for pandemic mitigation with multiple control inputs. Using previous results on the dynamical modeling of symptom-based testing, the testing intensity is introduced as a new manipulable input to the control system model in addition to the stringency of non-pharmaceutical measures. The control objective is the minimization of the severity of interventions, while the main constraints are the bounds on the daily number of hospitalized people and on the total number of available tests. For the control design and simulation, a nonlinear dynamical model containing 14 compartments is used, where the effect of vaccination is also taken into consideration. The computation results clearly show that the optimization-based design of testing intensity significantly reduces the stringency of the measures to be introduced to reach the control goal and fulfill the prescribed constraints.

3.2.1 Compartmental model of transmission dynamics

Model description

In order to describe the evolution of the COVID-19 epidemic with adequate precision, we create a compartmental model based on the one originally published in [J1], with its variations being used in [C1] and [J3] as well. The model was presented in subsection 3.1.1.

In both the original and the new model, the overall infection rate parameter is written as $(1-v)\beta$ which includes the effect of disturbances (e.g., varying infectiousness of the virus, seasonal effects, changes in behaviour and mobility of the population) in β, and also that of the introduced measures and restrictions (from mandatory mask wearing to total lockdown) which are considered manipulable within appropriate limits and represented by the scaling term $1 - v$.

In this work, the original model was modified to include the effect of vaccinations, and is equipped with a second input (κ), which is the number of symptom-based tests carried out during a unit time interval. Symptom-based test means that people who are developing special, a-priori defined symptoms are selected at high probability for PCR testing. If the test is positive, the person is quarantined. Following the concept of [63] the control input enters the model through the transition rate φ defined as follows:

$$\varphi = \kappa \frac{1}{\mathbf{I} + x_{\mathrm{VI}} + \sigma}, \tag{3.25}$$

where σ is the so-called secondary symptom pool, i.e. the proportion of individuals who are not infected with COVID-19, but produce the same set of symptoms. Comparing (3.25) with the formula originally introduced in [63], it can be seen that the original formula contains an additional parameter ρ, which is the probability that an individual from compartment I or VI[1] produces the symptoms on which the testing is based. In our model, we omit this parameter and investigate various choices of the symptom pool using a slightly different methodology as described later in one of the case studies.

People who have tested positive are quarantined. Therefore, a new compartment x_{Q} is added for quarantined individuals: these are symptomatic infected people (from $\mathbf{I}$), whose infection was confirmed by a test, and who are legally obliged to stay at a given location, and thus are unable

[1] Compartment I of the symptomatic infected individuals is detailed in section 3.1.1. VI is a clone of the I compartment for vaccinated individuals, detailed below.

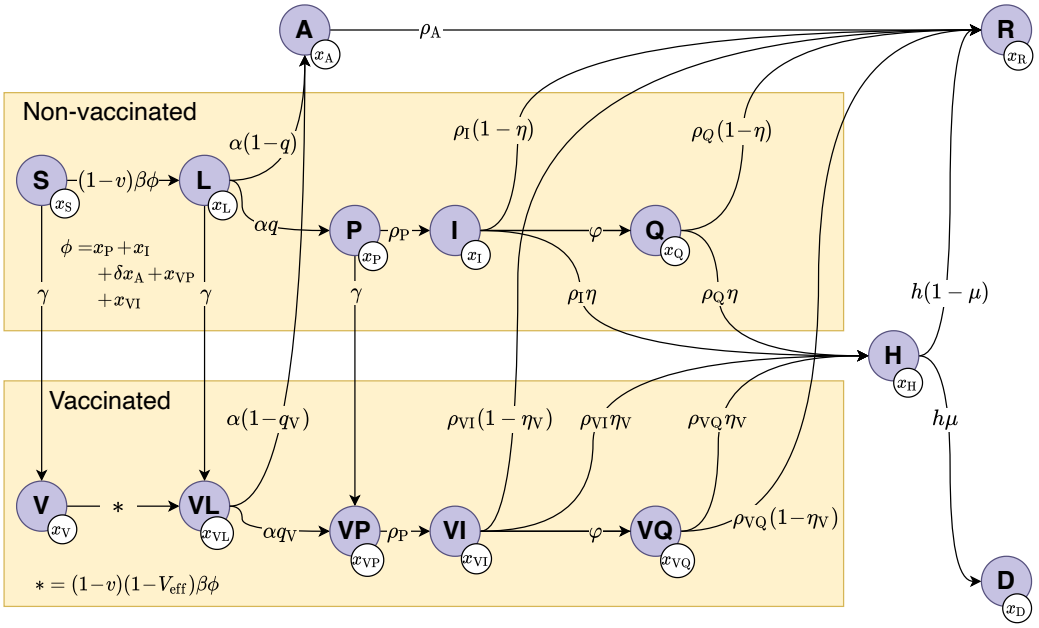

Figure 3.14: Transition diagram of the extended, 14-compartment nonlinear epidemic model. Circles represent compartments and arrows represent transitions between these compartments.

to get in contact with susceptibles and transmit the disease. The rate of transition from **I** to x_Q depends on the intensity of the testing policy (φ).

Also, we have slightly changed the definition of compartment A to adapt the model to the concept of symptom-based testing. In our model the 'Asymptomatic' compartment collects those individuals who do not develop the specific set of symptoms on which the testing is based. So in contrast to the original definition used in [J1], in the present model, symptomatic individuals may also be admitted to compartment A if their symptoms differ from the a-priori defined symptom set.

Next, a copy is created for compartments **S**, **L**, **P**, **I**, x_Q, with identical meaning, only for those individuals who already have some level of immunity due to vaccination: $\mathbf{V}, x_{VL}, x_{VP}, x_{VI}, x_{VQ}$ respectively. The possible transitions from these new compartments remain unchanged, only the parameters (e.g., probability of hospitalization) are different. The transition from non-vaccinated compartments to vaccinated ones is determined by parameter γ, standing for the ratio of total population being vaccinated in a unit time interval.

The model may suggest that only the people in compartments S, L, P can get vaccinated. Actually, this is not the case. When a vaccination campaign is carried out, people in A and R compartments can get the vaccine as well, since they can not be distinguished from the members of the other compartments. As the vaccinated Asymptomatic or Recovered individuals remain in their A or R compartments, they do not influence the transition dynamics. By definition, people in compartment I show symptoms, so they are declared ill; therefore, they are not vaccinated either. The $I \to VI$ transition can thus be neglected.

The final layout of the model, showing all the compartments, transitions, and the parameters influencing them, can be seen in Fig. 3.14. Formally, the model is described by dynamic equations (3.26) as follows:

$$\dot{x}_{\mathrm{S}} = -(1-v)\beta\left(\mathbf{P}+\mathbf{I}+x_{\mathrm{VP}}+x_{\mathrm{VI}}+\delta\mathbf{A}\right)\mathbf{S}-\gamma\mathbf{S} \tag{3.26a}$$

$$\dot{x}_{\mathrm{L}} = (1-v)\beta\left(\mathbf{P}+\mathbf{I}+x_{\mathrm{VP}}+x_{\mathrm{VI}}+\delta\mathbf{A}\right)\mathbf{S}-\alpha\mathbf{L}-\gamma\mathbf{L}, \tag{3.26b}$$

$$\dot{x}_{\mathrm{P}} = \alpha q\mathbf{L}-\rho_P\mathbf{P} \ - \ \gamma\mathbf{P}, \tag{3.26c}$$

$$\dot{x}_{\mathrm{I}} = \rho_P\mathbf{P}-\rho_I\mathbf{I} \ - \ \varphi\mathbf{I}, \tag{3.26d}$$

$$\dot{x}_{\mathrm{Q}} = \varphi\mathbf{I}-\rho_Q x_{\mathrm{Q}}, \tag{3.26e}$$

$$\dot{x}_{\mathrm{V}} = -(1-v)(1-V_{\mathrm{eff}})\beta\left(\mathbf{P}+\mathbf{I}+x_{\mathrm{VP}}+x_{\mathrm{VI}}+\delta\mathbf{A}\right)\mathbf{V}+\gamma\mathbf{S}, \tag{3.26f}$$

$$\dot{x}_{\mathrm{VL}} = (1-v)(1-V_{\mathrm{eff}})\beta\left(\mathbf{P}+\mathbf{I}+x_{\mathrm{VP}}+x_{\mathrm{VI}}+\delta\mathbf{A}\right)\mathbf{V}-\alpha x_{\mathrm{VL}}+\gamma\mathbf{L} \tag{3.26g}$$

$$\dot{x}_{\mathrm{VP}} = \alpha q_V x_{\mathrm{VL}} \ - \ \rho_P x_{\mathrm{VP}} \ + \ \gamma\mathbf{P}, \tag{3.26h}$$

$$\dot{x}_{\mathrm{VI}} = \rho_P x_{\mathrm{VP}} \ - \ \rho_{VI} x_{\mathrm{VI}} \ - \ \varphi x_{\mathrm{VI}}, \tag{3.26i}$$

$$\dot{x}_{\mathrm{VQ}} = \varphi x_{\mathrm{VI}} \ - \ \rho_{VQ} x_{\mathrm{VQ}}, \tag{3.26j}$$

$$\dot{x}_{\mathrm{A}} = \alpha(1-q)\mathbf{L} \ + \ \alpha(1-q_V)x_{\mathrm{VL}} \ - \ \rho_A\mathbf{A}, \tag{3.26k}$$

$$\dot{x}_{\mathrm{H}} = \rho_{\mathrm{I}}\eta\mathbf{I}+\rho_Q\eta x_{\mathrm{Q}}+\rho_{\mathrm{VI}}\eta_V x_{\mathrm{VI}}+\rho_{\mathrm{VQ}}\eta_V x_{\mathrm{VQ}}-h\mathbf{H}, \tag{3.26l}$$

$$\begin{aligned}\dot{x}_{\mathrm{R}} = {} & \rho_A\mathbf{A}+\rho_I(1-\eta)\mathbf{I}+\rho_{\mathrm{Q}}(1-\eta)x_{\mathrm{Q}}+\rho_{\mathrm{VI}}(1-\eta_{\mathrm{V}})x_{\mathrm{VI}}+\ldots \\ & \rho_{\mathrm{VQ}}(1-\eta_{\mathrm{VQ}})x_{\mathrm{VQ}}+h(1-\mu)\mathbf{H},\end{aligned} \tag{3.26m}$$

$$\dot{x}_{\mathrm{D}} = h\mu\mathbf{H}, \tag{3.26n}$$

It is visible from the above equations that separate birth/death processes are neglected, and the state variables denote the proportion of individuals in the corresponding compartments, i.e. the sum of the state variables is 1 in each time instant. As a result, the compartment values shown in the constraints and the results are scaled with the total population Π.

In a more compact form, we can write the system as $\dot{x} = f(x,u)$, with $x = [\mathbf{S} \ \mathbf{L} \ \mathbf{P} \ \mathbf{I} \ x_{\mathrm{Q}} \ \mathbf{V} \ x_{\mathrm{VL}} \ x_{\mathrm{VP}} \ x_{\mathrm{VI}} \ x_{\mathrm{VQ}} \ \mathbf{A} \ \mathbf{H} \ \mathbf{R} \ \mathbf{D}]^T$, $u = [v \ \kappa]^T$, and f is standing for the right hand side of the equations. As commonly done in literature, we suppress the time argument t of the variables x and u.

Model parameters

Model parameters characterizing the transitions among non-vaccinated compartments were set in accordance with related literature [66, 190] with slight modifications to include the effect of measures specific to Hungary [31], [C1] [J1]. The parameters of the vaccinated compartments are distinguished from the parameters of the non-vaccinated by the V subscript.

The parameters of the "vaccinated" part of the model have been chosen based on the following considerations. First, due to the vaccination, the transmission rate of infection (transition $V \rightarrow VL$) is significantly smaller than in the non-vaccinated case. Specifically, we use $\beta(1-V_{\mathrm{eff}})$ for vaccinated compartments, where V_{eff} is the vaccine efficiency taking values from the interval $[0.4, 0.9]$. Secondly, since a vaccinated individual is less likely to develop symptoms than a non-vaccinated person, q_V is smaller than q. The nominal value has been chosen by using the related literature (see, e.g. [191, 192]). Thirdly, the probability of hospitalization is also different for the vaccinated and non-vaccinated cases [193, 194]. These specific values have been fine-tuned by studying the epidemiological data registered in Hungary. By analysing Hungarian statistical data, we have found that the other parameters of the two model parts can be chosen to be identical.

There are two new parameters in the model that were not introduced in the earlier model derived in [J1]. The first is σ, i.e. the size of the secondary symptom pool. This parameter influences the effectiveness of testing through equation (3.25). Predominantly, we assume that testing is based

Parameter		Interpretation	Value	
NV	V		NV	V
β		Transmission rate	0.75	
V_{eff}		Efficiency of vaccination	$0.4 - 0.9$	
α^{-1}		Latent period (days)	2.5	
ρ_{P}^{-1}		Pre-symptomatic infectious period (days)	3	
δ		Relative transmissibility of asymptomatic	0.8	
ρ_{A}^{-1}		Infectious period of asymptomatic (days)	4	
q	q_V	Prob. of developing symptoms	0.6	0.012
ρ_{I}^{-1}	ρ_{VI}^{-1}	Infectious period of symptomatic cases (days)	4	4
ρ_{Q}^{-1}	ρ_{VQ}^{-1}	Quarantine period (days)	4	4
η	η_{V}	Hospitalization probability of symptomatic cases	0.076	0.0152
h^{-1}		Average length of hospitalization (days)	10	
μ		Probability of fatal outcome, given hospitalization	0.145	
σ		Secondary symptom pool	0.001	
γ		Rate of vaccination	0.0025	
Π		Population size (Hungary)	9 800 000	

Table 3.4: Parameters and values for non-vaccinated (NV) and vaccinated (V) subjects, applied in the simulations

on the whole set of common symptoms of COVID-19. Taking a typical influenza epidemic as a baseline, we set $\sigma = 10^{-3}$ (equivalent to about 10000 individuals) in accordance with the average number of individuals developing similar symptoms without COVID-19 infection. By restricting the symptom set and considering more severe disease progression as a candidate for testing, this value gets smaller. A preliminary analysis of the impact of different σ values on the efficiency of testing is presented in [63].

The next important parameter is γ, which is the rate of vaccination. By analysing the Hungarian statistical data we have chosen for γ to represent a reduced intensity vaccination after the initial vaccination peak, between the lowest and highest values documented. The current value of γ, which is 0.0025, corresponds approximately to 2500 new vaccinated individuals per day.

Discretization

The control design procedure presented in the next section requires a discrete-time model. Therefore, the above equations were discretized using the fourth-order Runge-Kutta method with sampling time $T_s = 1$ day. Numerical simulations have been carried out with various input signals (v, κ) to verify that the discrete time model approximates the continuous dynamics with sufficient accuracy. The discrete time model is denoted by $F(\cdot)$, that is, the dynamical equations can be written in compact form as follows: $x(k+1) = F(x(k), v(k), \kappa(k))$.

3.2.2 Control policy design by nonlinear optimization

The aim of a mitigation strategy is to control the epidemic course such that the epidemic peak is reduced and the harmful effects of the disease caused by the virus are minimized. This can be achieved by keeping the population size in certain compartments under a predefined limit. For example, to avoid overwhelming healthcare capacity, compartment H is constrained from above by the maximum number of available hospital beds. Since the interventions (social distancing, testing, vaccination, etc.) have social and financial costs, the mitigation goals have to be achieved

by using the minimal necessary control actions. To meet all of these requirements, a constrained optimization problem can be formulated as follows:

$$\min_{\mathbf{v},\boldsymbol{\kappa}} \quad \frac{1}{\overline{v}^2}\sum_{k=1}^{N} v(k)^2 \tag{3.27a}$$

w.r.t.

$$x(i+1) = F(x(i), v(j(i)), \kappa(i)),\ x(0) = x_0 \tag{3.27b}$$

$$i = 0 \dots N+K-1 \tag{3.27c}$$

$$j(i) = \begin{cases} \lfloor i/L \rfloor & \text{if } i \leq N \\ \lfloor N/L \rfloor & \text{if } i > N \end{cases} \tag{3.27d}$$

$$\kappa(i) = 0, \quad \text{if } i > N \tag{3.27e}$$

$$0 \leq \kappa(i) \leq (x_{\mathrm{I}}(i) + x_{\mathrm{VI}}(i) + \sigma) \tag{3.27f}$$

$$0 \leq v(j(i)) \leq \overline{v} \tag{3.27g}$$

$$\sum_{k=0}^{N-1} \kappa(k) \leq \bar{\kappa} \tag{3.27h}$$

$$x_{\mathrm{H}} \leq \bar{x}_{\mathrm{H}} \tag{3.27i}$$

where the notations and variables are explained as follows:

- $\mathbf{v} = [v(0), \dots v(\lfloor N/L \rfloor)]$, $\boldsymbol{\kappa} = [\kappa(0), \dots \kappa(N-1)]$.
- N is the length of the time horizon the input sequence is computed over. Using the concept of model predictive control, the input sequence is determined over a finite time horizon. As k starts from 0, we obtain an input sequence for the time interval $[0, (N-1) \cdot T_s]$. In this section we take this step and analyze the result obtained. In closed-loop control, the process could be continued: the first element of the control sequence would be applied to the system for T_s time period, then the state vector x_1 would be measured (or estimated) and the optimization (3.27) restarts to obtain the next control sequence for time interval $[T_s, N \cdot T_s]$. Feedback control is necessary in real applications to attenuate modeling uncertainties and possible measurement noises. Now, we focus on the analysis and optimization-based design of the control policy; therefore, we stop after the first step and do not implement a full feedback controller.
- The cost function evaluates the cumulative squared norm of the first control input, which quantifies the non-pharmaceutical measures applied to the society. The aim is to find a control policy that applies only the minimal necessary restrictions. The squared norm of the inputs is normalized by $1/\overline{v}^2$, where $\overline{v}$ is the upper bound of v. $\overline{v}$ corresponds to the strictest measure, which is the total lockdown of the cities (see below). By this normalization, a unit cost is assigned to the total lockdown, so the control cost measures the stringency of the interventions relative to the strictest measure. Currently each control action $v(i)$ has the same weight in the cost function, but naturally it is possible to choose a different weighting strategy as well.
- K is the length of the safety time window. This is a short (a few weeks long) time interval following the control window, where the control input is not updated, but the constraints have to be satisfied. This prevents the optimization to simply improve the cost function by generating less effective (in our case, smaller) control actions at the end of the horizon.

Turning off the controller in the last few steps leads to a high increase in the constrained state variable, which can therefore easily exceed the limit right after leaving the control window. In our case, the control action in the safety time window is defined as follows: the first input is kept at its last (N-th) value, the second input (testing) is turned off, i.e. no test is performed after the control horizon.

- Constraint (3.27g) defines upper and lower bounds for control input v. Setting $v = 0$ corresponds to applying no intervention. The upper bound quantifies the effect of the strictest measure, i.e. the total lockdown of the cities. Based on [78], we have chosen $\bar{v} = 0.8$ for this upper bound.

- Constraint (3.27f) comes from the definition of κ: the number of tests carried out in a unit time interval cannot be larger than the total number of symptomatic individuals.

- Constraint (3.27h) describes the assumption that the total number of PCR tests available on the control horizon is a-priori fixed. This maximal value is denoted by $\bar{\kappa}$. The constraint prescribes that the number of all tests performed in the control period should not exceed $\bar{\kappa}$. With this constraint the optimization algorithm tries to find the optimal distribution of available test capacity.

- Parameter L and definition of index j. Since the first control input determines rules and restrictions that have to be performed by the society, it takes time to have an impact on the dynamics. Therefore, it is of no use to change the control input at each sampling instant. We therefore prescribe that v is updated only at every L-th time step.

- Constraint (3.27i) introduces an upper bound for the number of hospitalized patients. This is now $\bar{x}_{\mathrm{H}} = 10^{-3}$ corresponding to the maximal number of available hospital beds safely usable for COVID-treatment in Hungary (note: this is a value scaled with the total population Π, which corresponds to roughly 10.000 places in the hospitals).

- Note that there is no terminal constraint introduced for the final state $x(N)$. In a general MPC design this constraint is used to guarantee recursive feasibility of the optimization and the stability of the closed-loop system. In our case, this is not necessary for two reasons. First, we focus on the computation of the control policy and do not implement a feedback controller (see the second bullet point above). Second, in the numerical examples we will choose the control horizon N long enough to cover the entire "lifetime" of the epidemic: by the end of the control horizon the critical compartments ($SLPA$) will start emptying and the corresponding states converge to zero. The convergence to the origin follows from the structure of the model: the model does not contain feedback branches: the individuals migrate only forward from compartment S to compartments D and H.

The optimization problem to be solved is nonlinear and nonconvex. Finding a solution to it is challenging mainly due to the complexity of the dynamical model and the long control horizon. To make it easier to solve we take three simplification steps.

- First, state variables $\mathbf{R}$ and $\mathbf{D}$ do not affect the dynamics of the others, there are no constraints prescribed for them, and they do not appear in the cost. Therefore, these two state variables can be removed from the model. The reduced state vector and dynamical model will be denoted by $\tilde{x}$ and $\tilde{F}$, respectively.

- Second, instead of κ, we choose $\varphi = \kappa/(\mathbf{I} + x_{\mathrm{VI}} + \sigma)$ as the input variable. In this way, the rational term $1/(\mathbf{I} + x_{\mathrm{VI}} + \sigma)$ is removed from the optimization problem. To satisfy the constraints prescribed for κ, we first introduce an additional state variable z with the following discrete time dynamics: $z(i+1) = z(i) + \varphi(i) \cdot (\mathbf{I}(i) + x_{\mathrm{VI}}(i) + \sigma)$. Clearly, z integrates input κ, so $z(N-1) = \sum_{k=0}^{N-1} \kappa(i)$. Therefore, (3.27h) can be replaced by $z(N-1) \leq \bar{\kappa}$, which is also linear. Although changing the input variable involves a new state with polynomial dynamics, we have found that, this solution is still better from a computational point of view than leaving rational terms in the optimization problem. After determining input sequence φ, the actual control input κ can be obtained by using the formula $\kappa(i) = \varphi(j(i)) \cdot (\mathbf{I}(i) + x_{\mathrm{VI}}(i) + \sigma)$.
- The third modification we make is to replace the hard constraint (3.27i) with a soft one. For this, a new nonnegative decision variable ε is introduced and added to the right-hand side of (3.27i). This allows for a small violation of the constraint. Large values for ε are penalized in the cost by an additive term $c\varepsilon$, where $c > 0$ is a suitably chosen scaling factor. With the original hard constraint, the solver tends to run into infeasibility as x_H approaches its limit. Using the proposed soft constraint, this issue can be eliminated.
- Finally, to avoid oscillations in control input κ, we constrained φ to change only weekly, together with v. As $\mathbf{I}$ and x_{VI} still change daily, this constraint does not imply that κ remains constant for a week, but the control input is suitably smoothed out. The constraint can be interpreted as limiting the percentage of symptomatic patients tested in each week.

The final form of the optimization problem is summarized below.

$$\min_{\mathbf{v},\varphi} \quad \frac{1}{\bar{v}^2} \sum_{i=1}^{N} v(k)^2 + c\varepsilon \tag{3.28a}$$

w.r.t.

$$\begin{bmatrix} \tilde{x}(i+1) \\ z(i+1) \end{bmatrix} = \begin{bmatrix} \tilde{F}(\tilde{x}(i), v(j(i)), \varphi(j(i))) \\ z(i) + \varphi(j(i))(x_{\mathrm{I}}(i) + x_{\mathrm{VI}}(i) + \sigma) \end{bmatrix}, \tag{3.28b}$$

$$\tilde{x}(0) = \tilde{x}_0 \tag{3.28c}$$

$$i = 0 \dots N + K - 1 \tag{3.28d}$$

$$j(i) = \begin{cases} \lfloor i/L \rfloor & \text{if } i \leq N \\ \lfloor N/L \rfloor & \text{if } i > N \end{cases} \tag{3.28e}$$

$$\varphi(\lfloor N/L \rfloor) = 0 \tag{3.28f}$$

$$0 \leq \varphi(j(i)) \leq 1 \tag{3.28g}$$

$$0 \leq v(j(i)) \leq \bar{v} \tag{3.28h}$$

$$z(N-1) \leq \bar{\kappa} \tag{3.28i}$$

$$x_{\mathrm{H}} \leq \bar{x}_{\mathrm{H}} + \varepsilon, \quad \varepsilon \geq 0 \tag{3.28j}$$

The above problem can be solved in a numerically stable way using the BARON solver (presented in subsection 2.6.3), for various parameters and initial conditions (in a reasonable range).

3.2.3 Case studies

In this section we present control strategies for different epidemic scenarios in order to demonstrate the applicability of the predictive algorithm and draw conclusions about optimal manage-

ment planning. Three main scenarios are considered: first, the effect of vaccination is examined in cases of different vaccine efficiency (subsection 3.2.3), then the effectiveness of the symptom-based testing as a control input is investigated (subsection 3.2.3). Finally, we analyse the effect of changing the symptom set, on which the testing is based 3.2.3). In all three scenarios the control horizon is $N = 168$ days, the safety period is $K = 30$ days (1 month). We constrain the control input v to change only weekly, i.e. $L = 7$. The initial state x_0 for every simulation test is chosen as follows:

$$\mathbf{L}(0) = 5000/\Pi,\ \mathbf{P}(0) = 4000/\Pi,\ \mathbf{A}(0) = 2000/\Pi, \tag{3.29a}$$

$$\mathbf{I}(0) = 100/\Pi,\ \mathbf{H}(0) = 200/\Pi,\ x_{\mathrm{Q}}(0) = 100/\Pi, \tag{3.29b}$$

$$x_{\mathrm{VL}}(0) = 200/\Pi,\ x_{\mathrm{VP}}(0) = 50/\Pi, \tag{3.29c}$$

$$x_{\mathrm{VI}}(0) = x_{\mathrm{VQ}}(0) = 0, \tag{3.29d}$$

$$\mathbf{R}(0) = \mathbf{D}(0) = 0, \tag{3.29e}$$

$$\mathbf{V}(0) = \text{depends on the scenario}, \tag{3.29f}$$

$$\mathbf{S}(0) = 1 - \text{"sum of the other states"} \tag{3.29g}$$

In the cost function the coefficient c penalizing the soft constraint violation is chosen to be $c = 1000$. The optimization problem has been formulated in CasADi [125] and solved by the off-the-shelf nonlinear solver IpOpt [126]. The computations have been performed on a Dell Vostro 5471 laptop equipped with an Intel i7 processor and 8GB RAM. On average, one simulation takes 1-2 minutes to complete. The resulting control input sequence is tested on the continuous time model in open loop configuration by using the ode45 solver of Matlab.

Testing strategies for different states of vaccination

In this scenario the optimization problem (3.28) was solved with different initial values for x_V and V_{eff}. Specifically, $x_{\mathrm{V}}(0) \in \{0.2, 0.3, 0.4, 0.5, 0.6, 0.7, 0.8\}$ and $V_{\mathrm{eff}} \in \{0.4, 0.5, 0.6, 0.7, 0.8, 0.9\}$. We examined the impact of the initial vaccination coverage ($x_{\mathrm{V}}(0)$) and vaccine effectiveness on the control strategy and the course of the epidemic. In all cases the optimization returns a feasible solution, i.e. all constraints can be satisfied. The values of the cost function for every studied $(x_{\mathrm{V}}(0), V_{\mathrm{eff}})$ pairs are shown in Fig. 3.15. It can be seen that initial vaccination is an important factor, as it fundamentally determines the course of the epidemic. On the other hand, choosing an efficient vaccine is also essential: increasing the efficiency by 0.1 can reduce the total cost to its fifth: see e.g. the row corresponding to $x_{\mathrm{V}}(0) = 5 \cdot 10^6$. The second (bottom) figure of Fig. 3.15 shows that the total cost depends approximately linearly on both variables.

Figs. 3.16 and 3.17 plot the state evolution and corresponding control inputs in two representative cases: First, the optimization was carried out with a fixed vaccine efficiency of 0.8 and different $x_V(0)$ values (Fig. 3.16). The significant effect of the ratio of vaccinated people is clear from the plots. With an approximately 60% ratio of vaccinated, we could prescribe a lower constraint for x_{H} by setting $\bar{H} = 5 \cdot 10^{-4}$. Still, a medium-intensity testing is enough to keep the number of hospitalized people well under the predefined limit, and there is no need for further restrictions. Conversely, a low rate of vaccination requires strict measures and intensive testing in parallel to keep the main constraints.

Secondly, $x_V(0)$ was fixed and V_{eff} was changed (Fig. 3.17). As it can be expected, a less efficient vaccine implies the need for significantly stricter measures. Note that in this scenario the upper bound of hospitalized people is reached, and the majority of the available tests are used in all cases. Comparing these results with the previous ones suggests that a high vaccination coverage

is definitely preferred even with a less efficient vaccine.

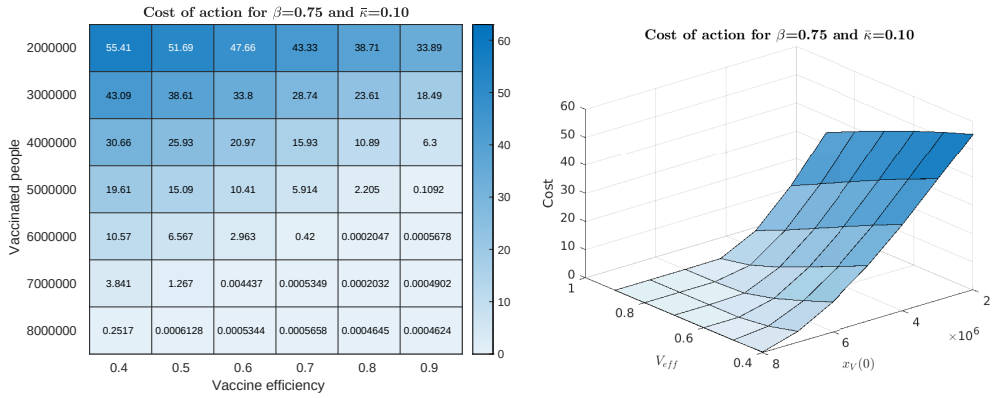

Figure 3.15: Cost of intervention in function of initially vaccinated people and vaccine efficiency (left), with $\beta = 0.75$ (virus variant delta) and $\bar{\kappa} = 0.1$, ie. approximately one million tests available for the length of the control horizon ($N = 168$ days). Three-dimensional plot of the cost of intervention (right) illustrating the convexity and close to linear nature of the function.

In addition, we have run all simulations without precise planning of κ in order to see how important it is to systematically design the testing strategy. The results are plotted in Figs. 3.16 and 3.17 by dashed lines. In these scenarios we have designed κ to be approximately constant when maximal testing intensity is reached, and prescribed that the majority of the tests should be used (if possible, i.e. there are sufficient number of infected) by the end of the control horizon. It is visible that the price of not carefully planned testing can be that significantly stricter measures have to be applied to the society. The difference is particularly striking at a medium vaccination coverage, i.e. when $x_{\mathrm{V}}(0) = 0.6$. In this case the total intervention cost can be halved by a carefully planned test strategy. Besides the reduction of the total cost, the high peaks of control input v are avoided as well. This implies that extremely strict interventions (such as the closing of schools or a total lockdown) could be avoided by thoughtful use of testing capacity. It is important to note that the above results were obtained by assuming the least strict quarantine policy when only the officially recorded infected are quarantined.

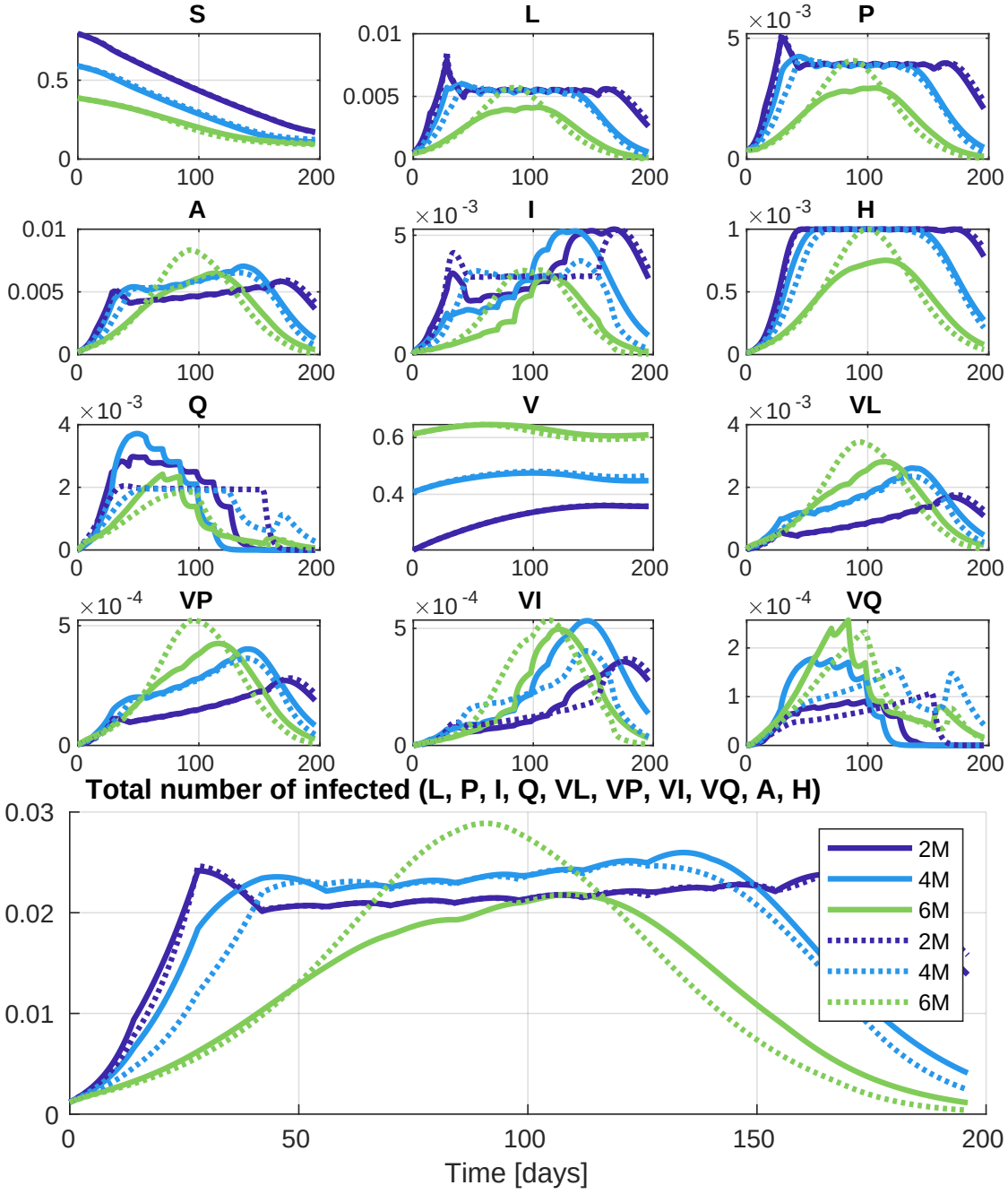

Figure 3.16a: Representative figure of the model states and total number of infections, showing the effect of the initial value of the number of vaccinated people, with $\beta = 0.75$, $\bar{\kappa} = 0.1$, and $V_{\text{eff}} = 0.8$. Colors represent values $\mathbf{V}(0) = 2 \cdot 10^6$ (dark blue), $\mathbf{V}(0) = 4 \cdot 10^6$ (light blue) and $\mathbf{V}(0) = 6 \cdot 10^6$ (light green). Dotted lines show the trajectories for the same scenarios, but with approximately constant (non-optimized) κ.

.

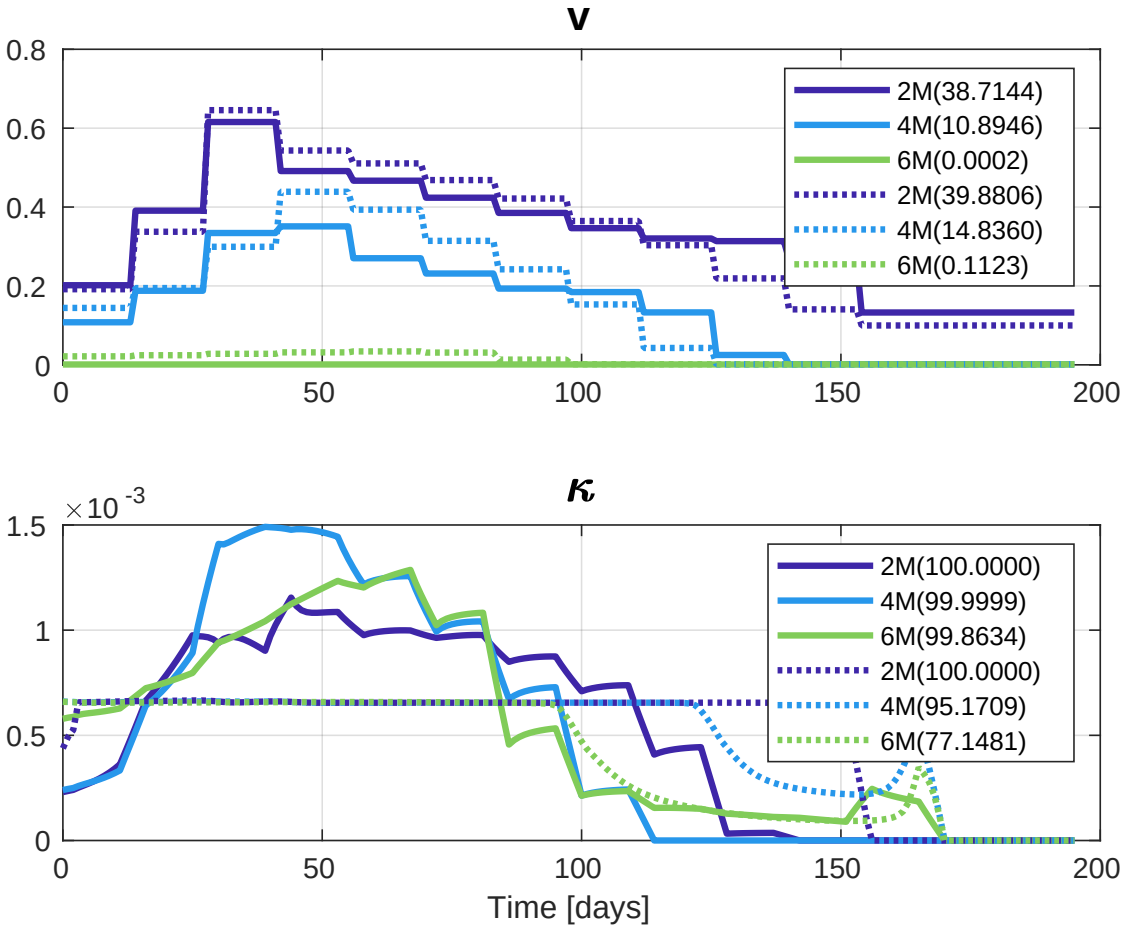

Figure 3.16b: Representative figure of the control inputs, showing the effect of the initial value of the number of vaccinated people, with $\beta = 0.75$, $\bar{\kappa} = 0.1$, and $V_{\text{eff}} = 0.8$. Colors represent values $\mathbf{V}(0) = 2{\cdot}10^6$ (dark blue), $\mathbf{V}(0) = 4 \cdot 10^6$ (light blue) and $\mathbf{V}(0) = 6 \cdot 10^6$ (light green). Dotted lines show the optimal inputs for the same scenarios, but with predefined suboptimal testing strategies (additional constraints on κ). We can see the percentage of tests used (compared to the number of tests available) in the legend of the bottom figure. Control costs are shown in parentheses in the legend of the control input diagram v.

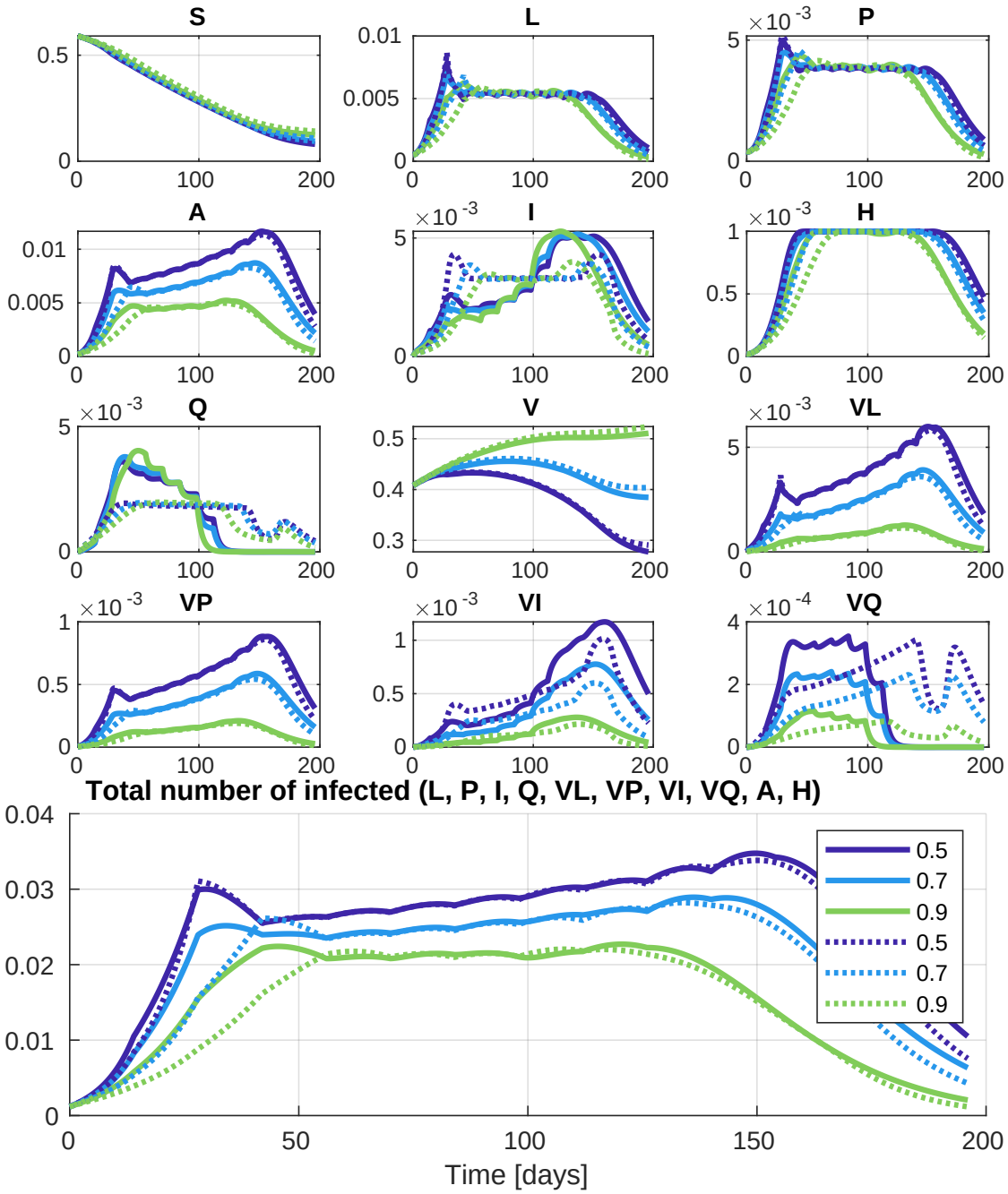

Figure 3.17a: Representative figure of the model states and number of infections, showing the effect of vaccine efficiency with $\beta = 0.75$, $\bar{\kappa} = 0.1$, and number of initially vaccinated people $\mathbf{V}(0) = 4 \cdot 10^6$ (appr. 40% of the population). Colors represent values $V_{\text{eff}} = 0.5$ (dark blue), $V_{\text{eff}} = 0.7$ (light blue) and $V_{\text{eff}} = 0.9$ (light green). Dotted lines show the trajectories for the same scenarios, but with approximately constant (non-optimized) κ.

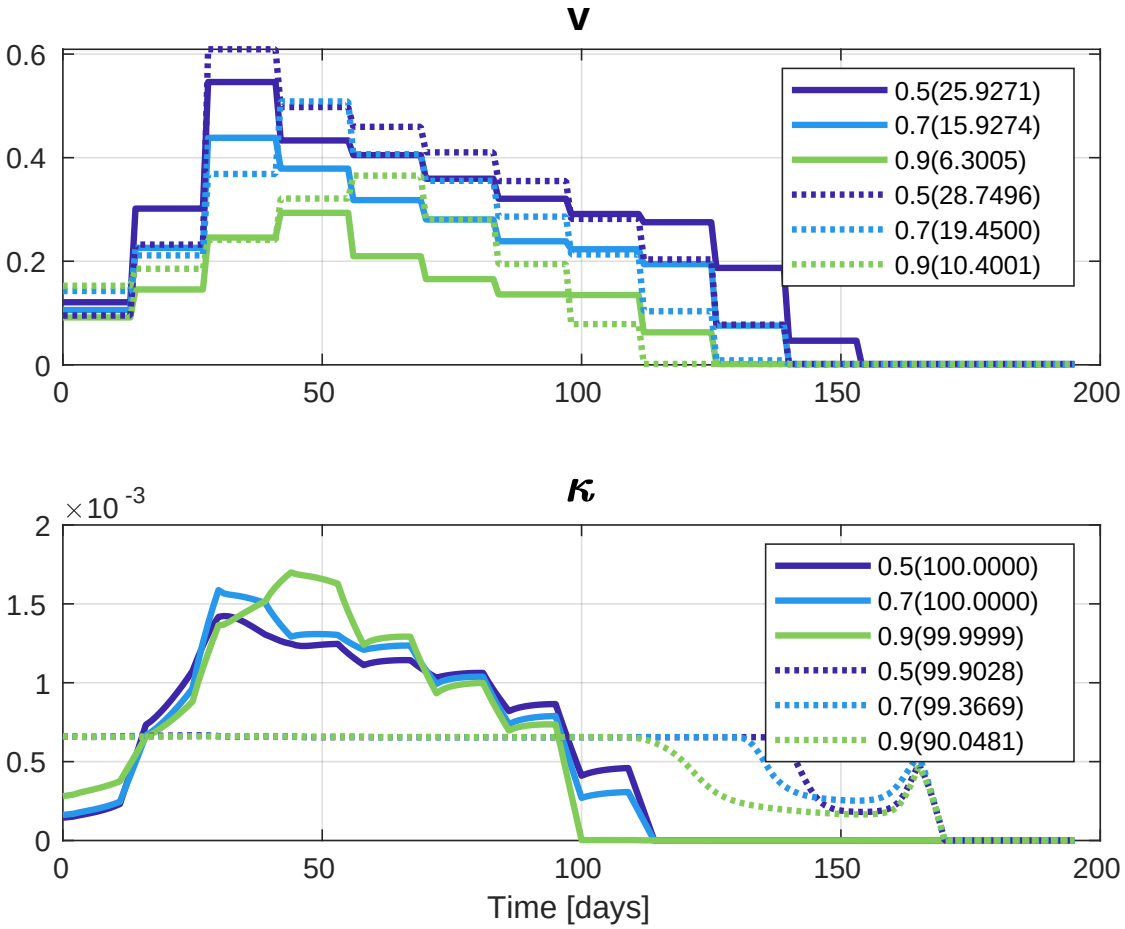

Figure 3.17b: Representative figure of the control inputs, showing the effect of vaccine efficiency with $\beta = 0.75$, $\bar{\kappa} = 0.1$, and number of initially vaccinated people $\mathbf{V}(0) = 4{\cdot}10^6$ (appr. 40% of the population). Colors represent values $V_{\text{eff}} = 0.5$ (dark blue), $V_{\text{eff}} = 0.7$ (light blue) and $V_{\text{eff}} = 0.9$ (light green). Dotted lines show the optimal inputs for the same scenarios, but with predefined suboptimal testing strategies (additional constraints on κ).We can see the percentage of tests used (compared to the number of tests available) in the legend of the bottom figure. Control costs are shown in parentheses in the legend of the control input diagram v.

Compensating less efficient vaccination by testing

This scenario focuses on the potential usefulness of symptom-based testing. The same set of optimization problems as in the previous section is solved with different upper bounds for the testing capacity. The values of the cost function obtained in the examined 2×36 simulation cases are collected in Fig. 3.18. We examined whether strict non-pharmaceutical measures (v) induced by the use of a less efficient vaccine can be alleviated by applying more intensive testing. By analysing the results in Fig. 3.18 it can be seen that testing is an effective auxiliary control input: if the test capacity is high enough, then even a really low (about 20%) vaccination coverage with an average vaccine efficiency can be successfully compensated by intensive testing and quarantining.

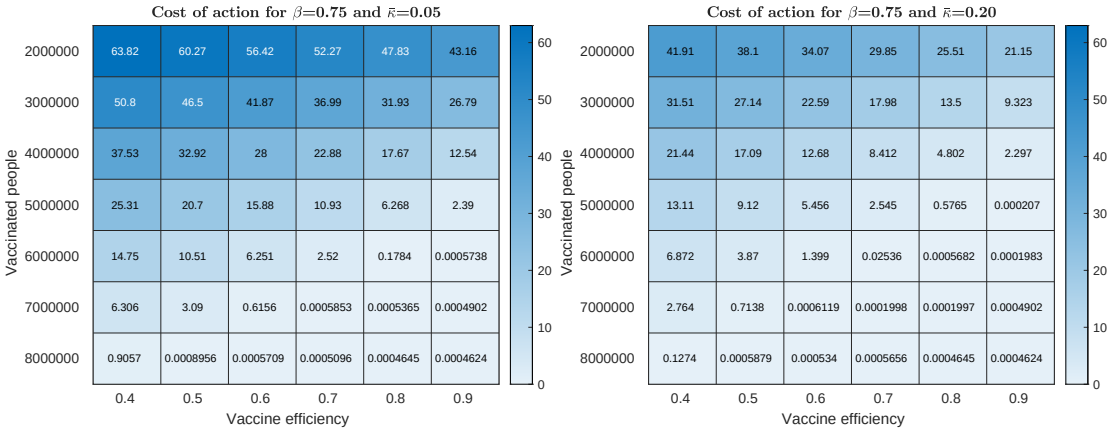

Figure 3.18: Comparison of the values of the cost function, if different number of tests are available: $\bar{\kappa} = 0.05$ (left) and $\bar{\kappa} = 0.2$ (right). Properly divided over the length of the horizon, a higher number of tests can significantly reduce the cost, and thus compensate for a less efficient vaccine.

Fig. 3.19 presents the control input and state trajectories in two particular cases selected from the simulations collected in Fig. 3.18. The first case corresponds to initial values $x_{\mathrm{V}}(0) = 0.4$, $V_{\mathrm{eff}} = 0.5$, $\bar{\kappa} = 0.2$, i.e. a low-efficiency vaccine is applied but a large number of tests is available. In the second case, the initial value of the vaccinated compartment is the same ($x_{\mathrm{V}}(0) = 0.4$), but $V_{\mathrm{eff}} = 0.8$ and $\bar{\kappa} = 0.05$, i.e. an efficient vaccine is used but the testing capacity is limited. It can be seen that the values of the cost function in the two cases are very close to each other (0.0558 in the first, and 0.0516 in the second case), i.e. the strictness of the social distancing measures (control input v) is similar. Although a less effective vaccine would result in stricter interventions, this can be avoided by allowing more intensive testing.

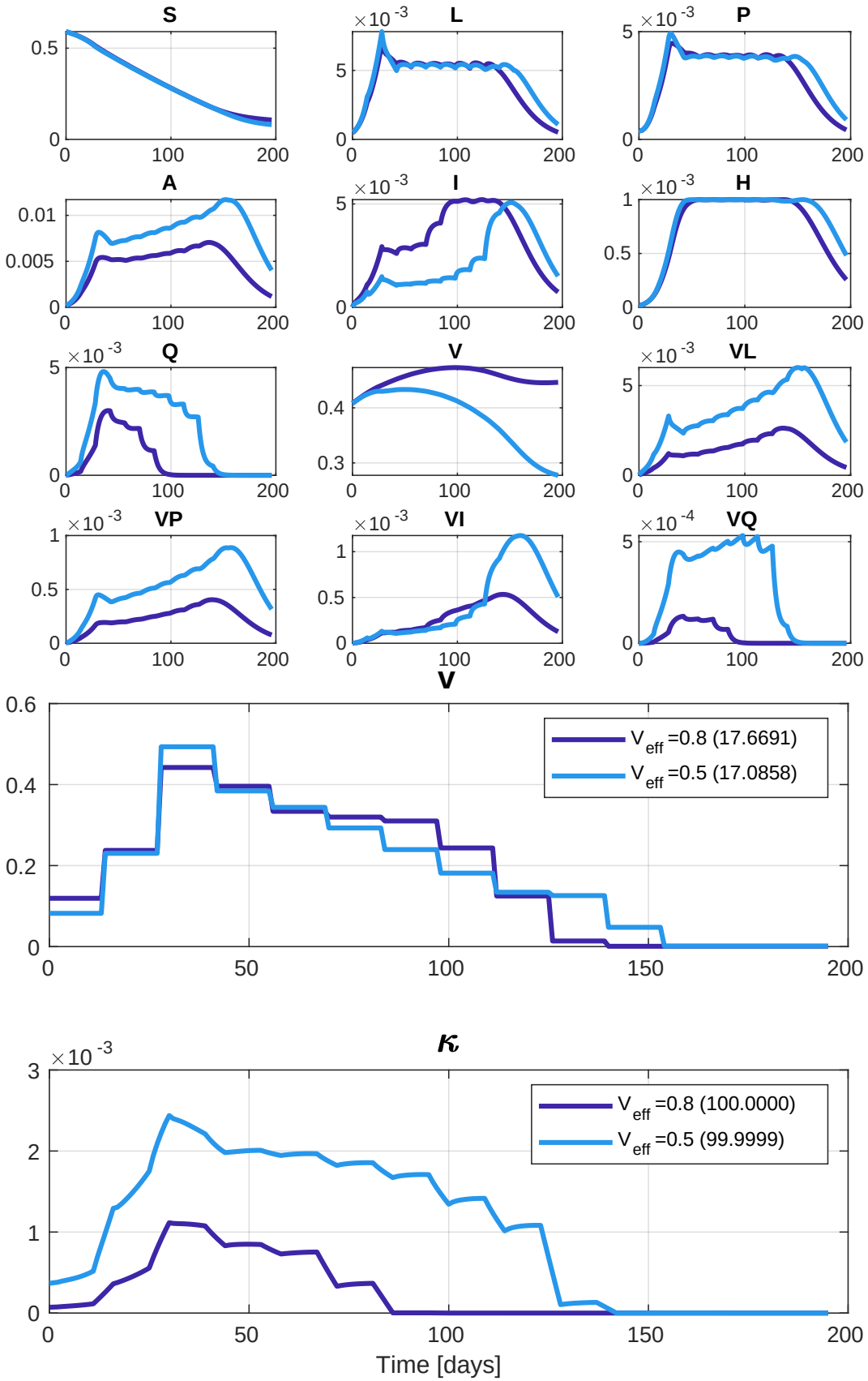

Figure 3.19: Comparison of model states (top) and control inputs (bottom) for two scenarios with similar intervention cost: strong vaccine and low amount of tests ($V_{\text{eff}} = 0.8$, $\bar{\kappa} = 0.05$, dark blue) against weak vaccine and high amount of tests ($V_{\text{eff}} = 0.5$, $\bar{\kappa} = 0.2$, light blue). Control costs are shown in parentheses in the figure of v, next to the V_{eff} parameter values.

Testing strategies by modifying the indicator symptom

The proposed model is readily capable of studying various testing strategies characterized by the choice of the indicator symptom as long as the assumption holds that hospitalization is unlikely for other symptomatic infections. A change from the whole set of common symptoms to a more severe disease course will affect the model parametrization in numerous ways. On the positive side, the secondary symptom pool shrinks, hence, the raw testing efficacy is increased. Nevertheless, by channeling more individuals to the A branch will increase its relative transmissibility and average infectious period. Moreover, that branch is not subject to testing, hence, more infections can stay potentially undetected. Finally, the infected individuals in the (indicator) symptomatic I branch have an increased possibility of hospitalization corresponding to a more severe disease course.

We investigated a plausible scenario by introducing a new parameter ζ to the model capturing the probability that a symptomatic infected displays the indicator symptom. The baseline corresponding to the parametrization in Table 3.4 is $\zeta = 1$. As in the model q itself represents the probability of developing an indicator symptom, and η is the probability of hospitalization thereafter, it is straightforward to see that they are directly and inversely proportional to ζ, respectively. The change in relative infectivity δ may be obtained as a weighted average of the baseline δ and 1 (the latter being the relative infectivity of the I branch wrt. to itself) with weights $(1-q)/(1-q\zeta)$ and $(q-q\zeta)/(1-q\zeta)$ referring to the original A branch and the newly redirected individuals, respectively. The effect on the infectious period of the A branch ρ_{A} may be treated analogously. Summarizing these basic considerations led to the following adjustment of the aforementioned parameters as functions of ζ.

$$q(\zeta) = q \cdot \zeta, \tag{3.30a}$$

$$\eta(\zeta) = \eta/\zeta, \tag{3.30b}$$

$$\delta(\zeta) = \frac{\delta(1-q) + q(1-\zeta)}{1 - q \cdot \zeta}, \tag{3.30c}$$

$$\rho_{\mathrm{A}}(\zeta) = \frac{\rho_{\mathrm{A}}(1-q) + \frac{1}{\rho_{\mathrm{P}}^{-1}+\rho_{\mathrm{I}}^{-1}} q(1-\zeta)}{1 - q \cdot \zeta}, \tag{3.30d}$$

where $q, \eta, \delta, \rho_{\mathrm{A}}, \rho_{\mathrm{P}}, \rho_{\mathrm{I}}$ on the right-hand side of the equations refer to the baseline values presented in Table 3.4. We assumed that a change of $\zeta = 0.75$ results in the shrinking of the secondary symptom pool σ from 10^{-3} to 10^{-4} and collected the results of the simulations in Fig. 3.20. Comparing with Fig. 3.16, we observe a potential for overall cost reduction due to a more optimal choice of the indicator symptom.

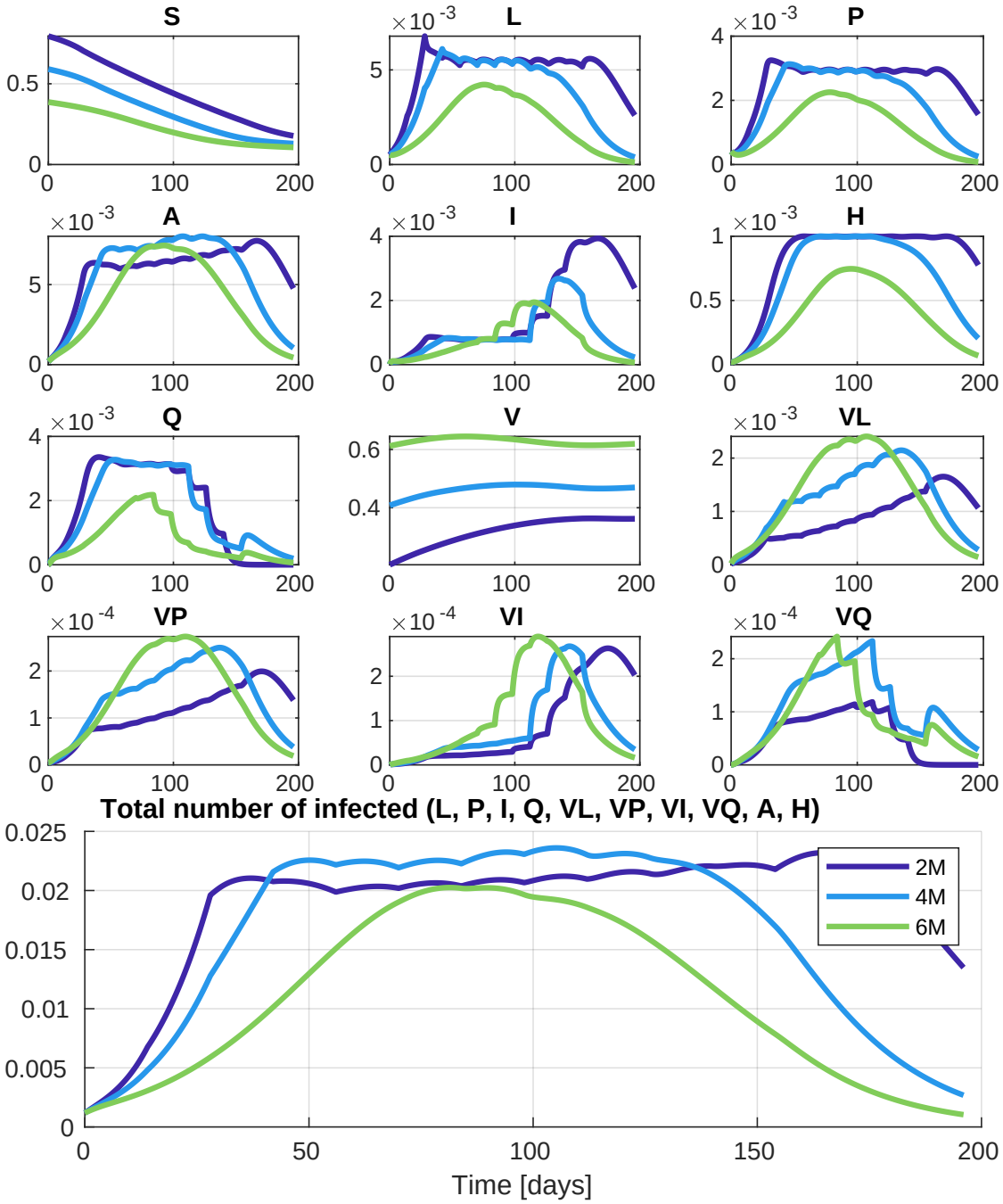

Figure 3.20a: Representative figure of the model states and total number of infections, showing the effect of the initial value of the number of vaccinated people using an altered indicator symptom characterized by $\zeta = 0.75$ and $\sigma = 10^{-4}$ with parameters $\beta = 0.75$, $\bar{\kappa} = 0.1$, and $V_{\text{eff}} = 0.8$. Colors represent values $\mathbf{V}(0) = 2 \cdot 10^6$ (dark blue), $\mathbf{V}(0) = 4 \cdot 10^6$ (light blue) and $\mathbf{V}(0) = 6 \cdot 10^6$ (light green).

.

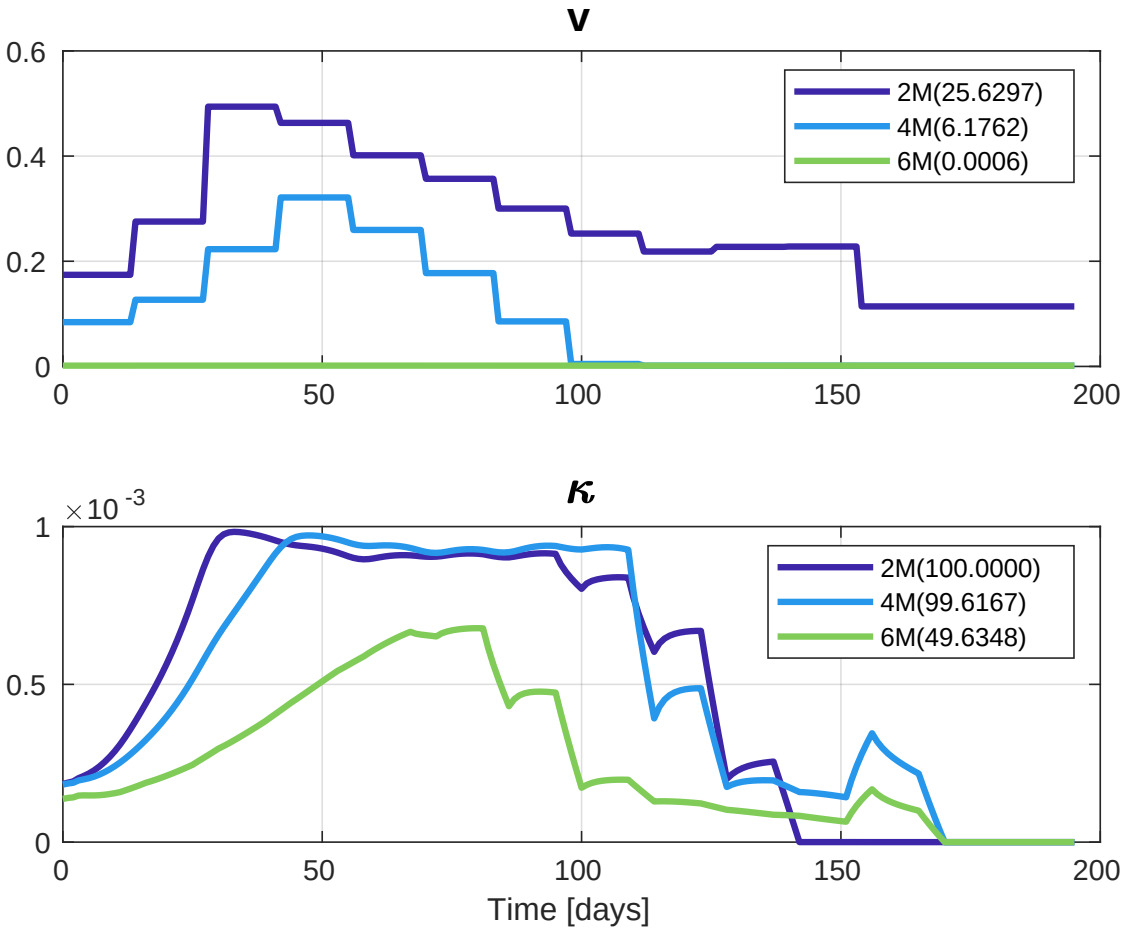

Figure 3.20b: Representative figure of the control inputs, showing the effect of the initial value of the number of vaccinated people using an altered indicator symptom characterized by $\zeta = 0.75$ and $\sigma = 10^{-4}$ with parameters $\beta = 0.75$, $\bar{\kappa} = 0.1$, and $V_{\text{eff}} = 0.8$. Colors represent values $\mathbf{V}(0) = 2 \cdot 10^6$ (dark blue), $\mathbf{V}(0) = 4 \cdot 10^6$ (light blue) and $\mathbf{V}(0) = 6 \cdot 10^6$ (light green). We can see the percentage of tests used (compared to the number of tests available) in the legend of the bottom figure. Control costs are shown in parentheses in the legend of the control input diagram v.

3.3 Summary

This chapter presented a control theoretic approach for dynamic epidemic management, with the primary purpose of controlling the spread of the COVID-19 pandemic.

Based on [J1], Section 3.1 introduced a detailed 8 compartment epidemic model, given in the form of a set of nonlinear ODEs, incorporating the specific elements of COVID-19's transmission dynamics. The model parameters are determined from the literature and the epidemic data recorded in Hungary between March and May, 2020. The assumed manipulable control input with strict upper and lower bounds is the time-varying transmission rate affected by different restrictive measures planned and implemented by the authorities to slow down disease spread. As a direct continuation, Section 3.2 (based on [J2]) further extends the model by the integration of alternative intervention measures. The resulting 14-compartment structure includes a simplified model of the vaccination and introduces the testing effort as an additional manipulable input, defining a multivariable nonlinear control problem.

The central methodological contribution is the application of MPC to this problem, using a formulation that supports complex logical constraints and predefined discrete intervention levels, specified using temporal logic expressions. Generally, the design goal is the minimization of the unwanted effects of the restrictive measures and the number of fatalities, while the constraints are focused on the maximum tolerable burden of the healthcare system and the limited nature of resources (e.g. number of available tests). These somewhat contradicting aspects are translated to a constrained mixed-integer nonlinear programming (MINLP) problem, handled using available numerical solvers. To address the realistic situation when not all state variables are observed continuously, a state observer is proposed using the theory of LPV systems, assuming that only the number of hospitalized and deceased patients are known on a daily basis.

In Section 3.1, five control scenarios were shown and analyzed with different goals and assumptions. The scenarios cover the well-known cases of mitigation, when the direct cost of the intervention (control) is minimized with a constraint on healthcare capacity, and also suppression, where the cost is assigned to infection, hospitalization and fatalities. The evolution of the time-varying effective reproduction number R_t - which has become a widely-used, standard measure of the current epidemic situation during the COVID-19 pandemic - is monitored across all of the simulations, providing a comparable measure between the different strategies.

For suppression, we see that very strict measures (lockdown) are necessary initially, and they can be slowly relaxed later. This corresponds to a sharp drop in R_t to levels way below one. On the other hand, for mitigation, the stringency of the control is increased much more slowly, and maximized at a moderate level, while R_t is being kept around the critical value 1 for a long time period. It is worthwhile to note that the computed control inputs (both for the mitigation and suppression strategies) show a striking resemblance to real-world government responses in different countries, as measured by publicly available stringency indices.

Justified by the computational results, the study underscores that an early intervention is of key importance in satisfying the control goals and constraints. The feasibility analysis corresponding to the model predictive control problem is also useful to assess the practical (physical, biological) limits of the planned interventions and identify late actions.

The case studies have shown, that the proposed model has numerically weakly observable regions due to the possible different orders of magnitudes of the susceptible and the infected population. However, the numerical simulations demonstrate, that even in this case a suitably accurate state reconstruction is feasible if the susceptible population (which is a scheduling parameter in the

state observer) can be regularly estimated. In practice, this underlines the importance of large scale serological surveys, which can significantly improve the real-time in-silico estimation of the other, directly unmeasurable states.

For a more realistic control setup, output feedback design case (i.e., the combination of the controller and observer) was also examined through several simulations assuming uncertainties in selected parameters.

In Section 3.2, several scenarios have been studied with different vaccination coverages, different possible vaccine efficiencies and various choices of the indicator symptom. The obtained computation results have clearly shown that the integrated design can efficiently reduce the severity of non-pharmaceutical measures. It has also been shown that reduced vaccine efficiency or a lower vaccine coverage can be successfully compensated by appropriately scheduled testing. Finally, the effect of changing the indicator symptoms is investigated. It has been shown, that careful selection of the symptom set can further enhance the overall cost reduction. These results clearly prove that testing can be an important auxiliary control input in pandemic management even if the available number of tests is limited.

From today's perspective, it must be emphasized, that the proposed approach is able to directly handle predefined discrete levels of restrictions. It was shown later (e.g. in [90]), that these prescribed levels can be subsequently mapped to actual, real-world interventions, paving the way for effective, realistic control applications.

Furthermore, it is worth to mention, that [J1], published in the August of 2020, accurately predicted the second COVID-19 wave of Hungary, quickly emerging after the strict interventions (corresponding to a suppression strategy) were lifted around the end of the summer.

Overall, Section 3.1 underlines the importance of early and decisive action, the benefits of regular, robust, wide-scale monitoring of the situation, and the increased costs and limits of late interventions. Through computational experiments, Section 3.2 shows that dynamically optimizing testing strategies can significantly reduce the need for stringent non-pharmaceutical interventions while still achieving comparable public healthcare goals. Altogether, this chapter illustrates how control-theoretic tools can be effectively applied to achieve cost-effective and long term sustainable epidemic responses: the described methodologies offer a practical framework, tested on real-world epidemiological data, that due to its flexible design can be easily tuned, extended and adapted for new types of pathogens and pandemics of the future.

Chapter 4

Trajectory reconstruction of nonlinear epidemic models

This chapter presents the second pillar of the nonlinear analysis and control framework built throughout this thesis, containing two dynamic model-based robust solutions for the accurate estimation and reconstruction of unmeasurable states and past trajectories of nonnegative compartmental systems. The contributions presented here were published in [J3] (2022) and [J4] (2025), and illustrate the effectiveness of two completely different methodologies on real-world epidemic data measured in different European countries during the COVID-19 pandemic. Preliminary studies were also published in [C1–C4].

In the first study [J3], a generic optimization-based approach is proposed to estimate the time-dependent quantities of stochastic nonlinear models by reformulating the reconstruction problem as a stochastic nonlinear model predictive control computation. The unknown inputs and parameters, approximated by Gaussian distributions, are searched as functions of the uncertain states, such that the model output follows the previous measurements. While the results come at the cost of solving a computationally intensive optimization problem, the obtained expected values and variances provide both an estimation for the unknown data and the uncertainty of the estimation itself.

In the second paper [J4] a suboptimal, but robust and computationally inexpensive, real-time solution is provided, where the estimates can be computed by simply simulating the trajectories of a feedback-controlled compartmental system. The reconstruction problem is again reformulated as a control scenario, however, in this case it is solved by a robustified feedback-linearization based asymptotic output tracking controller, constructed for a simplified epidemic model. The study explores the performance of this approach through multiple simulations in a highly realistic setup, where inaccurate output measurements, uncertain parameters and serious model mismatch must be taken into account.

4.1 Optimization-based stochastic model-predictive control

In this section, a model-based method is proposed for the reconstruction of not directly measured epidemiological data. To solve this task, a generic optimization-based approach is developed to compute unknown time-dependent quantities (such as states, inputs, and parameters) of discrete-time stochastic nonlinear models using a sequence of output measurements. The problem is reformulated as a stochastic nonlinear model predictive control computation, where the unknown inputs and parameters are searched as functions of the uncertain states, such that the model output tracks the observations. The unknown data are approximated by Gaussian distributions, where the expected value and variances have to be determined.

The predictive control problem is solved over a relatively long time window in three steps. First the expected trajectories of the unknown quantities are approximated through a nonlinear deterministic problem. In the next step the expected trajectories are fixed and the corresponding variances are computed using closed-form expressions. Finally, the obtained mean and variance values are used as an initial guess to solve the stochastic control problem.

To reduce the estimated uncertainty of the computed states, a closed-loop input policy is considered during the optimization, where the state-dependent gain values are determined heuristically. The applicability of the approach is illustrated through the estimation of the epidemiological data of the second and third COVID-19 wave of the pandemic in Hungary. To describe the epidemic spread, we use a slightly modified version of the previously published and validated compartmental model, in which the vaccination process is taken into account. The mean and the variance of the unknown data (e.g., the number of susceptible, infected, or recovered people) are estimated using only the daily number of hospitalized patients. The problem is reformulated as a finite horizon predictive control problem, where the unknown time-dependent parameter, the daily transmission rate of the disease, is computed such that the expected value of the computed number of hospitalized patients fits the truly observed data as much as possible.

Notations and abbreviations

Due to the increased need of variables for the more detailed probabilistic computations, the notations applied in this section slightly differ from the rest of this thesis. For clarification, a full explanation is provided below. All random variables are distinguished from the deterministic variables in notation by the accent $\hat{\bullet}$. Namely, $\hat{x}$ is a random variable, whereas, x is deterministic. When $\hat{x}$ is normally distributed with expected value μ and variance Σ, we write that $\hat{x} \sim \mathcal{N}(\mu, \Sigma)$. When $\hat{x} \sim \mathcal{N}(\mu, \sigma^2)$ is a scalar-valued Gaussian variable, the confidence intervals $\mu \pm 1\sigma = [\mu - 1\sigma, \mu + 1\sigma]$ and $\mu \pm 2\sigma = [\mu - 2\sigma, \mu + 2\sigma]$ of probability levels 68.2% and 95.4% are called the 1σ and 2σ confidence intervals, respectively. The value of a time series $x : \{0, 1, \dots\} \to \mathbb{R}^n$ at time instant k is denoted by x_k. Each constant or variable, which denotes a given number of people is denoted by a boldface letter, e.g., $\mathbf{N}$ constitutes the number or people in a community or the population of a country.. When $A \in \mathbb{R}^{n \times m}$ is a matrix, $\mathrm{He}\{A\}$ stands for $A^\top + A$, where $A^\top$ is the transposition of A. Let $x = (x_1, x_2, \dots, x_n)$ denote $x = \begin{pmatrix} x_1^\top & x_2^\top & \dots & x_n^\top \end{pmatrix}^\top$. The matrix-valued functions $\frac{\partial f}{\partial x} : \mathbb{R}^{n+m} \to \mathbb{R}^{p \times n}$ and $\frac{\partial f}{\partial (x,y)} : \mathbb{R}^{n+m} \to \mathbb{R}^{p \times (n+m)}$ (with arguments $(x, y) \in \mathbb{R}^{n+m}$) denote the Jacobian of function $f : \mathbb{R}^{n+m} \to \mathbb{R}^p$ with respect to (w.r.t.) $x \in \mathbb{R}^n$ and $(x, y) \in \mathbb{R}^{n+m}$, respectively. Furthermore, the value of $\frac{\partial f}{\partial x}$ at $x_0 \in \mathbb{R}^n$ and $y_0 \in \mathbb{R}^m$ is referred to as $\frac{\partial f}{\partial x}(x_0, y_0) \in \mathbb{R}^{p \times n}$. The Euclidean norm of a vector $x \in \mathbb{R}^n$ is $\|x\|$, whereas, the weighted norm of x w.r.t. the symmetric and positive definite matrix Q is referred to as $\|x\|_Q$, namely, $\|x\|_Q^2 = x^\top Q\, x$. Finally, let $\mathbb{I}_a^b = \{a, a+1, \dots, b\}$ denote the set of integers between a and b.

4.1.1 Compartmental model of the spread of the COVID-19

Compartments and transitions of the augmented model

In this part, the compartmental model used for describing the evolution of the epidemic is presented, reiterating the the original 8-compartment version presented in section 3.1.1, and underlining the key modification performed in it.

The original model divides the population of **N** individuals into eight classes, representing the different stages of the illness. The compartments correspond to the following subsets/groups of the population: susceptible individuals (**S**), infected people in the latent (**L**) and the pre-symptomatic (**P**) phases, infected people in the main sequence of the disease (**A**, **I**), infected people who need hospital treatment (**H**), finally, the recovered (**R**) and deceased (**D**) people. The main phase of the disease is further divided to those who remain asymptomatic (**A**), and those who produce symptoms (**I**).

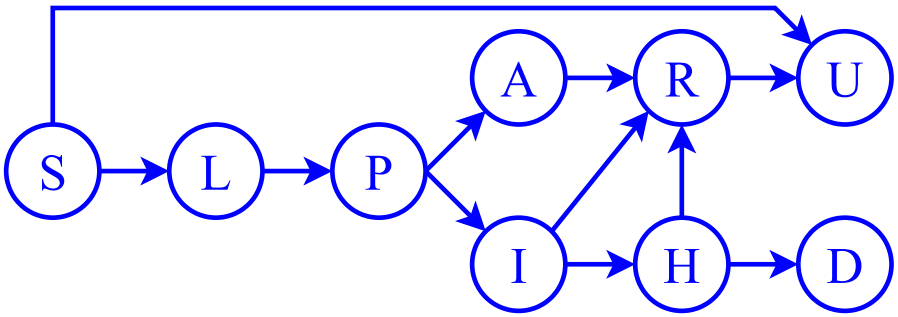

Figure 4.1: Transition graph of the epidemic model. Compartments and transitions are represented by the nodes and edges respectively.

In this section, this is complemented with a new compartment (**U**) comprising all individuals who became immune through vaccination. The members of this compartment are governed by the daily number of vaccinated people (**V**), treated as an external, uncontrollable input of the system, the value of which is obtained from published governmental data.

A discrete-time (DT) version of the augmented continuous-time model is obtained through the explicit Euler method with a 1-day long sampling period. The dynamic equations are given as follows:

$$
\begin{cases}
\mathbf{S}_{k+1} = \mathbf{S}_k - \beta_k\,(\mathbf{P}_k{+}\mathbf{I}_k{+}\delta\mathbf{A}_k)\,\mathbf{S}_k/\mathbf{N} - \nu\,\frac{\mathbf{S}_k}{\mathbf{S}_k{+}\mathbf{R}_k}\mathbf{V}_k, & (4.1a)\\
\mathbf{L}_{k+1} = \mathbf{L}_k + \beta_k\,(\mathbf{P}_k{+}\mathbf{I}_k{+}\delta\mathbf{A}_k)\,\mathbf{S}_k/\mathbf{N} - \alpha\,\mathbf{L}_k, & (4.1b)\\
\mathbf{P}_{k+1} = \mathbf{P}_k + \alpha\,\mathbf{L}_k - \pi\,\mathbf{P}_k, & (4.1c)\\
\mathbf{I}_{k+1} = \mathbf{I}_k + \gamma\,\pi\,\mathbf{P}_k - \rho_I\mathbf{I}_k, & (4.1d)\\
\mathbf{A}_{k+1} = \mathbf{A}_k + (1{-}\gamma)\,\pi\,\mathbf{P}_k - \rho_A\,\mathbf{A}_k, & (4.1e)\\
\mathbf{H}_{k+1} = \mathbf{H}_k + \rho_I\,\eta\,\mathbf{I}_k - \hbar\,\mathbf{H}_k, & (4.1f)\\
\mathbf{R}_{k+1} = \mathbf{R}_k + \rho_I(1{-}\eta)\,\mathbf{I}_k + \rho_A\,\mathbf{A}_k + (1{-}\mu)\,\hbar\,\mathbf{H}_k - \nu\,\frac{\mathbf{R}_k}{\mathbf{S}_k{+}\mathbf{R}_k}\mathbf{V}_k, & (4.1g)\\
\mathbf{D}_{k+1} = \mathbf{D}_k + \mu\,\hbar\,\mathbf{H}_k, & (4.1h)\\
\mathbf{U}_{k+1} = \mathbf{U}_k + \nu\,\mathbf{V}_k. & (4.1i)
\end{cases}
$$

The transitions between the compartments are illustrated in Figure 3.1. It is worth mentioning, that the recovered's compartment **R** contains the recovered people *who are not yet vaccinated*. To represent all the recovered people including vaccinated, we can consider the following additional

equation:

$$\mathbf{R}_{k+1}^{(\mathrm{all})} = \mathbf{R}_{k}^{(\mathrm{all})} \quad + \quad \rho_I(1-\eta)\,\mathbf{I}_k \;+\; \rho_A\,\mathbf{A}_k \;+\; (1-\mu)\,\hbar\,\mathbf{H}_k, \tag{4.2}$$

which clearly does not affect the dynamics of other states.

Updated parameter set of the augmented model

The detailed worldwide [195] and local serological [102] and dynamical [77, 110, 196, 197] analysis results provide estimates for the average lengths of the phases of the illness and the probabilities of transitions between the compartments. These parameters are aligned with the Hungary-specific data and are presented in detail in [J1]. After infection, the latent period of the disease (**L**) usually lasts approximately $\alpha^{-1} = 2.5$ days. This period is followed by a pre-symptomatic phase (**P**) of $\pi^{-1} = 3$ days. A person in the main sequence of the disease (**I** or **A**) remains infectious for about $\rho_I^{-1} = \rho_A^{-1} = 4$ days. The empirical probability of producing symptoms in the main sequence is $\gamma = 0.6$, furthermore, $\eta = 0.076$ portion of the symptomatic cases require hospitalization. The average length of a hospital treatment is $\hbar^{-1} = 10$ days. A hospitalized patient dies with a probability of $\mu = 0.205$, or recovers. The recovered people are assumed to be immune to reinfection. We assume that the disease is transmitted by the members of compartments **P**, **A**, and **I**, such that the relative infectiousness of the asymptomatic individuals (**A**) is $\delta = 0.75$, compared to those who produce symptoms (**I**). The transmission rate β of the disease is the most prominent parameter of the epidemic spread, which is typically time-dependent. The nominal values of the above mentioned model parameters and their assumed uncertainty are collected in Table 4.1.

For convenience, each uncertain parameter is assumed to have a normal distribution such that its nominal value (μ) is the expectation and its uncertainty ($\pm a\%$) gives the 2σ confidence interval with the standard deviations $\sigma = a\mu/200$. Nevertheless, it must be emphasized that rather than limiting generality by arbitrarily selecting a distribution, this choice was based on common engineering practice applied in similar scenarios. As presented in the above paragraphs, there exists *prior knowledge* about the parameter values (obtained through real-world measurements and statistical methods), as well as *realistic, practical bounds* for the range of each parameter. E.g. the length of the latent period was mostly the same for all individuals (2-3 days), and while outliers are certainly possible (like someone entering the next stage just in 1.5 or only in 5 days), the probability of distant values rapidly decreases. The choice of 2σ and $10-30\%$ is more a question of definition. At the time of writing the related study [J3], there were few detailed statistics available for parameter uncertainty, so we tried to find biologically meaningful ranges (based on related literature), which could accommodate the majority of the infections.

Here we examine the evolution of the epidemic in a fixed time window between the 1st of Match, 2020 ($k = 0$) and the 30th of June, 2021 ($k = T$). This interval contains the first three waves of the epidemic in Hungary. Subscript $k \in \{0, 1, \ldots, T\}$ denotes the number of days elapsed in the given time window of length $T + 1$.

Description	Nominal value	Uncertainty
The population of Hungary	$\mathbf{N} = 9.8 \cdot 10^6$	
Inverse of ... [1/days]		
latent period	$\alpha = 1/2.5$	$\pm 20\%$
presymptomatic infectious period	$\pi = 1/3$	$\pm 30\%$
infectuous period of symptomatic individuals	$\rho_I = 1/4$	$\pm 25\%$
infectuous period of asymptomatic individuals	$\rho_A = 1/4$	$\pm 25\%$
average length of hospitalization	$\hbar = 1/10$	$\pm 10\%$
Relative infectiousness of asymptomatic	$\delta = 0.75$	$\pm 10\%$
Probability of developing symptoms	$\gamma = 0.6$	$\pm 10\%$
Hospitalization probability of symptomatic cases	$\eta = 0.076$	$\pm 10\%$
Probability of fatal outcome (if already hospitalized)	$\mu = 0.205$	$\pm 10\%$
Effectiveness of vaccination	$\nu = 0.75$	$\pm 10\%$

Table 4.1: Presumed model parameters with their short description and their estimated uncertainty.

Vaccination model

For simplicity, our vaccination model assumes that only susceptible and recovered people are eligible for vaccination, and we neglect those rare cases, when the shot is given during an unidentified infection. Based on the serological test data [198], our model assumes that a subject, becomes immune $T_{\mathrm{V}} = 21$ days after the first dose with an average probability of $\nu = 0.75$. Correspondingly, variable $\mathbf{V}_k$ in (3.1) denotes the number of individuals who received the first dose of vaccine on day $k - T_{\mathrm{V}}$. In our model,

> *an individual is said to be* immune *to the disease if he/she will not be infected within the modeled time horizon.*

With this simplification, the people in the $\mathbf{R}$ and $\mathbf{U}$ compartments do not transmit the disease any more, as well as those who are still in hospital. It is worth remarking that a positive IgG test does not necessarily ensure immunity in this sense. Serological tests suggest that even a relatively high IgG level does not exclude the possibility of reinfection [199].

On the other hand, we assume that the willingness of the susceptible and recovered patients to vaccinate is roughly the same. Namely, the proportion of susceptible and recovered people vaccinated coincides with the proportion of all susceptibles and recovereds on each day. Therefore, the model counts with $\nu \mathbf{S}_k \mathbf{V}_k/(\mathbf{S}_k + \mathbf{R}_k)$ susceptible and $\nu \mathbf{R}_k \mathbf{V}_k/(\mathbf{S}_k + \mathbf{R}_k)$ recovered individuals who got immunity at time k. It is worth remarking that the value of $\mathbf{V}_k$ is known but cannot be manipulated as the computations are performed on *past* data of the epidemic spread. Correspondingly, $\mathbf{V} : k \mapsto \mathbf{V}_k$ can be considered as a preliminarily known input, or a *scheduling variable* [200], or a *measured disturbance* [120, 201]. The official European vaccination data including Hungary are available at [202]. Official Hungarian COVID-related data with additional analyses are also available at [203].

Available measurements

It is commonly stated in the literature [99, 100] that the daily number of infected people is not well-observable, as the measurement relies on aggressive and exhaustive contact tracing and testing strategies [32,61]. Though, it is reasonable to assume that testing is wide-spread and quick enough in the hospitals, the registered numbers of hospitalized patients [204] are still influenced by practical considerations. The limited healthcare capacity on weekends and holidays usually results in a lower number of performed and documented tests, as well as in a delayed hospital

discharge. Therefore, following the common engineering practice, we apply a 7-day long moving average filter to the published data ($\mathbf{H}_k^{\text{Off,raw}}$) [204] to avoid biased estimates caused by these administrative inaccuracies. The smoothed time series $\mathbf{H}_k^{\text{Off}}$ is formally calculated as:

$$\mathbf{H}_k^{\text{Off}} = \frac{1}{\min(3,T-k)+\min(3,k)+1} \sum_{i=-\min(3,k)}^{\min(3,T-k)} \mathbf{H}_{k+i}^{\text{Off,raw}}. \tag{4.3}$$

Obviously, the 7-day long sliding window must be truncated at both ends of the series. Finally, the filtered hospitalization data are considered as the single available processed measurement, which reveal relevant information about the time-evolution of the process.

4.1.2 Optimization-based reconstruction of past epidemiological data

Problem statement

We have already presented the fundamental dynamic equations (4.1) of the epidemic spread; introduced a possible vaccination model, where $\mathbf{V}_k$ acts like a *measured disturbance input* of the dynamical model; explained why parameter β_k can be considered as a *unknown input* of the system and finally, we have proposed to consider the hospitalization data ($\mathbf{H}$) as the *model output*. Using these, we define the compact notation for out discrete-time state-space model as:

$$x_{k+1} = f(x_k, u_k, \theta, v_k), \quad y_k = Cx_k, \tag{4.4}$$

where $x_k = \left(\mathbf{S}_k, \mathbf{L}_k, \mathbf{P}_k, \mathbf{I}_k, \mathbf{A}_k, \mathbf{H}_k, \mathbf{R}_k, \mathbf{D}_k, \mathbf{U}_k\right) \in \mathbb{R}^n$ is the state, $u_k = \beta_k \in \mathbb{R}^m$ is the unknown input, $\theta = \left(\alpha, \pi, \rho_I, \rho_A, \hbar, \delta, \gamma, \eta, \mu, \nu\right) \in \mathbb{R}^p$ is the vector of model parameters, $v_k = \mathbf{V}_k \in \mathbb{R}^q$ is a measured disturbance, and $y_k = \mathbf{H}_k \in \mathbb{R}^s$ is the output with $C = (0\,0\,0\,0\,0\,1\,0\,0\,0)$.
As a preliminary study, in [C1], we have presented two possible linear time-invariant (LTI) methods to reconstruct the past states x_{k+1} and the unknown inputs u_k using the measured output y_k, $k = \mathbb{I}_0^{T-1}$, both techniques relying on the dynamic inversion of the LTI subsystem of model (4.1). This type of reconstruction is discussed with more details in Section 4.2.
In this part, we revisit just the *unknown input filtering* problem and reformulate it as an *optimal predictive tracking control* problem. Namely, we compute an optimal input sequence u_k, $k = \mathbb{I}_0^{T-1}$ such that the output y_k of the system follows the reference signal $r_k = \mathbf{H}_k^{\text{Off}}$, which contains the past output measurements, i.e., the daily number of hospitalized patients ($\mathbf{H}_k^{\text{Off}}$). The simultaneous unknown input and state reconstruction can be formulated as the following optimization task.

Problem 4.1.1 (NMPC for epidemiological data reconstruction with fixed model parameters)**:** *Given the dynamical model* (4.4) *with initial condition* x_0*, a vector of constants* θ*, a measured disturbance* v_k*, and a reference output trajectory* r_{k+1} *to track* ($k \in \mathbb{I}_0^{T-1}$)*. We are looking for a sequence of inputs* u_k *and states* x_{k+1}*, which solve the state recursion* (4.4)*, satisfy the constraint* $u_k \in \mathcal{U}$*, and minimizes the following weighted cost function:*

$$J(X,U) = \sum\nolimits_{k=0}^{T-1} \|Cx_{k+1} - r_{k+1}\|_Q^2 + \sum\nolimits_{k=0}^{T-2} \|u_{k+1} - u_k\|_R^2, \tag{4.5}$$

where $X = \left(x_1 \ \dots \ x_T\right)$ *and* $U = \left(u_0 \ \dots \ u_{T-1}\right)$ *collect the free decision variables of the optimization,* Q*,* R *are positive definite weight matrices, and* $\mathcal{U}$ *is a closed subset of the input-space* $\mathbb{R}^m$*.*

In Problem 4.1.1, we have formulated a *data assimilation* problem in the form of a *nonlinear model predictive controller* (NMPC) computation. The available numerical optimization tools [124–127] make it possible to solve Problem 4.1.1 precisely in a reasonable time. From an epidemiological

point of view, the first term of the cost function (4.5) minimizes the deviation of the computed number of hospitalized patients from the official data, whereas, the second term minimizes the slope of the transmission rate of the pathogen. In this way, the NMPC design provides a optimal *smooth* solution for the unknown transmission rate function $\beta : \{0, \dots, T-1\} \to \mathcal{U} = [0.06, 1]$, which does not have sudden changes.

Remark The daily transmission rate of the disease β_k is an unknown time-dependent (but supposedly not abruptly varying) parameter. During an outbreak of the epidemic, the number of infected people is not negligible, namely, the sum $\mathbf{P}_k + \mathbf{I}_k + \delta\mathbf{A}_k$ is significant. In this case, the transmission rate function $\beta : k \mapsto \beta_k$ influences the overall dynamics significantly, and determines the shape of the epidemic wave. Therefore, parameter β_k is generally well-identifiable from the measurements during an outbreak of the epidemic, and it becomes uncertain when the number of infectious people is small.

The unknown input filtering task becomes complicated, when the model parameters and the initial state (from where the state reconstruction is performed) are probabilistic variables. In the next section, we address the stochastic extension of Problem 4.1.1.

4.1.3 Statistical analysis of the proposed methodology

We made several assumptions over the course of developing the proposed algorithm, based on similar research and results found in available literature. These are essential from a mathematical perspective, however, to avoid getting lost in the details, and sustain readability, most of the derivations were moved to the Appendix, section 7.3.1.

4.1.4 Results and discussion

In this section, we present the numerical results we obtained through the MPC-based reconstruction of the unknown epidemiological data. The results were computed in the MATLAB environment with Control System Toolbox [205]. For algorithmic differentiation we used CasADi [124, 125]. To solve nonlinear MPC problems we used IPOPT [126], an interior point line search algorithm, with the MUltifrontal Massively Parallel sparse direct Solver (MUMPS) [206, 207]. The computations were processed on a laptop PC with Intel Core i7-4710MQ CPU at 2.50 GHz and 16 GB of RAM. The MPC implementations are available online in the public repository [208].

To compute the unknown epidemiological data, we followed the operations of Algorithm 1 to find a pseudo-optimal solution for the $\mu\Sigma$-NMPC in Problem 7.3.1. On the 1st of March, 2020 ($k = 0$), we assumed a susceptible and almost healthy population, with a small uncertainty as follows:

$$\mu_0^x = (\mathbf{N} - 40 \;\; 10 \;\; 10 \;\; 10 \;\; 10 \;\; 0 \;\; 0 \;\; 0 \;\; 0)^\top, \; \Sigma_0^x = \mathrm{diag}(7, 1, 1, 1, 1, 1, 1, 1, 0). \tag{4.6}$$

(We note that the effect of the initial number of infected people on the reconstructed state vanishes after a transient period due to the stability properties of the compartmental model (4.1).) Furthermore, we considered pairwise independent random parameters with μ^θ and a diagonal Σ^θ as presented in Table 4.1. We fixed the initial value for β to $\mu_0^u = 1/3$ [J1]. We solved the ordinary NMPC in Problem 4.1.1 to find the candidate mean functions for $\hat{x}$ and $\hat{u}$. Then, we computed the gain matrices and the variances of the joint distribution (7.6). Using the obtained *feasible* solution as an initial guess, we solved the $\mu\Sigma$-NMPC in Problem 7.3.1. We learnt that the local optimum (M^*, S^*, V^*) found for Problem 7.3.1 is qualitatively the same as

Quantitative properties of the optimization	**Problem 4.1.1**	**Problem 7.3.1**
Total number of variables	4 869	70 614
Number of variables with only lower bounds	4 383	4 383
Number of variables with lower and upper bounds	486	486
Total number of equality constraints	4 383	70 128
Number of nonzeros in Lagrangian Hessian	10 826	386 575
Number of iterations	212	74
Elapsed time [sec]	8	1 187

Table 4.2: Computational complexity of Problems 4.1.1 and 7.3.1 illustrated through the epidemiological data assimilation case study. In this comparison, the cumulative number of recovered people $\mathbf{R}^{(\mathrm{all})}$ as an additional state variable is *not* considered. Accordingly, the number of state variables is $n = 9$, the number of uncertain parameters is $p = 10$, the number of inputs and the measured disturbances are $m = 1$ and $q = 1$, respectively.

the initial guess (M, S, V). The relative difference in the cost obtained by the optimal and the pseudo-optimal solution is negligible, namely:

$$\frac{J(M,S,V)-J(M^*,S^*,V^*)}{J(M^*,S^*,V^*)} \approx 7.1 \cdot 10^{-7}, \text{ where } J(M^*, S^*, V^*) \approx 17075.129. \tag{4.7}$$

If $\mathfrak{X}, \mathfrak{X}^* \in \mathbb{R}^{(n+m+np+n(n+1)/2)\cdot T-1}$ denote the vectors of independent variables of (M, S, V) and (M^*, S^*, V^*), respectively, the relative difference between $\mathfrak{X}$ and $\mathfrak{X}^*$ is

$$\|\mathfrak{X} - \mathfrak{X}^*\| \,/\, \|\mathfrak{X}^*\| \approx 2.86 \cdot 10^{-11}, \text{ where } \|\mathfrak{X}^*\| \approx 3.1978 \cdot 10^{11}. \tag{4.8}$$

In Table 4.2, we present the dimensional differences between the ordinary NMPC and the $\mu\Sigma$-NMPC if the length of time window is $T = 487$ days. In Figure 4.2, we illustrate the computed marginal distributions of the transmission rate of the pathogen, and the daily numbers of people in the different stages of the disease. The expectation for the states are presented in Plot 1 of Figure 4.2, which were computed through the ordinary NMPC design in Problem 4.1.1. In each of Plots 2–12 of Figures 4.2 and 4.3, the time evolution of the marginal distributions of scalar quantities are visualized, such that the shaded dark and light areas highlight the 1σ and 1σ confidence intervals, respectively. The shape of the epidemic curves clearly show the three waves of the epidemic until summer 2021.

As it was noted in Remark 4.1.2, the daily transmission rate becomes uncertain when the number of infectious people reduces significantly. In this case, the input constraint with the computed gain K_k may be violated, therefore, we increase the input weight $\mathbf{R}_k^{\mathrm{LQR}}$ to obtain a lower gain K_k. These heuristic operations to compute an admissible gain was relevant only when the 3rd wave of the epidemic suddenly dropped after the end of April, 2021. The scaled logarithm of the input weights on each day k are illustrated in Plot 2 of Figure 4.2. In Plot 3 of Figure 4.2, we present the reconstructed number of hospitalized patients in comparison with the official (i.e., reference) data. Plots 4, 5, and 6 of Figure 4.2 illustrate three derived probabilistic quantities $\hat{z}_k = h(\hat{x}_k, \hat{u}_k, \hat{\theta})$, namely, the time-dependent effective reproduction number (3.12) ($[\hat{z}_k]_1 = R_k$), the number of all infected people ($[\hat{z}_k]_2 = \hat{\mathbf{L}}_k + \hat{\mathbf{P}}_k + \hat{\mathbf{I}}_k + \hat{\mathbf{A}}_k + \hat{\mathbf{H}}_k$), and the number of daily new infections ($[\hat{z}_k]_3 = \hat{\beta}_k\,(\hat{\mathbf{P}}_k + \hat{\mathbf{I}}_k + \hat{\delta}\,\hat{\mathbf{A}}_k)\frac{\hat{\mathbf{S}}_k}{\mathbf{N}}$). The first and third coordinates of $\hat{z}_k$ are nonlinear functions of random variables. Therefore, the mean and the variance of $\hat{z}_k$ is approximated by the first-order Taylor polynomial of function h, namely,

$$\hat{z}_k \approx \frac{\partial h}{\partial(x,u,\theta)}(\mu_k) \begin{pmatrix} \hat{x}_k \\ \hat{u}_k \\ \hat{\theta}_k \end{pmatrix} + h(\mu_k) - \frac{\partial h}{\partial(x,u,\theta)}(\mu_k)\,\mu_k \sim \tag{4.9}$$

$$\sim \mathcal{N}\Big(h(\mu_k)\ ,\ \frac{\partial h}{\partial(x,u,\theta)}(\mu_k)\ \Sigma_k\ \Big(\frac{\partial h}{\partial(x,u,\theta)}(\mu_k)\Big)^{\top}\Big). \tag{4.10}$$

The yellow curve in Plot 4 illustrates the estimated reproduction number published online by Atlo Team in [209].

In Plot 12 of Figure 4.3, we present three uncertain time-series, namely, the number of recovered but not yet vaccinated people (blue), the cumulative number of recovered people (red), and the cumulative number of immune people (green).

In Figures 4.2 and 4.3 we can observe the successfully suppressed first wave with a dramatic effect of the strict lockdown introduced in March, 2020. As a result, the disease was mainly confined to closed institutions such as certain hospital wards and elderly homes. This policy could not be maintained in the autumn of 2020, and therefore, a substantially larger 2nd wave occurred causing a huge burden on the healthcare system. Therefore, further restrictions (online education in secondary schools, closure of certain public spaces, banning of most gatherings and curfew from 8pm to 5am) had to be introduced in the first half of November, 2020. These measures had the planned effect in terms of the significant reduction of the transmission rate as it is visible in Plot 2 of Figure 4.3. Then, from January 2021, R_t began to increase again due to the appearance of the more contagious alpha (B.1.1.7) variant although all of the former restrictions remained in effect. The alpha variant caused the largest peak of the epidemic so far in the spring of 2021 with a maximum of 12553 hospitalized people on March 30, 2021. Further restrictions had to be introduced on March 8, 2021, where the main component was the closing of all schools. Together with the intensive vaccination in the first half of 2021, this made the decrease in the number of infected people definitely fast. The ratio of the peaks of the estimated β in February 2021 and December 2020 is approximately 1.62, which matches well with literature reports (1.4 – 1.8) in the UK [210]. We note that we can compare these data since they were estimated under the same restriction level. Plot 12 in Figure 4.3 shows the estimated number of people gaining immunity by infection and/or vaccination. According to this estimation, more than 30 percent of the population might have gone through the COVID infection until the end of June 2021. This suggests an approximately 26% detection rate. This is significantly lower than the value of certain European countries such as Germany, Italy or Spain reaching or sometimes exceeding 50%, but the number of performed tests per population is also much lower in Hungary than in the mentioned countries [211].

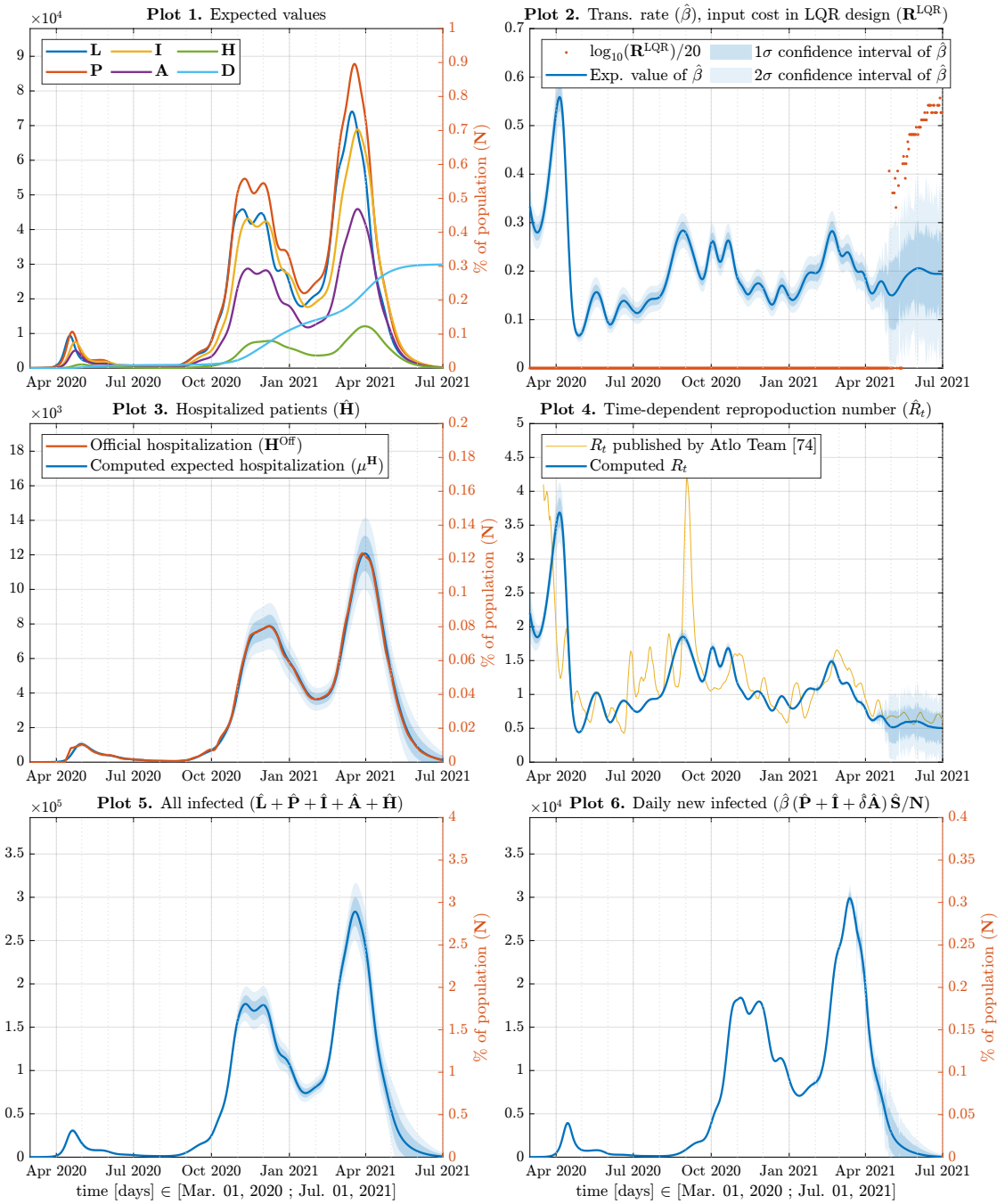

Figure 4.2: Reconstructed epidemiological data computed for system (3.1) with Gaussian model parameters: expected value of states (Plot 1), transmission rate of the pathogen (Plot 2), time-dependent reproduction number (Plot 4), number of reconstructed hospitalized patients compared to the recorded data (Plot 3), sum of all infected compartments (Plot 5), and the daily new infections (Plot 6). The gray dotted vertical grid lines show the first days of the months.

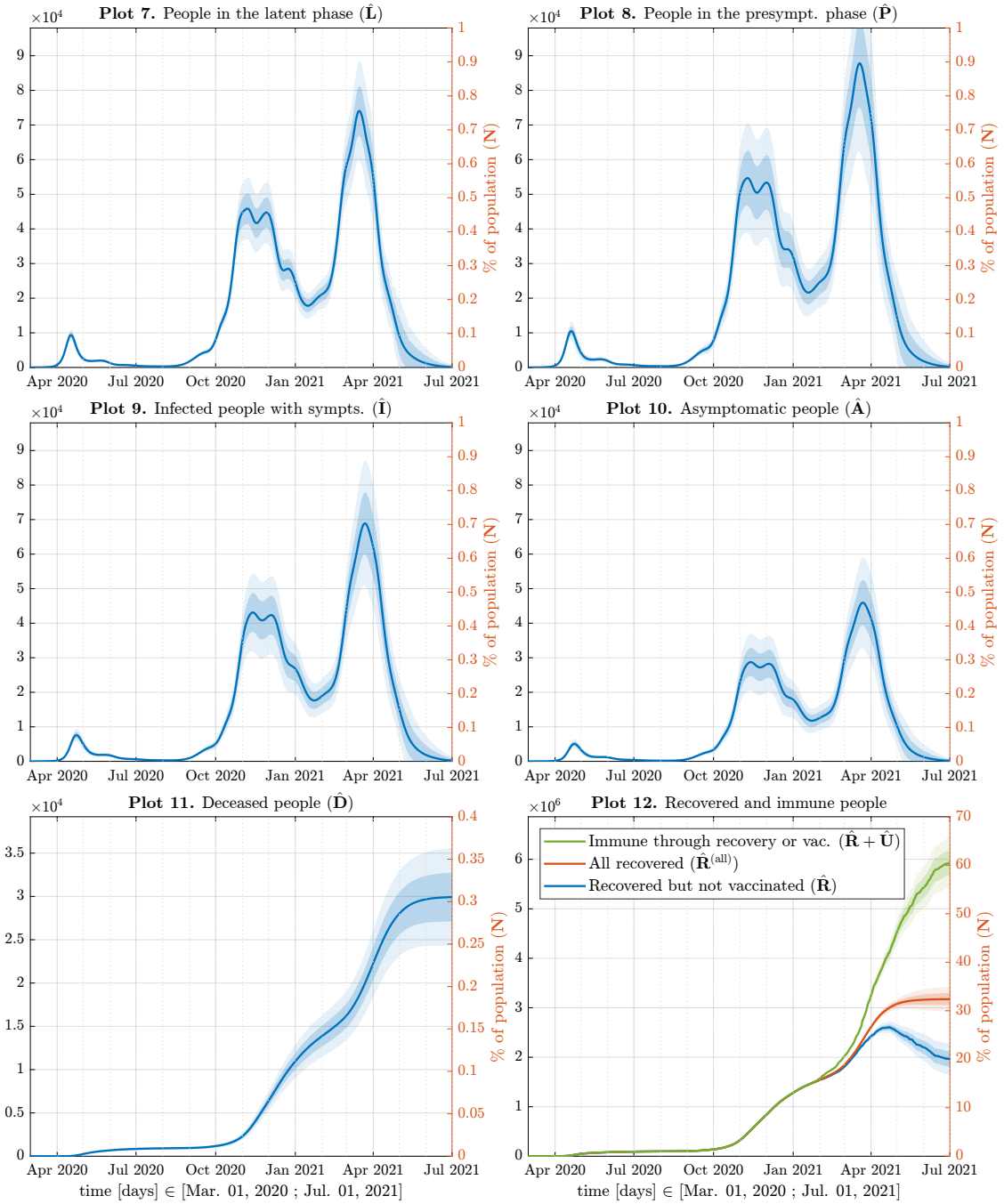

Figure 4.3: Unknown epidemiological data computed for system (3.1) with Gaussian model parameters: number of people in the different phases of the disease (Plots 7–10), number of deceased people (Plot 11), number of recovered and/or immune people (Plot 12). The gray dotted vertical grid lines emphasize the first days of the months.

4.1.5 Conclusions

In this section, we proposed an optimization-based data assimilation approach to compute the unknown inputs and states of discrete-time compartmental epidemic models with uncertain normally distributed parameters. We started from the assumption that the joint state-input-parameter distribution is Gaussian. Then, a deterministic mean-variance recursion was developed, which made possible to formulate the stochastic data assimilation problem as a single model predictive control design with a nonlinear mean-variance prediction model. We noted and demonstrated that the resulting $\mu\Sigma$-NMPC is computationally intensive, but its local optimum can be well approximated by a more efficient ordinary NMPC and further closed-form variance computations.

We proposed simple heuristics to predict appropriate feedback gains, which realize state-dependent control actions along the prediction horizon. In this way, a trade-off can be made between the uncertainty of the computed states and inputs as the predicted control action is scheduled by the deviation between the actual realization of the state and its predicted expectation. As the approach does not make a difference between the unknown parameters and inputs, the joint state observation, change detection, and parameter estimation is also possible.

Through the finite horizon *predictive* control computation, we estimated the unknown data of the *past* evolution of the COVID-19 epidemic spread within a fixed time window in Hungary. Among the unknown quantities, we considered the daily number of people in the different phases of the disease and the transmission rate of the pathogen, which highly depends on the actual social distancing rules, mobility restrictions, and virus mutations. The unknown time-series are computed such that the expected value of the computed number of hospitalized patients fits the truly observed data as much as possible. Compared to our previous results [J1] [C1], we considered an augmented and uncertain compartmental epidemiological model with *normally distributed random model parameters* and a simple *vaccination model* as well. With a few modifications, the approach can be applied to compute multiple uncertain possibly time-dependent parameters but also to give prediction to the future behaviour of the epidemic spread. The proposed methodology is able to extract and reconstruct detailed information from the whole time horizon of the epidemic process beyond giving estimates for the cumulative number of infected and recovered people. Future work will be focused on the analysis of other European countries.

4.2 Analytic solution using robust feedback linearization

In this section, a computational approach is presented for the state estimation based reference tracking control and historical data reconstruction of nonlinear compartmental (epidemic) models. The control model is given in nonlinear input-affine form, where the manipulable input is the disease transmission rate influenced by possible measures and restrictions, while the observed or computed output is the number of infected people.

The control design is built around a simple SEIR model and relies on a feedback linearization technique. We examine and compare different control setups distinguished by the availability of state information, complementing the directly measurable data with an extended Kalman filter used for state estimation. To illustrate the capabilities and robustness of the proposed method, we carry out multiple case studies for output tracking and data reconstruction on Swedish and Hungarian data, all in the presence of serious model and parameter mismatch.

4.2.1 Process modeling

Simulation model (SLPIAHRD)

To show the applicability of our control and estimation setup in realistic scenarios, we use different nonlinear dynamic models and parameters for the simulation of the epidemic process and for the estimation and control steps.

The epidemic simulation relies on the comprehensive eight-compartment model, abbreviated as SLPIAHRD (for susceptible, latent, presymptomatic, infected, asymptomatic, hospitalized, recovered, and deceased), which was designed with key characteristics of COVID-19 in mind. Already described in section 3.1.1, with different augmentations shown in section 3.2.1 and section 4.1.1, it can accommodate various factors such as different latent periods (infectious and noninfectious), the impact of presymptomatic and asymptomatic infections on the spread, the waning of immunity, and countermeasures like symptom-based testing and quarantines. Additionally, it can be adjusted to account for new virus variants by gradually modifying the model parameters based on their prevalence in the population.

In this section, we utilize the original model (from section 3.1.1) as ground truth, accepting its outputs as an accurate representation of a real-world complex epidemic process. For clarification, we mention that state variables in the model are the continuous numbers of individuals belonging to the compartments. The trajectory of the model is computed using accurate numerical solvers, such as 4-th and 5-th or 8-th and 9-th order Runge-Kutta method. For readability, we omit time arguments of the variables unless they are essential for understanding.

The simulations presented in this section rely on public epidemiological data from Hungary and Sweden during the second and third waves of the epidemic (15/08/2020 – 15/08/2021) to generate reference outputs for tracking. The data source is the Our World in Data (OWID) database [212], which keeps records of reported infections and hospitalizations provided by the responsible governmental institutions. The model parameters, shown in Table 4.3 and detailed in [J3], are aligned with the dominant virus variants (original and Alpha) of this period, to ensure that the simulations are as realistic as possible. Parameter values for the specific variants and time periods in Hungary were obtained from relevant scientific literature, computed using standard parameter estimation or statistics-based techniques. Although they are slightly different, we decided to use the same parameters for Hungary and Sweden in this model to simplify the approach and to illustrate the robustness of the computations.

Control design model (SEIR)

For feedback computation and part of the state observer design, we will use a largely simplified model compared to the previously described simulation model. This will be the well-known SEIR nonlinear compartmental model, which is widely used for describing epidemic processes, including COVID-19, despite its known limitations.

The model identifies four stages of infection for each individual, categorizing the population into four compartments: Susceptibles (**S**), who are unprotected, and may become Exposed (**E**) to the disease upon contact with Infected (**I**) individuals, who are already spreading the virus. Exposed individuals carry the disease, but take some time to begin spreading it, at which point they move to the **I** compartment. Infected individuals eventually recover and move to the Recovered (**R**) compartment, gaining full immunity against future infections. The model operates with three parameters: the transmission rate β of the virus (which is influenced by administrative countermeasures and thus considered a bounded manipulable input for the system), the latent period k_2^{-1} (time spent in the Exposed compartment), and the infectious period k_3^{-1} (time spent in **I**).

To consistently denote all variables, we use overline notation for the compartments in the control design model. With this notation, the differential equations of the continuous model can be expressed as:

$$\dot{\mathbf{S}} = -\beta\,\mathbf{S}\,\mathbf{I}\,/\,\mathbf{N}, \tag{4.11a}$$

$$\dot{\mathbf{E}} = \beta\,\mathbf{S}\,\mathbf{I}\,/\,\mathbf{N} - k_2\,\mathbf{E}, \tag{4.11b}$$

$$\dot{\mathbf{I}} = k_2\,\mathbf{E} - k_3\,\mathbf{I}, \tag{4.11c}$$

$$\dot{\mathbf{R}} = k_3\,\mathbf{I}. \tag{4.11d}$$

Nominal values for the model parameters k_2 and k_3 were selected by approximately lumping the corresponding compartments of the simulation model based on their role in the epidemic spread ($\mathbf{E} \approx \mathbf{L}$, $\mathbf{I} \approx \mathbf{P} + \mathbf{I} + \mathbf{A}$), summing the time an individual spends in them. Additionally, we took the averages of the parameters for the original and Alpha virus variants, obtaining a time-invariant model. While this matching process could easily be refined, the applied model mapping is straightforward to use in real-world scenarios and underscores the robustness of our feedback approach to parameter uncertainty. Choosing a simpler model for control computation introduces model mismatch, a common issue in realistic setups where no single model can exactly describe the epidemic spread.

4.2.2 Control design

We implemented the control of the *simulation model* in the following steps: estimation or computation (depending on control setup) of the *control model*'s states based on output(s) of the simulation model, feedback linearization of the *control model*, computation of a control signal for the *linearized control model*, and, finally, application of this control input to the *simulation model*. Based on how we compute/estimate the states of the *control model*, we present three different control setups which are different in their degree of reality. This approach is also useful to compare how the results may be affected by the availability of data. For a more sound theoretical background, the computations concerning the controllability of the used epidemic models, as well as the analysis of the internal dynamics of the feedback-linearized systems, can be found in the Appendix, Sections 7.4 and 7.6.

Parameter	Notation	Value (by virus variant)	
		Original	Alpha
Reproduction rate	β	Treated as input	
Latent period (days)	α^{-1}	3	2.5
Presymptomatic period (days)	ζ^{-1}	3	3
Asymptomatic period (days)	ρ_A^{-1}	4	3
Infectious period (days)	ρ_I^{-1}	4	4
Hospitalization period (days)	λ^{-1}	10	10
Probability of infection	γ	0.6	0.6
Probability of hospitalization	η	0.076	0.07
Probability of death	μ	0.145	0.145
Relative infectiousness of $\mathbf{A}$	δ	0.75	0.75
Total population (Hungary)	$\mathbf{N}$	9.8M	
Reproduction rate	β	Treated as input	
Latent period (days in $\mathbf{E}$)	k_2^{-1}	$\alpha^{-1} = 2.75$	
Infectious period (days in $\mathbf{I}$)	k_3^{-1}	$1/(\zeta^{-1} + \rho_I^{-1}) = 6.5$	

Table 4.3: Parameters of the epidemic model used for the simulations. The listed values were obtained from related literature and from parameter identification applied to Hungarian data.

Control setup 0: no estimation

We originally introduced control setup 0 in [C3], although we had previously experimented with simple feedback-linearization of epidemic models in [C2]. The structure of the feedback loop is shown in Figure 4.4, depicting a setup where no estimation step is carried out, and we assume full knowledge of the simulation model's state.

Our goal is to control the simulation model to track the reference signal $r(t)$ with the number of individuals capable of spreading the disease (i.e., minimizing $|r-(\mathbf{P}+\mathbf{I}+\mathbf{A})| = |r-\mathbf{I}|$ by selecting the appropriate β). To compute the input, first we apply a modified feedback linearization based on [83, Chap 4.3], calculated for the control design model, as detailed below in Subsections 4.2.2 and 4.2.2. This technique requires the full state information of the SEIR model, which we compute directly from the states of the known SLPIAHRD states, and results in a transformed system (with state variables z, acting as a simple integrator cascade between the transformed input v and output y. Next, we compute a simple full-state feedback gain for this linearized control model, which has a proportional-integral-derivative (PID) structure due to the obtained set of state variables.

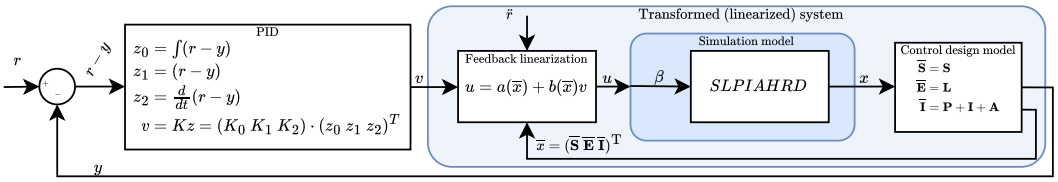

Figure 4.4: Control setup 0: simulation model's states are known, and control model states are directly computed.

Control setup I: partial state estimation

As knowledge of the full state information of the simulation model is problematic in a real-world application, we introduced control setup I. in [C4]. The feedback loop, as illustrated in Figure 4.5, contains one important modification compared to the previous approach, namely, we estimate the control model's state information $(\mathbf{S}, \mathbf{E}, \mathbf{I})$ using an extended Kalman filter (EKF).

It must be noted that this setup assumes that the control model state $\mathbf{I} = \mathbf{P} + \mathbf{I} + \mathbf{A}$ is a directly measurable output of the simulation model. Even though this might seem unrealistic at first as, e.g., the number of infected and virus-spreading asymptomatic individuals ($\mathbf{A}$) is hardly measurable, during the COVID-19 pandemic, several methods were proposed and tested for the estimation of these variables [110]. Thus, we assume in this scenario that a reliable estimation for $\mathbf{I}$ is already available.

Apart from this modification, we use the same extended feedback-linearization technique as in control setup 0, which again results in a PID-like control structure for the transformed, linearized model.

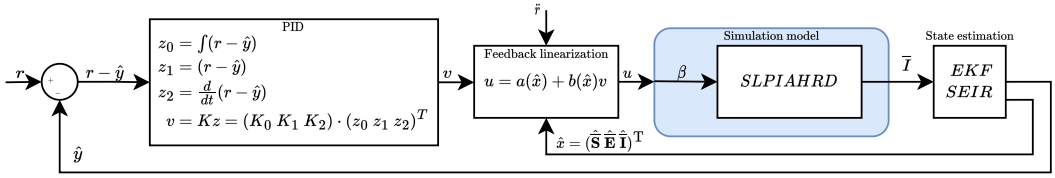

Figure 4.5: Control setup I: control model states are estimated from $\mathbf{I}$ and assumed to be obtained directly from the simulation model.

Control setup II: full state estimation

In order to overcome the limitations discussed above (i.e., the need for an extra estimation step) and to take into account the effect of that estimation's error on the whole system, we created control setup II. While similar to setup I., in this case we assume the only measurable output of the *simulation model* to be the daily number of hospitalizations ($\mathbf{H}(t)$). We apply an EKF constructed using the same model structure as the *simulation model*, but (not to move away from reality) having some of its parameters mismatched; we estimate the states of the *simulation model*, and finally we 'compute' the states of the *control model* by merging and matching the compartments of the *simulation model* as described above in the modeling section. Setup II can be seen in Figure 4.6.

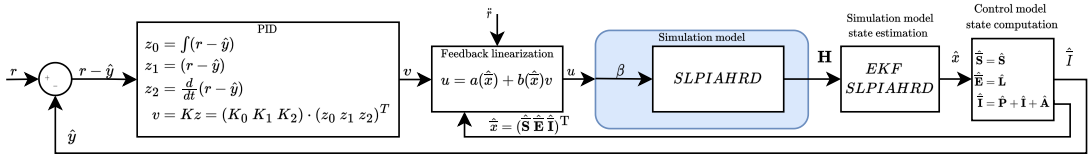

Figure 4.6: Control setup II: control model states computed from estimated simulation model states. The estimation is based solely on $\mathbf{H}$.

Feedback linearization and asymptotic output tracking

Based on [C3], we introduce the technique for feedback linearization following [83, Chap 4.3]. We derive the equations for nonlinear single-input single-output systems, written as:

$$\dot{x} = f(x) + g(x)\, u \tag{4.12a}$$

$$y = h(x), \tag{4.12b}$$

where $u \in \mathbb{R}$ is the system's input, $x \in \mathbb{R}^n_+$ is the state, and $y \in \mathbb{R}$ is the observed output. We assume that f, g, and h are well-defined and sufficiently smooth functions. Furthermore, we define a reference signal $r(t)$, as our ultimate control objective is calculating an input u such that y (asymptotically) converges to r.

Using the well-known definition of the Lie derivative of a scalar-valued function $h(x)$ along the vector field $f(x)$ as

$$L_f h(x) = \frac{\partial h(x)}{\partial x} f(x),$$

and the relative degree of a system being ρ if

$$1)\ L_g L_f^{\rho-1} h(x) \neq 0 \ \text{ and} \tag{4.13a}$$

$$2)\ L_g L_f^{k} h(x) = 0, \quad \forall x, \quad k = 0, 1, \ldots, \rho - 2 \tag{4.13b}$$

a state transformation z can be defined as:

$$z = \Phi(x) = \begin{pmatrix} y \\ \dot{y} \\ \ddot{y} \\ \vdots \\ y^{(\rho-1)} \end{pmatrix} = \begin{pmatrix} h(x) \\ L_f h(x) \\ L_f^2 h(x) \\ \vdots \\ L_f^{\rho-1} h(x) \end{pmatrix} \tag{4.14}$$

Applying the nonlinear state feedback:

$$u = \underbrace{-\frac{L_f^{\rho} h(x)}{L_g L_f^{\rho-1} h(x)}}_{a(x)} + \underbrace{\frac{1}{L_g L_f^{\rho-1} h(x)}}_{b(x)} v, \tag{4.15}$$

for the transformed system results in the closed-loop (from input v to output y) acting in a way equivalent to a cascade of ρ integrators:

$$\dot{z} = Az + Bv, \quad y = Cz \tag{4.16a}$$

$$A = \begin{pmatrix} 0 & 1 & 0 & \cdots & 0 \\ 0 & 0 & 1 & \cdots & 0 \\ & & & \cdots & \\ 0 & 0 & 0 & \cdots & 1 \\ 0 & 0 & 0 & \cdots & 0 \end{pmatrix} \in \mathbb{R}^{\rho \times \rho}, \ B = \begin{pmatrix} 0 \\ 0 \\ \cdots \\ 0 \\ 1 \end{pmatrix}, \ C = \begin{pmatrix} 1 & 0 & \cdots & 0 \end{pmatrix} \tag{4.16b}$$

Using the fact that such an integrator cascade can be stabilized by a simple state feedback, we can construct a stabilizing input driving the output to 0 in the form of:

$$v = -Kz = -\sum_{i=1}^{\rho} K_{i-1} \left(L_f^{i-1} h(x) \right), \tag{4.17}$$

where the constants $K = (K_0, K_1, ..., K_{\rho-1})$ can be arbitrary values that make $(A - BK)$ a stability matrix. In fact, the value of K can be obtained by applying any linear stabilization method to the system (4.16) such as pole placement, linear–quadratic regulator (LQR), or any other more advanced feedback approach.

Now, given a reference signal $r(t)$ to track with the output of the system, we can define the error output $e(t) = y(t) - r(t)$ and the corresponding state transformation as:

$$\bar{z} = \Phi(x) = \begin{pmatrix} y - r \\ \dot{y} - \dot{r} \\ \ddot{y} - \ddot{r} \\ \vdots \\ y^{(\rho-1)} - r^{\rho-1} \end{pmatrix} = \begin{pmatrix} h(x) - r \\ L_f h(x) - \dot{r} \\ L_f^2 h(x) - \ddot{r} \\ \vdots \\ L_f^{\rho-1} h(x) - r^{\rho-1} \end{pmatrix} \tag{4.18}$$

Analogously to (4.17), we can stabilize the system using the simple state feedback. Thus, the application of:

$$v = -K\bar{z} = -\sum_{i=1}^{\rho} K_{i-1}\left(L_f^{i-1}h(x) - r^{(i-1)}\right) \tag{4.19}$$

will result in $\lim_{t\to\infty} y(t) - r(t) = \lim_{t\to\infty} e(t) = 0$, if K is chosen such that $(A - BK)$ is a stability matrix [83, Chap 4.5]. For the sake of completeness, substituting v into the input mapping equation (4.15), we compute the asymptotic reference tracking input, which should be applied to the original system as:

$$u = -\frac{L_f^{\rho}h(x) - r^{(\rho)}}{L_g L_f^{\rho-1}h(x)} + \frac{-\sum_{i=1}^{\rho} K_{i-1}\left(L_f^{i-1}h(x) - r^{(i-1)}\right)}{L_g L_f^{\rho-1}h(x)} \tag{4.20}$$

Robust feedback linearization and output tracking

As it was previously shown in [C3], the robustness of the control loop may be significantly improved by the introduction of an extra integrator step into this cascade, given the same model structure as in Eq. (4.12), and effectively increasing the relative degree ρ by 1.

We define the new, transformed output $\overline{y}$ as $\dot{\overline{y}} = h(x) - r$, and modify the transformed system as:

$$z_0 = \overline{y} \tag{4.21a}$$

$$z_1 = \dot{z}_0 = \dot{\overline{y}} = h(x) - r = y - r \tag{4.21b}$$

$$z_2 = \dot{z}_1 = L_f h(x) - \dot{r} = \dot{y} - \dot{r} \tag{4.21c}$$

$$\dots \tag{4.21d}$$

$$z_\rho = L_f^{\rho-1}h(x) - r^{\rho-1} \tag{4.21e}$$

Analogously to the original case, we achieve asymptotic output tracking with a full state feedback gain $K = (K_0, K_1, ..., K_\rho)$, where K is an arbitrary constant making the augmented tracking error dynamics asymptotically stable.

By introducing the extra integrator into Eq. (4.15) and using the feedback $v = -Kz$ (Eq. (4.19)), we can conclude that the asymptotic output tracking input can be calculated as:

$$u = -\frac{L_f^{\rho}h(x) - r^{(\rho)}}{L_g L_f^{\rho-1}h(x)} + \frac{-\left(\sum_{i=1}^{\rho} K_i\overline{y}^{(i)} + K_0\overline{y}\right)}{L_g L_f^{\rho-1}h(x)} \tag{4.22}$$

It is clearly visible that the application of the technique to our SEIR control design model requires the state information $x = (\mathbf{S}, \mathbf{E}, \mathbf{I}, \mathbf{R})$ at any given time.

4.2.3 State estimation

In this section, we describe the state estimation approach with the corresponding control input computation. Using the definition and notations of the Extended Kalman Filter (EKF) as described in section 2.5, we transform and use both epidemic models for the state estimation. The detailed observability analysis of the models can be found in the Appendix, Section 7.5.

First, for Scenario I. we estimate the states of the *control design model*, assuming that the number of infected individuals **I** can be obtained directly from the simulation model. While this might seem an unrealistic approach, its feasibility is addressed in section 4.2.5.

Second, for Scenario II. the states of the simulation model are estimated from H, constructing the EKF around the 8-compartment simulation model. This introduces another challenge: as the reference input is available for **I**, the output of the system, used for the asymptotic reference tracking, is obtained through estimation. As a consequence, the *estimation error* appears directly in the tracking error computed using the *actual* value of **I**, an effect discussed in section 4.2.4 (Control Setup II).

Control input computation with estimated SEIR states

First of all, to obtain a suitable model (corresponding to the structure (2.24)), we introduce the notations $x_k = (\mathbf{S}_k\ \mathbf{E}_k\ \mathbf{I}_k\ \mathbf{R}_k)$, $y_k = \mathbf{I}_k$, $u = \beta$, and discretize our control design model (SEIR) using a simple forward Euler method and time step dt:

$$f(x_k, u_k) = \begin{pmatrix} \mathbf{S}_k - dt\beta_k \mathbf{S}_k \mathbf{I}_k / N \\ \mathbf{E}_k + dt(\beta_k \mathbf{S}_k \mathbf{I}_k / N - k_2 \mathbf{E}_k) \\ \mathbf{I}_k + dt(k_2 \mathbf{E}_k - k_3 \mathbf{I}_k) \\ \mathbf{R}_k + dt k_3 \mathbf{I} \end{pmatrix},\ h(x_k) = \mathbf{I}_k \tag{4.23}$$

As we need the Jacobians for substitution into 2.25 and 2.26, we compute them as:

$$\frac{\partial f}{\partial x} = \begin{pmatrix} 1 - dt\beta\mathbf{I}/N & 0 & -dt\beta\mathbf{S}/N & 0 \\ dt\beta\mathbf{I}/N & 1 - dtk_2 & dt\beta\mathbf{S}/N & 0 \\ 0 & dtk_2 & 1 - dtk_3 & 0 \\ 0 & 0 & dtk_3 & 1 \end{pmatrix},\ \frac{\partial h}{\partial x} = \begin{pmatrix} 0 \\ 0 \\ 1 \\ 0 \end{pmatrix}^T \tag{4.24}$$

Second, we derive the state transformation and the required output mapping as detailed in (4.21) - (4.22). We compute the required Lie-derivatives for the continuous system (4.12) as follows

$$f(x) = \begin{pmatrix} 0 \\ -k_2 x_2 \\ k_2 x_2 - k_3 x_3 \\ k_3 x_3 \end{pmatrix},\ g(x) = \begin{pmatrix} -k_1 x_3 \\ k_1 x_3 \\ 0 \\ 0 \end{pmatrix},\ h(x) = x_3 \tag{4.25a}$$

$$L_g h(x) = 0 \tag{4.25b}$$

$$L_f h(x) = k_2 x_3 + k_3 x_3 \tag{4.25c}$$

$$L_g L_f h(x) = k_2 x_1 x_3 \tag{4.25d}$$

$$L_f^2 h(x) = k_3 k_2 x_2 - k_3^2 x_3 + k_2^2 x_2, \tag{4.25e}$$

and conclude from the definition (4.13) that $\rho = 2$. However, as our technique for robustifying the controller defines a transformed output (4.21) and effectively increases the relative degree by 1, we have to consider the relative degree to be $\rho = 3$, and thus construct the input mapping required for asymptotic output tracking as:

$$u = \frac{\ddot{r} + k_3 k_2 x_2 + k_2^2 x_2 - k_3^2 x_3 + v}{k_2 x_1 x_3} \tag{4.26}$$

creating a system equivalent to:

$$\dot{z} = \begin{pmatrix} 0 & 1 & 0 \\ 0 & 0 & 1 \\ 0 & 0 & 0 \end{pmatrix} z + \begin{pmatrix} 0 \\ 0 \\ 1 \end{pmatrix} v, \tag{4.27a}$$

$$y = \begin{pmatrix} 1 & 0 & 0 \end{pmatrix} z, \tag{4.27b}$$

$$A \in \mathbb{R}^{\rho \times \rho}, B \in \mathbb{R}^{\rho \times 1}, C \in \mathbb{R}^{1 \times \rho} \tag{4.27c}$$

Now, by introducing the notation $\hat{x}_k = (\hat{x}_{1,k}\ \hat{x}_{2,k}\ \hat{x}_{3,k}) = (\hat{\mathbf{S}}_k\ \hat{\mathbf{E}}_k\ \hat{\mathbf{I}}_k)$ for the state information computed by the EKF, we can substitute the estimated state values into the above formulae, resulting in:

$$u_k = \frac{\ddot{r}_k + k_3 k_2 \hat{x}_{2,k} + k_2^2 \hat{x}_{2,k} - k_3^2 \hat{x}_{3,k} + v_k}{k_2 \hat{x}_{1,k} \hat{x}_{3,k}}, \tag{4.28}$$

Moreover, applying the input required for the asymptotic output tracking, we obtain:

$$u_k = \frac{\ddot{r}_k + (k_3 k_2 + k_2^2)\hat{x}_{2,k} - k_3^2 \hat{x}_{3,k}}{k_2 \hat{x}_{1,k} \hat{x}_{3,k}} - \frac{K_0 \overline{y}_k + K_1 \dot{\overline{y}}_k + K_2 \ddot{\overline{y}}_k}{k_2 \hat{x}_1 \hat{x}_3} \tag{4.29}$$

Thus, the obtained feedback has the following PID structure:

$$v_k = K_0 \int (r_k - y_k) + K_1 (r_k - y_k) + K_2 \frac{d}{dt}(r_k - y_k). \tag{4.30}$$

Here, we must take two important notes. First, the formulae for feedback linearization require the derivatives of signals r and y, which, due to the EKF estimation, are available only at discrete time instants. Therefore, we use the numerical derivatives, computed as $\dot{y}_k = (y_{k+1} - y_k)/dt$, $\dot{r}_k = (r_{k+1} - r_k)/dt$, and provide a two-times continuously differentiable reference signal for the system. If the reference signal is not differentiable, we can ensure the required smoothness by basic preprocessing techniques (see, e.g., [C1]). Second, we emphasize, that despite the PID-like structure of (4.30), the constants of the state feedback can be computed using a simple pole placement (computed for the system presented in Eq. (4.27)). In our experiments, we chose the desired poles of the controlled system to be $-(0.339, 0.407, 0.475)$, values obtained empirically during the creation of our first modified feedback-linearization based controller in [C2]. For the EKF, we used $dt = 0.5$ (days) and assumed $Q = \mathrm{diag}(1,\ 1,\ 1,\ 1)$, $R = 0.01$, and initial estimation error covariance $P_{0|-1} = 0.01$. We chose an initial state different from the true state value as follows: $\hat{x}_{0|-1} = \mathbf{N} \cdot ((1 - 10^{-5}),\ 5 \cdot 10^{-6},\ 5 \cdot 10^{-6},\ 0)^T$, inducing a short transient period at the beginning of the simulation. The estimator used the same (possibly mismatched) k_2 and k_3 parameters as the SEIR-based controller.

Control input computation with estimated SLPIAHRD states

For control setup II, we apply the discrete state estimation to the detailed simulation model given in Eq. (3.1), and compute the estimated control model states by merging the respective compartments. Compared to the previous case, instead of substituting Eq. (4.24) into Eq. (2.24), we derive the discrete transition and measurement functions (using the Euler method), as well

as their Jacobi matrices for the SLPIAHRD model as follows:

$$f(x_k,u_k)=\begin{pmatrix}\mathbf{S}_k-dt\left[\beta_k\,\mathbf{S}_k\left(\mathbf{P}_k+\mathbf{I}_k+\delta\mathbf{A}_k\right)/\mathbf{N}\right]\\ \mathbf{L}_k+dt\left[\beta_k\,\mathbf{S}_k\left(\mathbf{P}_k+\mathbf{I}_k+\delta\mathbf{A}_k\right)/\mathbf{N}-\alpha\,\mathbf{L}\right],\\ \mathbf{P}_k+dt\left[\alpha\,\mathbf{L}_k-\zeta\,\mathbf{P}_k\right],\\ \mathbf{I}_k+dt\left[\gamma\,\zeta\,\mathbf{P}_k-\rho_{\mathrm{I}}\mathbf{I}_k\right],\\ \mathbf{A}_k+dt\left[(1-\gamma)\,\zeta\,\mathbf{P}_k-\rho_{\mathrm{A}}\,\mathbf{A}_k\right],\\ \mathbf{H}_k+dt\left[\rho_{\mathrm{I}}\,\eta\,\mathbf{I}_k-\lambda\,\mathbf{H}_k\right],\\ \mathbf{R}_k+dt\left[\rho_{\mathrm{I}}(1-\eta)\,\mathbf{I}_k+\rho_{\mathrm{A}}\,\mathbf{A}_k+\lambda\,(1-\mu)\,\mathbf{H}_k\right]\\ \mathbf{D}_k+dt[\,\mu\,\lambda\,\mathbf{H}_k]\end{pmatrix},\ h(x_k)=\mathbf{H}_k,\ \frac{\partial h}{\partial x}=\begin{pmatrix}0\\0\\0\\0\\0\\1\\0\\0\end{pmatrix}^T \tag{4.31a}$$

$$\frac{\partial f}{\partial x}=\begin{pmatrix}\frac{1-dt\beta_k(\mathbf{P}_k+\mathbf{I}_k+\delta\mathbf{A}_k)}{\mathbf{N}} & 0 & -\frac{dt\beta_k\mathbf{S}_k}{N} & -\frac{dt\beta_k\mathbf{S}_k}{N} & -\frac{dt\beta_k\mathbf{S}_k\delta}{N} & 0 & 0 & 0\\ \frac{dt\beta_k(\mathbf{P}_k+\mathbf{I}_k+\delta\mathbf{A}_k)}{\mathbf{N}} & 1-dt\alpha & \frac{dt\beta_k\mathbf{S}_k}{N} & \frac{dt\beta_k\mathbf{S}_k}{N} & \frac{dt\beta_k\mathbf{S}_k\delta}{N} & 0 & 0 & 0\\ 0 & dt\alpha & 1-dt\zeta & 0 & 0 & 0 & 0 & 0\\ 0 & 0 & dt\gamma\zeta & 1-dt\rho_I & 0 & 0 & 0 & 0\\ 0 & 0 & dt(1-\gamma)\zeta & 0 & 1-dt\rho_A & 0 & 0 & 0\\ 0 & 0 & 0 & dt\rho_I\eta & 0 & 1-dt\lambda & 0 & 0\\ 0 & 0 & 0 & dt\rho_I(1-\eta) & dt\rho_A & dt\lambda(1-\mu) & 1 & 0\\ 0 & 0 & 0 & 0 & 0 & dt\mu\lambda & 0 & 1\end{pmatrix} \tag{4.31b}$$

For the controller, we used the same parameter combinations as above. For the EKF, we used $dt = 0.5$ (day) and assumed $Q = \mathrm{diag}(10^{-6},\ 0,\ 0,\ 10^{-6},\ 10^{-6},\ 10^{-6},\ 0,\ 0)$, $R = 1$, and initial estimation error covariance $P_{0|-1} = 10^{-3}$. For the initial state, we used $\hat{x}_{0|-1} = \mathbf{N}\cdot(0.9999869,\ 10^{-5},\ 10^{-6},\ 10^{-6},\ 10^{-6},\ 10^{-7},\ 0,\ 0)^T$. The estimator used the same parameters as the simulation model, apart from the mismatched parameters γ and δ, detailed in the next section.

Synthesis of continuous and discrete-time subsystems

As we are using both discrete-time and continuous models for the control and estimation steps, we would like to clarify the connection of all the components. We carry out all computations regarding the feedback-linearization and control on the continuous SEIR model. The output of the simulation model, which is continuous as well, is sampled for the discrete-time EKF, which in turn produces discrete state estimations. These estimations are used for computing the input of the system by substituting the obtained values into the state-feedback and input-mapping formulae. The obtained discrete-time input signal is fed back into the simulation model using a zero-order hold. The derivatives of the discrete-time signals (where needed) are approximated by the differences of the consecutive data samples.

4.2.4 Results and discussion

To illustrate and test the operation of the previously presented control setups, we carried out five experiments for the control and reconstruction of historical epidemic data, altering some parameters of the control model and the EKF (compared in Table 4.4).

We chose Sweden's and Hungary's estimated infection data from the interval 15/08/2020 – 15/08/2021 as a base for our reference signals, an interval containing two epidemic peaks for both countries. For the sake of simplicity, in both cases, we assumed the same model parameters as in the case of Hungary (as shown in Table 4.3, and obtained through parameter estimation and statistical methods detailed in [J1]). We set the parameters of the simulation model as

	k_2	k_3	γ	δ
Control setup 0.	20-200%	20-200%	-	-
Control setup I.	15-300%	15-300%	-	-
Control setup II.	10-300%	10-300%	40-165%	40-132%

Table 4.4: Listing of parameter errors applied in different control setups.

slowly-varying with the weighted average of the parameter values being used according to the dominance of the respective virus variant at the given time (detailed in [C2]).

The simulations were run in Matlab/Simulink using the ode45 solver with relative tolerance 10^{-10}, on a computer with processor Intel Core i7-8565u (1.8 - 4.6 GHz) and 16GB RAM, requiring between 45-90s per simulation (appr. 1.5 hours per control setup). To illustrate the robustness of the different scenarios, we altered the parameters of the model(s) used for control and estimation in the different controller setups. The comparison of the applied parameter errors in the different scenarios is shown in Table 4.4.

Control setup 0: robustness without state estimation (Sweden)

In this experiment, we used control setup 0 (Section 4.2.2) for reference tracking control of the SLPIAHRD model using Sweden's data. This setup assumes that all state variables of the simulation model are known at all times, and we computed the states of the control model through the lumping of the respective compartments.

We altered the parameters k_2 and k_3 on a 10×10 grid (i.e., $(k_2, k_3) \in \{(0.2 \cdot m_2 k_2, 0.2 \cdot m_3 k_3) | m_2, m_3 = 1 \dots 10\}$ applying $20 - 200\%$ relative error compared to the nominal value. In total, we ran 100 simulations, the results (nominal trajectories and the computed standard deviation) being illustrated in Figures 4.7–4.9. We can observe that the reference signal is closely followed by the controlled system's output even for significant changes of the parameter values, showing the robustness of the proposed controller setup. Additionally, Figure 4.9 confirms that even for the simulations with high inaccuracies, there is no significant change in the computed input, which, apart from the transient period at the beginning, remains in a feasible range for the observed epidemic.

Control setup I: robustness with SEIR state estimation (Sweden)

In this scenario, we examined the performance of the system in control setup I. (Section 4.2.2), using an EKF constructed around the SEIR model and Sweden's infection data as a reference signal.

Similarly to the previous scenario, we altered the relative error of parameters k_2, k_3 for the control model (affecting both the state estimation and the feedback linearization) on a 9×9 size grid $\{0.1, 0.3, 0.5, 0.75, 1, 1.5, 2, 2.5, 3\}^2$ (the middle of the grid $(1, 1)$ being the nominal parameter values).

The simulation results are illustrated in Figures 4.10, 4.11, 4.12. Figure 4.10 compares the estimated and simulated values of susceptible and recovered individuals: compartments $\mathbf{S}$ and $\mathbf{R}$ of the simulation model plotted alongside the estimated compartments $\hat{\mathbf{S}}$ and $\hat{\mathbf{R}}$ of the control design model, as computed by the EKF algorithm.

Similarly, Figure 4.11 displays the same comparison for estimated and simulated $\mathbf{E} = \mathbf{L}$ and $\mathbf{I} = \mathbf{P} + \mathbf{I} + \mathbf{A}$ compartments. It should be noted, however, that deviations of the simulated compartments are scarcely visible in any of the figures (being several magnitudes lower than

other plotted quantities).

Finally, Figure 4.12 contains the computed input fed into the simulation model.

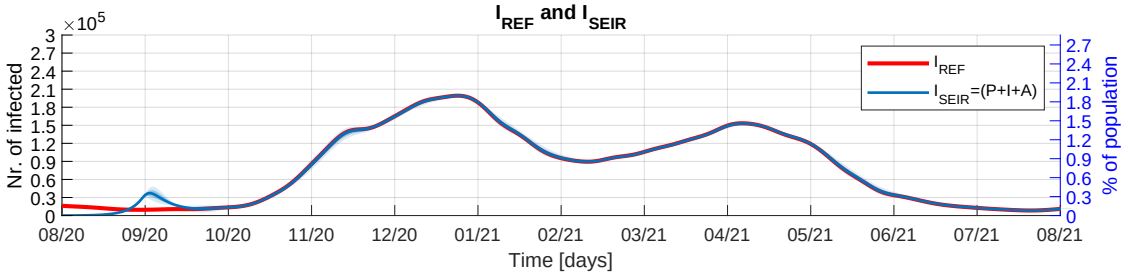

Figure 4.7: Control Setup 0: illustration of the Susceptible and Recovered compartments of the control design model.

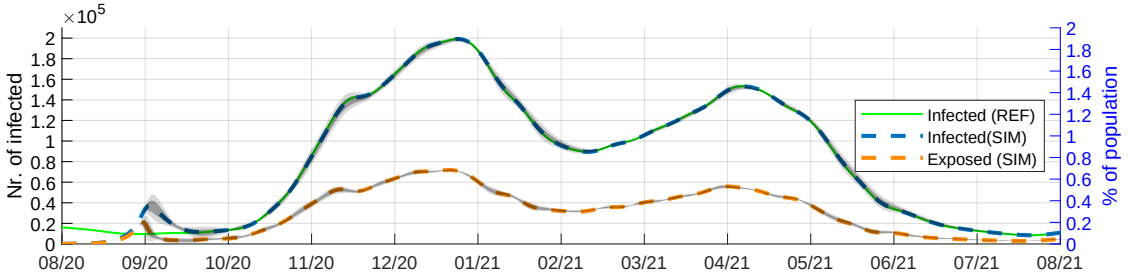

Figure 4.8: Control setup 0: illustration of the simulated Exposed and Infected (Exposed SIM, Infected SIM) compartments of the control design model along the reference signal (Infected REF). The dashed lines show the trajectory obtained using the nominal k_2 and k_3 parameters, and the shaded area shows the deviation σ and 2σ resulting from the parameter alterations.

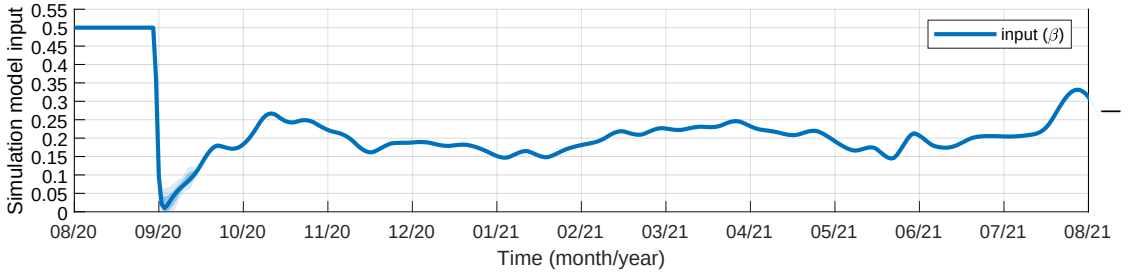

Figure 4.9: Control setup 0: the computed control input (i.e., the reproduction rate), applied to the simulation model. Following a transient period at the beginning (resulting from initial state mismatch), the curve shows almost no deviation in spite of the parameter uncertainties.

Qualitatively matching the results described in [C4], where an experiment with a similar setup but different aim and data (i.e., stricter reference curve, to evaluate performance in case of more intense epidemic control based on Hungary's data) was carried out, we can observe that the controller performed in an acceptable range for all examined parameter combinations.

First, as we can see looking at the continuous and dashed lines in Figure 4.10 and 4.11, the EKF produces precise estimation of states in the case of nominal parameters, regardless of the fact that these nominal values were obtained by the simple intuitive matching of compartments based on their functionality, rather than any kind of formal parameter computation (e.g., by fitting through optimization). As for the mismatched parameters, expectedly they produce significant estimation errors, especially in compartments which do not affect the system's output (like **R**). On the other hand, simulation model trajectories show minimal deviance (approx. 2 magnitudes lower, considering the mean tracking error). The input visible in Figure 4.12 also shows a small variation, emphasizing the error-prone operation of the proposed control law and EKF-based estimation setup.

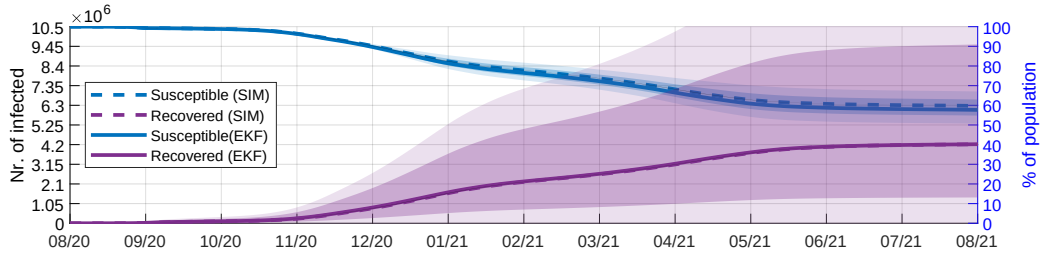

Figure 4.10: Control Setup I: Comparison of simulated and estimated trajectories for Susceptible and Recovered compartments. Dashed lines show the trajectories of the simulation model compartments: Susceptible (SIM) $\mathbf{S}$ and Recovered (SIM) $\mathbf{R}$; continuous lines represent the values computed by the EKF $\hat{\mathbf{S}}$ and $\hat{\mathbf{R}}$ using the nominal k_2 and k_3 parameters. The shaded area around each curve shows the deviation σ and 2σ of the respective variable caused by the mismatched k_2 and k_3 values.

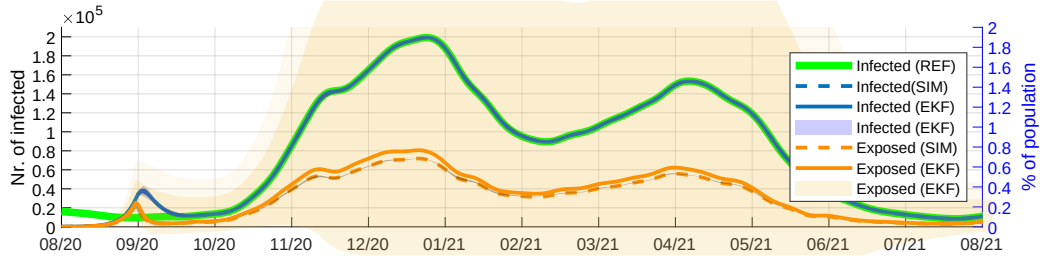

Figure 4.11: Control setup I: Comparison of simulated and estimated trajectories for Exposed and Infected compartments. Dashed lines show the trajectories of the simulation model compartments: Exposed (SIM) $\mathbf{E} = \mathbf{L}$ and Infected (SIM) $\mathbf{I} = \mathbf{I} + \mathbf{A} + \mathbf{P}$; continuous lines represent the estimations of the EKF: Exposed (EKF) $\hat{\mathbf{E}}$ and Infected (EKF) $\hat{\mathbf{I}}$ using the nominal k_2 and k_3 parameters. The shaded area around each curve (hardly visible for dashed lines) illustrates the deviation σ and $2 \cdot \sigma$ of the respective variable caused by the mismatched k_2 and k_3 values. The green continuous line shows the reference signal r, closely tracked by the controller in spite of the significant state estimation errors.

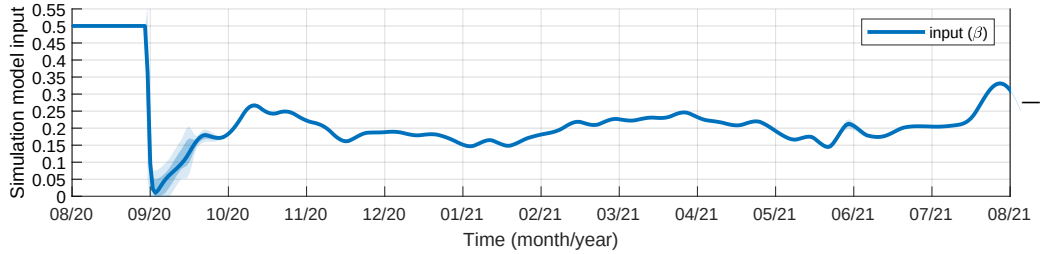

Figure 4.12: Control setup I: Input β of the simulation model (i.e. the desired reproduction rate). The continuous lines show the input computed by the controller with nominal k_2 and k_3, and the shaded area shows the deviation (σ and $2 \cdot \sigma$) resulting from mismatched parameters. The small deviation values show the robustness of the solution (the input calculated for tracking the same reference curve is barely affected by the parameters used for computing the state observation and feedback linearization.)

Control setup II: robustness with SLPIAHRD state estimation (Sweden)

In this experiment, we examined the performance of the system in control setup II (Section 4.2.2). Differently from the previous case, this time we used an EKF constructed around the SLPIAHRD model with mismatched parameters. Inspired by our experience during the Hungarian COVID-19 waves, we chose the uncertain parameters to be γ (probability of symptomatic infection) and δ (relative infectiousness of asymptomatic individuals), as these are the hardest to accurately determine using statistical methods. Similarly to the previous scenario, we also altered the parameters k_2, k_3 of the control model.

We ran 81 simulations, altering k_2, k_3, γ, δ on a $3\times3\times3\times3$ sized grid: $k_2, k_3 \in \{0.5, 1, 1.5\}$ of their nominal values. We used $\gamma \in \{0.25, 0.6, 0.99\}$ and $\delta \in \{0.3, 0.750.99\}$ (these being parameters showing probability, thus having a feasible range $[0, 1]$; the middle value for both parameters corresponds to their nominal value, as shown in the parameter table).

The results of the computations can be seen in Figures 4.13 - 4.19. From Figures 4.13 and 4.14 we can see that the applied parametric uncertainties cause significant deviations in the state variable values of the simulation model. Specifically, the presymptomatic and asymptomatic numbers are affected, while the number of hospitalized people shows a relatively smaller variation. Naturally, these uncertainties have a huge impact on the state estimations of the EKF which uses the nominal model, as it is shown in Figures 4.15 and 4.16. The deviation of the infected compartment is shown separately in Figure 4.17. We can observe that the uncertainty is the largest at the most critical point, i.e., around the peak of the first massive wave. However, as Figure 4.18 shows, this deviation can be greatly reduced using the proposed feedback scheme, even with a highly uncertain state estimation. Finally, Figure 4.19 shows the computed transmission rate. Although the deviation of β is naturally larger than in the previous scenario, the estimation quality is still acceptable in this realistic situation.

From the results of control setup II, two significant conclusions can be drawn. First, as it is visible in Figure 4.17, asymptotically tracking a reference for a non-measurable 'output' of the simulation model ($\mathbf{P}+\mathbf{I}+\mathbf{A}$) estimated using mismatched parameters will result in the estimation error directly appearing in the reference tracking performance - hence the high deviation in the $\mathbf{I}$ compartment. However, as shown in Figure 4.18, the controller – in spite of the serious state estimation errors, combined with the also mismatched control model parameters distorting the input mapping – can effectively minimize the difference between the *estimated* model output and the reference signal. Not surprisingly, as we can observe in Figures 4.13 and 4.14, this estimation bias (effectively causing the *simulation model* to follow different references in the simulations) can be seen in the deviation of the model states as well. However, as the much higher deviance values in Figures 4.15 and 4.16 show (especially in the case of compartments $\mathbf{I}$ and $\mathbf{A}$ highly affected by the uncertain parameters), the controller even in this case greatly reduces the spread caused by the incorrect state estimation, and maintains all important qualitative properties of the trajectory to be tracked. As a second observation, the small deviance values of the input β (visible in Figure 4.19) must be emphasized, showing that the incorrect controller and estimation parameters do not influence the input significantly. Consequently, even though imperfectly estimated output used for reference tracking can naturally decrease the tracking performance, we haven't experienced problematic inputs (abrupt changes, out-of-bound values, etc).

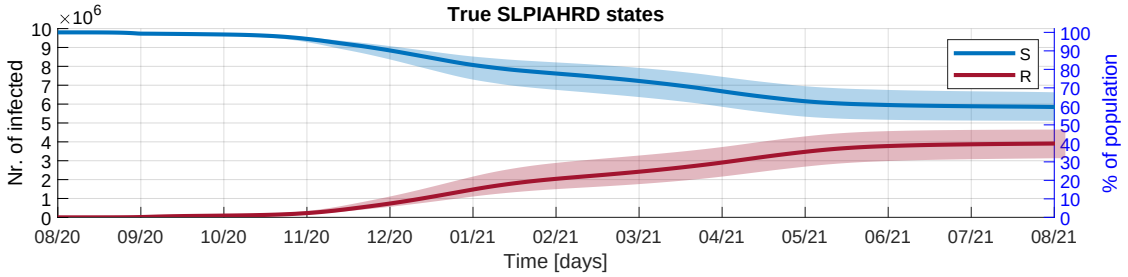

Figure 4.13: Control setup II: simulated states **S** and **R** of the *simulation model* and their standard deviation (shaded area) resulting from the parameter uncertainties

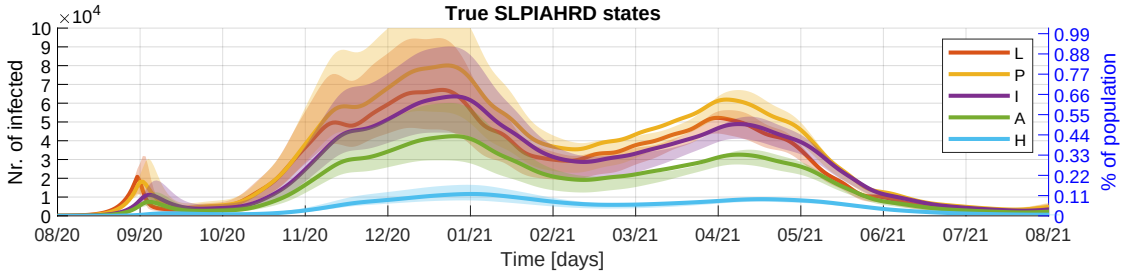

Figure 4.14: Control setup II: simulated states $\mathbf{L} - \mathbf{H}$ of the *simulation model*, and their standard deviation (shaded area) resulting from the parameter uncertainties

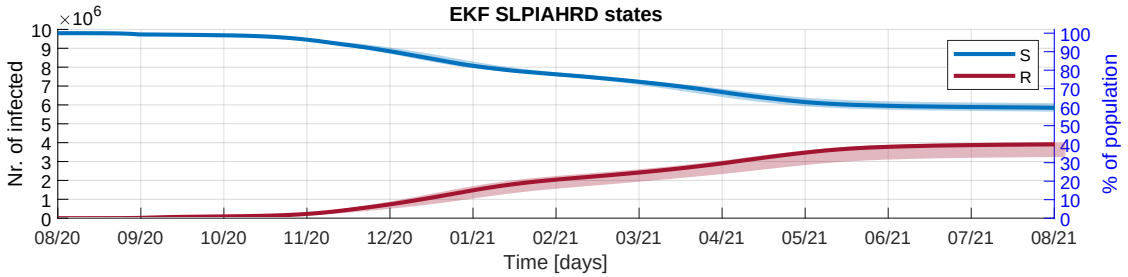

Figure 4.15: Control setup II: estimated states **S** and **R** of the *simulation model* and their standard deviation (shaded area) resulting from the parameter uncertainties

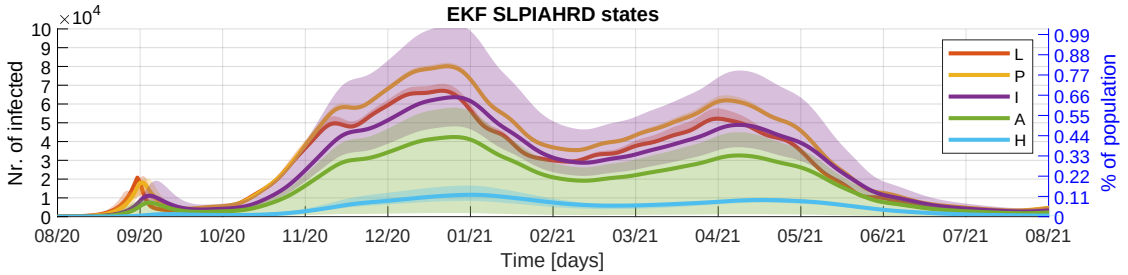

Figure 4.16: Control setup II: estimated states $\mathbf{L} - \mathbf{H}$ of the *simulation model*, and their standard deviation (shaded area) resulting from the parameter uncertainties

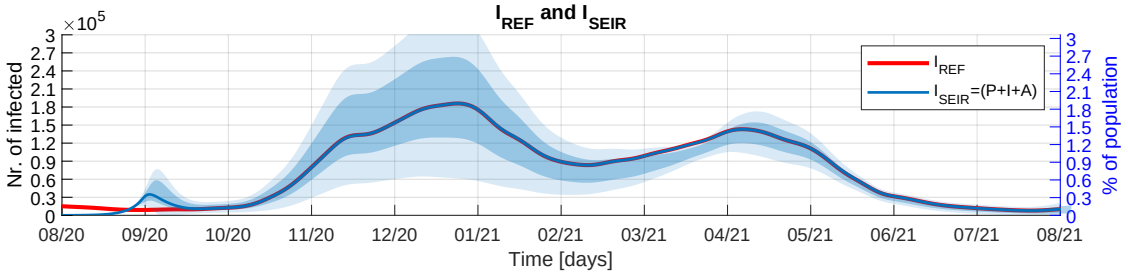

Figure 4.17: Control setup II: comparison of reference signal with the *real* output of the *simulation model*.

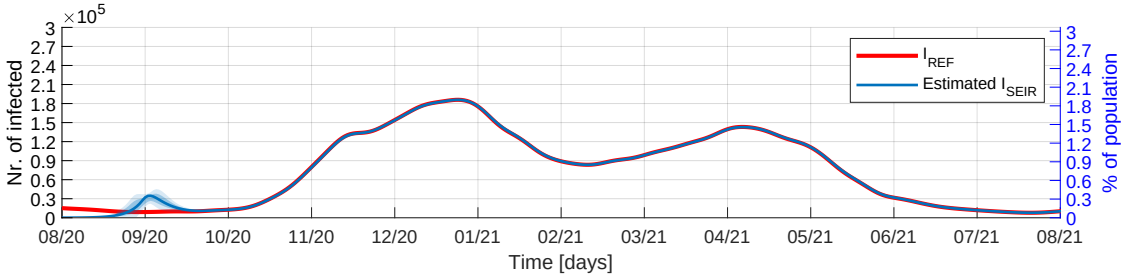

Figure 4.18: Control setup II: comparison of reference signal with the *estimated* output of the *simulation model*, as seen by the controller.

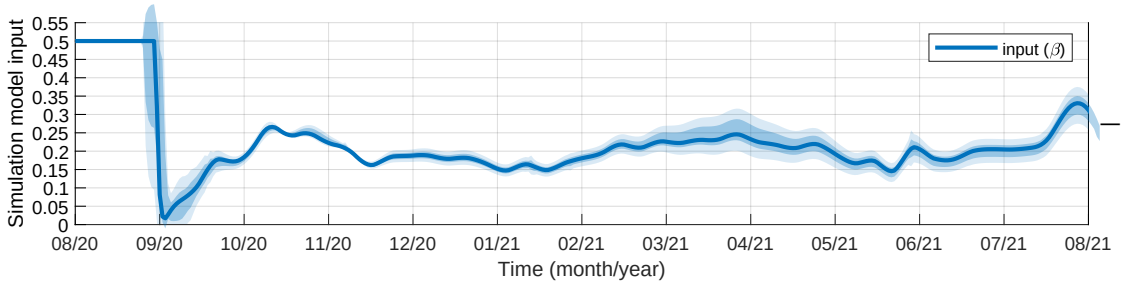

Figure 4.19: Control setup II: Input (i.e. the desired reproduction rate) applied to the *simulation model* in the simulations. The shaded areas represent the standard deviation (σ and $2\cdot\sigma$) of the signal resulting from the parameter uncertainties.

Testing: data reconstruction using SLPIAHRD state estimation (Hungary)

As it is summarized e.g., in [213], such a reference tracking scenario can also be viewed as an inversion of a dynamical model. By trying to track / reproduce the actual output of the epidemic process (as observed during the pandemic) with our model, the model's input (desired reproduction rate, computed by the controller) effectively becomes an estimation of the actual reproduction rate of the epidemic. In this way, the reproduction of model trajectories from the output can be transformed into a control problem, solved by the presented feedback-linearization technique.

In this scenario, we use control setup II. to track the transmission rate and the number of active infections measured (or more precisely, estimated from multiple factors) in Hungary between 15/08/2020 – 15/08/2021. Similarly to the previous scenario, we alter the parameters k_2, k_3, γ, δ on the same grid, totaling 81 simulations.

Similarly to the previous sections, we cannot use β directly to compare our results to those published in the relevant literature, thus we compute the effective reproduction number of the epidemic from it. As explained in section 3.1.2, the time-varying effective reproduction number of an epidemic corresponds to the number of susceptible individuals an infectious person will infect on average, given the circumstances at the given time. The effective reproduction number obtained as a result of this simulation can be seen in Figure 4.20, along with the effective reproduction number estimated for Hungary by the OWID [212] and by the ÁtlóTeam [214], both using a classical statistical approach.

For comparison, we also include our own previous estimation published in [C3], created using the same robust controller setup, but without any state estimation (assuming all states of the simulation model to be directly measurable). In that case, we used the SEIR model to compute the effective reproduction number from β, derived using the SEIR model's compartments as:

$$R_c(t) = \beta(t)\frac{\mathbf{S}(t)}{N}\frac{1}{k_3} \tag{4.32}$$

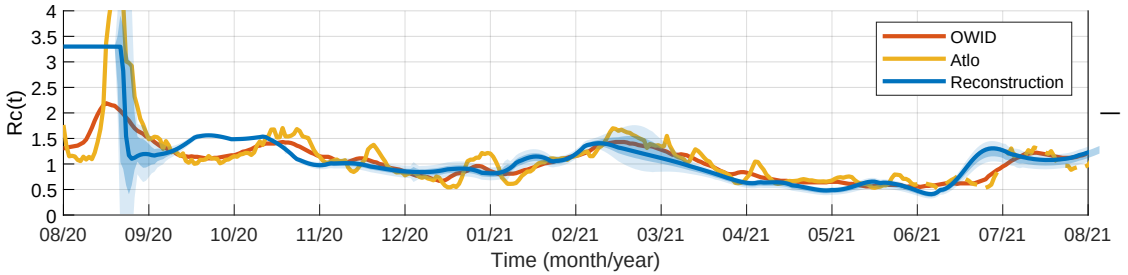

Figure 4.20: Reconstruction: Comparison of reproduction numbers, as estimated in Hungary by OWID [212], by the ÁtlóTeam [214], and as reconstructed using control setup II. The shaded blue area shows the standard deviation of our estimation for the different simulations.

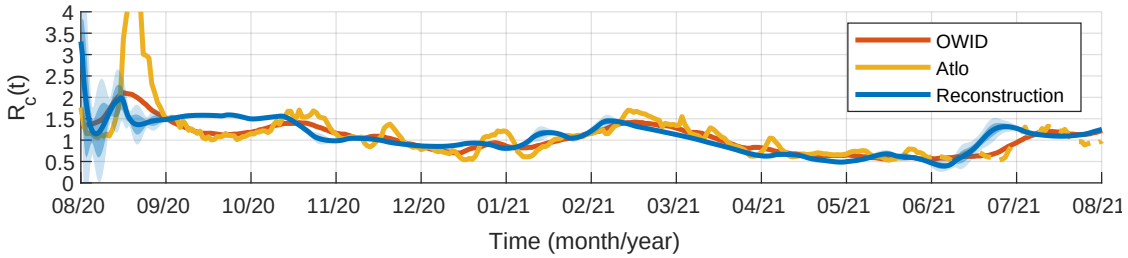

Figure 4.21: Reconstruction: Comparison of reproduction numbers, as estimated in Hungary by OWID [212], by the ÁtlóTeam [214], and as reconstructed by our algorithm using the true SLPIAHRD states without EKF estimation, but with serious parameter mismatch between the simulation and the control design model). The shaded blue area shows the standard deviation of our estimation for the different simulations.

The results of those simulations are shown in Figure 4.21, compared again with the results of the OWID and the ÁtlóTeam.

Testing: data reconstruction using public data of Sweden

Similarly to the Hungarian reconstruction scenario above, for the sake of completeness and validation, we also compute the effective reproduction number for Sweden, using control setup II (EKF based on the SLPIAHRD model, with altered k_2, k_3, γ, δ parameters). In this case, we could only compare our results to the reproduction number computed by OWID. As it is visible in Figure 4.22, following a brief transient period (while the state estimator and the controller converge), we could track the reproduction number with high accuracy (and low deviation, in spite of the serious parameter mismatch).

Comparison: Hungarian and Swedish data

During the COVID-19 outbreak, Hungary and Sweden opted for drastically different measures for dealing with the high number of infections and the burden it put on the country's healthcare

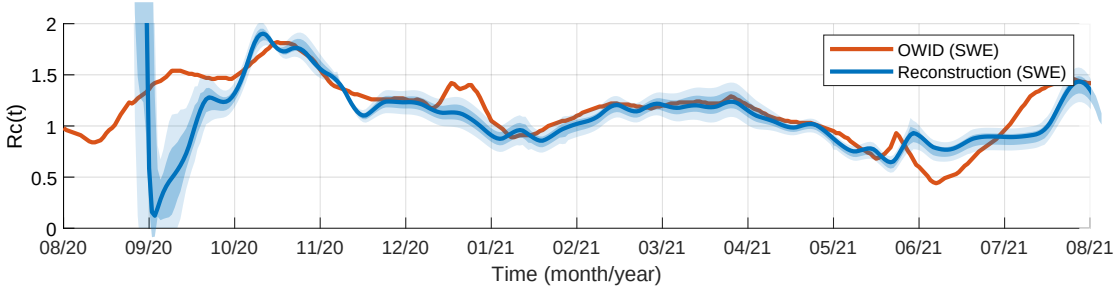

Figure 4.22: Reconstruction: Comparison of reproduction numbers, as estimated in SWEDEN by OWID [212] and as reconstructed using control setup II. The shaded blue area shows the standard deviation of our estimation for the different simulations.

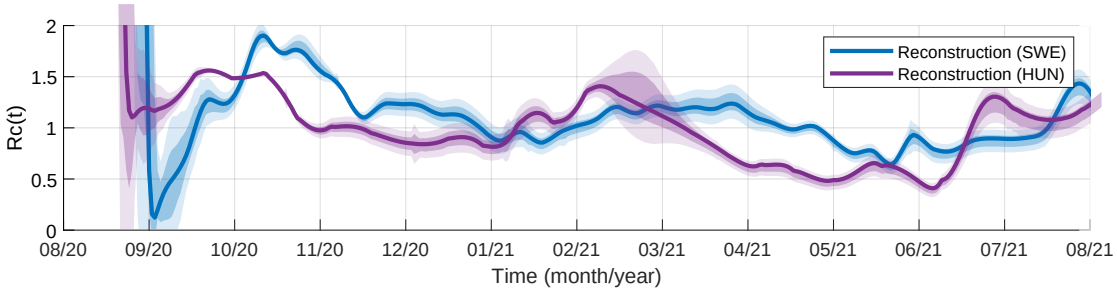

Figure 4.23: Reconstruction: comparison of reproduction numbers, as estimated in Sweden and Hungary, using control setup II. The shaded area shows the standard deviation for the different simulations.

system. Hungary initially opted for a strict suppression strategy, practically eliminating the first epidemic wave, and gradually releasing restrictions later, resulting in serious peaks in the second (around 10/20-11/20) and third (02/21) waves. Sweden, on the other hand, adopted a more permissive intervention strategy in the beginning, trying not only to mitigate the effects of the pandemic, but also minimizing the negative effects of the restrictions on the economy. As a result, more serious first and second waves were followed by smaller outbreaks. This difference of strategy appears in the reconstructions of the pathogen's reproduction numbers in the two countries, as illustrated in Figure 4.23.

4.2.5 Conclusion

The goal of this section was to study the possibilities of feedback linearization-based epidemic control combined with state estimation in the presence of parametric and modeling uncertainties. For this, we first proposed a reference tracking control scheme for a nonlinear 8-compartment epidemic model. The system input is the transmission rate, while the controlled output is the number of infected people within the population. The model used for control design is a simplified 4-compartment SEIR system where the state variables are mapped to those of the more detailed model. The control law is based on feedback linearization and asymptotic output tracking in a servo configuration. The state information for the feedback is computed by an extended Kalman filter. Two control setups containing state estimation were tested: in the first one, the state estimator was based on the simplified model, while in the second scenario, the EKF also used the detailed simulation model. The robustness of both scenarios was studied for several different parameter combinations in a range of 10% - 300% of their nominal values. Although the state estimation errors were significant in the case of uncertain parameters and model mismatch, the tracking performance was good in all studied cases. The proposed approach was also illustrated as a possible tool for retrospective data (especially, transmission rate) reconstruction. From this respect, we can say that the applied model is 'well invertible' in the sense that the variance of the transmission rate was small in all computations. In summary, the most important message of the study is that the combination of a state estimator and an appropriately designed nonlinear state feedback can be successful even if the control model contains significant modeling and/or parametric uncertainties. This is promising from the point of view of possible applications.

The main limitations of the study are the following. First, the number of infected people was used as observed 'performance' output, while it is known that it is challenging to determine it in real time. However, there are several statistical and dynamical-model-based methods to refine this number, e.g., from the number of hospitalized people and/or from wastewater samples [215–217]. Second, the manipulated input is assumed to be a variable that can be changed in each sampling instant. This makes the proposed methodology more suitable for data reconstruction, as it was illustrated in the case studies. However, the generated inputs and trajectories can be used as

feasible starting points for more realistic approaches such as model predictive control (MPC). Moreover, MPC generally also requires state estimation in a similar setup, and an important message of this study is that an appropriate feedback may still be operational with high estimation uncertainties caused by model mismatch. Additionally, we have to note that the properties of the entire control loop were not mathematically analyzed. In this respect, the most relevant results from the literature mentioned in the introduction are [51,147,154]. However, model uncertainties are not considered in these articles.

Chapter 5

Parameter synthesis of nonnegative systems

In this chapter, based on the previously published paper [J5], I propose an optimization-based approach for finding parameters that guarantee by design a predefined qualitative behavior for a nonnegative nonlinear dynamical system. Similarly to a model predictive control setup, the model states and parameters are considered as free decision variables, while the system dynamics as well as the desired behavioral properties are incorporated into the optimization constraints.

I show the feasibility of the idea, I present three case studies on models with increasing complexity and number of state dimensions: the classical Brussellator (for easy theoretical validation of the obtained results), a three-dimensional Lotka-Volterra (which introduces a numerically complex problem), and a four-dimensional epidemic model (which investigates the phenomena of oscillating epidemic processes without seasonality, and adds another pillar to the epidemic analysis and control framework developed in the previous chapters). The goal of all experiments is to induce oscillatory behavior with predefined frequency and possibly decay, which can be specified manually or - currently with limitations - temporal logic formulas.

The obtained results clearly underline the importance of novel, computationally-intensive methods in designing system behavior, which, due to the increased availability of highly-optimized numerical solvers and appropriate hardware are capable of handling problems with practical complexity.

5.1 Methodology

Our aim is to compute the parameters providing the desired qualitative dynamical properties by creating an appropriate nonlinear optimization problem, having the parameters as decision variables. To achieve this, we apply a strategy motivated by model predictive control (MPC). Along the parameters, all future states of the time-discretized system up to a predefined finite horizon of N steps are considered decision variables, while the system dynamics is introduced in the form of constraints between these variables. The desired behavior is also described using appropriate constraints on the state and input variables, either derived by hand or translated algorithmically from Signal Temporal Logic (STL) formulae. Similarly to the classical MPC framework, we can use the objective function of the optimization problem (typically given in a quadratic form involving the decision variables) to choose the preferred solution from the set of

feasible solutions. However, we are mainly interested in finding a feasible solution.
To formalize the approach, let us consider a continuous dynamical system in the form:

$$\dot{x}(t) = f(x(t), p) \tag{5.1}$$

where the state function f has parameters collected into a vector p. We assume that the parameters are constant in time, which leads to a time-invariant system.

5.1.1 Discretization

As previously, to apply an MPC framework, the first necessary step is finding a suitably precise discrete representation of the originally continuous system with sampling time dt:

$$x_{k+1} = F(x_k, p) \tag{5.2a}$$
$$x_k = x(k \cdot dt) \tag{5.2b}$$

Considering the two classical numerical ODE solutions detailed in subsection 2.1.6, in the end, we chose the Euler method for all three experiments.
Even with its well-known drawback of quickly accumulating the errors in case of higher derivatives, we experienced that choosing a smaller dt and thus working with longer horizons (in terms of variables) can provide the necessary precision, while avoiding the higher-order terms introduced in the equations by the Runge-Kutta method.
As future work, the usage of the Runge-Kutta method with some of its intermediary variables introduced into the optimization problem might be beneficial to consider. Even though this would induce a significant increase in the number of optimization variables, dealing with more variables might be a smaller challenge for the solver compared to the otherwise increased high-order numerical constraints.

5.1.2 The optimization problem and its solution

To formalize the nonlinear optimization problem, we introduce the notation: $\mathbf{x} = \{x_0,\ldots,x_N\}$, collecting the future state variables for N steps. Using this, we are looking for the parameters p which satisfy:

$$p^* = \arg\min_p J(\mathbf{x}, p) \tag{5.3a}$$
$$\text{w.r.t. } x_{k+1} = F(x_k, p),\ k = 0 \ldots (N-1) \tag{5.3b}$$
$$G_x(\mathbf{x}) \leq h_x,\ G_p(p) \leq h_p, \tag{5.3c}$$

where $J(\mathbf{x}, p)$ is the cost function, and (5.3b) are equality constraints for incorporating the system dynamics. Moreover, (5.3c) are additional constraints for the states, inputs, and parameters, respectively, including the nonnegativity constraint for the dynamics. Due to the nonlinear dynamics encoded in (5.3b), and the generality of the constraints, (5.3a) - (5.3c) is a nonlinear programming problem. The logical constraints are encoded using the big-M method. It must be noted, that the structure of the cost function is theoretically not limited in any way, but a convex (e.g. quadratic, like $J(\mathbf{x}, p) = \mathbf{x}^\intercal P_x \mathbf{x} + p^\intercal P_p p$ with positive definite P_x and P_p weighting matrices) function is generally recommended for a computationally more efficient numerical solution. In

this setup, even a constant cost function is sufficient: using this, solving the problem becomes a question of *feasibility*, when any kind of parameter set is accepted as long as the predefined behavioral constraints are met. However, if more complex behavior (e.g. approximate tracking of a given reference signal) is expected, the quadratic difference could also be incorporated in J.

Behavioral constraints

There are several possibilities to encode the desired qualitative behavior into the additional constraints (5.3c). For a simple required behavior, it can be straightforward to manually define the constraints. For example, if the states should converge to 0 after a given finite time, we can define

$$G_x(x_0, x_1, \dots, x_i, \dots x_N) = (0\ 0 \dots 0\ x_i \dots x_N)^\intercal \tag{5.4a}$$

$$h_x = (0\ 0\ \dots \varepsilon\ \varepsilon \dots \varepsilon)^\intercal \tag{5.4b}$$

where ε is sufficiently small.

For more complex behaviors, mathematical formalisms like Signal Temporal Logic can be used. While STL is typically used for behavior checking and validation of dynamical models, there exist algorithms and toolboxes for transforming STL formulae into optimization constraints [26], and there exist applications of MPC-based nonlinear system control using these constraints (e.g. [218]). A successful application is also discussed in Chapter 3, where STL is used to formulate time-varying constraints related to epidemic management. It must be noted, however, that the use of these toolboxes is far from being routine: the automatically generated constraint sets often have undue high dimensions, possibly resulting in a practically non-manageable computational problem for the solver. Additionally, STL specifications generally bring integer variables into the optimization task (5.3a) - (5.3c), making it a MINLP.

Enforcing oscillatory behavior

In this work, we chose to encode the oscillatory behavior we want to enforce for the examined systems. For this, we introduce the following notations. Let the ith state variable (x_i) at time step k be denoted by x_{ki}. Let the desired oscillation period for x_i be t_i, the oscillation threshold τ_i, and the constraint filling ratio be r_i. We prescribe that the system state variables go above and below the threshold at specific times, and remain there for a time period corresponding to the filling ratio. This dynamic constraint can be written as

$$l = r \cdot t/4 \tag{5.5a}$$

$$x_{ki} \leq \tau_i - \epsilon \quad \forall k \ : \ k \cdot dt \in S_1,\ 0 \leq k \leq N \tag{5.5b}$$

$$S_1 = \bigcup_{j \in \mathbb{N}} \left[t_{0i} + j \cdot t_i - l_i; t_{0i} + j \cdot t_i + l_i \right] \tag{5.5c}$$

$$x_{ki} \geq \tau_i + \epsilon \quad \forall k \ : \ k \cdot dt \in S_2,\ 0 \leq k \leq N \tag{5.5d}$$

$$S_2 = \bigcup_{j \in \mathbb{N}} \left[t_{0i} + \left(j + \tfrac{1}{2}\right) t_i - l_i; t_{0i} + \left(j + \tfrac{1}{2}\right) t_i + l_i \right] \tag{5.5e}$$

Numerical solution

In our setup, we used `MATLAB R2022b` as the base computation environment, and assembled the optimization problem using `YALMIP` (version 20210331 [162]), and solved it with `BARON 19.3.24` [163]. Baron is a proprietary MINLP solver that applies a polyhedral branch and

bound approach, and shows outstanding solution capabilities and excellent performance in complex nonlinear optimization [30, 219]. The experiments were carried out on a Lenovo Thinkpad T590 notebook with an i7-8568U (4 cores, 1.8-4.0 GHz) processor and 16GB RAM.

The obtained results were validated in continuous time using the built-in Ode45 solver of Matlab (using the 4th and 5th order Runge-Kutta method) with default settings (except for the absolute tolerance `AbsTol`=10^{-10}) for simulating the system trajectory given the solver-computed values of the decision variables.

5.2 Computation results

In order to find the boundaries and illustrate the capabilities of the proposed approach, we carried out three case studies for models with increasing state space dimension and number of parameters. Each of the presented nonnegative and kinetic models is capable of showing some kind of oscillatory behavior, and our aim is to find the appropriate parameters for it.

5.2.1 Brussellator

The Brusselator is a classic two-dimensional model, proposed initially by Prigogine and Lefever for describing chemical reaction networks capable of showing complex behavioral patterns [220]. As a starting point, it is widely used for modeling (bio)chemical systems with oscillatory behavior, e.g. the Belousov-Zhabotinsky reaction, chemical reactions regulating circadian clocks, or certain neuron models. Since many theoretical results are known on the oscillation conditions of general two-dimensional models and specifically on the Brusselator, this case is intended to be an introductory illustration and testing of our approach.

Model and nominal parameters

The model shows the trajectory of the concentrations of two reagents ($\mathbf{B_1}, \mathbf{B_2}$) present in a chemical reaction (the concentration of the remaining materials being constant), and is formally given by the following nonlinear ordinary differential equation (ODE) system in *dimensionless* form:

$$\dot{\mathbf{B}}_\mathbf{1} = k_1\, a - k_2\, b\, \mathbf{B_1} + k_3\, \mathbf{B_1}^2\, \mathbf{B_2} - k_4\, \mathbf{B_1} \tag{5.6a}$$

$$\dot{\mathbf{B}}_\mathbf{2} = k_2\, b\, \mathbf{B_1} - k_3\, \mathbf{B_1}^2\, \mathbf{B_2}. \tag{5.6b}$$

In our study, we use the Brussellator with the simplest nominal set of parameter values, choosing $k_1 = k_2 = k_3 = k_4 = 1$, and consider a and b as unknown parameters to be determined. It must be noted that to the dimensionless form, this simplification can be performed without loss of generality [220].

Our goal is that the system produces sustained oscillations with predefined period lengths, starting from the initial state $x_0 = [1\ 1]^\intercal$. We remark that the necessary and sufficient condition of oscillations is well-known as

$$a^2 + 1 \leq b. \tag{5.7}$$

However, we won't use this condition among the constraints.

Optimization parameters and results

In our first experiment, we chose the oscillatory period to be $t = 8$ time units. We discretized

the system using the Euler method using $dt = 0.2$ units and chose a time horizon of $T = 40$ units, resulting in $N = 200$ steps. We introduced the following periodicity constraints (see, eq. (5.5)): $t_1 = t_2 = 8$, $t_{01} = 4, t_{02} = 8$, $\epsilon = 0.1$, $r_1 = r_2 = 0.1$. As we did not want to overspecify the problem and decide on a suitable oscillation threshold $\tau_1$and τ_2, we also introduced these as decision variables (i.e., we only want each state variable to have a threshold that periodically outgrows and then goes back below, but we do not specify where that threshold is between the realistic bounds $\epsilon \leq \tau_1, \tau_2 \leq 10$). As we are only looking for a feasible solution (and do not want to choose from them any specific one), we set the cost function J to a constant value. The problem took approximately 6 seconds for the solver, resulting in parameter values $a = 0.808, b = 1.690$, and trajectories illustrated in Fig. 5.1a.

Consequently, we repeated the computation for a series of growing periods $t = \{10, 12, 15, 20\}$, using the same approach to derive the constraints, resulting in parameters and trajectories shown in Figs. 5.1b-5.1e. The solver times needed for the computation are shown in Table 5.1.

Looking at the results, it can be checked that for the cases shown in Figs. 5.1b-5.1d, the condition (5.7) holds, meaning that the system indeed produces stable oscillations with these parameters. In the last case in Fig. 5.1e, however, the condition is not satisfied, although the prescribed oscillations are fulfilled. Here, we can observe a limitation imposed by the finite horizon $T = 40$ of the optimization, barely able to include two full periods of $t = 20$. Thus, while the system satisfies each constraint and produces oscillations, the trajectories converge to a stable equilibrium in the long term. Essentially, the same results were obtained using the Runge-Kutta 4 discretization.

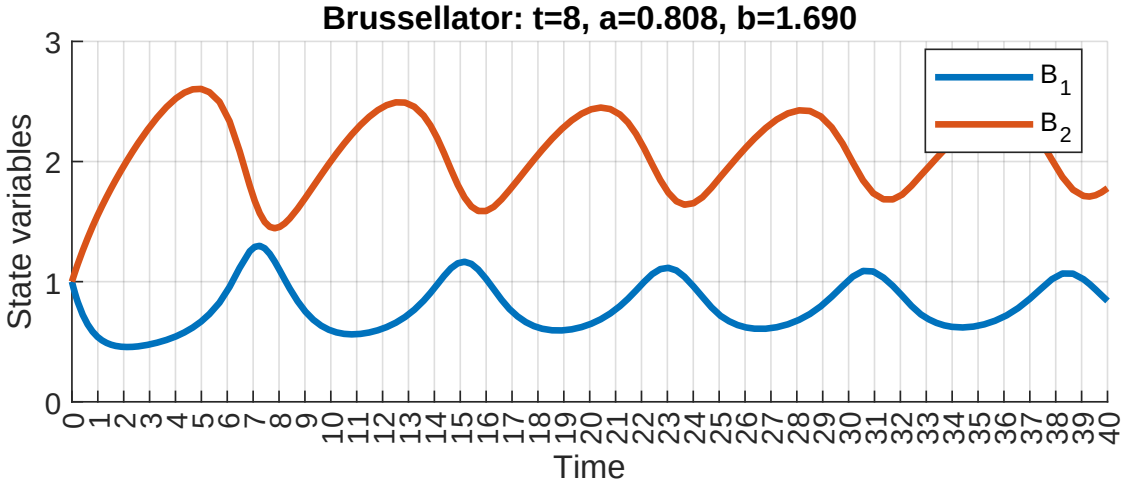

(a)

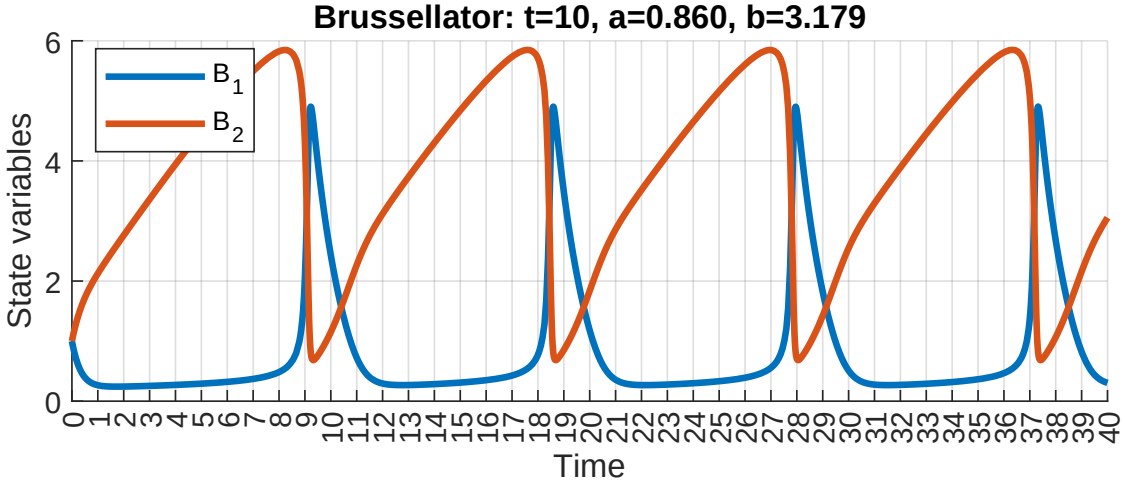

(b)

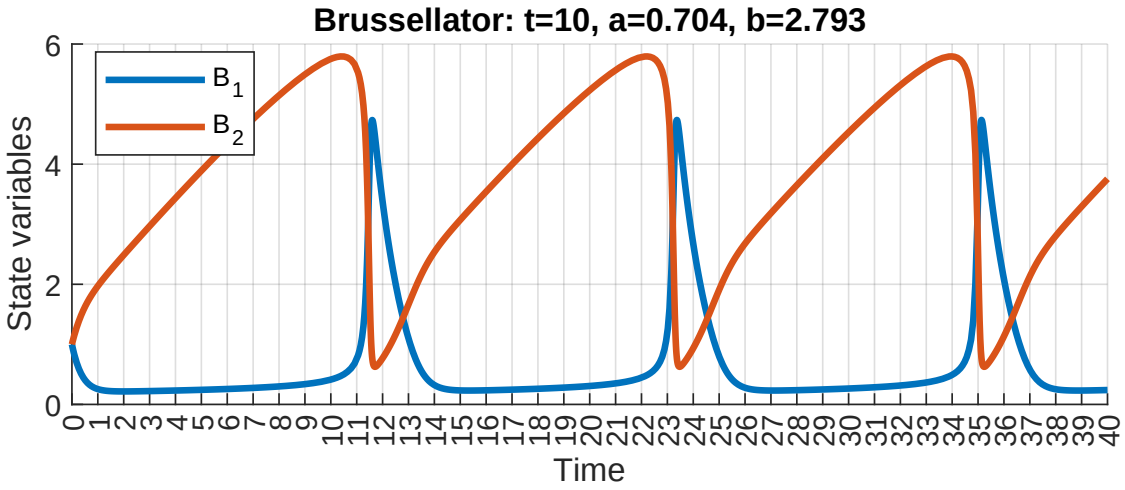

(c)

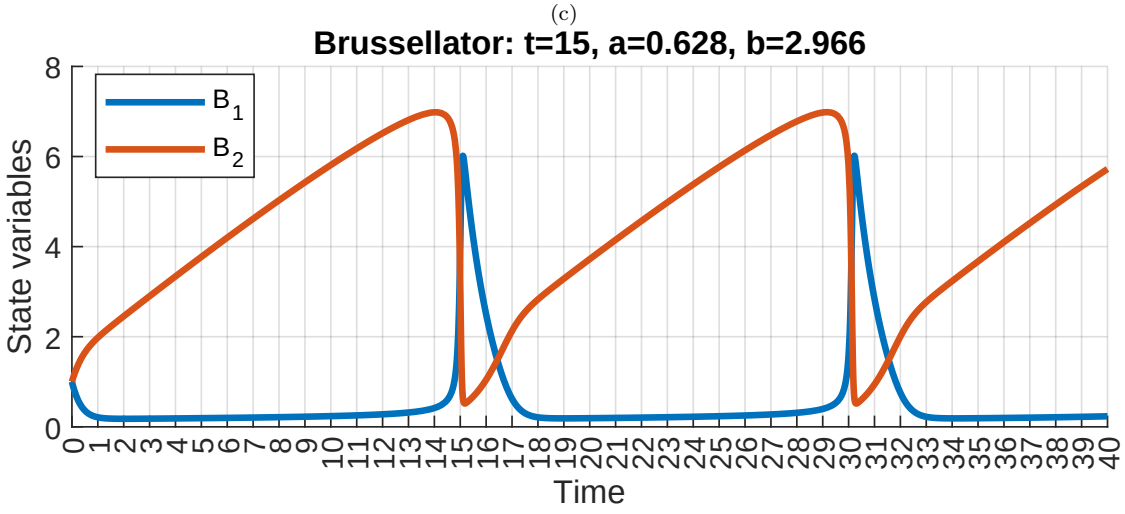

(d)

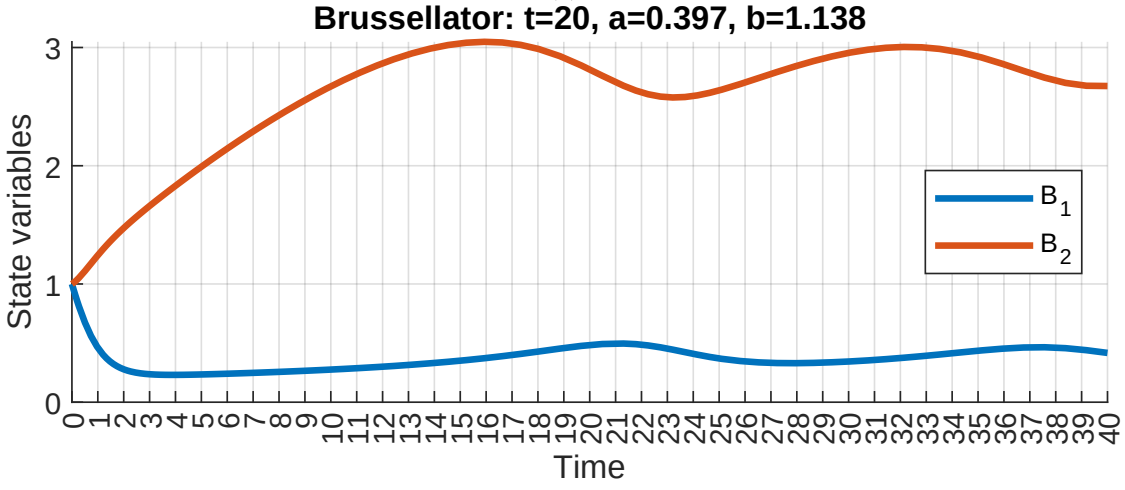

(e)

Figure 5.1: Computed parameters and their simulated trajectories for the Brussellator model

5.2.2 A food chain model in Lotka-Volterra form

Lotka-Volterra-type (LV) models were originally derived independently for two purposes: modeling (then only hypothetical) chemical reactions in which the concentrations of reagents oscillate, and describing population dynamics of interacting species in a habitat [13, 221]. It is important to mention that generalized Lotka-Volterra models can be considered as universal descriptors of nonlinear dynamics; therefore, their analysis and application reach far beyond population models [222].

Model and nominal parameters

We analyze the system proposed in [223], which models a linear three-species food chain consisting of a low-level prey ($\mathbf{L_1}$), its mid-level predator ($\mathbf{L_2}$), and a high-level predator ($\mathbf{L_3}$) hunting for $\mathbf{L_2}$. The interaction between the species is modeled by the differential equation system below

$$\dot{\mathbf{L}}_\mathbf{1} = a\,\mathbf{L_1} - b\,\mathbf{L_1}\,\mathbf{L_2}, \tag{5.8a}$$

$$\dot{\mathbf{L}}_\mathbf{2} = -c\,\mathbf{L_2} + d\,\mathbf{L_1}\,\mathbf{L_2} - e\,\mathbf{L_2}\,\mathbf{L_3}, \tag{5.8b}$$

$$\dot{\mathbf{L}}_\mathbf{3} = -f\,\mathbf{L_3} + g\,\mathbf{L_2}\,\mathbf{L_3}. \tag{5.8c}$$

with the following parameters:

- a, c, f representing the natural growth and decay rate of populations $\mathbf{L_1}, \mathbf{L_2}$, and $\mathbf{L_3}$, respectively (without being hunted and without prey being available);
- b, e representing the negative effect of being hunted on populations $\mathbf{L_1}, \mathbf{L_2}$; and
- d, g representing the positive effect of prey being available for populations $\mathbf{L_2}, \mathbf{L_3}$.

The model is known to show oscillations and periodic behavior for certain parameter combinations, specific behaviors being shown in the case of different parameter regions [223]. For our study, we opted for nominal parameter values: $b = 1/2, e = 1, d = 1/6, g = 1/8$, fixing the effect of interaction between the species, and let the solver find the natural growth and decay rates a, c, f for which the task specification holds. We prescribed (stable) oscillations for the system with predefined period lengths, starting from the initial state $x_0 = [10\ 3\ 1]^\intercal$

Optimization parameters and results

As the Lotka-Volterra model showed serious approximation errors in case of the Euler method, we used different dt values and time horizons in the three case studies, as detailed in Table 5.1. Similarly to the Brussellator experiment, we manually set the periodicity constraint for the first state variable (substituting Eq. (5.5) with $t_1 = 10, t_{01} = 4, \epsilon = 0.1, r_1 = 0.1, 1 \leq \tau_1 \leq 20$ and setting J constant. For the second and third state variables no constraints were set.

We carried out three computations, with results shown in Figures 5.2a - 5.2c. It is visible that the oscillations fulfill the prescribed periods. It can also be seen from Table 5.1 that the average solution time was the highest in the case of this model.

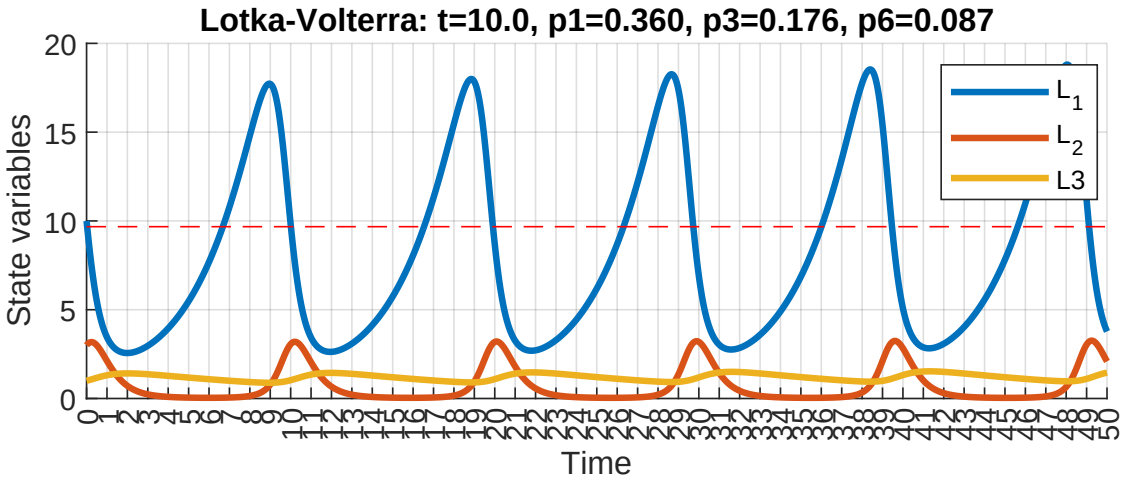

(a)

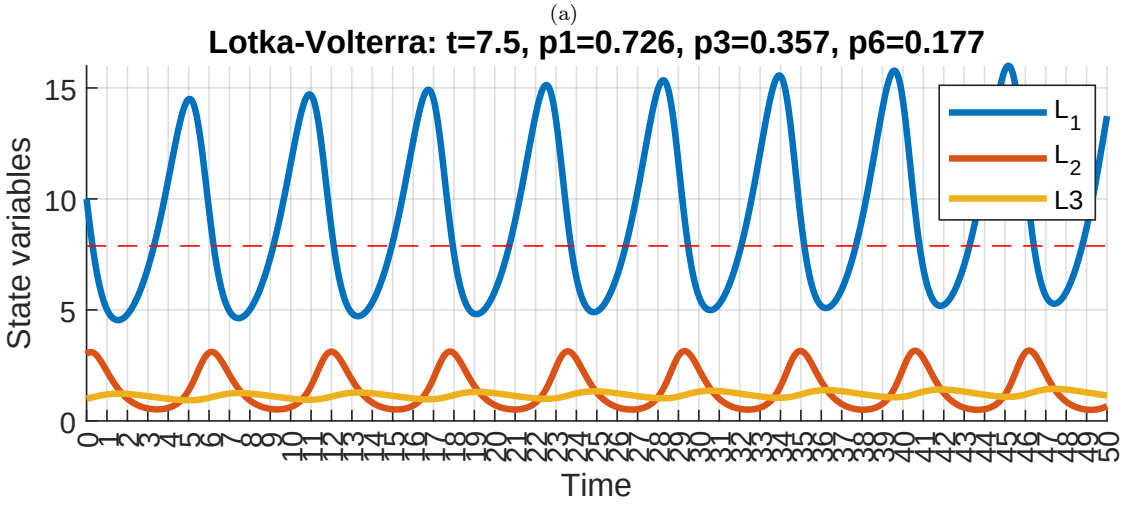

(b)

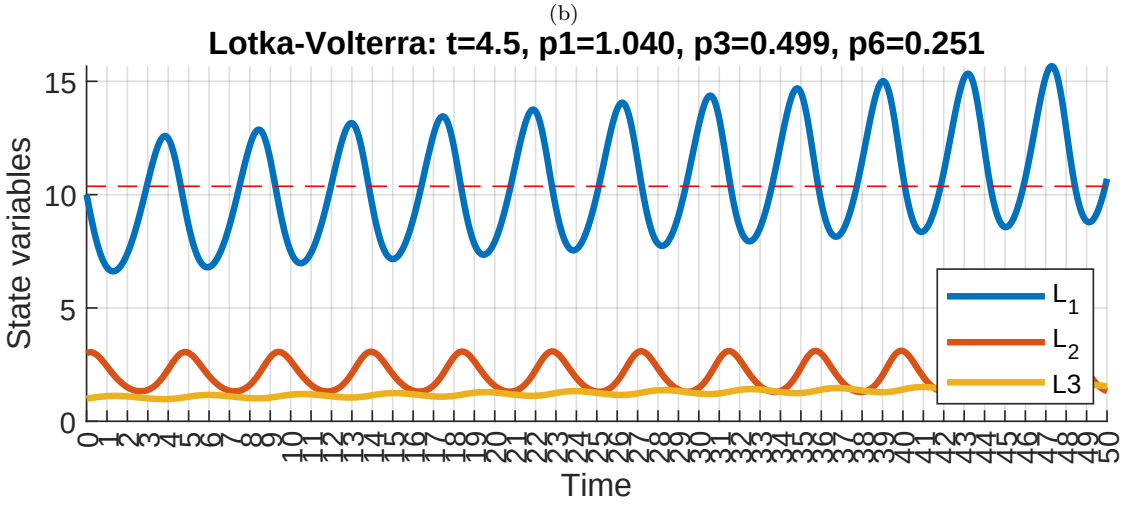

(c)

Figure 5.2: Computed parameters and corresponding trajectories for the Lotka-Volterra model. The red dashed line shows the computed threshold τ_1.

5.2.3 A SEIR(S) epidemic model with immunity waning

The SEIR(S) is a four-dimensional nonlinear compartmental model widely used for describing various epidemic processes. As already detailed in subsection 4.2.1, the SEIR model divides the population into four compartments, representing the different states of the disease, and people transition from one compartment to another based on their current health condition. Susceptible individuals (in compartment **S**) are assumed to have no protection against the virus and may become ill if exposed to the pathogen. Those in the exposed compartment (**E**) already carry the disease, but can not spread it yet, and transition automatically to the infected group (**I**) after the incubation period. Infected people (**I**) can infect those in **S** and are assumed to recover over time. Recovered individuals (**R**) are assumed to have perfect immunity against the pathogen.

Complementing the basic SEIR model, in our case, recovered people lose their immunity after a given time and are moved back into the susceptible compartment. As disambiguation, this version is commonly referred to as SEIR**S** in scientific literature. Compartments of the model and the possible transitions can be observed in Fig. 5.3.

Formally, the dynamics of the model is given by the following differential equations:

$$\dot{\mathbf{S}} = -\beta\,\mathbf{S}\,\mathbf{I}\,/\,\mathbf{N} + \omega\,\mathbf{R}, \tag{5.9a}$$

$$\dot{\mathbf{E}} = \beta\,\mathbf{S}\,\mathbf{I}\,/\,\mathbf{N} - k_2\,\mathbf{E}, \tag{5.9b}$$

$$\dot{\mathbf{I}} = k_2\,\mathbf{E} - k_3\,\mathbf{I}, \tag{5.9c}$$

$$\dot{\mathbf{R}} = k_3\,\mathbf{I} - \omega\,\mathbf{R}. \tag{5.9d}$$

where **N** is the total population size, which is assumed to be constant.

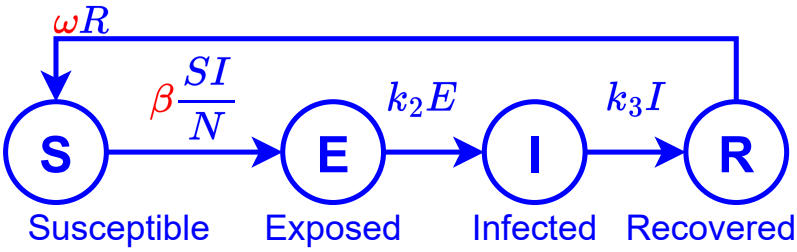

Figure 5.3: Compartmental transitions of SEIRS epidemic model with waning of immunity

The model has four parameters: the transmission rate of the virus (β), the average incubation period (k_2^{-1}), the average time it takes to recover (k_3^{-1}), and the average time the immunity obtained by recovery lasts (ω^{-1}). Thus, the parameter vector was defined as $p = [\beta\ k_2\ k_3\ \omega]^T$. Typical values of the parameters, roughly corresponding to the evolution of COVID-19 in Hungary between 15/08/2020 - 15-08-2021, are $\beta \approx 0.1 - 0.7, k_2 \approx 1/2.65, k_3 \approx 1/6.5, \omega \approx 1/150$.

As it has actually been observed during the COVID-19 epidemic, with appropriately selected parameters, the model can show damped oscillations even considering the same virus variant: people moving back and forth between **S** and **R** cause multiple epidemic peaks. There exist proofs for similar systems (e.g., for SIRS models) to be globally asymptotically stable by the construction of appropriate Lyapunov functions [224]. Therefore, we cannot expect sustained oscillations in the solutions. Thus, we prescribed that the solutions show oscillations with a specific time period without altering the parameters or explicitly specifying the oscillation threshold. Moreover, we wanted to influence the rate of convergence by prescribing a minimum for the oscillation amplitude at the end of the time horizon.

Case study	oscillation period (t)	time horizon (T)	sampling time dt	no. of timesteps (N)	free parameters	no. of decision variables	computation time (s)
Brussellator (a)	8						5.23
Brussellator (b)	10						262.72
Brussellator (c)	12	40	0.2	200	a, b	403	21.17
Brussellator (d)	15						3.65
Brussellator (e)	20						29.89
Lotka-Volterra (a)	10	20	0.02	1000		3004	604.74
Lotka-Volterra (b)	7.5	16	0.02	800	a, c, f	2404	385.37
Lotka-Volterra (c)	5	12	0.015	800		2404	185.75
SEIR (a)	30	100		400		1605	4.50
SEIR (b)	40	100	0.25	400	β, k_2, k_3, ω	1605	6.72
SEIR (c)	50	100		400		1605	5.32
SEIR (d)	50	150		600		2405	12.88

Table 5.1: Comparison of the case studies involving three models

Optimization parameters and results

For each simulation, we discretized the system using $dt = 0.25$ (days). Periodicity constraints were derived for only the first compartment ($\mathbf{S}$), by substituting into Eq. (5.5): $t_{01} = t_1/2, \epsilon_1 = 0.01, r_1 = 0.001, J(\mathbf{x}, p) = 0$, and $t_1 = \{30, 40, 50, 50\}$ (cases (a), (b), (c), (d)). Additionally, we used the following constraints: $0.01 \leq \tau_1 \leq 0.9$, $\beta \leq 5$, $0 \leq k_2, k_3, \omega \leq 1$ to ensure the optimizer remains within the selected model class. In the last simulation (d), to induce stronger oscillations, we increased the parameter value ϵ_1 to 0.025 and the time horizon to $T = 150$ (days).

We carried out four experiments, as seen in Figures 5.4a-5.4d. In experiments (a)-(c), we computed the parameter values for oscillation periods 30,40, and 50 days, respectively, for a time horizon of $T = 100$ days. For the last experiment (d), in order to produce stronger oscillations (with higher amplitude), we repeated case (c) with a higher ϵ (i.e., a higher deviation from the threshold was required), and a longer horizon. Although the dynamical constraints could be satisfied, the obtained transition rates were (sometimes unrealistically) high, partly caused by the short time horizon. It is also apparent from Table 5.1. that the computation times were significantly lower than in the case of the Lotka-Volterra model.

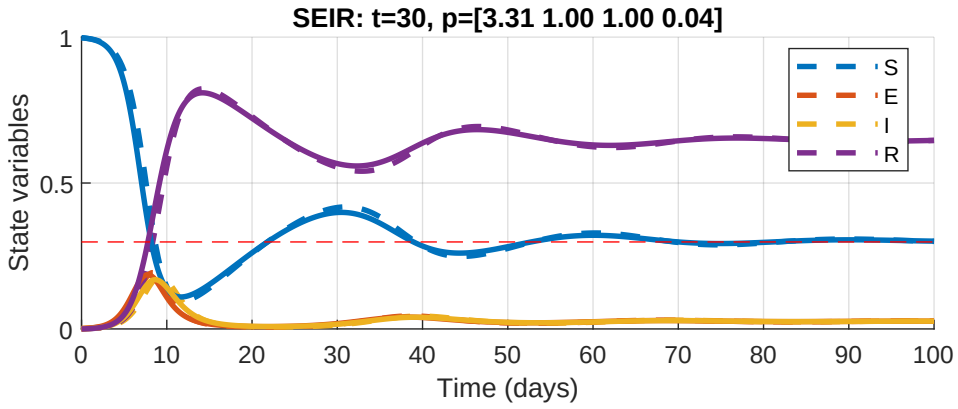

(a)

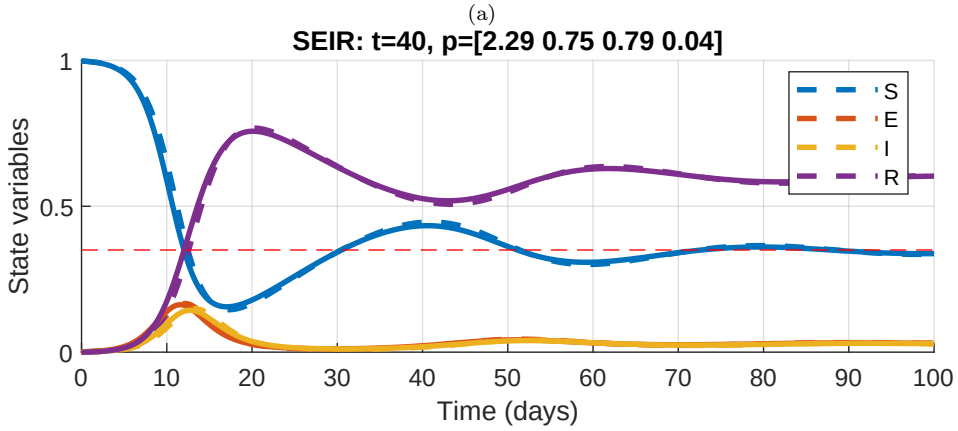

(b)

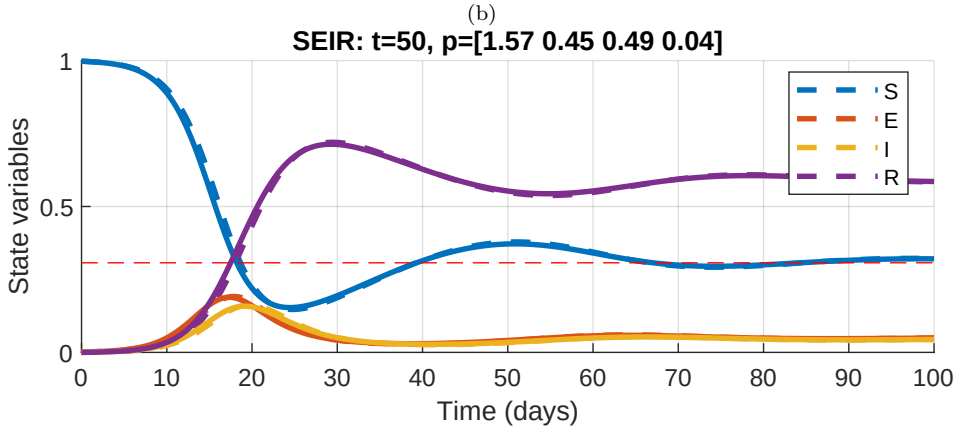

(c)

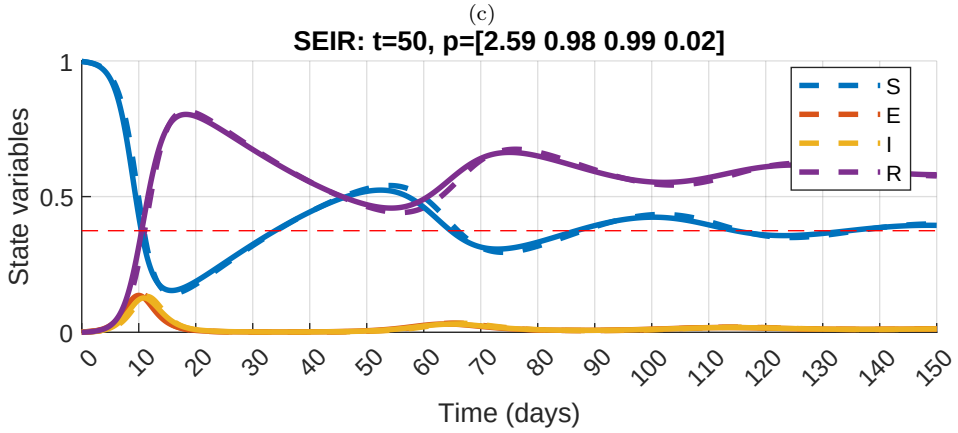

(d)

Figure 5.4: Computed parameters and their simulated trajectories for the SEIR model. Dashed lines represent the trajectories created by the optimizer (using the Euler method), while continuous lines show the simulated trajectories produced by the Ode45 solver using the previously computed parameters.

5.3 Conclusions

This chapter presents an optimization-based method for finding parameter values ensuring a prescribed dynamical behavior for nonlinear nonnegative models. The approach was inspired by nonlinear model predictive control with complex constraints, applied extensively for epidemic management in Chapter 3. Therefore, the computations used the discrete-time dynamics of the models. Clearly, the choice of the discretization method is fundamentally important in balancing between computability and the satisfactory approximation of the nonlinear dynamics. In contrast to simulation-based global optimization approaches, the applied setup requires one optimization run. The price of this is the increased number of decision variables, which are, however, strictly constrained. The methodology was illustrated using three kinetic nonlinear models, where the goal was to induce some kind of oscillatory behavior (sustained or damped) with a given frequency. The computations were successfully performed using the proprietary BARON solver.

It must be noted that even though the whole chapter revolves around the parameter synthesis of nonnegative models (including all the illustrative examples), there were no hard limits determined regarding the applicability of the proposed methodology. The sign constraint on the state variables clearly eliminates numerous possible problems during the nonlinear optimization run (e.g. degrading observability or not well-defined parameter values in the neighborhood of 0); however, the procedure could be extended to other classes of nonlinear systems.

On the other hand, even though not specified exactly, the methodology might be infeasible on some classes of positive systems as well. As the complexity of the system dynamics and the prescribed behavior can strongly influence the time required to solve the nonlinear optimization problem, it is possible to create scenarios that are computationally untractable. E.g., systems dynamics with exponential terms, or with state variables spanning several orders of magnitude, are probably out of scope for such an approach - during our preliminary experiments, we have encountered some obstacles, but we did not delve deeper regarding the exact causes.

Nevertheless, based on empirical evidence and a high number of experiences, the methodology can be applied without modification for many kinds of polynomial systems, and adaptation for other classes is certainly possible.

Future work will be focused on defining the qualitative dynamical requirements in STL form and automatically translating the constraints from those, and also incorporating other solvers for which the current solutions may possibly be used as feasible initial values. Furthermore, our goals also include a more exact specification of the methodology's theoretical capabilities.

Chapter 6

Conclusions

6.1 New scientific contributions

Thesis 1. I have presented a model predictive control-based methodology for the optimal control of nonlinear compartmental epidemic models allowing discrete intervention levels and intervals, in the presence of complex constraints specified by temporal logic formulas.

Thesis 1.1 I developed a method based on nonlinear model predictive control to compute the required stringency of epidemiological restrictions, ensuring the fulfillment of complex, time-varying and logical conditions, while balancing between possibly contradictory goals and expectations. The method is capable of handling predefined discrete intervention levels and time intervals.
Publication: [J1]

Thesis 1.2 I proposed a control theoretic approach for the integrated design of non-pharmaceutical interventions, vaccination and testing intensity for epidemic mitigation, introducing additional manipulable inputs and compartments to complex epidemic models. By accounting for the limited number of resources and the complex logical constraints, the optimization-based controller is capable of computing a comprehensive strategy for the timely deployment of the different measures.
Publication: [J2]

Related chapters: 3 (thesis), 3.1 (thesis booklet)

Thesis 2. I have designed novel methods for the retrospective trajectory reconstruction and parameter synthesis of nonlinear nonnegative systems, constructing and solving complex optimization problems inspired by the structure of deterministic or stochastic model predictive control.

Thesis 2.1 I have proposed optimization-based deterministic and stochastic methods for estimating the unmeasurable quantities of epidemic processes, together with error estimations. Using these, I gave precise approximations for the time-dependent transmission rate, the likely actual number of infections, and the number of latent, pre-symptomatic, and asymptomatic cases based solely on the daily number of hospitalizations.
Publications: [C1], [J3]
Related chapters: 4.1 (thesis), 3.2 (thesis booklet)

Thesis 2.2 I have proposed a novel optimization-based parameter synthesis method, suitable to ensure a predefined qualitative behavior in nonlinear nonnegative systems. I

have illustrated the methodology on three kinetic models, with the goal of inducing sustained or damped autonomous oscillatory behavior with given frequencies.
Publication: [J5]
Related chapters: 5 (thesis), 3.3 (thesis booklet)

Thesis 3. I have developed a robust, computationally efficient approach for historical data reconstruction of epidemic processes, using a robustified feedback-linearization based asymptotic reference tracking scheme together with nonlinear state estimation. The resulting setup showed appropriate robustness with respect to mismatch and inaccuracies in model structure, estimated model parameters, and measured output.
Publications: [C2], [C3], [C4], [C5], [J4]
Related chapters: 4.2 (thesis), 3.2 (thesis booklet)

6.2 Applications and future work

Due to the fact that we have developed new methodologies for a wide class of nonnegative systems, there are numerous application possibilities. Actually, some of the presented approaches were already applied in practice to address real-world data reconstruction needs.

During the COVID-19 pandemic, we used the presented framework to regularly estimate the number of individuals in unmeasurable categories (e.g. asymptomatic infections) in Hungary, providing insight into the progress of the current epidemic wave. Using these, we also computed accurate forecasts. Our results were always comparable (and sometimes even better) than the data published by independent research groups (e.g. [209, 225]).

The research concerning the robustification of the feedback-linearization technique to tolerate high model and parameter mismatch directly paved the way for the combination of compartmental-model-based control and agent-based modeling and simulation [90]. Being directly applicable in an upcoming epidemic (naturally, after tailoring the parameters to the spread and behavior of the potential new pathogen), the solution can be used to evaluate and balance between real-world epidemic control goals and intervention possibilities in rapidly changing environments.

Finally, as chemical oscillators play a fundamental role in numerous biological processes (e. g. circadian clock or other time-dependent cell decisions in living organisms), the possibility to synthesize such systems with predefined frequency and behavior might be helpful or thought-provoking in a wide area of biological and medical research.

There are several interesting directions left for future exploration:

1. The connection between the ODE and agent-based model could be made more realistic by optimally matching the combination of real-world interventions (e.g. school closure) to the intended strictness. Moreover, the ODE-based methodologies with multiple inputs (e.g. testing intensity, vaccination, etc) could also be complemented with agent-based approaches for optimized planning of an even more comprehensive epidemic management strategy.
2. Epidemic management aside, this kind of connection between robust controllers and agent-based models could provide a computationally feasible planning solution for all kinds of mechanical or ecological systems (population dynamics, vehicle traffic flows, etc.) Without connection to the epidemic management, preliminary studies were already carried out for optimized vehicle scheduling and route-planning in industrial environments using MPC and temporal logic [O1], [O2].
3. As kinetic models can be used to describe a wide range of processes, the application of the parameter synthesis methodology for e.g. ribosome flow models, calls for further investigation.

The Author's publications

The Author's journal papers

[J1] T. Péni, B. Csutak, G. Szederkényi, and G. Röst, "Nonlinear model predictive control with logic constraints for COVID-19 management," *Nonlinear Dynamics*, vol. 102, no. 4, pp. 1965–1986, Dec. 2020, SJR: **Q1** / **D1**.

[J2] T. Péni, B. Csutak, F. A. Bartha, G. Röst, and G. Szederkényi, "Optimizing symptom based testing strategies for pandemic mitigation," *IEEE Access*, vol. 10, pp. 84 934–84 945, 2022, SJR: **Q1**.

[J3] P. Polcz, B. Csutak, and G. Szederkényi, "Reconstruction of epidemiological data in Hungary using stochastic model predictive control," *Applied Sciences*, vol. 12, no. 3, p. 1113, 2022, SJR: **Q2**. [Online]. Available: https://www.mdpi.com/2076-3417/12/3/1113

[J4] B. Csutak and G. Szederkényi, "Robust control and data reconstruction for nonlinear epidemiological models using feedback linearization and state estimation," *Mathematical Biosciences and Engineering*, vol. 22, no. 1, pp. 109–137, 2025, SJR: **Q2**.

[J5] B. Csutak and G. Szederkényi, "Optimization-based parameter computation for nonnegative systems to achieve prescribed dynamic behaviour," *Acta Polytechnica Hungarica*, vol. 21, no. 10, pp. 457–474, 2024, SJR: **Q2**.

The Author's conference papers

[C1] B. Csutak, P. Polcz, and G. Szederkenyi, "Computation of COVID-19 epidemiological data in Hungary using dynamic model inversion," in *2021 IEEE 15th International Symposium on Applied Computational Intelligence and Informatics (SACI)*. IEEE, 2021, pp. 91–96.

[C2] B. Csutak, P. Polcz, and G. Szederkényi, "Model-based epidemic data reconstruction using feedback linearization," in *2022 International Conference on Electrical, Computer and Energy Technologies (ICECET)*, 2022, pp. 1–6.

[C3] B. Csutak, K. M. Jenei, and G. Szederkényi, "Linearization based robust reference tracking control of a compartmental epidemiological model," in *2023 24th International Conference on Process Control (PC)*, 2023, pp. 66–71.

[C4] B. Csutak and G. Szederkényi, "Reference tracking control of a nonlinear epidemiological model with state estimation," in *2023 9th International Conference on Control, Decision and Information Technologies (CoDIT)*, 2023, pp. 2311–2316.

[C5] B. Csutak, P. Polcz, and G. Szederkényi, "Magyarországi járványadatok elemzése rendszerelméleti megközelítéssel," *XXXIV. Neumann Kollokvium*, 2021.

The Author's other papers

[O1] B. Csutak, T. Péni, and G. Szederkényi, "An optimization based algorithm for conflict-free navigation of autonomous guided vehicles," in *Proceedings of the Pannonian Conference on Advances in Information Technology (PCIT'2019)*. Veszprém: University of Pannonia, Faculty of Information Technology, 2019, pp. 90–97. [Online]. Available: https://eprints.sztaki.hu/9762/

[O2] B. Csutak, T. Péni, and G. Szederkényi, "Hierarchical routing algorithm for industrial mobile robots by signal temporal logic specifications," *StuCoSReC. Proceedings of the 2019 6th Student Computer Science Research Conference*, 2019. [Online]. Available: https://doi.org/10.26493/978-961-7055-82-5.43-47

Bibliography

[1] S. H. Strogatz, *Nonlinear dynamics and chaos: with applications to physics, biology, chemistry, and engineering*. Chapman and Hall/CRC, 2024.

[2] M. W. Hirsch, S. Smale, and R. L. Devaney, *Differential equations, dynamical systems, and an introduction to chaos*. Academic press, 2013.

[3] H. K. Khalil and J. W. Grizzle, *Nonlinear systems*. Prentice hall Upper Saddle River, NJ, 2002, vol. 3.

[4] S. Boyd and L. Vandenberghe, *Convex Optimization*. Cambridge University Press, 2004.

[5] E. Camacho and C. Bordons, *Model Predictive Control*. Springer, 01 2004, vol. 13.

[6] W. M. Haddad, V. Chellaboina, and Q. Hui, *Nonnegative and Compartmental Dynamical Systems*. Princeton University Press, 2010.

[7] L. Farina and S. Rinaldi, *Positive Linear Systems: Theory and Applications*. John Wiley & Sons, 2000.

[8] M. Feinberg, *Foundations of Chemical Reaction Network Theory*. Springer, 2019.

[9] P. Érdi and J. Tóth, *Mathematical Models of Chemical Reactions: Theory and Applications of Deterministic and Stochastic models*. Manchester University Press, 1989.

[10] N. Samardzija, L. D. Greller, and E. Wasserman, "Nonlinear chemical kinetic schemes derived from mechanical and electrical dynamical systems," *The Journal of Chemical Physics*, vol. 90, no. 4, pp. 2296–2304, 1989.

[11] G. Lipták, G. Szederkényi, and K. M. Hangos, "Kinetic feedback design for polynomial systems," *Journal of Process Control*, vol. 41, p. 56–66, May 2016.

[12] M. Pereira, B. Kulcsár, G. Lipták, M. Kovács, and G. Szederkényi, "The traffic reaction model: A kinetic compartmental approach to road traffic modeling," *Transportation Research Part C: Emerging Technologies*, vol. 158, p. 104435, Jan. 2024. [Online]. Available: http://dx.doi.org/10.1016/j.trc.2023.104435

[13] I. Epstein and J. Pojman, *An Introduction to Nonlinear Chemical Dynamics: Oscillations, Waves, Patterns, and Chaos*, ser. Topics in Physical Chemistry. Oxford University Press, 1998. [Online]. Available: https://books.google.ro/books?id=ci4MNrwSlo4C

[14] J. J. Tyson, K. C. Chen, and B. Novak, "Sniffers, buzzers, toggles and blinkers: dynamics of regulatory and signaling pathways in the cell," *Current Opinion in Cell Biology*, vol. 15, no. 2, pp. 221–231, 2003.

[15] C. Conradi and C. Pantea, *Multistationarity in Biochemical Networks: Results, Analysis, and Examples*. Academic Press, 2019, algebraic and Combinatorial Computational Biology, Ch. 9, Eds. Robeva R. and Macaulay M., Mathematics in Science and Computation.

[16] B. Boros and J. Hofbauer, "Some minimal bimolecular mass-action systems with limit cycles," *Nonlinear Analysis: Real World Applications*, vol. 72, p. 103839, Aug. 2023.

[17] R. J. Field and F. W. Schneider, "Oscillating chemical reactions and nonlinear dynamics," *Journal of Chemical Education*, vol. 66, no. 3, p. 195, 1989. [Online]. Available: https://doi.org/10.1021/ed066p195

[18] K. Beutel and E. Peacock-Lopez, "Chemical oscillations: Two-variable models," *The Chemical Educator*, vol. 12, pp. 224–235, 01 2007.

[19] I. Otero-Muras and J. R. Banga, "Automated design framework for synthetic biology exploiting Pareto optimality," *ACS Synthetic Biology*, vol. 6, no. 7, pp. 1180–1193, 2017.

[20] B. Shults and B. Kuipers, "Qualitative simulation and temporal logic: proving properties of continuous systems," *University of Texas Artificial Intelligence Laboratory TR AI96-244*, 1996.

[21] P. Ballarini and M. L. Guerriero, "Query-based verification of qualitative trends and oscillations in biochemical systems," *Theoretical Computer Science*, vol. 411, no. 20, pp. 2019–2036,

2010, hybrid Automata and Oscillatory Behaviour in Biological Systems. [Online]. Available: https://www.sciencedirect.com/science/article/pii/S0304397510001052

[22] A. Rizk, G. Batt, F. Fages, and S. Soliman, "On a continuous degree of satisfaction of temporal logic formulae with applications to systems biology," in *Computational Methods in Systems Biology*, M. Heiner and A. M. Uhrmacher, Eds. Berlin, Heidelberg: Springer Berlin Heidelberg, 2008, pp. 251–268.

[23] F. Fages and S. Soliman, *Model Revision from Temporal Logic Properties in Computational Systems Biology*. Berlin, Heidelberg: Springer Berlin Heidelberg, 2008, pp. 287–304. [Online]. Available: https://doi.org/10.1007/978-3-540-78652-8_11

[24] C. Banks, "Spatio-temporal logic for the analysis of biochemical models," Ph.D. dissertation, University of Edinburgh, 06 2015.

[25] L. Calzone, N. Chabrier-Rivier, F. Fages, and S. Soliman, "A machine learning approach to biochemical reaction rules discovery," in *Proceedings of Foundations of Systems Biology and Engineering (FOSBE'05)*, 2005, pp. 375–379.

[26] A. Donze and V. Raman, "BluSTL: Controller synthesis from signal temporal logic specifications," in *2nd International Workshop on Applied Verification for Continuous and Hybrid Systems (ARCH 2015)*, 2015. [Online]. Available: http://terraswarm.org/pubs/570.html

[27] E. A. Gol, E. Bartocci, and C. Belta, "A formal methods approach to pattern synthesis in reaction diffusion systems," in *53rd IEEE Conference on Decision and Control*, 2014, pp. 108–113.

[28] E. Bartocci, E. Aydin Gol, I. Haghighi, and C. Belta, "A formal methods approach to pattern recognition and synthesis in reaction diffusion networks," *IEEE Transactions on Control of Network Systems*, vol. 5, no. 1, pp. 308–320, 2018.

[29] S. S. Farahani, V. Raman, and R. M. Murray, "Robust model predictive control for signal temporal logic synthesis," *IFAC-PapersOnLine*, vol. 48, no. 27, pp. 323–328, 2015. [Online]. Available: http://dx.doi.org/10.1016/j.ifacol.2015.11.195

[30] J. Kronqvist, D. E. Bernal, A. Lundell, and I. E. Grossmann, "A review and comparison of solvers for convex MINLP," *Optimization and Engineering*, vol. 20, pp. 397–455, 2019.

[31] G. Röst, F. A. Bartha, N. Bogya, P. Boldog, A. Dénes, T. Ferenci, K. J. Horváth, A. Juhász, C. Nagy, T. Tekeli *et al.*, "Early phase of the COVID-19 outbreak in Hungary and post-lockdown scenarios," *Viruses*, vol. 12, no. 7, p. 708, June 2020. [Online]. Available: http://dx.doi.org/10.3390/v12070708

[32] R. Steinbrook, "Contact tracing, testing, and control of COVID-19 – Learning from Taiwan," *JAMA Internal Medicine*, vol. 180, no. 9, pp. 1163–1164, Sep. 2020.

[33] S. e. Stoecklin, "First cases of coronavirus disease 2019 (covid-19) in france: Surveillance, investigations and control measures," *Euro Surveill.*, vol. 25, no. 6, January 2020, doi:10.2807/1560-7917.es.2020.25.6.2000094. 2019 (COVID-19) in France: Surveillance, Investigations and Control Measures, . em Euro Surveill. bf 2020, em). url. [Online]. Available: https://doi.org/10.2807/1560-7917.es.2020.25.6.2000094

[34] A. Deslandes, "Sars-cov-2 was already spreading in france in late december 2019." *Int. J. Antimicrob. Agents*, 2020, doi:10.1016/j.ijantimicag.2020.106006.

[35] M. M. Böhmer, U. Buchholz, V. M. Corman, M. Hoch, K. Katz, D. V. Marosevic, S. Böhm, T. Woudenberg, N. Ackermann, R. Konrad *et al.*, "Investigation of a covid-19 outbreak in germany resulting from a single travel-associated primary case: a case series," *The Lancet Infectious Diseases*, vol. 20, no. 8, pp. 920–928, 2020.

[36] G. Sebastiani, M. Massa, and E. Riboli, "Covid-19 epidemic in italy: evolution, projections and impact of government measures," *European Journal of Epidemiology*, vol. 35, no. 4, pp. 341–345, April 2020, doi:10.1007/s10654-020-00631-6. [Online]. Available: http://dx.doi.org/10.1007/s10654-020-00631-6

[37] E. C. for Disease Prevention and C. (ECDC), "Rapid risk assessment from ecdc: Resurgence of reported cases of covid-19 in the eu/eea, the uk and eu candidate and potential candidate countries," *Eurosurveillance*, vol. 25, no. 26, July 2020. [Online]. Available: http://dx.doi.org/10.2807/1560-7917.es.2020.25.26.2007021

[38] W. H. O. (WHO), "Who situation report - 191, coronavirus disease 2019 (covid-19) 29 july 2020," July 2020, accessed: June 2025. [Online]. Available: https://www.who.int/docs/default-source/coronaviruse/situation-reports/20200729-covid-19-sitrep-191.pdf

[39] C.-H. Hsieh, "On robust economic control of epidemics with application to COVID-19," *IEEE Access*, vol. 9, pp. 167 948–167 958, 2021. [Online]. Available: https://doi.org/10.1109/access.2021.3136191

[40] Z. Feng, *Applications of Epidemiological Models to Public Health Policymaking: The Role of Heterogeneity in Model Predictions*. Applications of epidemiological models to public health policymaking: WORLD SCIENTIFIC, 2013, world Scientific. [Online]. Available: http://dx.doi.org/10.1142/8884

[41] I. F. Miller, A. D. Becker, B. T. Grenfell, and C. J. E. Metcalf, "Disease and healthcare burden of COVID-19 in the United States," *Nature Medicine*, vol. 26, no. 8, pp. 1212–1217, 2020.

[42] S. R. Baker, N. Bloom, S. J. Davis, and S. J. Terry, "COVID-induced economic uncertainty," National Bureau of Economic Research, Tech. Rep., 2020.

[43] E. Sontag, *Mathematical Control Theory: Deterministic and Finite Dimensional Systems*. Springer, 1998.

[44] C. Kuttler and N. G. Becker, "Modeling to inform infectious disease control. boca raton, crc press." *Biometrics*, vol. 74, no. 1, pp. 382–383, March 2018. [Online]. Available: http://dx.doi.org/10.1111/biom.12852

[45] E. A. Hernandez-Vargas, *Modeling and control of infectious diseases in the host: with MATLAB and R*. Academic Press, 2019.

[46] A. D. Ames, T. G. Molnar, A. W. Singletary, and G. Orosz, "Safety-critical control of active interventions for covid-19 mitigation," *IEEE Access*, vol. 8, pp. 188 454–188 474, 2020, doi:urlhttps://doi.org/10.1101/2020.06.17.2013326. [Online]. Available: http://dx.doi.org/10.1109/access.2020.3029558

[47] K. Muqbel, G. Vas, and G. Röst, "Periodic orbits and global stability for a discontinuous sir model with delayed control," *Qualitative Theory of Dynamical Systems*, vol. 19, p. 59, 2020.

[48] Z. Wang, G. R"ost, and S. Moghadas, "Delay in booster schedule as a control parameter in vaccination dynamics," *Journal of Mathematical Biology*, vol. 79, pp. 2157–2182, 2019.

[49] C. Nowzari, V. Preciado, and G. Pappas, "Analysis and control of epidemics: A survey of spreading processes on complex networks," *IEEE Control Systems Magazine*, vol. 36, pp. 26–46, February 2016, textbf36(1). [Online]. Available: http://dx.doi.org/10.1109/mcs.2015.2495000

[50] O. Sharomi and T. Malik, "Optimal control in epidemiology," *Annals of Operations Research*, vol. 251, no. 1, pp. 55–71, 2017.

[51] S. Alonso-Quesada, M. De la Sen, R. P. Agarwal, and A. Ibeas, "An observer-based vaccination control law for an SEIR epidemic model based on feedback linearization techniques for nonlinear systems," *Advances in Difference Equations*, vol. 2012, no. 1, pp. 1–32, September 2012. [Online]. Available: http://dx.doi.org/10.1186/1687-1847-2012-161

[52] F. Sélley, A. Besenyei, I. Z. Kiss, and P. L. Simon, "Dynamic control of modern, network-based epidemic models," *SIAM Journal on applied dynamical systems*, vol. 14, no. 1, pp. 168–187, 2015.

[53] J. Köhler, L. Schwenkel, A. Koch, J. Berberich, P. Pauli, and F. Allgöwer, "Robust and optimal predictive control of the COVID-19 outbreak," *Annual Reviews in Control*, vol. 51, pp. 525–539, 2021.

[54] M. M. Morato, I. M. Pataro, M. V. da Costa, and J. E. Normey-Rico, "A parametrized nonlinear predictive control strategy for relaxing COVID-19 social distancing measures in Brazil," *ISA transactions*, 2020.

[55] M. M. Morato, S. B. Bastos, D. O. Cajueiro, and J. E. Normey-Rico, "An optimal predictive control strategy for covid-19 (sars-cov-2) social distancing policies in brazil," *Annual Reviews in Control*, vol. 50, pp. 417–431, 2020.

[56] J. Sereno, A. D'Jorge, A. Ferramosca, E. Hernandez-Vargas, and A. González, "Model predictive control for optimal social distancing in a type SIR-switched model," *IFAC-PapersOnLine*, vol. 54, no. 15, pp. 251–256, 2021.

[57] T. Péni and G. Szederkényi, "Convex output feedback model predictive control for mitigation of COVID-19 pandemic," *Annual Reviews in Control*, vol. 52, pp. 543–553, 2021.

[58] E. H. Bussell, C. E. Dangerfield, C. A. Gilligan, and N. J. Cunniffe, "Applying optimal control theory to complex epidemiological models to inform real-world disease management," *Phylosophical Transactions B of the Royal Society*, vol. 374, p. 20180284, 2018.

[59] N. Watkins, C. Nowzari, and G. Pappas, "Robust economic model predictive control of continuous-time epidemic processes," *IEEE Transactions on Automatic Control*, vol. 65, no. 3, pp. 1116–1131, 2020.

[60] L. C. Lopes-Júnior, E. Bomfim, D. S. da Silveira, R. M. Pessanha, S. I. Schuab, and R. A. Lima, "Effectiveness of mass testing for control of covid-19: a systematic review protocol," *BMJ Open*, vol. 10, no. 8, p. e040413, 2020.

[61] M. Salath, C. L. Althaus, R. Neher, S. Stringhini, E. Hodcroft, J. Fellay, M. Zwahlen, G. Senti, M. Battegay, A. Wilder-Smith, I. Eckerle, M. Egger, and N. Low, "COVID-19 epidemic in Switzerland: On the importance of testing, contact tracing and isolation," *Swiss Medical Weekly*, Mar. 2020.

[62] E. A. Yarmol-Matusiak, L. E. Cipriano, and S. Stranges, "A comparison of COVID-19 epidemiological indicators in Sweden, Norway, Denmark, and Finland," *Scandinavian Journal of Public Health*, vol. 49, no. 1, pp. 69–78, 2021.

[63] F. A. Bartha, J. Karsai, T. Tekeli, and G. Röst, "Symptom-based testing in a compartmental model of COVID-19," in *Analysis of Infectious Disease Problems (COVID-19) and Their Global Impact*. Springer, 2021, pp. 357–376.

[64] K. Hangos and I. Cameron, *Process modelling and model analysis*. Academic Press, 2001.

[65] R. M. Anderson and R. M. May, *Infectious diseases of humans: Dynamics and control*. Oxford University Press, 1992.

[66] G. Giordano, F. Blanchini, R. Bruno, P. Colaneri, A. Di Filippo, A. Di Matteo, and M. Colaneri, "Modelling the COVID-19 epidemic and implementation of population-wide interventions in Italy," *Nature Medicine*, vol. 26, no. 6, pp. 855–860, 2020.

[67] A. d'Onofrio, M. Iannelli, P. Manfredi, and G. Marinoschi, "Epidemic control by social distancing and vaccination: Optimal strategies and remarks on the COVID-19 Italian response policy," *Mathematical Biosciences and Engineering*, vol. 21, no. 7, p. 6493–6520, 2024. [Online]. Available: http://dx.doi.org/10.3934/mbe.2024283

[68] L. Cao, Q. Liu, and W. Hou, "COVID-19 modeling: A review," *arXiv preprint arXiv:2104.12556*, 2021.

[69] O. Tutsoy, S. Colak, A. Polat, and K. Balikci, "A novel parametric model for the prediction and analysis of the COVID-19 casualties," *IEEE Access*, vol. 8, pp. 193 898–193 906, 2020. [Online]. Available: https://doi.org/10.1109/access.2020.3033146

[70] A. Vespignani, H. Tian, C. Dye, J. O. Lloyd-Smith, R. M. Eggo, M. Shrestha, S. V. Scarpino, B. Gutierrez, M. U. Kraemer, J. Wu *et al.*, "Modelling Covid-19," *Nature Reviews Physics*, vol. 2, no. 6, pp. 279–281, 2020.

[71] G. R. Shinde, A. B. Kalamkar, P. N. Mahalle, N. Dey, J. Chaki, and A. E. Hassanien, "Forecasting models for coronavirus disease (COVID-19): A survey of the state-of-the-art," *SN Computer Science*, vol. 1, no. 4, pp. 1–15, 2020.

[72] M. H. A. Biswas, , L. T. Paiva, and M. de Pinho, "A SEIR model for control of infectious diseases with constraints," *Mathematical Biosciences and Engineering*, vol. 11, no. 4, pp. 761–784, 2014.

[73] R. M. Anderson and R. M. May, "Population biology of infectious diseases: Part i," *Nature*, vol. 280, no. 5721, pp. 361–367, 1979.

[74] R. M. May and R. M. Anderson, "Population biology of infectious diseases: Part ii," *Nature*, vol. 280, no. 5722, pp. 455–461, 1979.

[75] F. Brauer, "Compartmental models in epidemiology," in *Mathematical Epidemiology*. Springer Berlin Heidelberg, 2008, pp. 19–79.

[76] F. Brauer, C. Castillo-Chavez, and C. Castillo-Chavez, *Mathematical models in population biology and epidemiology*. Springer, 2012, vol. 2.

[77] S. He, Y. Peng, and K. Sun, "SEIR modeling of the COVID-19 and its dynamics," *Nonlinear Dynamics*, vol. 101, no. 3, pp. 1667–1680, 2020.

[78] H. Wang, Z. Wang, Y. Dong, R. Chang, C. Xu, X. Yu, S. Zhang, L. Tsamlag, M. Shang, J. Huang *et al.*, "Phase-adjusted estimation of the number of coronavirus disease 2019 cases in Wuhan, China," *Cell Discovery*, vol. 6, no. 1, pp. 1–8, 2020, article number 10.

[79] M. de la Sen and S. Alonso-Quesada, "Vaccination strategies based on feedback control techniques for a general SEIR-epidemic model," *Applied Mathematics and Computation*, vol. 218, pp. 2888–3904, 2011.

[80] W. O. Kermack and A. G. McKendrick, "A contribution to the mathematical theory of epidemics," *Proceedings of the Royal Society of London. Series A, Containing Papers of a Mathematical and Physical Character*, vol. 115, no. 772, pp. 700–721, 2024/09/16/ 1927, full publication date: Aug. 1, 1927. [Online]. Available: http://www.jstor.org/stable/94815

[81] R. Pastor-Satorras, C. Castellano, P. Van Mieghem, and A. Vespignani, "Epidemic processes in complex networks," *Rev. Mod. Phys.*, vol. 87, pp. 925–979, Aug 2015. [Online]. Available: https://link.aps.org/doi/10.1103/RevModPhys.87.925

[82] L. Stella, A. P. Martínez, D. Bauso, and P. Colaneri, "The role of asymptomatic infections in the COVID-19 epidemic via complex networks and stability analysis," *SIAM Journal*

on Control and Optimization, vol. 60, no. 2, p. S119–S144, Jan. 2022. [Online]. Available: http://dx.doi.org/10.1137/20M1373335

[83] A. Isidori, *Nonlinear Control Systems*. Springer Berlin, 1999.

[84] R. Riobello, "On some new mathematical models of infectious diseases: analysis, equilibrium, positivity and vaccination controls," Ph.D. dissertation, University of Basque Country, Spain, 2015, ph.D. thesis, University of Basque Country, Spain.

[85] N. Hoertel, M. Blachier, C. Blanco, M. Olfson, M. Massetti, M. S. Rico, F. Limosin, and H. Leleu, "A stochastic agent-based model of the SARS-CoV-2 epidemic in France," *Nature medicine*, vol. 26, no. 9, pp. 1417–1421, 2020.

[86] R. J. Rockett, A. Arnott, C. Lam, R. Sadsad, V. Timms, K.-A. Gray, J.-S. Eden, S. Chang, M. Gall, J. Draper *et al.*, "Revealing COVID-19 transmission in Australia by SARS-CoV-2 genome sequencing and agent-based modeling," *Nature Medicine*, vol. 26, no. 9, pp. 1398–1404, 2020.

[87] A. Rajabi, A. V. Mantzaris, E. C. Mutlu, and O. O. Garibay, "Investigating dynamics of COVID-19 spread and containment with agent-based modeling," *Applied Sciences*, vol. 11, no. 12, p. 5367, 2021.

[88] I. Z. Reguly, D. Csercsik, J. Juhász, K. Tornai, Z. Bujtár, G. Horváth, B. Keömley-Horváth, T. Kós, G. Cserey, K. Iván *et al.*, "Microsimulation based quantitative analysis of COVID-19 management strategies," *PLoS computational biology*, vol. 18, no. 1, p. e1009693, 2022, to appear in PLoS Computational Biology. [Online]. Available: https://doi.org/10.1371/journal.pcbi.1009693

[89] J. de Mooij, P. Bhattacharya, D. Dell'Anna, M. Dastani, B. Logan, and S. Swarup, "A framework for modeling human behavior in large-scale agent-based epidemic simulations," *Simulation*, vol. 99, no. 12, pp. 1183–1211, 2023.

[90] P. Polcz, I. Z. Reguly, K. Tornai, J. Juhász, S. Pongor, A. Csikász-Nagy, and G. Szederkényi, "Smart epidemic control: A hybrid model blending odes and agent-based simulations for optimal, real-world intervention planning," *PLOS Computational Biology*, vol. 21, no. 5, p. e1013028, May 2025. [Online]. Available: http://dx.doi.org/10.1371/journal.pcbi.1013028

[91] S. Lalmuanawma, J. Hussain, and L. Chhakchhuak, "Applications of machine learning and artificial intelligence for COVID-19 (SARS-CoV-2) pandemic: A review," *Chaos, Solitons & Fractals*, vol. 139, p. 110059, 2020.

[92] M. Satu, K. C. Howlader, M. Mahmud, M. S. Kaiser, S. I. S. M., J. M. Quinn, S. A. Alyami, and M. A. Moni, "Short-term prediction of COVID-19 cases using machine learning models," *Applied Sciences*, vol. 11, no. 9, p. 4266, 2021.

[93] S. Ghafouri-Fard, H. Mohammad-Rahimi, P. Motie, M. Minabi, M. Taheri, and S. Nateghinia, "Application of machine learning in the prediction of COVID-19 daily new cases: A scoping review," *Heliyon*, p. e08143, 2021.

[94] G. Pinter, I. Felde, A. Mosavi, P. Ghamisi, and R. Gloaguen, "Covid-19 pandemic prediction for hungary; A hybrid machine learning approach," *Mathematics*, vol. 8, no. 6, p. 890, 2020.

[95] S. F. Ardabili, A. Mosavi, P. Ghamisi, F. Ferdinand, A. R. Varkonyi-Koczy, U. Reuter, T. Rabczuk, and P. M. Atkinson, "COVID-19 outbreak prediction with machine learning," *Algorithms*, vol. 13, no. 10, p. 249, 2020.

[96] G. Rzadkowski and G. Figlia, "Logistic wavelets and their application to model the spread of COVID-19 pandemic," *Applied Sciences*, vol. 11, no. 17, p. 8147, 2021.

[97] Ministry of Health of the Czech Republic, "COVID-19: Overview of the current situation in the Czech Republic," https://onemocneni-aktualne.mzcr.cz/covid-19, (Accessed on 04/28/2021).

[98] Government of Hungary, "3 million 774 thousand vaccinated, 1,692 new infected, 188 patients deceased," https://koronavirus.gov.hu/cikkek/3-millio-774-ezer-beoltott-1692-az-uj-fertozott-elhunyt-188-beteg, (Accessed on 04/28/2021).

[99] S. J. Phipps, R. Q. Grafton, and T. Kompas, "Robust estimates of the true (population) infection rate for COVID-19: A backcasting approach," *Royal Society Open Science*, vol. 7, no. 11, p. 200909, 2020.

[100] I. Rocchetti, D. Böhning, H. Holling, and A. Maruotti, "Estimating the size of undetected cases of the COVID-19 outbreak in Europe: An upper bound estimator," *Epidemiologic Methods*, vol. 9, no. s1, 2020.

[101] "Hungary coronavirus (live): 391 170 cases | The coronavirus app," https://coronavirus.app/tracking/hungary, (Accessed on 04/26/2021).

[102] B. Merkely, A. J. Szabó, A. Kosztin, E. Berényi, A. Sebestyén, C. Lengyel, G. Merkely, J. Karády, I. Várkonyi, C. Papp *et al.*, "Novel coronavirus epidemic in the Hungarian population, a cross-

sectional nationwide survey to support the exit policy in Hungary," *GeroScience*, vol. 42, no. 4, pp. 1063–1074, 2020.

[103] E. D. Sontag, *Mathematical control theory: Deterministic finite dimensional systems*. Springer Science & Business Media, 2013, vol. 6.

[104] L. Lennart, "System identification: Theory for the user," *PTR Prentice Hall, Upper Saddle River, NJ*, vol. 28, 1999.

[105] K. M. Gostic, L. McGough, E. B. Baskerville, S. Abbott, K. Joshi, C. Tedijanto, R. Kahn, R. Niehus, J. A. Hay, P. M. De Salazar *et al.*, "Practical considerations for measuring the effective reproductive number, Rt," *PLoS Computational Biology*, vol. 16, no. 12, p. e1008409, 2020.

[106] C. Fraser, "Estimating individual and household reproduction numbers in an emerging epidemic," *PLoS One*, vol. 2, no. 8, p. e758, 2007.

[107] A. Cori, N. M. Ferguson, C. Fraser, and S. Cauchemez, "A new framework and software to estimate time-varying reproduction numbers during epidemics," *American Journal of Epidemiology*, vol. 178, no. 9, pp. 1505–1512, 2013.

[108] A. J. Kucharski, T. W. Russell, C. Diamond, Y. Liu, J. Edmunds, S. Funk, R. M. Eggo, F. Sun, M. Jit, J. D. Munday *et al.*, "Early dynamics of transmission and control of COVID-19: A mathematical modelling study," *The lancet infectious diseases*, vol. 20, no. 5, pp. 553–558, 2020.

[109] S. Koyama, T. Horie, and S. Shinomoto, "Estimating the time-varying reproduction number of COVID-19 with a state-space method," *PLoS Computational Biology*, vol. 17, no. 1, p. e1008679, 2021.

[110] C. Tsay, F. Lejarza, M. A. Stadtherr, and M. Baldea, "Modeling, state estimation, and optimal control for the US COVID-19 outbreak," *Scientific reports*, vol. 10, no. 1, p. 10711, 2020.

[111] J. C. Lemaitre, J. Perez-Saez, A. Azman, A. Rinaldo, and J. Fellay, "Assessing the impact of non-pharmaceutical interventions on SARS-CoV-2 transmission in Switzerland," *Swiss Medical Weekly*, p. 150:w20295, 2020.

[112] F. Allgöwer and A. Zheng, Eds., *Nonlinear model predictive control*, 1st ed., ser. Progress in Systems and Control Theory 26. Birkhäuser Basel, 2000.

[113] A. Apte, C. K. R. T. Jones, A. M. Stuart, and J. Voss, "Data assimilation: Mathematical and statistical perspectives," *International Journal for Numerical Methods in Fluids*, vol. 56, no. 8, pp. 1033–1046, 2008.

[114] J. Bröcker, "On variational data assimilation in continuous time," *Quarterly Journal of the Royal Meteorological Society*, vol. 136, no. 652, pp. 1906–1919, Oct. 2010.

[115] J. Schumann-Bischoff, U. Parlitz, H. D. I. Abarbanel, M. Kostuk, D. Rey, M. Eldridge, and S. Luther, "Basin structure of optimization based state and parameter estimation," *Chaos: An Interdisciplinary Journal of Nonlinear Science*, vol. 25, no. 5, p. 053108, May 2015.

[116] J. Schumann-Bischoff and U. Parlitz, "State and parameter estimation using unconstrained optimization," *Phys. Rev. E*, vol. 84, p. 056214, Nov. 2011.

[117] T. Chen, N. F. Kirkby, and R. Jena, "Optimal dosing of cancer chemotherapy using model predictive control and moving horizon state/parameter estimation," *Computer Methods and Programs in Biomedicine*, vol. 108, no. 3, pp. 973–983, 2012.

[118] A. Das, "Chance-constrained optimization-based parameter estimation for Muskingum models," *Journal of Irrigation and Drainage Engineering*, vol. 133, no. 5, pp. 487–494, Oct. 2007.

[119] D. Amlan, "Parameter estimation for Muskingum models," *Journal of Irrigation and Drainage Engineering*, vol. 130, no. 2, pp. 140–147, Apr. 2004.

[120] N. Al-Hemeary, P. Polcz, and G. Szederkényi, "Optimal solar panel area computation and temperature tracking for a cubesat system using model predictive control," *SPIIRAS Proceedings*, vol. 19, no. 3, pp. 564–593, 2020.

[121] P. Courtier and O. Talagrand, "Variational assimilation of meteorological observations with the direct and adjoint shallow-water equations," *Tellus A: Dynamic Meteorology and Oceanography*, vol. 42, no. 5, pp. 531–549, 1990.

[122] L. Blackmore, B. Açıkmeşe, and J. M. Carson, "Lossless convexification of control constraints for a class of nonlinear optimal control problems," *Systems & Control Letters*, vol. 61, no. 8, pp. 863–870, 2012.

[123] Y. Mao, M. Szmuk, and B. Açıkmeşe, "Successive convexification of non-convex optimal control problems and its convergence properties," in *2016 IEEE 55th Conference on Decision and Control (CDC)*, 2016, pp. 3636–3641.

[124] J. Andersson, J. Gillis, and M. Diehl, *User documentation for CasADi v3.4.4*, May 2018.

[125] J. A. E. Andersson, J. Gillis, G. Horn, J. B. Rawlings, and M. Diehl, "CasADi: A software framework for nonlinear optimization and optimal control," *Mathematical Programming Computation*, vol. 11, no. 1, pp. 1–36, Jul. 2018.

[126] A. Wächter and L. T. Biegler, "On the implementation of an interior-point filter line-search algorithm for large-scale nonlinear programming," *Mathematical Programming*, vol. 106, no. 1, pp. 25–57, Apr. 2005.

[127] A. Zanelli, A. Domahidi, J. Jerez, and M. Morari, "Forces NLP: an efficient implementation of interior-point methods for multistage nonlinear nonconvex programs," *International Journal of Control*, vol. 93, no. 1, pp. 13–29, 2017.

[128] A. Mesbah, "Stochastic model predictive control: An overview and perspectives for future research," *IEEE Control Systems Magazine*, vol. 36, no. 6, pp. 30–44, Dec. 2016.

[129] D. de la Penad, A. Bemporad, and T. Alamo, "Stochastic programming applied to model predictive control," in *Proceedings of the 44th IEEE Conference on Decision and Control*, Dec. 2005, pp. 1361–1366.

[130] D. Bernardini and A. Bemporad, "Stabilizing model predictive control of stochastic constrained linear systems," *IEEE Transactions on Automatic Control*, vol. 57, no. 6, pp. 1468–1480, Jun. 2012.

[131] S. Thangavel, R. Paulen, and S. Engell, "Robust multi-stage nonlinear model predictive control using sigma points," *Processes*, vol. 8, no. 7, 2020.

[132] ——, "Dual multi-stage NMPC using sigma point principles." *IFAC-PapersOnLine*, vol. 53, no. 2, pp. 11 243–11 250, 2020, 21st IFAC World Congress.

[133] A. D. Bonzanini, J. A. Paulson, G. Makrygiorgos, and A. Mesbah, "Fast approximate learning-based multistage nonlinear model predictive control using Gaussian processes and deep neural networks," *Computers & Chemical Engineering*, vol. 145, p. 107174, 2021.

[134] C. J. Ostafew, A. P. Schoellig, and T. D. Barfoot, "Conservative to confident: Treating uncertainty robustly within learning-based control," in *2015 IEEE International Conference on Robotics and Automation (ICRA)*, May 2015, pp. 421–427.

[135] L. Hewing, J. Kabzan, and M. N. Zeilinger, "Cautious model predictive control using Gaussian process regression," *IEEE Transactions on Control Systems Technology*, vol. 28, no. 6, pp. 2736–2743, Nov. 2020.

[136] J. Q. Candela, A. Girard, and C. E. Rasmussen, "Prediction at an uncertain input for Gaussian processes and relevance vector machines application to multiple-step ahead time-series forecasting," *Tech. Report IMM-2003-18, Technical University of Denmark*, Jul. 2003.

[137] M. P. Deisenroth, "Efficient reinforcement learning using Gaussian processes – Revised version," Ph.D. dissertation, Faculty of Informatics Institute for Anthropomatics Intelligent Sensor-Actuator-Systems Laboratory (ISAS, 2017.

[138] A. Ibeas, M. De la Sen, S. Alonso-Quesada *et al.*, "Robust sliding control of SEIR epidemic models," *Mathematical Problems in Engineering*, vol. 2014, 2014.

[139] A. Ibeas, M. de la Sen, and S. Alonso-Quesada, "Sliding mode robust control of SEIR epidemic models," in *2013 21st Iranian Conference on Electrical Engineering (ICEE)*. IEEE, 2013, pp. 1–6.

[140] M. W. Spong, "On feedback linearization of robot manipulators and Riemannian curvature," in *Essays on Mathematical Robotics*. Springer, 1998, pp. 185–202.

[141] T. A. Le, G.-H. Kim, M. Y. Kim, and S.-G. Lee, "Partial feedback linearization control of overhead cranes with varying cable lengths," *International Journal of Precision Engineering and Manufacturing*, vol. 13, pp. 501–507, 2012.

[142] C. Lascu, S. Jafarzadeh, M. S. Fadali, and F. Blaabjerg, "Direct torque control with feedback linearization for induction motor drives," *IEEE Transactions on Power Electronics*, vol. 32, no. 3, pp. 2072–2080, 2016.

[143] W. H. Kim, "Feedback Linearization of Nonlinear Systems: Robustness and Adaptive Control," Ph.D. dissertation, Louisiana State University and Agricultural & Mechanical College, 1991.

[144] M. Kaheni, M. H. Zarif, A. A. Kalat, and L. Chisci, "Robust feedback linearization for input-constrained nonlinear systems with matched uncertainties," in *2018 European Control Conference (ECC)*. IEEE, 2018, pp. 2947–2952.

[145] M. De la Sen, A. Ibeas, and S. Alonso-Quesada, "Feedback linearization-based vaccination control strategies for true-mass action type SEIR epidemic models," *Nonlinear Analysis: Modelling and Control*, vol. 16, no. 3, pp. 283–314, 2011.

[146] S. Zhai, G. Luo, T. Huang, X. Wang, J. Tao, and P. Zhou, "Vaccination control of an epidemic model with time delay and its application to COVID-19," *Nonlinear Dynamics*, vol. 106, no. 2, pp. 1279–1292, may 2021.

[147] A. Iggidr and M. O. Souza, "State estimators for some epidemiological systems," *Journal of Mathematical Biology*, vol. 78, no. 1–2, pp. 225–256, July 2019. [Online]. Available: http://dx.doi.org/10.1007/s00285-018-1273-3

[148] D. Simon, "Optimal state estimation: Kalman, H∞, and nonlinear approaches," 2006.

[149] D. M. Sheinson, J. Niemi, and W. Meiring, "Comparison of the performance of particle filter algorithms applied to tracking of a disease epidemic," *Mathematical Biosciences*, vol. 255, pp. 21–32, 2014.

[150] W. Yang, A. Karspeck, and J. Shaman, "Comparison of filtering methods for the modeling and retrospective forecasting of influenza epidemics," *PLoS Computational Biology*, vol. 10, no. 4, p. e1003583, 2014.

[151] X. Zhu, B. Gao, Y. Zhong, C. Gu, and K.-S. Choi, "Extended Kalman filter based on stochastic epidemiological model for COVID-19 modelling," *Computers in Biology and Medicine*, vol. 137, p. 104810, 2021.

[152] V. Azimi, M. Sharifi, S. Fakoorian, T. Nguyen, and V. Van Huynh, "State estimation-based robust optimal control of influenza epidemics in an interactive human society," *Information Sciences*, vol. 592, pp. 340–360, 2022.

[153] A. Rajaei, M. Raeiszadeh, V. Azimi, and M. Sharifi, "State estimation-based control of COVID-19 epidemic before and after vaccine development," *Journal of Process Control*, vol. 102, pp. 1–14, 2021.

[154] A. Ibeas, M. de la Sen, S. Alonso-Quesada, and I. Zamani, "Stability analysis and observer design for discrete-time SEIR epidemic models," *Advances in Difference Equations*, vol. 2015, no. 1, April 2015. [Online]. Available: http://dx.doi.org/10.1186/s13662-015-0459-x

[155] K. Hangos, J. Bokor, and G. Szederkényi, *Computer controlled systems*. Veszprém: Veszprémi Egyetemi Kiadó, 2002. [Online]. Available: https://eprints.sztaki.hu/2869/

[156] M. Kvasnica, *Real-Time Model Predictive Control Via Multi-Parametric Programming: Theory and Tools*. VDM Publishing, 2009.

[157] J. A. Jacquez, *Compartmental analysis in biology and medicine: kinetics of distribution of tracer-labeled materials*. Elsevier Publishing Company New York, 1972.

[158] J. A. Jacquez and C. P. Simon, "Qualitative theory of compartmental systems," *Siam Review*, vol. 35, no. 1, pp. 43–79, 1993.

[159] C. Belta, B. Yordanov, and E. Aydin Gol, *Formal Methods for Discrete-Time Dynamical Systems*, ser. E. A.: Formal methods for discrete-time dynamical systems, vol. 89. newblock: Springer International Publishing, 2017. [Online]. Available: http://dx.doi.org/10.1007/978-3-319-50763-7

[160] A. Donzé and V. Raman, "Blustl: Controller synthesis from signal temporal logic specifications," in *EPiC Series in Computing*. EasyChair, 2015, pp. 160–150.

[161] J. Rawlings, D. Mayne, and M. Diehl, *Model Predictive Control: Theory, Computation, and Design*, 01 2017.

[162] J. Lofberg, "YALMIP : a toolbox for modeling and optimization in MATLAB," in *2004 IEEE International Conference on Robotics and Automation (IEEE Cat. No.04CH37508)*, 2004, pp. 284–289.

[163] A. Khajavirad and N. V. Sahinidis, "A hybrid LP/NLP paradigm for global optimization relaxations," *Mathematical Programming Computation*, vol. 10, pp. 383 – 421, 2018. [Online]. Available: http://dx.doi.org/10.1007/s12532-018-0138-5

[164] S. Sadraddini, J. Rudan, and C. Belta, "Formal synthesis of distributed optimal traffic control policies," in *Proceedings of the 8th international conference on cyber-physical systems*, 2017, pp. 15–24.

[165] P. Ashcroft, J. S. Huisman, S. Lehtinen, J. A. Bouman, C. L. Althaus, R. R. Regoes, and S. Bonhoeffer, "Covid-19 infectivity profile correction," *Swiss Medical Weekly*, vol. 150, no. 3132, p. w20336, August 2020. [Online]. Available: http://dx.doi.org/10.4414/smw.2020.20336

[166] W. J. S. (2020) Covid-19 epidemic risk assessment for georgia. [Online]. Available: https://github.com/jsweitz/covid-19-ga-summer-2020

[167] M. V. Barbarossa, J. Fuhrmann, J. H. Meinke, S. Krieg, H. V. Varma, N. Castelletti, and T. Lippert, "The impact of current and future control measures on the spread of covid-19 in germany," *medRxiv*, pp. 2020–04, 2020.

[168] L. Di Domenico, G. Pullano, C. E. Sabbatini, P.-Y. Boëlle, and V. Colizza, "Impact of lockdown on covid-19 epidemic in Île-de-france and possible exit strategies," *BMC Medicine*, April 2020, doi:10.1101/2020.04.13.20063933. [Online]. Available: http://dx.doi.org/10.1186/s12916-020-01698-4

[169] S. M. Moghadas, A. Shoukat, M. C. Fitzpatrick, C. R. Wells, P. Sah, A. Pandey, J. D. Sachs, Z. Wang, L. A. Meyers, B. H. Singer, and A. P. Galvani, "Projecting hospital utilization during the covid-19 outbreaks in the united states," *Proceedings of the National Academy of Sciences*, vol. 117, no. 16, pp. 9122–9126, April 2020. [Online]. Available: http://dx.doi.org/10.1073/pnas.2004064117

[170] R. Moss, J. Wood, D. Brown, F. Shearer, A. Black, A. Cheng, J. McCaw, and J. McVernon, "Modelling the impact of covid-19 in australia to inform transmission reducing measures and health system preparedness," *medRxiv*, April 2020, doi:10.1101/2020.04.07.20056184. [Online]. Available: http://dx.doi.org/10.1101/2020.04.07.20056184

[171] S. A. Lauer, K. H. Grantz, Q. Bi, F. K. Jones, Q. Zheng, H. R. Meredith, and J. Lessler, "The incubation period of coronavirus disease 2019 (covid-19) from publicly reported confirmed cases: estimation and application," *Annals of internal medicine*, vol. 172, no. 9, pp. 577–582, 2020.

[172] L. Zou, F. Ruan, H. M., and et al., "Sars-cov-2 viral load in upper respiratory specimens of infected patients," *N Engl J Med*, vol. 382, no. 12, pp. 1177–1179, 2020.

[173] J. H. Tanne, "Covid-19: Antimicrobial resistance rose dangerously in us during pandemic, cdc says," *BMJ*, p. o1755, July 2022. [Online]. Available: http://dx.doi.org/10.1136/bmj.o1755

[174] A. B. Docherty, E. M. Harrison, C. A. Green, H. Hardwick, R. Pius, L. Norman, K. A. Holden, J. M. Read, F. Dondelinger, G. Carson *et al.*, "Features of 16,749 hospitalised uk patients with covid-19 using the isaric who clinical characterisation protocol," *MedRxiv*, pp. 2020–04, 2020.

[175] Covid-net, a weekly summary of u. s. covid-19 hospitalization data. [Online]. Available: https://gis.cdc.gov/grasp/COVIDNet/COVID19_5.html

[176] Ksh, hungarian central statistical office. [Online]. Available: http://www.ksh.hu/?lang=en

[177] S. Flaxman, S. Mishra, A. Gandy, and et al, "Estimating the effects of non-pharmaceutical interventions on covid-19 in europe," *Nature*, 2020.

[178] J. Wu, B. Tang, N. Bragazzi, K. Nah, and Z. McCarthy, "Quantifying the role of social distancing, personal protection and case detection in mitigating covid-19 outbreak in ontario, canada." *Journal of Mathematics in Industry*, vol. 10, no. 1, 2020.

[179] S. Ullah and M. A. Khan, "Modeling the impact of non-pharmaceutical interventions on the dynamics of novel coronavirus with optimal control analysis with a case study," *Chaos, Solitons and Fractals*, vol. 139, 2020. [Online]. Available: http://dx.doi.org/10.1016/j.chaos.2020.110075

[180] T. Hale, N. Angrist, B. Kira, A. Petherick, T. Phillips, and S. Webster, "Variation in government responses to covid-19. blavatnik school of government working paper," 2020.

[181] J. Lofberg, "Yalmip: a toolbox for modeling and optimization in matlab," in *2004 IEEE International Conference on Robotics and Automation (IEEE Cat. No.04CH37508)*. IEEE, 2004, pp. 284–289.

[182] N. M. Ferguson, D. Laydon, G. Nedjati-Gilani, N. Imai, K. Ainslie, M. Baguelin, S. Bhatia, A. Boonyasiri, Z. Cucunubá, G. Cuomo-Dannenburg *et al.*, *Report 9: Impact of non-pharmaceutical interventions (NPIs) to reduce COVID19 mortality and healthcare demand.* Imperial College London London, 2020, vol. 16.

[183] J. Köhler, L. Schwenkel, A. Koch, J. Berberich, P. Pauli, and F. Allgöwer, "Robust and optimal predictive control of the covid-19 outbreak," *Annual Reviews in Control*, vol. 51, pp. 525–539, 2021. [Online]. Available: http://dx.doi.org/10.1016/j.arcontrol.2020.11.002

[184] A. Bandyopadhyay and et al., "Helmholtz-initiative 'systemische epidemiologische analyse der covid-19-epidemie'," *Stellungnahme der Helmholtz-Initiative 'Systemische Epidemiologische Analyse der*, vol. COVID-19-Epidemie, 2020.

[185] T. W. Russell, N. Golding, J. Hellewell, S. Abbott, L. Wright, C. A. B. Pearson, K. v. Zandvoort, C. I. Jarvis, H. Gibbs, Y. Liu, R. M. Eggo, W. J. Edmunds, and A. J. Kucharski, "Reconstructing the early global dynamics of under-ascertained covid-19 cases and infections," *medRxiv*, vol. 2020, 2020, doi:urlhttps://doi.org/10.1101/2020.07.07.20148460.

[186] A. Pugliese and S. Sottile, "Inferring the covid-19 infection curve in italy," 2020, arXiv preprint.

[187] G. Millerioux, L. Rosier, G. Bloch, and J. Daafouz, "Bounded state reconstruction error for lpv systems with estimated parameters," *IEEE Transactions on Automatic Control*, vol. 49, no. 8, pp. 1385–1389, August 2004. [Online]. Available: http://dx.doi.org/10.1109/tac.2004.832669

[188] J. Daafouz, G. Millerioux, and L. Rosier, "Observer design with guaranteed bound for lpv systems," *IFAC Proceedings Volumes*, vol. 38, no. 1, pp. 107–112, 2005. [Online]. Available: http://dx.doi.org/10.3182/20050703-6-cz-1902.00962

[189] W. P. M. H. Heemels, J. Daafouz, and G. Millerioux, "Observer-based control of discrete-time lpv systems with uncertain parameters ," *IEEE Transactions on Automatic Control*, vol. 55, no. 9, pp. 2130–2135, September 2010. [Online]. Available: http://dx.doi.org/10.1109/tac.2010.2051072

[190] A. Leontitsis, A. Senok, A. Alsheikh-Ali, Y. Al Nasser, T. Loney, and A. Alshamsi, "SEAHIR: A specialized compartmental model for covid-19," *International Journal of Environmental Research and Public Health*, vol. 18, no. 5, p. 2667, 2021.

[191] L. Tang, D. R. Hijano, A. H. Gaur, T. L. Geiger, E. J. Neufeld, J. M. Hoffman, and R. T. Hayden, "Asymptomatic and symptomatic SARS-CoV-2 infections after BNT162b2 vaccination in a routinely screened workforce," *Jama*, vol. 325, no. 24, pp. 2500–2502, 2021.

[192] M. G. Thompson, E. Stenehjem, S. Grannis, S. W. Ball, A. L. Naleway, T. C. Ong, M. B. DeSilva, K. Natarajan, C. H. Bozio, N. Lewis *et al.*, "Effectiveness of Covid-19 vaccines in ambulatory and inpatient care settings," *New England Journal of Medicine*, vol. 385, no. 15, pp. 1355–1371, 2021.

[193] T. Nyberg, N. M. Ferguson, S. G. Nash, H. H. Webster, S. Flaxman, N. Andrews, W. Hinsley, J. L. Bernal, M. Kall, S. Bhatt *et al.*, "Comparative analysis of the risks of hospitalisation and death associated with SARS-CoV-2 omicron (B. 1.1. 529) and delta (B. 1.617. 2) variants in England: a cohort study," *The Lancet*, vol. 399, no. 10332, pp. 1303–1312, 2022.

[194] P. Bager, J. Wohlfahrt, J. Fonager, M. Rasmussen, M. Albertsen, T. Y. Michaelsen, C. H. Møller, S. Ethelberg, R. Legarth, M. S. F. Button *et al.*, "Risk of hospitalisation associated with infection with SARS-CoV-2 lineage B. 1.1. 7 in Denmark: an observational cohort study," *The Lancet Infectious Diseases*, vol. 21, no. 11, pp. 1507–1517, 2021.

[195] D. T. H. de Moura, T. R. McCarty, I. B. Ribeiro, M. P. Funari, P. V. A. G. de Oliveira, A. A. de Miranda Neto, E. S. do Monte Júnior, F. Tustumi, W. M. Bernardo, E. G. H. de Moura, and C. C. Thompson, "Diagnostic characteristics of serological-based COVID-19 testing: A systematic review and meta-analysis," *Clinics*, vol. 75, 2020.

[196] A. Sedaghat, S. A. A. Oloomi, M. A. Malayer, S. Band, A. Mosavi, and L. Nadai, "Modeling and sensitivity analysis of coronavirus disease (COVID-19) outbreak prediction," in *2020 IEEE 3rd International Conference and Workshop in Óbuda on Electrical and Power Engineering (CANDO-EPE)*, 2020, pp. 000 261–000 266.

[197] A. Sedaghat, S. A. A. Oloomi, M. A. Malayer, S. Band, N. Rezaei, A. Mosavi, and L. Nadai, "Coronavirus (COVID-19) outbreak prediction using epidemiological models of Richards Gompertz Logistic Ratkowsky and SIRD," in *2020 IEEE 3rd International Conference and Workshop in Óbuda on Electrical and Power Engineering (CANDO-EPE)*. Cold Spring Harbor Laboratory Press, 2020, pp. 000 289–000 298.

[198] S. Y. Tartof, J. M. Slezak, H. Fischer, V. Hong, B. K. Ackerson, O. N. Ranasinghe, T. B. Frankland, O. A. Ogun, J. M. Zamparo, S. Gray, S. R. Valluri, K. Pan, F. J. Angulo, L. Jodar, and J. M. McLaughlin, "Effectiveness of mRNA BNT162b2 COVID-19 vaccine up to 6 months in a large integrated health system in the USA: a retrospective cohort study," *The Lancet*, vol. 398, no. 10309, pp. 1407–1416, Oct. 2021.

[199] X. Hu and A. Lindquist, *Geometric control theory*. Royal institute of technology SE-100 44 Stockholm, Sweden, 2012.

[200] P. S. González Cisneros and H. Werner, "Nonlinear model predictive control for models in quasi-linear parameter varying form," *International Journal of Robust and Nonlinear Control*, vol. 30, no. 10, pp. 3945–3959, 2020.

[201] A. Bemporad, N. L. Ricker, and M. Morari, *Model Predictive Control Toolbox™User's Guide (R2019b)*, 2019th ed., MathWorks, 2019.

[202] "Data on COVID-19 vaccination in the EU/EEA," https://www.ecdc.europa.eu/en/publications-data/data-covid-19-vaccination-eu-eea.

[203] Atlo Team, "Koronamonitor: Hungarian status of coronavirus vaccination," https://atlo.team/vakcinacio, 2021, (Accessed on 11/11/2021).

[204] "Data on hospital and ICU admission rates and current occupancy for COVID-19," https://www.ecdc.europa.eu/en/publications-data/download-data-hospital-and-icu-admission-rates-and-current-occupancy-covid-19, 2021, (Accessed on 04/28/2021).

[205] MathWorks, *Control System Toolbox™Reference (R2021b)*, 2021st ed., 2021. [Online]. Available: https://www.mathworks.com/help/pdf_doc/control/control_ref.pdf

[206] P. Amestoy, I. S. Duff, J. Koster, and J.-Y. L'Excellent, "A fully asynchronous multifrontal solver using distributed dynamic scheduling," *SIAM Journal on Matrix Analysis and Applications*, vol. 23, no. 1, pp. 15–41, 2001.

[207] P. Amestoy, A. Buttari, J.-Y. L'Excellent, and T. Mary, "Performance and scalability of the block low-rank multifrontal factorization on multicore architectures," *ACM Transactions on Mathematical Software*, vol. 45, pp. 2:1–2:26, 2019.

[208] P. Polcz, "Epidemiological data reconstruction for Hungary using stochastic nonlinear MPC computations." GitHub repository, https://github.com/ppolcz/MPC-monitoring-for-COVID-19, 2021, commit ab75b3a698b0f6540ab5cc738a64f003aa82284a.

[209] Atlo Team, "Koronamonitor: Detailed diagrams of the coronavirus outbreak," https://atlo.team/koronamonitor-reszletesadatok, 2021, (Accessed on 11/11/2021).

[210] E. Volz, S. Mishra, M. Chand, J. C. Barrett, R. Johnson, L. Geidelberg, W. R. Hinsley, D. J. Laydon, G. Dabrera, Á. O'Toole *et al.*, "Transmission of SARS-CoV-2 lineage B.1.1.7 in England: Insights from linking epidemiological and genetic data," *medRxiv*, pp. 2020–12, 2021.

[211] Institute for Health Metrics and Evaluation, "COVID-19 results briefing, European Union, July 1, 2021," https://www.healthdata.org/sites/default/files/files/Projects/COVID/2021/4743_briefing_European_Union_23.pdf, 2021, (Accessed on 12/17/2021).

[212] E. Mathieu, H. Ritchie, L. Rodés-Guirao, C. Appel, C. Giattino, J. Hasell, B. Macdonald, S. Dattani, D. Beltekian, E. Ortiz-Ospina, and M. Roser, "Coronavirus pandemic (covid-19)," *Our World in Data*, 2020, https://ourworldindata.org/coronavirus.

[213] R. Seifried, *Feedback Linearization and Model Inversion of Nonlinear Systems*. Springer International Publishing, November 2013, p. 55–111.

[214] AtloTeam, "Koronamonitor," 2022, https://atlo.team/koronamonitor/. [Online]. Available: https://atlo.team/koronamonitor/

[215] W. Rauch, H. Schenk, N. Rauch, M. Harders, H. Oberacher, H. Insam, R. Markt, and N. Kreuzinger, "Estimating actual SARS-CoV-2 infections from secondary data," *Scientific Reports*, vol. 14, no. 1, March 2024. [Online]. Available: http://dx.doi.org/10.1038/s41598-024-57238-0

[216] M. Pájaro, N. M. Fajar, A. A. Alonso, and I. Otero-Muras, "Stochastic SIR model predicts the evolution of COVID-19 epidemics from public health and wastewater data in small and medium-sized municipalities: A one year study," *Chaos, Solitons & Fractals*, vol. 164, p. 112671, 2022.

[217] P. Polcz, K. Tornai, J. Juhász, G. Cserey, G. Surján, T. Pándics, E. Róka, M. Vargha, I. Z. Reguly, A. Csikász-Nagy *et al.*, "Wastewater-based modeling, reconstruction, and prediction for COVID-19 outbreaks in Hungary caused by highly immune evasive variants," *Water Research*, vol. 241, p. 120098, 2023.

[218] I. Haghighi, N. Mehdipour, E. Bartocci, and C. Belta, "Control from signal temporal logic specifications with smooth cumulative quantitative semantics," in *2019 IEEE 58th Conference on Decision and Control (CDC)*. IEEE, 2019.

[219] L. Alkhalifa, "Comparison between five MINLP solvers and new results related to trigonometric functions," *Fractals*, vol. 30, no. 10, p. 2240249, 2022.

[220] R. Lefever, G. Nicolis, and P. Borckmans, "The Brusselator: it does oscillate all the same," *Journal of the Chemical Society, Faraday Transactions 1: Physical Chemistry in Condensed Phases*, vol. 84, no. 4, pp. 1013–1023, 1988.

[221] Y. Takeuchi, *Global dynamical properties of Lotka-Volterra systems*. World Scientific, 1996.

[222] L. Brenig, "Reducing nonlinear dynamical systems to canonical forms," *Philosophical Transactions of the Royal Society A: Mathematical, Physical and Engineering Sciences*, vol. 376, no. 2124, p. 20170384, 2018.

[223] E. Chauvet, J. E. Paullet, J. P. Previte, and Z. Walls, "A Lotka-Volterra three-species food chain," *Mathematics Magazine*, vol. 75, no. 4, pp. 243–255, 2002.

[224] J. Chen, "An SIRS epidemic model," *Applied Mathematics-A Journal of Chinese Universities*, vol. 19, no. 1, pp. 101–108, 2004.

[225] H. Ritchie, E. Mathieu, L. Rodés-Guirao, C. Appel, C. Giattino, E. Ortiz-Ospina, J. Hasell, B. Macdonald, D. Beltekian, and M. Roser, "Coronavirus pandemic (COVID-19)," *Our World in Data*, 2020, https://ourworldindata.org/coronavirus.

[226] A. Mesbah, S. Streif, R. Findeisen, and R. D. Braatz, "Stochastic nonlinear model predictive control with probabilistic constraints," in *2014 American Control Conference*. IEEE, Jun. 2014.

[227] P. De Larminat, *Analysis and control of linear systems*. John Wiley & Sons, 2013.

[228] M. Lorenzen, F. Dabbene, R. Tempo, and F. Allgöwer, "Constraint-tightening and stability in stochastic model predictive control," *IEEE Transactions on Automatic Control*, vol. 62, no. 7, pp. 3165–3177, 2017.

[229] R. Hermann and A. Krener, "Nonlinear controllability and observability," *IEEE Transactions on Automatic Control*, vol. 22, no. 5, pp. 728–740, 1977.

Appendix

7.3 Optimisation-based stochastic MPC

This section contains additional computations and clarifications to the approach presented in Chapter 4.1. Consequently, the notations applied here follow the rules outlined at the beginning of the referenced part.

7.3.1 Statistical analysis for normally distributed model parameters

Gaussian assumptions

In this section, we allow the model parameters to vary in time ($\hat{\theta} : k \mapsto \hat{\theta}_k$), but we assume that the parameter process $\hat{\theta}$ is a collection of *independent identically distributed* (i.i.d.) Gaussian random variables

$$\hat{\theta}_k \sim \mathcal{N}(\mu^\theta, \Sigma^\theta) \text{ for all } k = 0, 1, \dots, T-1, \tag{7.1}$$

where μ^θ is the expected value of $\hat{\theta}_k$ corresponding to the values presented in Section 4.1.1, and the diagonal Σ^θ is its variance. The expected value of the parameter vector contains the nominal values from Table 4.1, whereas, the variances are determined such that the uncertainty intervals from Table 4.1 resemble the 2σ confidence intervals. Moreover, we assume that the initial state, from where the prediction is performed, is itself a random variable, namely:

$$\hat{x}_0 \sim \mathcal{N}\big(\mu_0^x, \Sigma_0^x\big). \tag{7.2}$$

Consequently, every further state and output are random variables, which obey the following stochastic recursion and output equation:

$$\hat{x}_{k+1} = f(\hat{x}_k, \hat{u}_k, \hat{\theta}_k, v_k),\ \hat{y}_k = C\hat{x}_k. \tag{7.3}$$

Due to the nonlinear terms in the state transition function f, the distribution of the predicted states $\hat{x}_k$ becomes more and more complicated as we look forward in time ($k = 1, 2, \dots$). Therefore, it is very inefficient to compute or at least approximate the non-Gaussian probability density functions of the predicted states for the nonlinear stochastic model (7.3). As it is commonly done in the literature (see, e.g., [134–137]), we perform a tube-like trajectory estimation. With this technique each predicted state $\hat{x}_k$ is described by the first two moments, the expected value μ_k^x and the variance Σ_k^x, namely, the states are approximated by normal distributions:

$$\hat{x}_k \sim \mathcal{N}(\mu_k^x, \Sigma_k^x) \text{ for all } k = 0, 1, 2, \dots \tag{7.4}$$

Closed-loop control policy

In the literature [128], the values of the optimal control input u are often searched as functions of the states as follows:

$$\hat{u}_k = \mu_k^u - K(\mu_k^x)(\hat{x}_k - \mu_k^u), \tag{7.5}$$

where μ_k^u are free decision variables, and K is (not necessarily a closed-form) function of the expected state. Thus, the control input is inherently a random variable, and is normally distributed as the state (7.4) itself is approximated by a Gaussian. If $\Sigma_k^{x\theta} = (\Sigma_k^{\theta x})^\top$ denotes the covariance between $\hat{x}_k$ and $\hat{\theta}_k$, the joint distribution of $\hat{x}_k$, $\hat{u}_k$, and $\hat{\theta}_k$ is

$$\begin{pmatrix} \hat{x}_k \\ \hat{u}_k \\ \hat{\theta}_k \end{pmatrix} \sim \mathcal{N}(\mu_k, \Sigma_k), \text{ where } \mu_k = \begin{pmatrix} \mu_k^x \\ \mu_k^u \\ \mu^\theta \end{pmatrix}, \ \Sigma_k = \begin{pmatrix} \star \end{pmatrix}^\top \begin{pmatrix} \Sigma_k^x & \Sigma_k^{x\theta} \\ \Sigma_k^{\theta x} & \Sigma^\theta \end{pmatrix} \begin{pmatrix} I & -K^\top(\mu_k^x) & 0 \\ 0 & 0 & I \end{pmatrix}. \tag{7.6}$$

Remark[Nonlinear state-dependent input policy] When $K = 0$, the optimal tracking problem is said to be an **open-loop** MPC problem [226], whereas, $K \neq 0$ results in a so-called **closed-loop** MPC problem [135], where the optimal input policy is parameterized by the state. A stabilizing state feedback (7.5) is typically useful when the predicted states are random variables, and their actual realizations may deviate from the predicted expectations. When the prediction model is stochastic, a sequence of deterministic input values ($K = 0$) may result in a diverging sequence of state variances, and hence in a **conservative** (overly cautious) prediction. When the input is parameterized by the state ($K \neq 0$), the adaptability of the input may reduce the uncertainty of the predicted states significantly if the feedback function (7.5) is determined appropriately. In this sense, the **gain function quantifies the trade-off between the uncertainty of the state and the input**. Unfortunately, it is not straightforward to compute a stabilizing gain function K for the nominal model (4.4). Later, in Section 7.3.1, we will demonstrate that **a reference state trajectory** (if available) makes it possible to compute the values of K separately in each operating reference state through a classical LTI state feedback approach, e.g., a pole-placement or a linear quadratic regulator (LQR) design [227, Sec. 6.4.2].

Probabilistic cost and input constraint

Problem 4.1.1 with the stochastic state equations (7.3) and the joint distribution (7.6) results in a stochastic optimal control problem, where both the cost function (4.5) and the input constraint are probabilistic. Therefore, the inputs and the states are meant to be found such that they minimize the *expected cost*, namely:

$$J(M,S,V) = \sum_{k=0}^{T-1} \|C\mu_{k+1}^x - r_{k+1}\|_Q^2 + \sum_{k=0}^{T-2} \|\mu_{k+1}^u - \mu_k^u\|_R^2 + \sum_{k=0}^{T-1} \operatorname{Tr}\left(Q\,C\,\Sigma_{k+1}^x\,C^\top\right) \tag{7.7}$$
$$+ \sum_{k=0}^{T-2} \operatorname{Tr}\Big(R\,K(\mu_{k+1}^x)\,\Sigma_{k+1}^x\,K^\top(\mu_{k+1}^x) + R\,K(\mu_k^x)\,\Sigma_k^x\,K^\top(\mu_k^x) - R\,\mathrm{He}\Big\{K(\mu_{k+1}^x)\,\operatorname{Cov}(\hat{x}_{k+1},\hat{x}_k)\,K^\top(\mu_k^x)\Big\}\Big),$$

$$\text{where } M = \begin{pmatrix} \mu_1^x & \dots & \mu_T^x \end{pmatrix},\ S = \begin{pmatrix} \Sigma_1^x & \dots & \Sigma_T^x \\ \Sigma_1^{\theta x} & \dots & \Sigma_T^{\theta x} \end{pmatrix}, \text{ and } V = \begin{pmatrix} \mu_0^u & \dots & \mu_{T-1}^u \end{pmatrix}. \tag{7.8}$$

The expanded formula (7.7) of the expectation of cost (4.5) is derived in [J3, AppendixA].

Remark The term $\operatorname{Cov}(\hat{x}_{k+1},\hat{x}_k) = \operatorname{Cov}(f(\hat{x}_k,\hat{u}_k,v_k,\hat{\theta}_k),\hat{x}_k)$ in (7.7) is typically a non-quadratic function of the mean and the variance of the joint distribution (7.6). This term introduces a potential difficulty to the optimization, which will be addressed later in Section 7.3.1.

The conditions on the input can be formulated as chance constraints of the form $\Pr(\hat{u}_k \in \mathcal{U}) \geq p_u$, where p_u denotes the *probability level* of the *confidence set* $\mathcal{U}$. When $\hat{u}_k$ comprise a single input, and the input domain $\mathcal{U}$ is an interval, the chance constraint $\Pr(\hat{u}_k \in [\underline{u},\overline{u}]) \geq p_u$ is equivalent to the following deterministic interval constraint [135]:

$$\mu_k^u \in [\underline{u} + c, \overline{u} - c], \text{ with } c = \Phi^{-1}(\tfrac{p_u+1}{2})\sqrt{K(\mu_k^x)\,\Sigma_k^x\,K^\top(\mu_k^x)}, \tag{7.9}$$

where $\Phi : \mathbb{R} \to (0,1)$ denotes the (cumulative) distribution function of the standard normal distribution $\mathcal{N}(0,1)$. This technique for the reformulation of a probabilistic condition is referred to as *constraint tightening* [228].

Linear approximation of the state dynamics around the expectation

In the literature, there exist different stochastic sample-based optimization approaches for a predictive optimal controller design, see, e.g., [129–134]. However, these approaches are computationally tractable only for a shorter prediction horizon. Alternatively, we have the possibility to formulate deterministic recursions for the first two moments of the state vector. E.g., [135] proposed the state transition function f to be approximated by its first order Taylor polynomial around the expected values $\mu_k = (\mu_k^x, \mu_k^u, \mu^\theta)$ of the probabilistic variables $(\hat{x}_k,\, \hat{u}_k,\, \hat{\theta}_k)$, namely:

$$\hat{x}_{k+1} \approx \tfrac{\partial f}{\partial(x,u,\theta)}(\mu_k, v_k) \begin{pmatrix} \hat{x}_k \\ \hat{u}_k \\ \hat{\theta}_k \end{pmatrix} \quad + \quad f(\mu_k, v_k) - \tfrac{\partial f}{\partial(x,u,\theta)}(\mu_k, v_k)\,\mu_k. \tag{7.10}$$

This approach leads to a deterministic mean-variance ("$\mu\Sigma$") dynamics, that are typically nonlinear in the free variables μ_k^x and μ_k^u.

$$\begin{cases} \mu_{k+1}^x = f(\mu_k, v_k), & \text{(7.11a)} \\ \Sigma_{k+1}^{x\theta} = \tfrac{\partial f}{\partial(x,u,\theta)}(\mu_k, v_k) \begin{pmatrix} I & -K^\top(\mu_k^x) & 0 \\ 0 & 0 & I \end{pmatrix}^\top \begin{pmatrix} \Sigma_k^{x\theta} \\ \Sigma^\theta \end{pmatrix}, & \text{(7.11b)} \\ \Sigma_{k+1}^x = \tfrac{\partial f}{\partial(x,u,\theta)}(\mu_k, v_k)\,\Sigma_k \left(\tfrac{\partial f}{\partial(x,u,\theta)}(\mu_k, v_k)\right)^\top. & \text{(7.11c)} \end{cases}$$

Note that the linear Taylor approximation of $\hat{x}_{k+1}$ allows us to express the non-quadratic term in the cost function (7.7) as follows:

$$\mathrm{Cov}(\hat{x}_{k+1}, \hat{x}_k) = \tfrac{\partial f}{\partial(x,u,\theta)}(\mu_k, v_k) \begin{pmatrix} I & -K^\top(\mu_k^x) & 0 \\ 0 & 0 & I \end{pmatrix}^\top \begin{pmatrix} \Sigma_k^x \\ \Sigma_k^{\theta x} \end{pmatrix} \tag{7.12}$$

The dynamic equations in (7.11) constitute a possible deterministic *prediction model* for system (7.3), and results in the following nonlinear optimal predictive control problem.

Problem 7.3.1 ($\mu\Sigma$-NMPC for unknown-input state reconstruction)**:** *Given the dynamical model* (7.11) *with an initial state distribution* (7.2)*, an i.i.d. parameter process* (7.1)*, a measured disturbance* v_k*, an input policy* (7.5) *with a fixed gain function* K*, and a reference output trajectory* r_{k+1} *to track* ($k \in \mathbb{I}_0^{T-1}$)*. We are looking for a sequence of deterministic values* μ_k^u*, state moments* μ_{k+1}^x*,* Σ_{k+1}^x*, and covariance matrices* $\Sigma_{k+1}^{x\theta}$ *with* $\Sigma_0^{x\theta} = 0$*, which solve* (7.11)*, satisfy the input constraint* (7.9)*, and minimize the cost* (7.7)*. The free variables of the optimization are collected in* (7.8)*.*

Problem 7.3.1 is a *stochastic data assimilation* problem, reformulated as an optimal predictive tracking problem with a deterministic nonlinear $\mu\Sigma$-prediction model (7.3). Henceforth, we refer to Problem 7.3.1 as a *Gaussian* or *mean-variance* NMPC problem abbreviated as $\mu\Sigma$-NMPC. In general, the variance dynamics (7.11b) and (7.11c) significantly increase the complexity of the control problem. If n and p denote the dimension of the state $\hat{x}_k$ and the parameter $\hat{\theta}_k$, respectively, the equations in (7.11) comprise $np + n(n+1)/2$ separate scalar equations, whereas,

the deterministic model (4.4) constitutes a system of n scalar equations. Therefore, the $\mu\Sigma$-NMPC in Problem 7.3.1 is typically (at least) an order of magnitude more demanding than the ordinary NMPC in Problem 4.1.1. However, an appropriate initial guess for the solution of $\mu\Sigma$-NMPC may reduce the computational complexity of the optimization substantially by providing a fast convergence of the solution.

Initial solution for the $\mu\Sigma$-NMPC problem

In this section, we compute a pseudo-optimal (i.e., feasible but not necessarily optimal) solution of Problem 7.3.1, which satisfies the dynamic equations (7.3) and the input constraint (7.9) but it does not necessarily minimize the cost (7.7). The computed solution can be considered an initial value for the $\mu\Sigma$-NMPC problem. The solution relies on three observations.

First, observe that the mean equation in (7.11a) resembles the deterministic state recursion in (4.4) as the the mean dynamics is not affected by the variances nor the state-dependent feedback gain $K(\mu_k^x)$. Therefore, Problem 7.3.1 simplifies to Problem 4.1.1 if we neglect the variances ($S = 0$) and their dynamics (7.11b) and (7.11c) from the optimization. Accordingly, a possible guess for the expectation (M, V), which solves the mean equation (7.11a), can be given by the optimal solution (X^*, U^*) of Problem 4.1.1 with initial condition $x_0 \leftarrow \mu_0^x$ and parameter vector $\theta \leftarrow \mu^\theta$.

Secondly, we note that the gain function K depends (by design) on the expected states only. This allows to compute an appropriate gain K_k at each operating point $x_0^* = \mu_0^x$, x_k^*, $k \in \mathbb{I}_1^{T-1}$ along the computed mean solution. We determine K_k through the DT version of the LQR design applied to the controllable modes of the pair (A_k, B_k), where

$$A_k = \tfrac{\partial f}{\partial x}(\mu_k, v_k),\ B_k = \tfrac{\partial f}{\partial u}(\mu_k, v_k). \tag{7.13}$$

Through a sequence of DT-LQR computations, we select a static feedback gain matrix K_k at each time instant k, which minimizes the quadratic cost

$$\sum\nolimits_{t=k}^{\infty} \left(x_t^\top \mathbf{Q}_k^{\mathrm{LQR}}\, x_t + u_t^\top \mathbf{R}_k^{\mathrm{LQR}}\, u_t\right),\ \text{with } u_t = -K_k\, x_t. \tag{7.14}$$

For a DT-LTI state-space model $x_{t+1} = A_k x_t + B_k u_t$ (with $t = 0, 1, 2, \ldots$, but a fixed k), the constant gain matrix K_k can be computed through simple linear algebra operations [227, Sec. 6.4.2], which are implemented in function `dlqr` of the Control System Toolbox [205] for MATLAB. When selecting the weight matrices $\mathbf{Q}_k^{\mathrm{LQR}}$ and $\mathbf{R}_k^{\mathrm{LQR}}$ of the LQR problem at time $k \in \mathbb{I}_0^{T-1}$, we need to take into consideration that the value of K_k quantifies the trade-off between the uncertainty of $\hat{x}_{k+1}$ and $\hat{u}_k$. If the locally stabilizing gain has a higher value, the input $\hat{u}_k$ is more adaptive (hence more uncertain) but the uncertainty of $\hat{x}_{k+1}$ is smaller. However, the chance constraint (7.9) does not allow the uncertainty of $\hat{u}_k$ to increase beyond any bounds. Therefore, the gain should be selected carefully, such that it generates an input distribution satisfying (7.9). If the first computed value for K_k does not result in an admissible input distribution, we are allowed to compute K_k multiple times with a gradually decreasing value for $\mathbf{R}_k^{\mathrm{LQR}}$.

Finally, in the knowledge of μ_k, v_k, $K(\mu_k^x) = K_k$, $k \in \mathbb{I}_0^{T-1}$, Σ_0^x, and $\Sigma_0^{x\theta} = 0$, we compute the variances according to (7.11b) and (7.11c), which give the value of S in (7.8). If the expected values and K are fixed, the variances are well-defined by the variance equations (7.11b) and (7.11c). By construction, the tuple (M, S, V) is a feasible solution for Problem 7.3.1 as it satisfies both the $\mu\Sigma$-equations (7.11) and the input constraint (7.9). The computed solution is a good initial guess for the optimal solution of Problem 7.3.1. In Algorithm 1, we summarize the proposed operations with a single input $u_k \in \mathbb{R}$ and a simple LQR weight selection.

Algorithm 1 Computing a pseudo-optimal solution for Problem 7.3.1.

1: Fix $\hat{x}_0 \sim \mathcal{N}(\mu_0^x, \Sigma_0^x)$, $\Sigma_0^{x\theta} \leftarrow 0$, μ^θ, and Σ^θ. (Optionally, fix μ_0^u.)
2: Collect data v_k and r_{k+1}, then, solve Problem 4.1.1 to obtain μ_k^x and μ_k^u, where $k \in \mathbb{I}_0^{T-1}$.
3: **for** $k \in \mathbb{I}_0^{T-1}$ **do**
4: $\quad i \leftarrow 1$.
5: $\quad$ **repeat**
6: $\quad\quad$ Compute K_k for the pair (A_k, B_k) given in (7.13) through a DT-LQR design with weight matrices $\mathbf{Q}^{\text{LQR}} \leftarrow I_n$ and $\mathbf{R}_k^{\text{LQR}} \leftarrow 2^{i-1}$; $\quad i \leftarrow i+1$.
7: $\quad$ **until** condition (7.9) is met. (If not such K_k found, let $K_k \leftarrow 0$.)
8: $\quad$ Compute $\Sigma_{k+1}^{x\theta}$, Σ_{k+1}^x, as given in (7.11b) and (7.11c), respectively, using $K(\mu_k^x) = K_k$.
9: **end for**

Remark From the authors' experience, the computationally demanding $\mu\Sigma$-NMPC optimization for model (3.1), will generally not result in a significantly lower expected cost (7.7) compared to the computed pseudo-optimal solution (M, S, V).

7.4 Zero dynamics of the epidemic models

This part provides the detailed analysis of the feedback-linearized SEIR and SLPIAHRD models' zero dynamics, exploring the theoretical limitations where the method proposed in Chapter 4.2 is reliably applicable. While the derivations consider the original feedback-linearization (without the extra integrator introduced for robustness), this makes no difference regarding the stability of the internal states and the zero dynamics.

7.4.1 SEIR model

Reiterating the formulations used in Sections 4.2.2 - 4.2.3, the SEIR model can be expressed as:

$$\dot{x} = f(x) + g(x)u, \quad y = h(x), \quad \text{where} \tag{7.15a}$$

$$u = \beta, \quad x = \begin{pmatrix} \mathbf{S} \\ \mathbf{E} \\ \mathbf{I} \\ \mathbf{R} \end{pmatrix}, \quad f(x) = \begin{pmatrix} 0 \\ -k_2\mathbf{E} \\ k_2\mathbf{E} - k_3\mathbf{I} \\ k_3\mathbf{I} \end{pmatrix}, \quad g(x) = \begin{pmatrix} -\mathbf{SI} \\ \mathbf{SI} \\ 0 \\ 0 \end{pmatrix}, \quad h(x) = \mathbf{I} \tag{7.15b}$$

It was already computed that the relative degree of the system is $\rho = 2$, so we can write the transformed z states and the extra output derivative (required for the input mapping) as:

$$z_0 = y = h(x) = \mathbf{I} \tag{7.16a}$$

$$z_1 = \dot{y} = L_f h(x) = \dot{\mathbf{I}} = k_2\mathbf{E} - k_3\mathbf{I} \tag{7.16b}$$

$$\ddot{y} = L_f^2 h(x) = k_2\dot{\mathbf{E}} - k_3\dot{\mathbf{I}} = k_2\mathbf{SI}u - k_2^2\mathbf{E} - k_3k_2\mathbf{E} + k_3^2\mathbf{I} = v \tag{7.16c}$$

It must be noted, however, that the input appears in $\ddot{y}$ only if the term $k_2\mathbf{SI} \neq 0$. Considering that the parameter $k_2 > 0$ at all times, and that the system is nonnegative ($\mathbf{S}, \mathbf{I} \geq 0$), this means that the relative degree is not well-defined in parts of the state-space ($\{x \mid \mathbf{S} = 0 \; or \; \mathbf{I} = 0\}$), and consequently, the input-mapping can not be defined in this region either.

As the original system has four state variables, and the relative degree is $\rho = 2$, the transformed system will have $4 - 2 = 2$ internal states (η_1, η_2). Supplementing the two transformed states

$(z_1, z_2) = \Phi(x)$ with these, we can define the full transformation as $\Phi_f(x) = (z_1, z_2, \eta_1, \eta_2)^\intercal$. As a natural choice, selecting $\eta_1 = \mathbf{S}, \eta_2 = \mathbf{R}$ results in:

$$\Phi_f(x) = \begin{pmatrix} z_1 \\ z_2 \\ \eta_1 \\ \eta_2 \end{pmatrix} = \begin{pmatrix} \mathbf{I} \\ k_2\mathbf{E} - k_3\mathbf{I} \\ \mathbf{S} \\ \mathbf{R} \end{pmatrix} = \underbrace{\begin{pmatrix} 0 & 0 & 1 & 0 \\ 0 & k_2 & -k_3 & 0 \\ 1 & 0 & 0 & 0 \\ 0 & 0 & 0 & 1 \end{pmatrix}}_{D\Phi_f} \begin{pmatrix} \mathbf{S} \\ \mathbf{E} \\ \mathbf{I} \\ \mathbf{R} \end{pmatrix}. \tag{7.17}$$

We check that the transformation is invertible by computing the determinant:

$$\det(D\Phi_f) = -k_2 \neq 0, \tag{7.18}$$

which confirms that the zero dynamics of the system corresponds to the dynamics of the states $\mathbf{S}, \mathbf{R}$ when the output-zeroing input is applied to the system. Thus, the zero dynamics can be derived as:

$$y = \mathbf{I} \equiv 0 \tag{7.19a}$$

$$\dot{y} = k_2\mathbf{E} - k_3\mathbf{I} \equiv 0 \xrightarrow{(\mathbf{I}\equiv 0)} \mathbf{E} \equiv 0 \tag{7.19b}$$

$$\dot{\mathbf{S}} = -u\mathbf{S}\mathbf{I} \equiv 0 \tag{7.19c}$$

$$\dot{\mathbf{R}} = k_3\mathbf{I} \equiv 0 \tag{7.19d}$$

As we can see, the zero-dynamics of the internal states is marginally stable, and thus will always have bounded solutions. Even more generally, due to the nonnegative property of the system ($\mathbf{S}, \mathbf{R} \geq 0$) and the population conservation law ($\mathbf{S} + \mathbf{R} < \mathbf{N}$), these variables have bounded solutions for any admissible input, which allows a stable feedback-linearization based control in the whole state-space (except the above-mentioned regions where the relative degree is not well defined).

7.4.2 SLPIAHRD model

The zero-dynamics of the SLPIAHRD model was already briefly analyzed in [C2]. For the sake of completeness, this part reiterates the results, complementing them with more detailed calculations and interpretations.

Due to the complexity of the derivations, MATLAB's Symbolic Toolbox was used to validate the computed Lie derivatives and transformation matrices. The system has a relative degree of $\rho = 4$, with state variables on the infection path between the input (β, entering the model at $\mathbf{L}$) and output (measured at $\mathbf{H}$) being part of the equations. These are $\mathbf{L}, \mathbf{P}, \mathbf{I}, \mathbf{H}$. Consequently, the system has 4 internal states, the zero dynamics of which should be examined.

Writing out the equations, the transformed states can be computed as:

$$z_1 = y = \mathbf{H} \tag{7.20a}$$

$$z_2 = \dot{y} = \dot{\mathbf{H}} = \rho_I\eta\mathbf{I} - h\mathbf{H} \tag{7.20b}$$

$$z_3 = \ddot{y} = \rho_I\eta\dot{\mathbf{I}} - h\dot{\mathbf{H}} = \rho_I\eta(qp\mathbf{P} - \rho_I\mathbf{I}) - h(\rho_I\eta\mathbf{I} - h\mathbf{H}) = \tag{7.20c}$$
$$= \rho_I\eta qp\mathbf{P} - (\rho_I^2\eta - h\rho_I\eta)\mathbf{I} + h^2\mathbf{H}$$

$$z_4 = \dddot{y} = \rho_I\eta qp\dot{\mathbf{P}} - (\rho_I^2\eta - h\rho_I\eta)\dot{\mathbf{I}} + h^2\dot{\mathbf{H}} = \tag{7.20d}$$
$$= \rho_I\eta qp(\alpha\mathbf{L} - p\mathbf{P}) - (\rho_I^2\eta - h\rho_I\eta)(qp\mathbf{P} - \rho_I\mathbf{I}) + h^2(\rho_I\eta\mathbf{I} - h\mathbf{H}) =$$
$$= \rho_I\eta qp\alpha\mathbf{L} - \left(\rho_I\eta qp^2 + (\rho_I^2\eta - h\rho_I\eta)qp\right)\mathbf{P} + ((\rho_I^3\eta - h\rho_I^2\eta) + h^2\rho_I\eta)\mathbf{I} - h^3\mathbf{H}$$

Differentiating the output one more time the input β appears on the right:

$$\begin{aligned} d^4y/dt &= \rho_I\eta qp\alpha\dot{\mathbf{L}} - \left(\rho_I\eta qp^2 + (\rho_I^2\eta - h\rho_I\eta)qp\right)\dot{\mathbf{P}} + ((\rho_I^3\eta - h\rho_I^2\eta) + h^2\rho_I\eta)\dot{\mathbf{I}} - h^3\dot{\mathbf{H}} \qquad (7.21)\\ &= \rho_I\eta qp\alpha\left(\underset{\Uparrow}{\beta}[\mathbf{P}+\mathbf{I}+\delta\mathbf{A}]\mathbf{S} - \alpha\mathbf{L}\right) - \left(\rho_I\eta qp^2 + (\rho_I^2\eta - h\rho_I\eta)qp\right)(\alpha\mathbf{L} - p\mathbf{P}) + ...\\ &\quad ... + ((\rho_I^3\eta - h\rho_I^2\eta) + h^2\rho_I\eta)(qp\mathbf{P} - \rho_I\mathbf{I}) - h^3(\rho_I\eta\mathbf{I} - h\mathbf{H}), \end{aligned}$$

which confirms that the relative degree is $\rho = 4$ if $\rho_I\eta qp\alpha[\mathbf{P}+\mathbf{I}+\delta\mathbf{A}]\mathbf{S} \neq 0$. Similarly to the SEIR model, $\rho_I, \eta, q, p, \alpha, \delta > 0$ and $\mathbf{S}, \mathbf{P}, \mathbf{I}, \mathbf{A} \geq 0$, which means that the relative degree is not well defined only if $\mathbf{S} = 0$ or $\mathbf{P} = \mathbf{I} = \mathbf{A} = 0$ (i.e. no susceptible or no infectious individuals are present in the system).

As the original system has 8 state variables, the transformed system has $8-4 = 4$ internal states. Supplementing the state transformation with the state variables not appearing in equations (7.20), we can check that the full transformation $\Phi_f(x) = (z_1\ z_2\ z_3\ z_4\ \mathbf{S}\ \mathbf{A}\ \mathbf{R}\ \mathbf{D})^\intercal$ becomes a linear projection $\Phi_f(x) = T_f x,\ T_f \in \mathbb{R}^{8\times 8}$. Furthermore, it can be verified (using symbolic tools) that $\det T_f = \det(D\Phi_f(x)) \neq 0$ for all possible values of the model states and parameters, meaning that $\Phi_f(x)$ is invertible.

As a result, the system's zero dynamics corresponds to the dynamics of compartments **S**, **A**, **R**, and **D** when the output zeroing input is applied to the system, namely, the virus is eradicated. Due to the population conservation law, the union of the compartments is invariant; moreover, the cardinality of the compartments is non-negative. Therefore, the original system, and hence the zero dynamics, has bounded solutions for all admissible inputs. The boundedness of the zero dynamics ensures a stable feedback linearization control (except in regions where the relative degree is not well defined, and thus the input mapping law can not be constructed).

7.5 Observability analysis of the epidemic models

This part contains the detailed observability analysis for the SEIR and SLPIAHRD models used in Chapter 4.2. Instead of checking just local observability of the linearized system, we compute the Hermann-Krener nonlinear observability matrices using co-distributions [229].

Generally, considering a nonlinear system in the input-affine form:

$$\dot{x} = f(x) + G(x)u = f(x) + \sum_{i=1}^{m} g_j(x)u_j \qquad (7.22a)$$

$$y = [y_1\ y_2\ \ldots y_p]^\intercal = h(x), \qquad (7.22b)$$

and introducing the notation $g_0 = f$ for more compact formulations, the algorithm for constructing the observability matrix consists of the following steps:

1. Starting point: $\Omega_0 = \text{span}\{dh_1, dh_2, \ldots, dh_p\}$.
2. Developing the co-distribution: $\Omega_k = \Omega_{k-1} + \sum_{i=0}^{m} L_{g_i}\Omega_{k-1}$,
   where $L_{g_i}\Omega = \Omega\dfrac{\partial g_i}{\partial x}$ is the Lie-derivative defined for co-distributions.
3. Stopping criteria: if $\exists k^*$: rank Ω_k = rank Ω_{k+1} then $\Omega_{obs} = \Omega_k$; otherwise $\Omega_{obs} = \Omega_n$.

.

Using this, the below theorem states the sufficient (and almost necessary) condition for local nonlinear observability:

Theorem (Nonlinear observability sufficient condition)**.** If the observability matrix has maximal rank at a point x_0, i.e. rank $\Omega_{obs}(x_0) = n$, then the system is (locally) observable in some neighbourhood of x_0.

7.5.1 SEIR model

Computing the nonlinear observability matrix

Using the same input-affine description for the SEIR model as in equation (7.15), we iteratively compute the observability matrix following the above algorithm. For more efficient computations, we can precompute the values:

$$Df(x) = \begin{pmatrix} 0 & 0 & 0 & 0 \\ 0 & -k_2 & 0 & 0 \\ 0 & k_2 & -k_3 & 0 \\ 0 & 0 & k_3 & 0 \end{pmatrix}, \quad Dg(x) = \begin{pmatrix} -\mathbf{I} & 0 & -\mathbf{S} & 0 \\ \mathbf{I} & 0 & \mathbf{S} & 0 \\ 0 & 0 & 0 & 0 \\ 0 & 0 & 0 & 0 \end{pmatrix} \tag{7.23a}$$

It must also be noted that since the SEIR has a single input and a single output, $m = 1$ and $p = 1$, somewhat simplifying the required calculations.
Now, following the steps of the algorithm:

0. Starting point:

$$\Omega_0 = \operatorname{span}\{dh_1\} = \operatorname{span}\{(0 \;\; 0 \;\; 1 \;\; 0)\}; \quad \operatorname{rank}\,\Omega_0 = 1 \tag{7.24}$$

1. Iteration 1:

$$\Omega_1 = \Omega_0 + \sum_{i=0}^{m=1} L_{g_i}\Omega_0 \tag{7.25a}$$

$$L_{g_0}\Omega_0 = L_f\Omega_0 = (0 \;\; 0 \;\; 1 \;\; 0)\; Df(x) = (0 \;\; k_2 \;\; -k_3 \;\; 0) \tag{7.25b}$$

$$L_{g_1}\Omega_0 = (0 \;\; 0 \;\; 1 \;\; 0)\; Dg(x) = (0 \;\; 0 \;\; 0 \;\; 0) \tag{7.25c}$$

$$\Omega_1 = \operatorname{span}\left\{\begin{matrix}(0 & 0 & 1 & 0) \\ (0 & k_2 & -k_3 & 0)\end{matrix}\right\}; \quad \operatorname{rank}\,\Omega_1 = 2 \tag{7.25d}$$

2. Iteration 2:

$$\Omega_2 = \Omega_1 + \sum_{i=0}^{m=1} L_{g_i}\Omega_1 \tag{7.26a}$$

$$L_{g_0}\Omega_1 = (0 \quad -k_2^2 - k_2k_3 \quad -k_3^2 \;\; 0) \tag{7.26b}$$

$$L_{g_1}\Omega_1 = (k_2\mathbf{I} \;\; 0 \;\; k_2\mathbf{S} \;\; 0) \tag{7.26c}$$

$$\Omega_1 = \operatorname{span}\left\{\begin{matrix}(0 & 0 & 1 & 0) \\ (0 & k_2 & -k_3 & 0) \\ (0 & -k_2^2 - k_2k_3 & -k_3^2 & 0) \\ (k_2\mathbf{I} & 0 & k_2\mathbf{S} & 0)\end{matrix}\right\}; \quad \operatorname{rank}\,\Omega_2 = 3 \tag{7.26d}$$

At this point, we can terminate the algorithm. While the stopping criteria is not reached (yet), it is clearly visible that the Jacobians $Df(x), Dg(x)$ have only 0 values in their last columns, meaning that the last element in any $L_{g_i}\Omega_k$ term will be 0. For this reason, the last column in Ω_k will remain uniformly zero regardless of how many iterations we execute, and thus rank Ω_k can never increase to 4. As Ω_2 already has a structural rank of 3, this means rank $\Omega_2 =$ rank $\Omega_3 = 3$ will fulfill the stopping criteria, and $\Omega_{obs} = \Omega_2$.

Observability analysis

As the rank of the observability matrix is less than the number of state variables, we can conclude that the SEIR model is *not* fully observable. Moreover, it can be computed that the unobservability subspace is $\ker \Omega_{obs} = \{x \mid x = r \cdot (0\ 0\ 0\ 1)^\intercal, r \in \mathbb{R}\}$, meaning that the state variable $\mathbf{R}$ is not observable.

Intuitively, this is not a surprising result: $\mathbf{R}$ is a terminal compartment (integrating the value of $\mathbf{I}$), which has no influence on any other state variable, thus there is no way to detect a constant being added to its initial value without a direct measurement. Nevertheless, as $\mathbf{R}$ is not required for the feedback-linearization, this does not affect the control setup proposed in Chapter 4.2.

Furthermore, it must be noted that the value of $\Omega_{obs}(x)$ depends on the system state, and while it has a *structural* rank of 3, this might decrease in some regions of the state-space. To investigate where this reduction might happen, we compute the determinant of the $M_{3,4}$ minor:

$$\det M_{3,4} = \begin{vmatrix} 0 & 0 & 1 \\ 0 & k_2 & -k_3 \\ k_2\mathbf{I} & 0 & k_2\mathbf{S} \end{vmatrix} = -k_2^2\ \mathbf{I} \tag{7.27}$$

Solving this for $\det M_{3,4} = 0$ shows that the rank of Ω_{obs} can only decrease if $\mathbf{I} = 0$ (since the parameter $k_2 > 0$), meaning that there are no infectious individuals in the system. In practice, this can happen only at the end of an epidemic process, when the pathogen is fully eradicated.

7.5.2 SLPIAHRD model

We apply the same methodology for the SLPIAHRD model, presented in Section 3.1.1.

The model can be written out using the following input-affine equations:

$$\dot{x} = f(x) + g(x)u, \quad y = h(x), \quad \text{where} \tag{7.28a}$$

$$x = \begin{pmatrix} \mathbf{S} \\ \mathbf{L} \\ \mathbf{P} \\ \mathbf{I} \\ \mathbf{A} \\ \mathbf{H} \\ \mathbf{R} \\ \mathbf{D} \end{pmatrix}; f(x) = \begin{pmatrix} 0 \\ -\alpha\mathbf{L} \\ \alpha\mathbf{L} - p\mathbf{P} \\ qp\mathbf{P} - \rho_I\mathbf{I} \\ (1-q)p\mathbf{P} - \rho_A\mathbf{A} \\ \rho_I\eta\mathbf{I} - h\mathbf{H} \\ \rho_I(1-\eta)\mathbf{I} + \rho_A\mathbf{A} + (1-\mu)h\mathbf{H} \\ \mu h\mathbf{H} \end{pmatrix}; \ g(x) = \begin{pmatrix} -\mathbf{S}(\mathbf{P}+\mathbf{I}+\delta\mathbf{A}) \\ \mathbf{S}(\mathbf{P}+\mathbf{I}+\delta\mathbf{A}) \\ 0 \\ 0 \\ 0 \\ 0 \\ 0 \\ 0 \end{pmatrix}; \ h(x) = \mathbf{H} \tag{7.28b}$$

Unfortunately, the complexity of the calculations below exceeds the sensible limit which can be derived or validated by hand. Thus, I only present the final results obtained using MATLAB's Symbolic Toolbox.

The algorithm reached the stopping criteria for $k^* = 5$, meaning that $\Omega_{obs} = \Omega_5$, which has 10 rows and 8 columns. The matrix has a structural rank of 6 (rank $\Omega_{obs} = 6$), meaning that the system is not fully observable. Computing the unobservability subspace:

$$\ker \Omega_{obs} = \{x \mid x = r_1(0\ 0\ 0\ 0\ 0\ 0\ 1\ 0)^\intercal + r_2(0\ 0\ 0\ 0\ 0\ 0\ 0\ 1)^\intercal;\ r_1, r_2 \in \mathbb{R}\}, \tag{7.29}$$

it is clearly visible that compartments $\mathbf{R}, \mathbf{D}$ are not observable.

Similarly to the SEIR model's case, this is the expected result: both $\mathbf{R}$ and $\mathbf{D}$ are terminal, integrator compartments, which do not influence the dynamics of any other state variables. Analogously, they are not required for the feedback linearization input law either, and thus their unobservability does not affect the effectiveness of the EKF estimation relevant for the controller.

Contrary to the SEIR case, it is not trivial to see which 6×6 minor(s) of Ω_{obs} provide(s) the nonzero determinant ensuring the rank of 6. The last two columns, corresponding to $\mathbf{R}, \mathbf{D}$, contain only 0s, so they should be naturally omitted. However, finding the correct row combination(s) from the possible $\mathbf{C}_{10}^6 = 210$ possibilities was carried out by exhaustive search.

The search resulted in 45 possible candidates, minors having a determinant that the symbolic toolbox could not classify *structurally* to be always 0. Fortunately, there is no need to individually check all of them for possible singularities.

Choosing arbitrarily[1], we examine the minor $M = \left\{\Omega_{obs|i,j} \mid i \in \{1,2,3,4,6,9\}, j \in \{1,2,3,4,5,6\}\right\}$, and compute its determinant:

$$\det M = \mathbf{S}\alpha^3\delta\eta^5 p^4 q^4 \rho_A \rho_I^5 (\mathbf{I} + \mathbf{P} + \delta\mathbf{A}). \tag{7.30}$$

Knowing that the model parameters $\alpha, \delta, \eta, p, q, \rho_A, \rho_I > 0$, and $\mathbf{S}, \mathbf{I}, \mathbf{P}, \mathbf{A} \geq 0$, we can conclude that $\det M = 0$ if and only if $\mathbf{S} = 0$ or $\mathbf{P} = \mathbf{I} = \mathbf{A} = 0$ (i.e no susceptibles or no carriers of the pathogen present in the system).

Consequently, we can also conclude that:

$$x \notin Z = \{\mathbf{S} = 0\ \vee (\mathbf{P} = 0\ \wedge\ \mathbf{I} = 0\ \wedge\ \mathbf{A} = 0)\}\ \Rightarrow\ \det M \neq 0\ \Rightarrow\ \text{rank}\ \Omega_{obs}(x) = 6, \tag{7.31}$$

which means that the remaining six state variables $(\mathbf{S}, \mathbf{L}, \mathbf{P}, \mathbf{I}, \mathbf{A}, \mathbf{H})$ are fully observable everywhere in the state space except the above-defined Z singular manifold.

On the other hand, we can check by substitution the structural ranks:

$$\text{rank}\ \ \Omega_{obs}(x)|_{\mathbf{S}=0} = 5 \quad \text{and} \quad \text{rank}\ \ \Omega_{obs}(x)|_{\mathbf{P}=0,\mathbf{I}=0,\mathbf{A}=0} = 5, \tag{7.32}$$

so the rank of the observability matrix decreases below 6 when $x \in Z$. Whether there are parts of Z where the observability degrades even further remains an interesting and open question (which would require some further analysis); however, this is not significant from the EKF-based state estimation's point of view. The controller and the estimator are used generally outside of Z, with slight numerical problems possibly arising only in its neighbourhood (e.g. when the number of infected individuals in the system is close to 0 between two epidemic waves).

[1] Without loss of generality, the minor with the *seemingly simplest* determinant was chosen.

7.6 Controllability analysis of the epidemic models

This part contains the detailed controllability analysis of the SEIR and SLPIAHRD epidemic models controlled in Chapter 4.2. To check local accessibility, we compute the state-dependent controllability distribution and check its structural rank [83, 229]. We also investigate singularities, i.e, attempt to exactly determine the regions in which the models might not be controllable. Generally, considering a nonlinear system in the input-affine form seen in equations (7.22), we construct the controllability distribution using the following algorithm:

1. Starting point: $\Delta_0 = \text{span}\{g_1, g_2, \ldots, g_m\}$. Note: $g_0 = f$ by definition.

2. Iterative development of the distribution:

$$\Delta_k = \Delta_{k-1} + \sum_{i=0}^{m} [g_i, \Delta_{k-1}], \text{ where} \tag{7.33a}$$

$$[g_i, \Delta_{k-1}] = \text{span}\{[g_i, \phi_1], [g_i, \phi_2], \ldots, [g_i, \phi_l]\}, \text{where} \tag{7.33b}$$

$$\Delta_{k-1} = \text{span}\{\phi_1, \phi_2, \ldots, \phi_l\} \text{ and } [f, g] = \frac{\partial g}{\partial x} f - \frac{\partial f}{\partial x} g \text{ (i.e the Lie-bracket)} \tag{7.33c}$$

3. Stopping criteria: if $\exists k* : \text{rank } \Delta_{k^*} = \text{rank } \Delta_{k^*+1}$ then $\Delta_c = \Delta_{k^*}$; otherwise $\Delta_c = \Delta_n$.

We can check controllability based on the following theorem:

Theorem (Local accessibility)**.** If the controllability matrix $\Delta_c(x)$ has full rank at a point x_0, i.e rank $\Delta_c = n$, then the system is locally accessible in some neighborhood of x_0.

7.6.1 SEIR model

Using the same input-affine formulations as in equations (7.15), with $m = 1$, we compute the steps of the algorithm (using Matlab Symbolic Toolbox):

0. Starting point: $\Delta_0 = \text{span}\{g_1\} = \text{span}\{(-\mathbf{SI} \;\; \mathbf{SI} \;\; 0 \;\; 0)^\intercal\}$

1. Iteration 1:

$$\Delta_1 = \text{span}\left\{ \begin{pmatrix} -\mathbf{SI} \\ \mathbf{SI} \\ 0 \\ 0 \end{pmatrix} \begin{pmatrix} -\mathbf{S}(k_2\mathbf{E} - k_3\mathbf{I}) \\ \mathbf{S}(k_2\mathbf{E} - k_3\mathbf{I}) + k_2\mathbf{SI} \\ -k_2\mathbf{SI} \\ 0 \end{pmatrix} \right\} \tag{7.34}$$

2. Iteration 2:

$$\Delta_2 = \text{span}\left\{ \begin{pmatrix} -\mathbf{SI} \\ \mathbf{SI} \\ 0 \\ 0 \end{pmatrix} \begin{pmatrix} -\mathbf{S}(k_2\mathbf{E} - k_3\mathbf{I}) \\ \mathbf{S}(k_2\mathbf{E} - k_3\mathbf{I}) + k_2\mathbf{SI} \\ -k_2\mathbf{SI} \\ 0 \end{pmatrix} \begin{pmatrix} k_3\mathbf{S}(k_2\mathbf{E} - k_3\mathbf{I}) + k_2^2\mathbf{SE} \\ (k_2 - k_3)\mathbf{S}(k_2\mathbf{E} + k_2\mathbf{I} - k_3\mathbf{I}) \\ -k_2\mathbf{S}(2k_2\mathbf{E} + k_2\mathbf{I} - k_3\mathbf{I}) \\ k_2k_3\mathbf{IS} \end{pmatrix} \right\} \tag{7.35}$$

3. Stopping criteria: checked using symbolic tools that rank Δ_3 = rank Δ_2, meaning that $\Delta_c = \Delta_2$.

As a result, we can see that the structural rank of the system is rank $\Delta_c = 3$, so the SEIR model is *not* fully controllable. This was expected, as due to the population conservation law $\mathbf{S}(t) + \mathbf{E}(t) + \mathbf{I}(t) + \mathbf{R}(t) = \mathbf{N}$ at all times, efficiently reducing the system's degree of freedom

to 3. In line with the above intuition, we can also check the image (or column space) of the controllability matrix:

$$\text{Im } \Delta_c = \left\{ x \;\middle|\; x = r_1 \begin{pmatrix} 1 \\ 0 \\ 0 \\ -1 \end{pmatrix} + r_2 \begin{pmatrix} 0 \\ 1 \\ 0 \\ -1 \end{pmatrix} + r_3 \begin{pmatrix} 0 \\ 0 \\ 1 \\ -1 \end{pmatrix}, \quad r_1, r_2, r_3 \in \mathbb{R} \right\} \tag{7.36}$$

We can also check for local singularities, where the controllability rank decreases. Computing the determinant of the upper-left 3×3 minor of Δ_c:

$$\det M = k_2 k_3 \mathbf{S}^3 \mathbf{I}^3 \tag{7.37}$$

which means that the controllability becomes worse only if $\mathbf{S} = 0$ or $\mathbf{I} = 0$ (parameters $k_2, k_3 > 0$). It can be checked using substitution that in these cases rank $\Delta_c = 0$, since the 0-ness of either variable implies $g(x) = 0$ (i.e the input has absolutely no effect on the system's dynamics). This is the same manifold on which the model's observability is degraded: when there are no susceptible or infectious people in the system.

7.6.2 SLPIAHRD model

Using the input-affine formulation from equations (7.28), with $m = 1$, we compute the steps using the Symbolic Toolbox. Similarly to the observability analysis, due to the complexity of the equations, only the results are presented.

The algorithm reached the stopping condition at $k^* = 5$, where rank $\Delta_5 =$ rank $\Delta_6 = 6$. Again, the model is *not* fully controllable, which is not surprising because of the population conservation law. To analyze the controllable subspace, we can compute the image of the controllability matrix:

$$\Delta_c = \text{span} \left\{ \begin{pmatrix} 1 \\ 0 \\ 0 \\ 0 \\ 0 \\ 0 \\ \eta\mu q - 1 \\ -\eta\mu q \end{pmatrix}; \begin{pmatrix} 0 \\ 1 \\ 0 \\ 0 \\ 0 \\ 0 \\ \eta\mu q - 1 \\ -\eta\mu q \end{pmatrix}; \begin{pmatrix} 0 \\ 0 \\ 1 \\ 0 \\ 0 \\ 0 \\ \eta\mu q - 1 \\ -\eta\mu q \end{pmatrix}; \begin{pmatrix} 0 \\ 0 \\ 0 \\ 1 \\ 0 \\ 0 \\ \eta\mu q - 1 \\ -\eta\mu q \end{pmatrix}; \begin{pmatrix} 0 \\ 0 \\ 0 \\ 0 \\ 1 \\ 0 \\ -1 \\ 0 \end{pmatrix}; \begin{pmatrix} 0 \\ 0 \\ 0 \\ 0 \\ 0 \\ 1 \\ \mu - 1 \\ -\mu \end{pmatrix} \right\} \tag{7.38}$$

From this, we can see that generally the first six states of the model can be controlled independently, while the $\mathbf{R}, \mathbf{D}$ compartments can be expressed using their linear combination.

We can also check for singular points and conditions when the rank of the controllability matrix decreases even further. First, we check the determinant of the minor containing the first 6 columns of Δ_c.

$$\det M = \mathbf{S}^6 \alpha^5 \eta h p^4 q^2 \rho_A \rho_I^2 (h - \rho_A)(\rho_A - \rho_I)(q - 1)(\mathbf{I} + \mathbf{P} + \delta\mathbf{A})^6 \tag{7.39}$$

Similarly to the observability case, we can see the controllability rank possibly decreasing if $\mathbf{S} = 0$ or $\mathbf{P} = \mathbf{I} = \mathbf{A} = 0$ (i.e there are no susceptibles or infectious individuals in the system). Checking by substitution, we can see that rank $\Delta_c|_{\mathbf{S}=0} = 0$ and rank $\Delta_c|_{\mathbf{P}=\mathbf{I}=\mathbf{A}=0} = 0$, as these conditions imply $g(x) = 0$, i.e the input has no influence over the system dynamics.

However, here there are additional cases, depending on the parameters, when the rank of the matrix might further decrease. Below, I separately analyze each term that can make the above determinant 0.

1. First, $(1-q) = 0$ means that the probability of an asymptomatic infection is 0, and everyone transitions from **P** to the **I** compartment. In this case, $\mathbf{A}(t) = 0\ \forall t$, and only the $\mathbf{S}, \mathbf{L}, \mathbf{P}, \mathbf{I}, \mathbf{H}$ subsystem can remain fully controllable. It can also be checked by substitution that in this case rank $\Delta_c|_{q=1} = 5$, and that the image of Δ_c supports the above statement.

2. If $h - \rho_A = 0$, the time spent in the **A** and **H** compartment is equal. In this case, the image of Δ_c will be the subspace spanned by:

$$\text{span}\left\{\begin{pmatrix}1\\0\\0\\0\\0\\0\\\eta\mu q-1\\-\eta\mu q\end{pmatrix};\begin{pmatrix}0\\1\\0\\0\\0\\0\\\eta\mu q-1\\-\eta\mu q\end{pmatrix};\begin{pmatrix}0\\0\\1\\0\\0\\0\\\eta\mu q-1\\-\eta\mu q\end{pmatrix};\begin{pmatrix}0\\0\\0\\1\\0\\\eta\rho_I/(h-\rho_I)\\r_1^*\\-\eta h\mu/(h-\rho_I)\end{pmatrix};\begin{pmatrix}0\\0\\0\\0\\1\\-\eta q\rho_I/(h-\rho_I-hq+q\rho_I)\\r_2^*\\\eta\mu q\rho_I/(h-\rho_I-hq+q\rho_I)\end{pmatrix}\right\} \tag{7.40a}$$

$$r_1^* = -(h-\rho_I+\eta\rho_I-\eta h\mu)/(h-\rho_I) \tag{7.40b}$$

$$r_2^* = -(h-\rho_I-hq+q\rho_I-\eta q\rho_I+\eta\mu q\rho_I)/(h-\rho_I-hq+q\rho_I), \tag{7.40c}$$

   i.e the state **H** will be linearly dependent on the **I** and **A** compartments. Checking by substitution, in this case rank $\Delta_c|_{\rho_A=h} = 5$.

3. If $\rho_A = \rho_I$, the time spent in the **I** and **A** compartments is equal. In this case:

$$\text{Im}\ \Delta_c = \text{span}\left\{\begin{pmatrix}1\\0\\0\\0\\0\\0\\\eta\mu q-1\\-\eta\mu q\end{pmatrix};\begin{pmatrix}0\\1\\0\\0\\0\\0\\\eta\mu q-1\\-\eta\mu q\end{pmatrix};\begin{pmatrix}0\\0\\1\\0\\0\\0\\\eta\mu q-1\\-\eta\mu q\end{pmatrix};\begin{pmatrix}0\\0\\0\\1\\-(q-1)/q\\0\\(\eta\mu q-1)/q\\-\eta\mu q/q\end{pmatrix};\begin{pmatrix}0\\0\\0\\0\\0\\1\\\mu-1\\-\mu\end{pmatrix}\right\}, \tag{7.41}$$

   thus the number of individuals in **A** is proportional to the number of people in **I**, and the system has only 5 degrees of freedom. In this case, rank $\Delta_c|_{\rho_A=\rho_I} = 5$.

Altogether, as the aim of the controller is only achieving reference tracking with the $y = \mathbf{H}$ output, the fact that some intermediary states can not be independently controlled does not cause any problem for the control setups presented in Chapter 4.2.